AUTONOMIC NERVOUS SYSTEM AND CARDIOVASCULAR DISEASES: FROM BRAIN TO HEART

EDITED BY: Lilei Yu, Hong Jiang, Yan Yao, Deyong Long and Sunny Po
PUBLISHED IN: Frontiers in Physiology, Frontiers in Neurology and Frontiers in Neuroscience

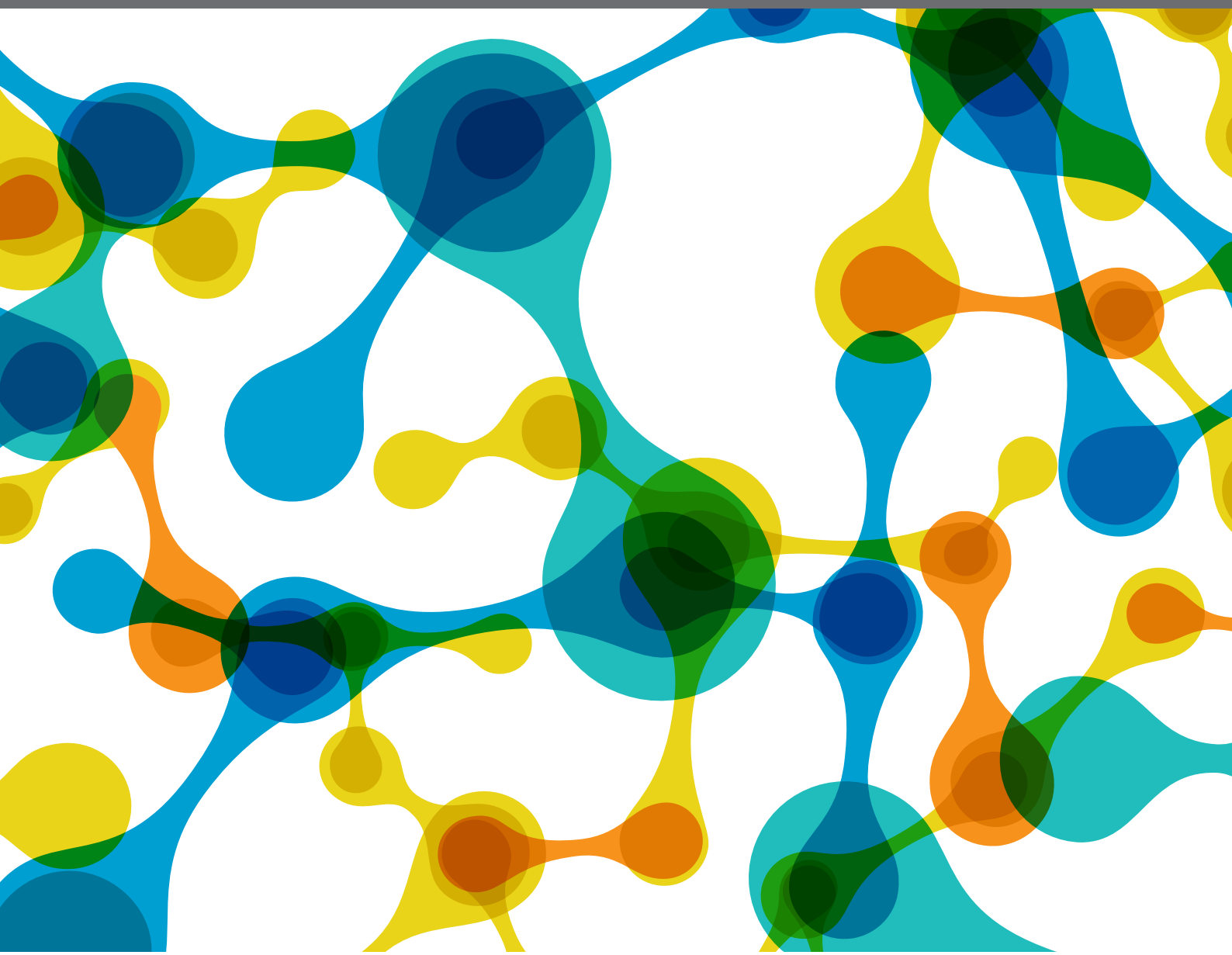

frontiers Research Topics

ISSN 1664-8714
ISBN 978-2-88976-213-2
DOI 10.3389/978-2-88976-213-2

About Frontiers

Frontiers is more than just an open-access publisher of scholarly articles: it is a pioneering approach to the world of academia, radically improving the way scholarly research is managed. The grand vision of Frontiers is a world where all people have an equal opportunity to seek, share and generate knowledge. Frontiers provides immediate and permanent online open access to all its publications, but this alone is not enough to realize our grand goals.

Frontiers Journal Series

The Frontiers Journal Series is a multi-tier and interdisciplinary set of open-access, online journals, promising a paradigm shift from the current review, selection and dissemination processes in academic publishing. All Frontiers journals are driven by researchers for researchers; therefore, they constitute a service to the scholarly community. At the same time, the Frontiers Journal Series operates on a revolutionary invention, the tiered publishing system, initially addressing specific communities of scholars, and gradually climbing up to broader public understanding, thus serving the interests of the lay society, too.

Dedication to Quality

Each Frontiers article is a landmark of the highest quality, thanks to genuinely collaborative interactions between authors and review editors, who include some of the world's best academicians. Research must be certified by peers before entering a stream of knowledge that may eventually reach the public - and shape society; therefore, Frontiers only applies the most rigorous and unbiased reviews.
Frontiers revolutionizes research publishing by freely delivering the most outstanding research, evaluated with no bias from both the academic and social point of view. By applying the most advanced information technologies, Frontiers is catapulting scholarly publishing into a new generation.

What are Frontiers Research Topics?

Frontiers Research Topics are very popular trademarks of the Frontiers Journals Series: they are collections of at least ten articles, all centered on a particular subject. With their unique mix of varied contributions from Original Research to Review Articles, Frontiers Research Topics unify the most influential researchers, the latest key findings and historical advances in a hot research area! Find out more on how to host your own Frontiers Research Topic or contribute to one as an author by contacting the Frontiers Editorial Office: frontiersin.org/about/contact

AUTONOMIC NERVOUS SYSTEM AND CARDIOVASCULAR DISEASES: FROM BRAIN TO HEART

Topic Editors:
Lilei Yu, Wuhan University, China
Hong Jiang, Renmin Hospital of Wuhan University, China
Yan Yao, State Key Laboratory of Cardiovascular Disease, Fuwai Hospital, Chinese Academy of Medical Sciences, China
Deyong Long, Capital Medical University, China
Sunny Po, University of Oklahoma Health Sciences Center, United States

Citation: Yu, L., Jiang, H., Yao, Y., Long, D., Po, S., eds. (2022). Autonomic Nervous System and Cardiovascular Diseases: From Brain to Heart.
Lausanne: Frontiers Media SA. doi: 10.3389/978-2-88976-213-2

Table of Contents

frontiers | Frontiers in Physiology

EDITORIAL
published: 29 April 2022
doi: 10.3389/fphys.2022.884832

Editorial: Autonomic Nervous System and Cardiovascular Diseases: From Brain to Heart

Yueyi Wang[1,2,3,4], *Liping Zhou*[1,2,3,4], *Hong Jiang*[1,2,3,4] *and Lilei Yu*[1,2,3,4]*

[1]Department of Cardiology, Renmin Hospital of Wuhan University, Wuhan, China, [2]Cardiac Autonomic Nervous Research Center of Wuhan University, Wuhan, China, [3]Cardiovascular Research Institute, Wuhan University, Wuhan, China, [4]Hubei Key Laboratory of Cardiology, Wuhan, China

Keywords: autonomic nervous system, sympathetic, parasympathetic, brain-heart connection, cardiovascular disease

Editorial on the Research Topic

Autonomic Nervous System and Cardiovascular Diseases: From Brain to Heart

The autonomic nervous system connects the control from brain to heart through the sympathetic and parasympathetic branches. Central nervous system diseases can induce cardiovascular diseases mediated by autonomic nervous system. For instance, patients with Parkinson's disease present autonomic dysfunction and α-synuclein deposition in cardiovascular system leading to catecholaminergic abnormalities and cardiac denervation, because of the high density of sympathetic innervation in the heart (Sharabi et al., 2021). Meanwhile, the brain-heart interaction is involved in the pathophysiology of cardiovascular diseases through autonomic nervous system, as patients with Takotsubo syndrome display deficient autonomic-limbic integration and fewer functionally connected parasympathetic- and sympathetic-subnetworks (Templin et al., 2019). All these findings highlight the autonomic nervous system as an essential target for prevention and control of the pathological process of cardiac diseases, and for further clinical transformation (Yu et al., 2010; Yu et al., 2017).

This research topic aimed to explore recent developments in this area focused on 1) the role of autonomic nervous system in cardiovascular diseases, 2) the role of autonomic nervous system in central nervous system diseases, and 3) the autonomic nervous system interaction between heart and brain.

The function of cardiac autonomic nervous system (CANS) is under influence of multiple factors, including pathophysiological processes. Hooper et al. showed that irritant-evoked pulmonary-cardiac reflexes were remodeled in spontaneously hypertensive (SH) rats. Inhalation of the selective transient receptor potential ankyrin 1 agonist allyl isothiocyanate evoked pulmonary-cardiac reflex, leading to morphological change in P waves in SH rats. Inhibition of either parasympathetic or sympathetic components of the pulmonary-cardiac reflex attenuated these effects. This study provides novel evidence for altered irritant-evoked pulmonary-cardiac reflex for AF initiation in SH rats, that deepens our understanding of autonomic mechanisms underlying cardiovascular diseases.

Kidney plays an important role in sympathetic activation and the pathogenesis of hypertension, and regulation of the renal afferents influences the sympathetic activity and blood pressure. Ye et al. demonstrated the contribution of renal afferents and the induced excitatory renal reflex (ERR) in the development of hypertension in SH rats. The study showed that ERR was enhanced in the early stage of hypertension, but attenuated in the later stage in the SHR, indicating the involvement of abnormal ERR in sympathetic activation and the development of hypertension. As the renal sympathetic denervation therapy gains extensive attention, this study proposed that selective renal afferent or efferent denervation may produce distinct output in hypertension, especially at the early stage.

Edited and reviewed by:
Joel C. Bornstein,
The University of Melbourne, Australia

***Correspondence:**
Lilei Yu
lileiyu@whu.edu.cn

Specialty section:
This article was submitted to Autonomic Neuroscience, a section of the journal Frontiers in Physiology

Received: *27 February 2022*
Accepted: *16 March 2022*
Published: *29 April 2022*

Citation:
Wang Y, Zhou L, Jiang H and Yu L (2022) Editorial: Autonomic Nervous System and Cardiovascular Diseases: From Brain to Heart. Front. Physiol. 13:884832. doi: 10.3389/fphys.2022.884832

The stellate ganglion (SG) is an autonomic nervous ganglion that provides sympathetic outflow and plays an integrative role in regulating cardiovascular function. Myocardial infarction (MI) results in neural remodeling in the SG, however, the expression and function of the proteins in SG tissue after MI remained unclear. Cheng et al. explored the expression characteristics of proteins in rabbit SG by the tandem mass tags quantitative proteomic sequencing, and found 383 differentially expressed proteins (DEPs) including 143 upregulated and 240 downregulated proteins. This study provides beneficial evidence for further studies on the SG in understanding the pathological process and developing therapeutic treatment of MI.

Along with the identification and investigation of the autonomic mechanisms in cardiovascular disease, major focus was put on the left-sided cardiac pathology and in animals. However, the structure, function and autonomic innervation of the right ventricle are distinct from the left. Zandstra et al. reviewed the asymmetry and regional differences with distinct anatomical, functional and molecular characteristics of the CANS in humans. Based on this review, further researches are needed to investigate the different autonomic innervation of the right ventricle and design accurate treatment in accordance with cardiac autonomic asymmetry and heterogeneity.

Cardiac autonomic imbalance is observed after acute ischemic stroke (AIS), and heart rate variability (HRV) can be used to predict clinical outcomes and neurological function. However, are other noninvasively measured cardiac parameters involved and associated with neurological improvement in AIS? Joseph Miller et al. conducted a pilot prospective observational study in AIS patients, and found that the cardiac stroke volume index (cSVI) and mean arterial blood pressure (MAP) were associated with 24-h neurological improvement. Of which, cSVI showed a linear correlation with NIH stroke scale improvement. This study proposed cSVI as a unique cardiac parameter in association with 24-h neurological outcomes in AIS patients, which provides valuable evidences for possible therapeutic and prognostic application.

Hydrogen sulfide (H_2S), as a vital endogenous gasotransmitter, is involved in a wide range of physiological and pathological processes. Basak Donertas Ayaz et al. studied the H_2S donor NaHS in a rat model of hypertension. They found that intracerebroventricular infusion of NaHS attenuated angiotensin II induced hypertension, autonomic dysfunction and microglia activation in paraventricular nucleus (PVN). Their results suggest an independent role of central H_2S from circulating H_2S in treatment of hypertension, and the mediated neuromodulating and neuroimmune pathways contributing H_2S a potentially beneficial autonomic and anti-hypertensive target.

Epilepsy is a disorder of central nervous system characterized by repeated seizures, leading to impaired CNAS function. However, there are few researches studied the CANS function in pre-school children with epilepsy. Yang et al. found that the measurements of heart rate variability (HRV), multiscale entropy (MSE) and Kurths-Wessel symbolization entropy (KWSE) were significantly lower in pre-school pediatric intractable epilepsy (PIE) patients, indicating the imbalance of CANS in both sympathetic and vagal tone. Meanwhile, an accurate prediction of PIE *via* the combination of HRV, MSE and KWSE was proposed based on noninvasive ECG. This study provides important implication in health control in pre-school PIE children.

Event-related potentials (ERPs) are commonly used to assess motor or cognitive events. But no study reported if other factors, such as changes in heartbeat-evoked potentials (HEPs), could influence ERPs. Park et al. revealed the effects of HEPs on the performance of the mental workload (MWL) classification based on ERPs. With a mental arithmetic task to distinguish low- and high- MWL, they found that HEPs affected the ERPs resulting in a decrease in the performance of MWL classification. HEPs reflected a synchronization in the communication between brain and heart, indicating that the cardiac activity is needed to be considered to obtain a clear and pure ERP response. This study suggested an accurate strategy to improve brain activity classification and provide a better application of ERPs to various fields.

Both sympathetic hyperactivation and baroreflex dysfunction are typical characteristics in heart failure patients with reduced ejection fraction (HFrEF), but it's unclear between the phasic activity of sympathetic nerve bursts and the baroreflex dysfunction. Toschi-Dias et al. investigated the rhythm of the muscle sympathetic nerve activity (MSNA) in HFrEF patients. They found that the oscillatory pattern of MSNA was directly associated with the gain and coupling of the sympathetic baroreflex function, and inversely associated with MSNA burst frequency. This study extended our knowledge about the oscillatory pattern of MSNA on the functional capacity and clinical condition of HFrEF patients.

Moyamoya disease is a rare cerebrovascular disease resulting in ischemic or hemorrhagic stroke, characterized by progressive stenosis of the intracranial internal carotid arteries and their proximal branches. Zou et al. presented a rare case of a postpartum woman with moyamoya disease, observed atypical posterior reversible encephalopathy syndrome (PRES). Based on this report, PRES can occur in patients with moyamoya disease and should be considered for the differential diagnosis of cerebral infarcts and hemorrhage in postpartum woman, providing both pathophysiological and clinical significance.

In conclusion, the present research topic collected some interesting papers and revealed better understanding of the autonomic nervous system interaction between heart and brain. We hope further researches about this topic will be continued, and will contribute to the clinical transformation of novel neuromodulate strategies.

AUTHOR CONTRIBUTIONS

All authors listed have made a substantial, direct and intellectual contribution to the work, and approved it for publication.

FUNDING

This work was supported by the grants from National Natural Science Foundation of China (No. 81871486, 81970287, 82100530), and Foundation for Innovative Research Groups of Natural Science Foundation of Hubei Province, China (2021CFA010).

REFERENCES

Sharabi, Y., Vatine, G. D., and Ashkenazi, A. (2021). Parkinson's Disease outside the Brain: Targeting the Autonomic Nervous System. *Lancet Neurol.* 20 (10), 868–876. doi:10.1016/S1474-4422(21)00219-2

Templin, C., Hänggi, J., Klein, C., Topka, M. S., Hiestand, T., Levinson, R. A., et al. (2019). Altered Limbic and Autonomic Processing Supports Brain-Heart axis in Takotsubo Syndrome. *Eur. Heart J.* 40 (15), 1183–1187. doi:10.1093/eurheartj/ehz068

Yu, L., Scherlag, B. J., Dormer, K., Nguyen, K. T., Pope, C., Fung, K.-M., et al. (2010). Autonomic Denervation with Magnetic Nanoparticles. *Circulation* 122 (25), 2653–2659. doi:10.1161/CIRCULATIONAHA.110.940288

Yu, L., Zhou, L., Cao, G., Po, S. S., Huang, B., Zhou, X., et al. (2017). Optogenetic Modulation of Cardiac Sympathetic Nerve Activity to Prevent Ventricular Arrhythmias. *J. Am. Coll. Cardiol.* 70 (22), 2778–2790. doi:10.1016/j.jacc.2017.09.1107

Conflict of Interest: The authors declare that the research was conducted in the absence of any commercial or financial relationships that could be construed as a potential conflict of interest.

frontiers in Physiology

ORIGINAL RESEARCH
published: 03 June 2021
doi: 10.3389/fphys.2021.673950

Dysregulation of the Excitatory Renal Reflex in the Sympathetic Activation of Spontaneously Hypertensive Rat

*Chao Ye[1], Fen Zheng[1], Jing-Xiao Wang[1], Xiao-Li Wang[1], Qi Chen[2], Yue-Hua Li[2], Yu-Ming Kang[3] and Guo-Qing Zhu[1,2]**

[1] Key Laboratory of Targeted Intervention of Cardiovascular Disease, Collaborative Innovation Center of Translational Medicine for Cardiovascular Disease, Department of Physiology, Nanjing Medical University, Nanjing, China, [2] Department of Pathophysiology, Nanjing Medical University, Nanjing, China, [3] Department of Physiology and Pathophysiology, Cardiovascular Research Center, Xi'an Jiaotong University School of Medicine, Xi'an, China

Excessive sympathetic activation plays crucial roles in the pathogenesis of hypertension. Chemical stimulation of renal afferents increases the sympathetic activity and blood pressure in normal rats. This study investigated the excitatory renal reflex (ERR) in the development of hypertension in the spontaneously hypertensive rat (SHR). Experiments were performed in the Wistar-Kyoto rat (WKY) and SHR aged at 4, 12, and 24 weeks under anesthesia. Renal infusion of capsaicin was used to stimulate renal afferents, and thus, to induce ERR. The ERR was evaluated by the changes in the contralateral renal sympathetic nerve activity and mean arterial pressure. At the age of 4 weeks, the early stage with a slight or moderate hypertension, the ERR was more enhanced in SHR compared with WKY. The pressor response was greater than the sympathetic activation response in the SHR. At the age of 12 weeks, the development stage with severe hypertension, there was no significant difference in the ERR between the WKY and SHR. At the age of 24 weeks, the later stage of hypertension with long-term several hypertensions, the ERR was more attenuated in the SHR compared with the WKY. On the other hand, the pressor response to sympathetic activation due to the ERR was smaller at the age of 12 and 24 weeks than those at the age of 4 weeks. These results indicate that ERR is enhanced in the early stage of hypertension, and attenuated in the later stage of hypertension in the SHR. Abnormal ERR is involved in the sympathetic activation and the development of hypertension.

Keywords: renal reflex, hypertension, sympathetic activity, blood pressure, kidney

OPEN ACCESS

Edited by:
Lilei Yu,
Renmin Hospital of Wuhan University, China

Reviewed by:
Jasenka Zubcevic,
University of Florida, United States
Hanjun Wang,
University of Nebraska Medical Center, United States
Jie Qi,
Xi'an Jiaotong University, China

***Correspondence:**
Guo-Qing Zhu
gqzhucn@njmu.edu.cn
orcid.org/0000-0002-3132-9592

Specialty section:
This article was submitted to Autonomic Neuroscience, a section of the journal Frontiers in Physiology

Received: *28 February 2021*
Accepted: *08 April 2021*
Published: *03 June 2021*

Citation:
Ye C, Zheng F, Wang J-X, Wang X-L, Chen Q, Li Y-H, Kang Y-M and Zhu G-Q (2021) Dysregulation of the Excitatory Renal Reflex in the Sympathetic Activation of Spontaneously Hypertensive Rat. Front. Physiol. 12:673950. doi: 10.3389/fphys.2021.673950

INTRODUCTION

Excessive sympathetic activity is closely associated with hypertension, chronic heart failure, and chronic kidney disease (Chen et al., 2015; Grassi and Ram, 2016; Cheng et al., 2019). Most of the patients with chronic kidney diseases have an excessive sympathetic activation and hypertension, which is closely related to the increased morbidity and mortality of cardiovascular events (Kaur et al., 2017). Sympathetic overactivity is found not only in various hypertensive animal models including the spontaneously hypertensive rat (SHR) (Fan et al., 2012), obesity-related hypertensive rats (Xiong et al., 2012), renovascular hypertensive rats (Chen et al., 2011), and DOCA-sal

hypertensive rats (Yemane et al., 2010), but also in patients with essential hypertension (Fisher and Fadel, 2010) and secondary hypertension (Vecchione et al., 2000; Lambert et al., 2007; Neumann et al., 2007). The excessive sympathetic activation plays a pathogenic role in the occurrence and development of hypertension and related organ damage (Grassi et al., 2015). Intervention of sympathetic overactivity is an important strategy for attenuating hypertension and its complication (Esler, 2014; Seravalle et al., 2014).

Kidney plays critical roles in the sympathetic activation in hypertension and chronic kidney diseases (Rettig et al., 1989, 1990; Iliescu et al., 2015). Renal nerves comprise of the afferent sensory fibers and efferent sympathetic fibers. The afferent sensory activity from the kidney to the brain is involved in regulating the sympathetic activity and blood pressure (Kopp, 2015; Bie and Evans, 2017; Milanez et al., 2020). Selective removal of renal afferent fibers reduces the blood pressure and sympathetic activity in a rat model of renovascular hypertension (Lopes et al., 2020). Recently, we have shown that the chemical stimulation of kidney in normal rats with capsaicin causes an excitatory renal reflex (ERR), which results in the sympathetic activation and pressor responses (Ye et al., 2020). The capsaicin-induced ERR is mediated by angiotensin II in the hypothalamic paraventricular nucleus (PVN), which acts on AT_1R, and in turn activates NADPH oxidase, causing oxidative stress and the subsequent NFκB activation and IL-1β production in the PVN in normal rats (Qiu et al., 2020; Zheng et al., 2020). The renal afferent input increases the activity of some neurons in the PVN (Xu et al., 2015), and destruction of the PVN neurons abolishing the capsaicin-induced ERR (Ye et al., 2020).

In the recent years, catheter-based renal sympathetic denervation (RDN) is the most extensively investigated approach for intervention of hypertension by interrupting the activity of both afferent and efferent renal nerves (Lauder et al., 2021; Weber and Osborn, 2021). It is important to know the changes of the ERR in the pathogenesis of hypertension. Unfortunately, the changes of the ERR-induced by the chemical stimulation of renal afferents in hypertension are still unknown. SHR is the most widely used animal model of essential hypertension. The genetic hypertension model has many similarities with human essential hypertension in the pathophysiological progress, neuroendocrine changes, clinical course, and secondary diseases (Bell et al., 2004; Graham et al., 2005). In the present study, we investigated the changes of the ERR in the occurrence and development of hypertension in the SHR.

MATERIALS AND METHODS

Animals

Male WKY and SHR at ages four, 12, and 24 weeks were obtained from the Vital River Laboratory Animal Technology Co., Ltd. (Beijing, China). The rats were kept in a temperature-controlled room on a 12-h cycle of light/darkness. Tap water and normal rat chow were available *ad libitum*. The experiments were approved by the Experimental Animal Care and Use Committee of Nanjing Medical University, and performed in accordance with the recommendations in the NIH guidelines (Eighth edition, 2011) listed in the Guide for the Care and Use of Laboratory Animals.

General Procedures

Rats were anesthetized intraperitoneally with a mixture of urethane (800 mg/kg) and α-chloralose (40 mg/kg). Depth of anesthesia was assessed by both the paw withdrawal and corneal reflexes (Zhang et al., 2014). The rats were kept in a supine position, and a vertical incision was made in the middle of the neck to expose the trachea and carotid artery. Positive pressure ventilation *via* endotracheal intubation with room air was performed using a small animal ventilator (51,600, Stoelting, Chicago, IL, United States). A PE50 catheter was implanted into the right common carotid artery for blood pressure recording. Right and left kidneys were, respectively, exposed *via* flank incisions for preparing renal stimulation to induce ERR and renal sympathetic nerve activity (RSNA) recording. After the surgery, rats were allowed to stabilize for more than 30 min before intervention. Finally, the rats were euthanized by a rapid intravenous injection of pentobarbital sodium (100 mg/kg).

Assessment of ERR

Our previous study has shown that the infusion of capsaicin into the cortico-medullary border of the kidney caused greater ERR effects than those in the cortex or medulla of the kidney. Infusion of capsaicin into the upper, lateral, or lower parts of the kidney showed similar ERR effects (Ye et al., 2020). Therefore, the cortico-medullary border of the lateral part of the kidney was selected for the infusion site in inducing ERR (Qiu et al., 2020; Zheng et al., 2020). Intravenous infusion of the same dose of capsaicin failed to cause significant effects on the RSNA, mean arterial pressure (MAP), and heart rate (HR), excluding the possibility that the effects of the renal infusion of capsaicin might be caused by leaking into the blood circulation (Ye et al., 2020). The right kidney was exposed through a flank incision. An outer diameter of 0.31 mm stainless steel tube was inserted horizontally from the lateral margin of the kidney to the hilum level of the kidney. The tip of the tube rested on the edge of the renal cortex and medulla, where the tube encountered a slight resistance. A PE50 catheter was connected to the tube with a PM2000B programmable pressure injector (MicroData Instrument, NJ, United States). The ERR was induced by a renal infusion of capsaicin (1 nmol/μL) at 1.0 μL/min for 20 min, and evaluated by the capsaicin-induced changes in the RSNA and MAP. The same amount of vehicle was used as a control. At the end of the experiment, the same volume of Evans Blue was infused for the histological identification of the infusion sites. Capsaicin was purchased from MedChemExpress (Monmouth Junction, NJ, United States).

RSNA Recording

Renal sympathetic nerve activity was continuously recorded as we reported previously (Ye et al., 2020). Left renal sympathetic nerve was exposed through a left retroperitoneal incision in a prone position. The nerve was separated, and cut at the distal end to eliminate the renal afferent activity. The renal nerve was placed on a pair of platinum electrode, and soaked in paraffin oil at

37°C. Renal nerve signal was amplified by 4-Channel Differential Amplifier (Warner Instrument, Hamden, CT, United States) with a band-pass between 100 and 3,000 Hz. RSNA was integrated at a 100-ms time constant using the LabChart 8 software (ADInstruments). Background noise was recorded after cutting the central end of the renal nerve. RSNA data were obtained by subtracting the background noise. The percentage change in the integrated RSNA from the baseline value was calculated after renal infusion.

Blood Pressure Recording

Before the acute experiment, blood pressure of tail artery was measured in a conscious state with a non-invasive computerized tail-cuff system (NIBP, ADInstruments). Rats were warmed at 28°C for 10–20 min so that the pulsation of the caudal artery could be detected to reach the pulse level. The systolic blood pressure (SBP) was determined by averaging 10 measurements. During the acute experiment, the right common carotid artery was exposed *via* a vertical incision in the middle of the neck. A PE50 catheter filled with normal saline containing heparin (50 IU/mL) was implanted into the right common carotid artery. Blood pressure was continuously recorded *via* a pressor transducer connected with the catheter using an 8SP PowerLab system with the data acquisition software (ADInstruments, Bella Vista, NSW, Australia).

Statistics

Renal sympathetic nerve activity, MAP, and HR changes were determined by a one-minute average at the time frame of the maximal RSNA responses to the chemicals. All data were expressed as mean ± SE. Student's *t*-test was used to compare the difference between two groups. Paired t test were used to compare the values before and after the intervention. One-way and two-way ANOVA followed by Bonferroni's *post hoc* analysis were used for multiple comparisons. $P < 0.05$ was considered statistically significant.

RESULTS

ERR in the WKY and SHR at the Age of 4 Weeks

Our previous study has shown that the renal infusion of capsaicin dose-dependently induces ERR in normal rats (Ye et al., 2020). The dose of capsaicin at 1 nmol/min for 20 min was selected to induce ERR, and the vehicle for renal infusion had no significant effects on the RSNA, MAP, and HR (Qiu et al., 2020; Ye et al., 2020; Zheng et al., 2020). At the age of 4 weeks, the early stage with slight or moderate hypertension, unilateral renal infusion of capsaicin caused immediate increases in the contralateral RSNA and MAP in both the WKY and SHR, lasting for at least 30 min. Capsaicin reached its maximal effect at about 15 min after the beginning of the renal infusion. However, capsaicin reduced the HR in SHR, which occurred a little later than the capsaicin-induced pressor response (**Figure 1A**). The ERR was significantly enhanced in the SHR compared with the WKY. However, capsaicin increased the HR in WKY, but decreased in SHR (**Figure 1B**).

ERR in WKY and SHR at the Age of 12 Weeks

Renal infusion of capsaicin caused a rapid increase in the RSNA and MAP in both the WKY and SHR at the age of 12 weeks, the development stage with severe hypertension (**Figure 2A**). Unexpectedly, the capsaicin-induced ERR was not significantly enhanced in the SHR compared with the WKY. Renal infusion of capsaicin increased the HR in WKY, but had no significant effects in SHR (**Figure 2B**).

ERR in WKY and SHR at the Age of 24 Weeks

At the age of 24 weeks, the later stage of hypertension with long-term several hypertensions, renal infusion of capsaicin increased the RSNA and MAP in both the WKY and SHR (**Figure 3A**). However, the capsaicin-induced ERR was significantly attenuated in the SHR compared with the WKY. Renal infusion of capsaicin had no significant effects on the HR in both the WKY and SHR (**Figure 3B**).

Comparison of ERR at Different Ages of Hypertension in WKY and SHR

There was no significant difference in the body weight between the WKY and SHR at the ages of 4, 12, and 24 weeks (**Table 1**). The SBP of the SHR in a conscious state at the ages of 4, 12, and 24 weeks were significantly higher than those in the WKY, and the SBP in the SHR at the ages of 12 and 24 weeks were higher than that in the SHR at the age of 4 weeks (**Table 1**). Similarly, the baseline MAP of the SHR under an anesthetic at the ages of 4, 12, and 24 weeks were significantly higher than those in the WKY, and the baseline MAP in the SHR at the ages of 12 and 24 weeks was higher than that in the SHR at the age of 4 weeks (**Figure 4A**). In order to better understand the changes of ERR in the different periods of hypertension, we presented the results mentioned above in another format (**Figure 4B**). The RSNA response to capsaicin in WKY at the ages of 12 and 24 weeks was more enhanced than that in the WKY at the age of 4 weeks, while the MAP response to capsaicin in the SHR at the ages of 12 and 24 weeks was more attenuated than that in the SHR at the age of 4 weeks. Capsaicin-induced reduction in HR only occurred in the SHR at the age of 4 weeks (**Figure 4B**).

Difference in the RSNA and MAP Responses to Capsaicin in the WKY and SHR

We further compared the difference in the RSNA and MAP responses to capsaicin with the ratio of the MAP change to the integrated RSNA change (P/A index), an index to evaluate the relationship of MAP and RSNA. The P/A index was calculated as the ratio of MAP change in mmHg to the integrated RSNA change in mV (**Figure 5A**) or to the integrated RSNA change in percentage (**Figure 5B**). The P/A index was greater in the SHR

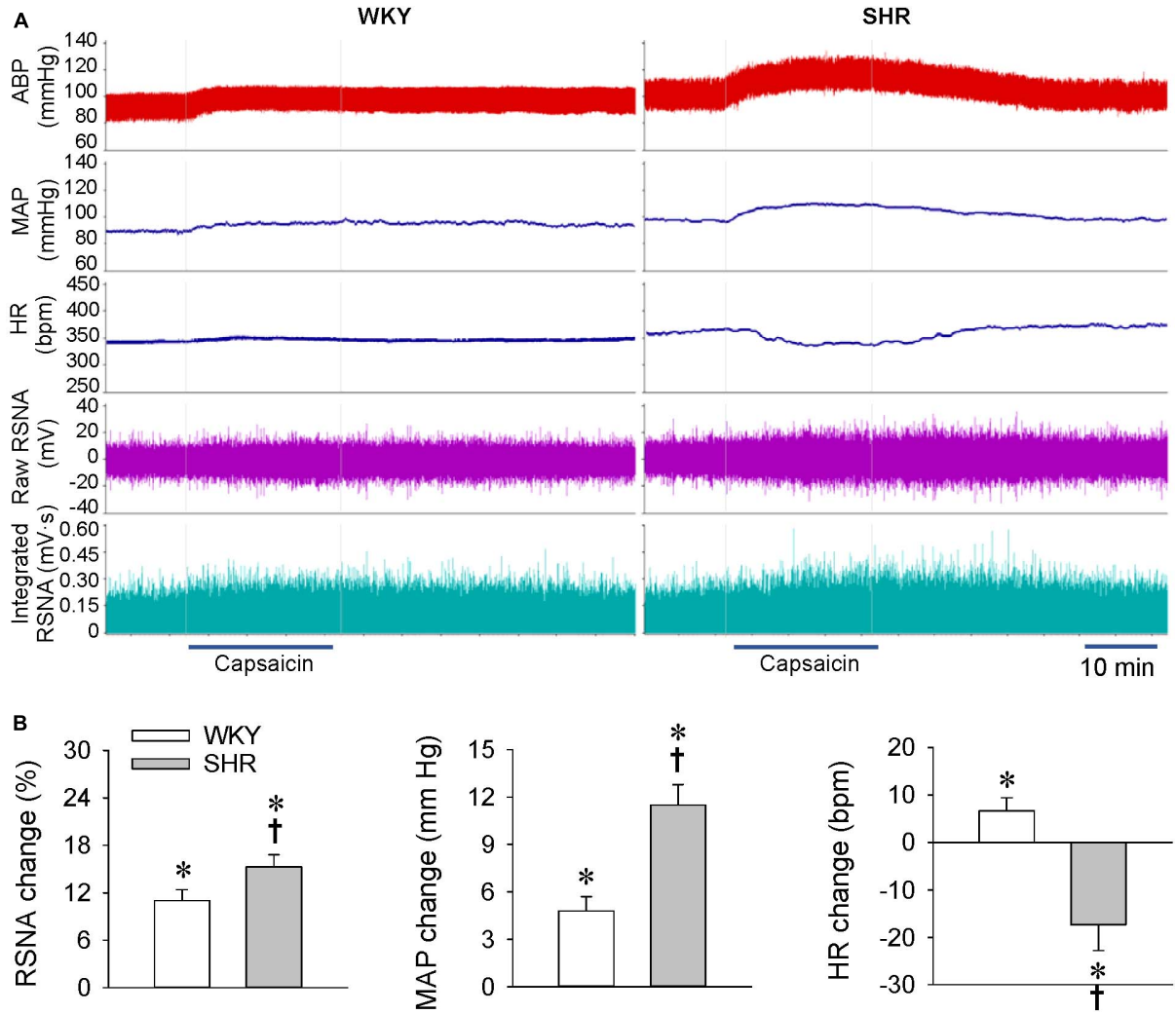

FIGURE 1 | ERR in the WKY and SHR at the age of 4 weeks. The ERR was induced by renal infusion of capsaicin at 1 nmol/min for 20 min. **(A)** representative recordings showing the recordings of the capsaicin-induced ERR. **(B)** bar graph showing the capsaicin-induced ERR. Values are mean ± SE. $^{*}P < 0.05$ vs the values before renal infusion; $^{\dagger}P < 0.05$ vs WKY. $n = 6$.

than that in the WKY at the age of 4 weeks, but there was no significant difference in the P/A index between the WKY and SHR at the age of 12 or 24 weeks. The upregulated P/A index in the SHR at the age of 4 weeks was reduced to the normal level at the ages of 12 and 24 weeks (**Figures 5A,B**).

DISCUSSION

Renal infusion of capsaicin to induce ERR dose-dependently increased the contralateral RSNA and MAP in normal rats. The ERR can be induced by renal infusion of several chemicals such as capsaicin, angiotensin II, bradykinin, and adenosine (Ye et al., 2020). Capsaicin stimulates afferents and increases the afferent nerve activity at a low concentration, but causes denervation at a high concentration (Fitzgerald, 1983). The concentration of capsaicin in the present study was used to stimulate the renal afferents and cause ERR (Qiu et al., 2020; Ye et al., 2020; Zheng et al., 2020), which was much lower than the concentration used for denervation in previous studies (Fitzgerald, 1983; Foss et al., 2015). The capsaicin-induced ERR existed in the SHR at the ages of four, 12, and 24 weeks, indicating that the ERR is involved in the sympathetic activation and hypertension from the early stage to the sustained stage of hypertension in SHR. It is noted that the ERR was enhanced in the SHR aged at 4 weeks compared with the WKY, indicating that the enhanced ERR is crucial for the sympathetic activation and the occurrence and development of hypertension in the early stage. The findings suggest the importance of early intervention of the enhanced ERR in retarding and attenuating sympathetic activation and hypertension. On the other hand, vascular remodeling contributes to the development and complications of hypertension (Schiffrin, 2012). Intervention of sympathetic activation or a variety of major targets in arteries at the early

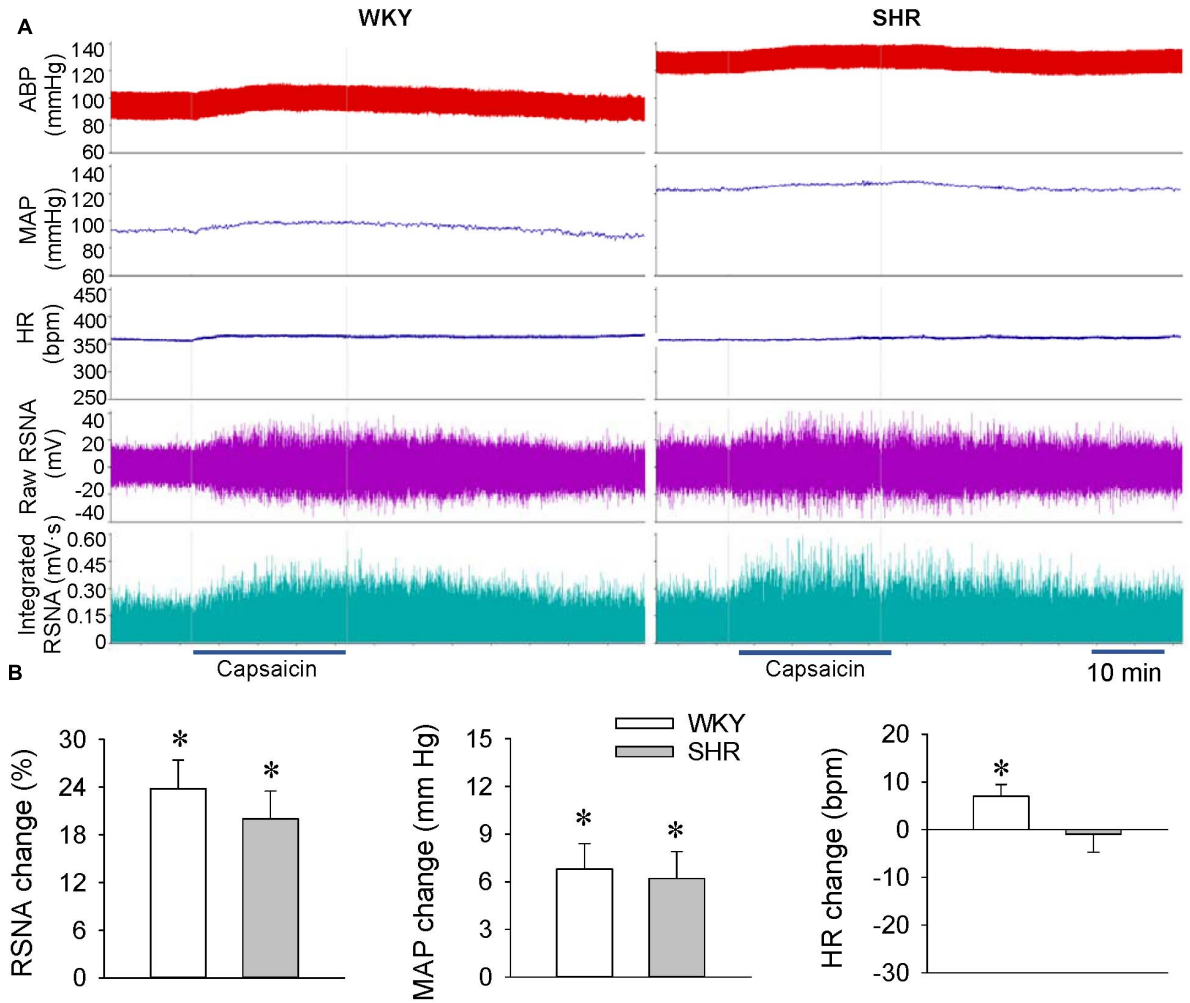

FIGURE 2 | ERR in the WKY and SHR at the age of 12 weeks. The ERR was induced by renal infusion of capsaicin at 1 nmol/min for 20 min. **(A)** representative recordings showing the recordings of the capsaicin-induced ERR. **(B)** bar graph showing the capsaicin-induced ERR. Values are mean ± SE. $^*P < 0.05$ vs the values before renal infusion. No significant difference was found between the WKY and SHR. $n = 6$.

stage of hypertension not only attenuates hypertension, but also vascular remodeling in the young SHR (Fan et al., 2012; Sun et al., 2017; Ren et al., 2020). We speculate that early intervention of the enhanced ERR may have beneficial effects in attenuating vascular remodeling in hypertension. Although the ERR was attenuated in the 24-weeks-old SHR compared with the WKY, the attenuated ERR was still an important factor to increase the sympathetic activity and blood pressure in a sustained hypertension.

An interesting finding in the present study was that the increase in RSNA was smaller but the increase in blood pressure was greater in the 4-week old SHR than those in the WKY. We propose to use the P/A index to reflect the relationship between the RSNA and MAP changes. The increased P/A index means that smaller changes in the renal sympathetic nerve activity (A) cause greater changes in the blood pressure (P). In this study, the P/A index in the young SHR was much greater than that in the young WKY or adult SHR, suggesting that an increased RSNA is more important for hypertension in the young SHR. In the WKY rats, capsaicin-induced the sympathetic activation increasing the HR. However, renal infusion of capsaicin in the four-weeks-old SHR reduced the HR, which may be secondary to the enhanced baroreceptor reflex because the capsaicin-induced HR reduction response appeared a little later than the pressor response. In the SHR at the ages of 12 and 24 weeks, renal infusion of capsaicin had no significant effects on the HR. The possible explanation may be that the role of sympathetic activation in increasing the HR is attenuated by the role of the baroreceptor reflex in reducing the HR, and/or the parasympathetic control of HR is dampened in the adult SHR.

Transient receptor potential vanilloid 1 (TRPV1) is a non-selective cation channel, which is primarily expressed in the sensory Aδ- and C-fibers and primary sensory neurons. The TRPV1 can be activated by capsaicin, endovanilloids, and a variety of chemical and physical stimuli such as lipid metabolites, acidic pH, and noxious heat (Zhong et al., 2019). Capsaicin, a selective TRPV1 agonist, increases the ipsilateral afferent renal

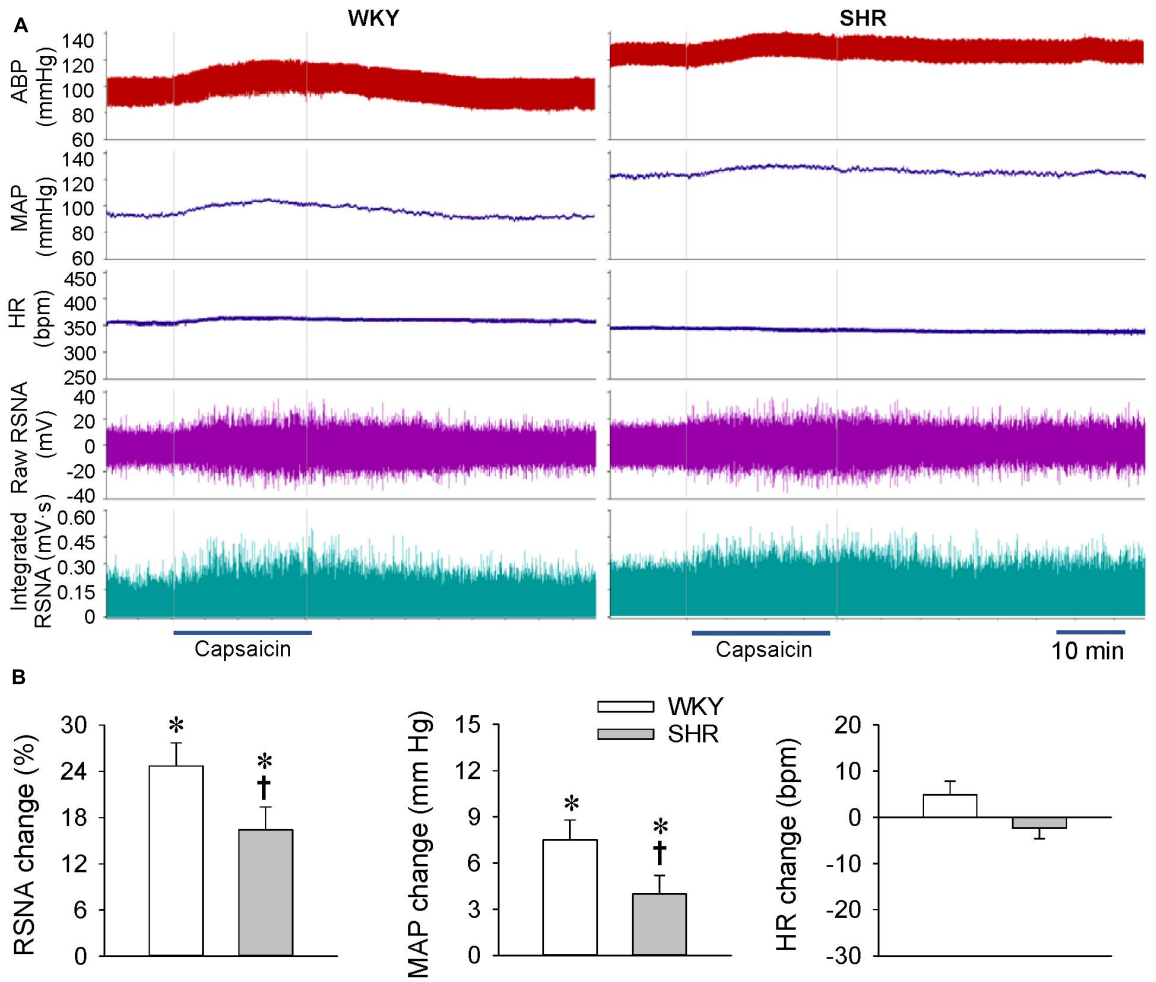

FIGURE 3 | ERR in the WKY and SHR at the age of 24 weeks. The ERR was induced by renal infusion of capsaicin at 1 nmol/min for 20 min. **(A)** representative recordings showing the recordings of the capsaicin-induced ERR. **(B)** bar graph showing the capsaicin-induced ERR. Values are mean ± SE. *$P < 0.05$ vs the values before renal infusion; †$P < 0.05$ vs WKY. $n = 6$.

nerve activity in the Wide-type mice but not in the TRPV1 knockout mice (Zhong et al., 2019). Pretreatment with a TRPV1 competitive antagonist capsazepine abolishes the capsaicin-induced ERR (Qiu et al., 2020). These findings indicate that the renal infusion of capsaicin-induced ERR is mediated by the TRPV1 receptors in the kidney.

TABLE 1 | Body weight and systolic blood pressure measured in a conscious state.

Age (weeks)	BW (g)		SBP (mm Hg)	
	WKY	SHR	WKY	SHR
4	99.7 ± 4.6	102.5 ± 5.6	118.0 ± 3.8	143.5 ± 5.7*
12	249.0 ± 8.2†	244.0 ± 7.9†	121.3 ± 3.9	182.2 ± 8.6*†
24	389.3 ± 7.5†‡	368.7 ± 9.8†‡	122.5 ± 4.9	191.0 ± 6.3*†

*Values are mean ± SE. *P < 0.05 vs WKY. †P < 0.05 vs four weeks. ‡P < 0.05 vs 12 weeks. n = 6. BW, body weight; SBP, systolic blood pressure.*

Renal stimulation induces two opposite sympathetic responses, the excitatory renal reflex (ERR) and inhibitory renal reflex (IRR), which may be related to the site of stimulation, types of stimuli, and pathophysiological state (Kopp, 2015). ERR can be induced by the renal infusion of capsaicin, bradykinin, adenosine, and angiotensin II at the cortico-medullary border of the kidney, which increases the sympathetic activity and blood pressure (Ye et al., 2020). IRR can be induced by increasing the ureteral pressure or retrograde ureteropelvic perfusion with 0.9 M NaCl, which increases the ipsilateral afferent renal nerve activity but decreases the contralateral efferent renal nerve activity in normal WKY rats, but not in SHR (Kopp et al., 1987). Activation of renal afferents by the increased renal pelvic pressure, bradykinin, prostaglandin E2, substance P, and norepinephrine exerts an inhibitory effect on RSNA to minimize sodium retention (Kopp, 2015). The function of sensory fibers containing TRPV1 is impaired in obesity, diabetes, and aging (Zhong et al., 2019). TRPV1 expression and function in renal sensory fibers were impaired in the Dahl salt-sensitive

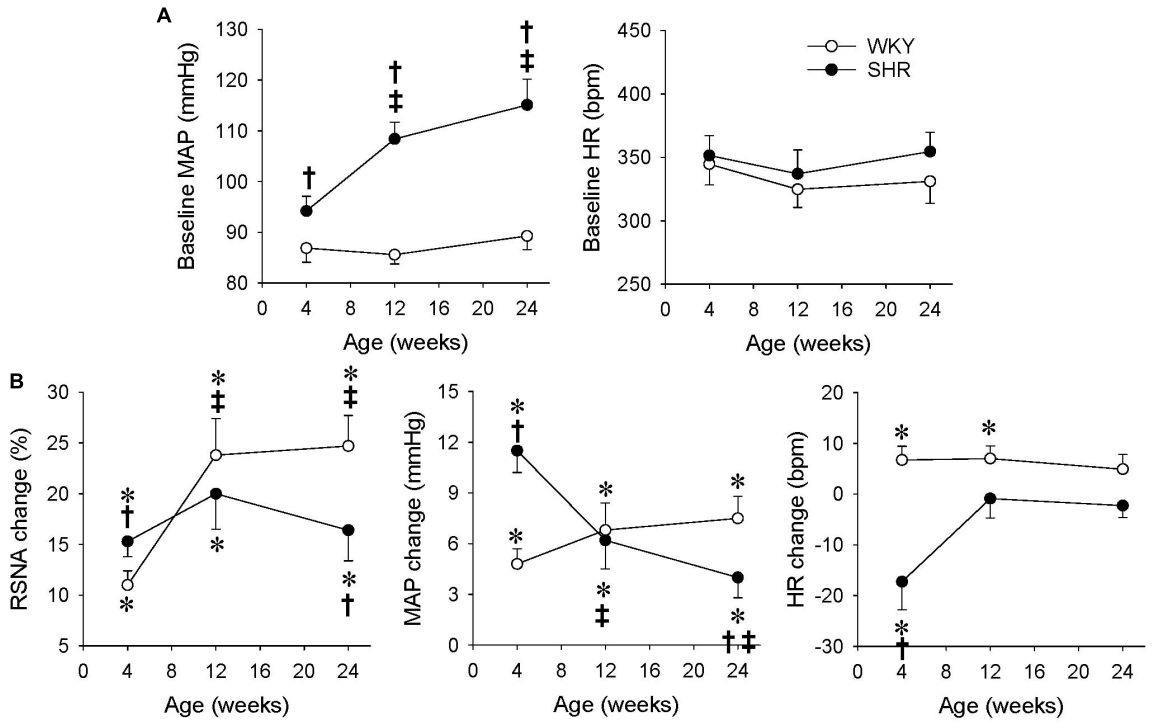

FIGURE 4 | Comparison of ERR in the WKY and SHR at the ages of 4, 12, and 24 weeks. The ERR was induced by renal infusion of capsaicin at 1 nmol/min for 20 min. **(A)** Baseline MAP and HR. †$P < 0.05$ vs WKY. ‡$P < 0.05$ vs 4 weeks. **(B)** capsaicin-induced ERR. Values are mean ± SE. *$P < 0.05$ vs the values before renal infusion; †$P < 0.05$ vs WKY. ‡$P < 0.05$ vs 4 weeks. $n = 6$.

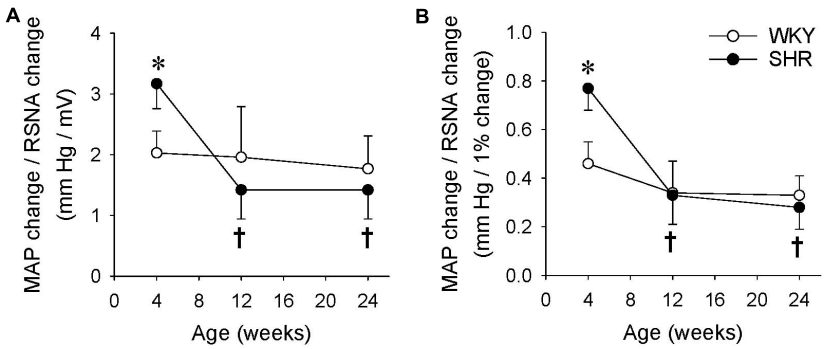

FIGURE 5 | Difference of the RSNA and MAP responses to renal infusion of capsaicin in the WKY and SHR at the ages of 4, 12, and 24 weeks. The ERR was induced by renal infusion of capsaicin at 1 nmol/min for 20 min. **(A)** The ratio of MAP change to RSNA change induced by capsaicin. The values were expressed as mmHg/mV. **(B)** The ratio of MAP change to RSNA change induced by capsaicin. The values were expressed as mm Hg/1% RSNA change. Values are mean ± SE. *$P < 0.05$ vs WKY. †$P < 0.05$ vs 4 weeks. $n = 6$.

hypertensive rats fed with a high-salt diet (Li and Wang, 2008). In the present study, the capsaicin-induced ERR was attenuated in the SHR at the age of 24 weeks compared with the WKY, which might be attributed to the impaired function of sensory fibers containing TRPV1. A limitation is that we did not measure the TRPV1 receptor expression in the kidneys between the WKY and SHR rats, which needs further investigation.

Excessive sympathetic activity plays crucial roles in the pathogeneses of hypertension, chronic heart failure, and chronic kidney disease (Fitzgerald, 1983; Chen et al., 2015; Grassi and Ram, 2016; Cheng et al., 2019). Renal afferent activity may contribute to the sympathetic overactivity in these diseases (Esler, 2014; Frame et al., 2016; Kaur et al., 2017). Catheter-based radiofrequency renal denervation (RFRD) was used as a therapy for hypertension, chronic kidney disease, and chronic heart failure (Veelken and Schmieder, 2014; Frame et al., 2016; Carlstrom, 2017). However, the renal denervation therapy destroys both the afferent and efferent renal nerves. The present

study shows the important roles of renal afferent activity in the sympathetic activation in hypertension, especially in the early stage of hypertension. Selectively renal afferent denervation or efferent denervation to interrupt ERR may have its unique advantage in the treatment of hypertension.

In conclusion, abnormal ERR is involved in the sympathetic activation and development of hypertension. ERR is enhanced in the early stage of hypertension, and is attenuated in the later stage of severe hypertension in SHR. ERR-induced sympathetic activation is associated with a stronger pressor response in the early stage of hypertension.

DATA AVAILABILITY STATEMENT

The original contributions presented in the study are included in the article/supplementary material, further inquiries can be directed to the corresponding author.

ETHICS STATEMENT

The animal study was reviewed and approved by Experimental Animal Care and Use Committee, Nanjing Medical University.

AUTHOR CONTRIBUTIONS

CY, QC, Y-HL, Y-MK, and G-QZ conceptualized and designed the study. CY, FZ, J-XW, and X-LW performed the research. CY, FZ, and G-QZ analyzed the data and contributed to the methods or models. CY and G-QZ wrote the original draft. All authors have read and agreed to the published version of the manuscript.

FUNDING

This study was supported by the National Natural Science Foundation of China (31871148, 32071106, and 81770426).

REFERENCES

Bell, D., Kelso, E. J., Argent, C. C., Lee, G. R., Allen, A. R., and McDermott, B. J. (2004). Temporal characteristics of cardiomyocyte hypertrophy in the spontaneously hypertensive rat. *Cardiovasc. Pathol.* 13, 71–78. doi: 10.1016/s1054-8807(03)00135-2

Bie, P., and Evans, R. G. (2017). Normotension, hypertension and body fluid regulation: brain and kidney. *Acta Physiol.* 219, 288–304. doi: 10.1111/apha.12718

Carlstrom, M. (2017). Therapeutic value of renal denervation in cardiovascular disease? *Acta Physiol.* 220, 11–13. doi: 10.1111/apha.12816

Chen, A. D., Zhang, S. J., Yuan, N., Xu, Y., De, W., Gao, X. Y., et al. (2011). AT_1 receptors in paraventricular nucleus contribute to sympathetic activation and enhanced cardiac sympathetic afferent reflex in renovascular hypertensive rats. *Exp. Physiol.* 96, 94–103. doi: 10.1113/expphysiol.2010.054353

Chen, W. W., Xiong, X. Q., Chen, Q., Li, Y. H., Kang, Y. M., and Zhu, G. Q. (2015). Cardiac sympathetic afferent reflex and its implications for sympathetic activation in chronic heart failure and hypertension. *Acta Physiol.* 213, 778–794. doi: 10.1111/apha.12447

Cheng, Z. J., Wang, R., and Chen, Q. H. (2019). Autonomic rregulation of the cardiovascular system: diseases, treatments, and novel approaches. *Neurosci. Bull.* 35, 1–3. doi: 10.1007/s12264-019-00337-0

Esler, M. (2014). Sympathetic nervous system moves toward center stage in cardiovascular medicine: from Thomas Willis to resistant hypertension. *Hypertension* 63, e25–32. doi: 10.1161/HYPERTENSIONAHA.113.02439

Fan, Z. D., Zhang, L., Shi, Z., Gan, X. B., Gao, X. Y., and Zhu, G. Q. (2012). Artificial microRNA interference targeting AT1a receptors in paraventricular nucleus attenuates hypertension in rats. *Gene Ther.* 19, 810–817. doi: 10.1038/gt.2011.145

Fisher, J. P., and Fadel, P. J. (2010). Therapeutic strategies for targeting excessive central sympathetic activation in human hypertension. *Exp. Physiol.* 95, 572–580. doi: 10.1113/expphysiol.2009.047332

Fitzgerald, M. (1983). Capsaicin and sensory neurones–a review. *Pain* 15, 109–130. doi: 10.1016/0304-3959(83)90012-x

Foss, J. D., Wainford, R. D., Engeland, W. C., Fink, G. D., and Osborn, J. W. (2015). A novel method of selective ablation of afferent renal nerves by periaxonal application of capsaicin. *Am. J. Physiol Regul. Integr. Comp. Physiol.* 308, R112–R122. doi: 10.1152/ajpregu.00427.2014

Frame, A. A., Carmichael, C. Y., and Wainford, R. D. (2016). Renal afferents. *Curr. Hypertens. Rep.* 18:69.

Graham, D., McBride, M. W., Brain, N. J., and Dominiczak, A. F. (2005). Congenic/consomic models of hypertension. *Methods Mol. Med.* 108, 3–15. doi: 10.1385/1-59259-850-1:003

Grassi, G., and Ram, V. S. (2016). Evidence for a critical role of the sympathetic nervous system in hypertension. *J. Am. Soc. Hypertens.* 10, 457–466. doi: 10.1016/j.jash.2016.02.015

Grassi, G., Mark, A., and Esler, M. (2015). The sympathetic nervous system alterations in human hypertension. *Circ. Res.* 116, 976–990. doi: 10.1161/circresaha.116.303604

Iliescu, R., Lohmeier, T. E., Tudorancea, I., Laffin, L., and Bakris, G. L. (2015). Renal denervation for the treatment of resistant hypertension: review and clinical perspective. *Am. J. Physiol. Renal Physiol.* 309, F583–94. doi: 10.1152/ajprenal.00246.2015

Kaur, J., Young, B. E., and Fadel, P. J. (2017). Sympathetic overactivity in chronic kidney disease: consequences and mechanisms. *Int. J. Mol. Sci.* 18:E1682. doi: 10.3390/ijms18081682

Kopp, U. C. (2015). Role of renal sensory nerves in physiological and pathophysiological conditions. *Am. J. Physiol. Regul. Integr. Comp. Physiol.* 308, R79–95. doi: 10.1152/ajpregu.00351.2014

Kopp, U. C., Smith, L. A., and DiBona, G. F. (1987). Impaired renorenal reflexes in spontaneously hypertensive rats. *Hypertension* 9, 69–75. doi: 10.1161/01.hyp.9.1.69

Lambert, E., Straznicky, N., Schlaich, M., Esler, M., Dawood, T., Hotchkin, E., et al. (2007). Differing pattern of sympathoexcitation in normal-weight and obesity-related hypertension. *Hypertension* 50, 862–868. doi: 10.1161/hypertensionaha.107.094649

Lauder, L., Bohm, M., and Mahfoud, F. (2021). The current status of renal denervation for the treatment of arterial hypertension. *Prog. Cardiovasc. Dis.* Online ahead of print. doi: 10.1016/j.pcad.2021.02.005

Li, J., and Wang, D. H. (2008). Role of TRPV1 channels in renal haemodynamics and function in Dahl salt-sensitive hypertensive rats. *Exp. Physiol.* 93, 945–953. doi: 10.1113/expphysiol.2008.042036

Lopes, N. R., Milanez, M. I. O., Martins, B. S., Veiga, A. C., Ferreira, G. R., Gomes, G. N., et al. (2020). Afferent innervation of the ischemic kidney contributes to renal dysfunction in renovascular hypertensive rats. *Pflugers Arch.* 472, 325–334. doi: 10.1007/s00424-019-02346-4

Milanez, M. I. O., Veiga, A. C., Martins, B. S., Pontes, R. B., Bergamaschi, C. T., Campos, R. R., et al. (2020). Renal sensory activity regulates the γ-aminobutyric acidergic inputs to the paraventricular nucleus of the hypothalamus in Goldblatt hypertension. *Front. Physiol.* 11:601237. doi: 10.3389/fphys.2020.601237

Neumann, J., Ligtenberg, G., Klein, I. H., Boer, P., Oey, P. L., Koomans, H. A., et al. (2007). Sympathetic hyperactivity in hypertensive chronic kidney disease patients is reduced during standard treatment. *Hypertension* 49, 506–510. doi: 10.1161/01.hyp.0000256530.39695.a3

Qiu, Y., Zheng, F., Ye, C., Chen, A. D., Wang, J. J., Chen, Q., et al. (2020). Angiotensin type 1 receptors and superoxide anion production in hypothalamic

paraventricular nucleus contribute to capsaicin-induced excitatory renal reflex and sympathetic activation. *Neurosci. Bull.* 36, 463–474. doi: 10.1007/s12264-019-00460-y

Ren, X. S., Tong, Y., Qiu, Y., Ye, C., Wu, N., Xiong, X. Q., et al. (2020). MiR155-5p in adventitial fibroblasts-derived extracellular vesicles inhibits vascular smooth muscle cell proliferation via suppressing angiotensin-converting enzyme expression. *J. Extracell. Vesicles* 9:1698795. doi: 10.1080/20013078.2019.1698795

Rettig, R., Folberth, C., Stauss, H., Kopf, D., Waldherr, R., and Unger, T. (1990). Role of the kidney in primary hypertension: a renal transplantation study in rats. *Am. J. Physiol.* 258, F606–11. doi: 10.1152/ajprenal.1990.258.3.F606

Rettig, R., Stauss, H., Folberth, C., Ganten, D., Waldherr, B., and Unger, T. (1989). Hypertension transmitted by kidneys from stroke-prone spontaneously hypertensive rats. *Am. J. Physiol.* 257, F197–F203. doi: 10.1152/ajprenal.1989.257.2.F197

Schiffrin, E. L. (2012). Vascular remodeling in hypertension: mechanisms and treatment. *Hypertension* 59, 367–374. doi: 10.1161/hypertensionaha.111.187021

Seravalle, G., Mancia, G., and Grassi, G. (2014). Role of the sympathetic nervous system in hypertension and hypertension-related cardiovascular disease. *High Blood Press. Cardiovasc. Prev.* 21, 89–105. doi: 10.1007/s40292-014-0056-1

Sun, H. J., Ren, X. S., Xiong, X. Q., Chen, Y. Z., Zhao, M. X., Wang, J. J., et al. (2017). NLRP3 inflammasome activation contributes to VSMC phenotypic transformation and proliferation in hypertension. *Cell Death. Dis.* 8:e3074. doi: 10.1038/cddis.2017.470

Vecchione, C., Argenziano, L., Fratta, L., Pompeo, F., and Trimarco, B. (2000). Sympathetic nervous system and hypertension in diabetic patients. *Diabetes Nutr. Metab.* 13, 327–331.

Veelken, R., and Schmieder, R. E. (2014). Renal denervation–implications for chronic kidney disease. *Nat. Rev. Nephrol.* 10, 305–313. doi: 10.1038/nrneph.2014.59

Weber, M. A., and Osborn, J. W. (2021). Improved understanding of renal nerve anatomy: an opportunity to enhance denervation treatment of hypertension. *JACC Cardiovasc. Interv.* 14, 316–318. doi: 10.1016/j.jcin.2020.11.003

Xiong, X. Q., Chen, W. W., Han, Y., Zhou, Y. B., Zhang, F., Gao, X. Y., et al. (2012). Enhanced adipose afferent reflex contributes to sympathetic activation in diet-induced obesity hypertension. *Hypertension* 60, 1280–1286. doi: 10.1161/hypertensionaha.112.198002

Xu, B., Zheng, H., Liu, X., and Patel, K. P. (2015). Activation of afferent renal nerves modulates RVLM-projecting PVN neurons. *Am. J. Physiol. Heart Circ. Physiol.* 308, H1103–H1111. doi: 10.1152/ajpheart.00862.2014

Ye, C., Qiu, Y., Zhang, F., Chen, A. D., Zhou, H., Wang, J. J., et al. (2020). Chemical stimulation of renal tissue induces sympathetic activation and pressor response via hypothalamic paraventricular nucleus. *Neurosci. Bull.* 36, 143–152. doi: 10.1007/s12264-019-00417-1

Yemane, H., Busauskas, M., Burris, S. K., and Knuepfer, M. M. (2010). Neurohumoral mechanisms in deoxycorticosterone acetate (DOCA)-salt hypertension in rats. *Exp. Physiol.* 95, 51–55. doi: 10.1113/expphysiol.2008.046334

Zhang, L. L., Ding, L., Zhang, F., Gao, R., Chen, Q., Li, Y. H., et al. (2014). Salusin-beta in rostral ventrolateral medulla increases sympathetic outflow and blood pressure via superoxide anions in hypertensive rats. *J. Hypertens.* 32, 1059–1067. doi: 10.1097/hjh.0000000000000143

Zheng, F., Ye, C., Wan, G. W., Zhou, B., Tong, Y., Lei, J. Z., et al. (2020). Interleukin-1β in hypothalamic paraventricular nucleus mediates excitatory renal reflex. *Pflugers Arch.* 472, 1577–1586. doi: 10.1007/s00424-020-02461-7

Zhong, B., Ma, S., and Wang, D. H. (2019). Ablation of TRPV1 elevates nocturnal blood pressure in Western diet-fed mice. *Curr. Hypertens. Rev.* 15, 144–153. doi: 10.2174/1573402114666181031141840

Conflict of Interest: The authors declare that the research was conducted in the absence of any commercial or financial relationships that could be construed as a potential conflict of interest.

frontiers in Neurology

ORIGINAL RESEARCH
published: 25 June 2021
doi: 10.3389/fneur.2021.632370

Impairment of Cardiac Autonomic Nerve Function in Pre-school Children With Intractable Epilepsy

*Zhao Yang[1], Tung-Yang Cheng[1], Jin Deng[1], Zhiyan Wang[1], Xiaoya Qin[1], Xi Fang[1], Yuan Yuan[1], Hongwei Hao[1], Yuwu Jiang[2,3], Jianxiang Liao[4], Fei Yin[5,6], Yanhui Chen[7,8], Liping Zou[9], Baomin Li[10], Yuxing Gao[11], Xiaomei Shu[12], Shaoping Huang[13], Feng Gao[14], Jianmin Liang[15,16] and Luming Li[1,17,18,19]**

[1] National Engineering Laboratory for Neuromodulation, School of Aerospace Engineering, Tsinghua University, Beijing, China, [2] Division of Pediatric Neurology, Pediatrics Department, Peking University First Hospital, Beijing, China, [3] Department of Pediatric Epilepsy Center, Peking University First Hospital, Beijing, China, [4] Department of Neurology, Shenzhen Children's Hospital, Shenzhen, China, [5] Department of Pediatrics, Xiangya Hospital of Central South University, Changsha, China, [6] Hunan Intellectual and Developmental Disabilities Research Center of Children, Changsha, China, [7] Division of Pediatric Neurology, Pediatrics Department, Fujian Medical University Union Hospital, Fuzhou, China, [8] Department of Epilepsy Center, Fujian Medical University Union Hospital, Fuzhou, China, [9] Department of Pediatric, The People's Liberation Army (PLA) General Hospital, Beijing, China, [10] Pediatics Department, Qilu Hospital of Shandong University, Jinan, China, [11] Division of Pediatrics Neurology, Provincial Hospital Affiliated to Shandong University, Jinan, China, [12] Department of Pediatrics, Affiliated Hospital of Zunyi Medical College, Zunyi, China, [13] Department of Pediatrics, The Second Affiliated Hospital of Xi'an Jiaotong University, Xi'an, China, [14] Department of Neurology, The Children's Hospital, ZheJiang University School of Medicine, Hangzhou, China, [15] Department of Pediatric Neurology, First Bethune Hospital, Jilin University, Changchun, China, [16] Research Center of Neuroscience, First Bethune Hospital, Jilin University, Changchun, China, [17] Precision Medicine and Healthcare Research Center, Tsinghua-Berkeley Shenzhen Institute, Shenzhen, China, [18] Institute of Human-Machine, School of Aerospace Engineering, Tsinghua University, Beijing, China, [19] Center of Epilepsy, Beijing Institute for Brain Disorders, Beijing, China

Objective: Intractable epilepsy and uncontrolled seizures could affect cardiac function and the autonomic nerve system with a negative impact on children's growth. The aim of this study was to investigate the variability and complexity of cardiac autonomic function in pre-school children with pediatric intractable epilepsy (PIE).

Methods: Twenty four-hour Holter electrocardiograms (ECGs) from 93 patients and 46 healthy control subjects aged 3–6 years were analyzed by the methods of traditional heart rate variability (HRV), multiscale entropy (MSE), and Kurths–Wessel symbolization entropy (KWSE). Receiver operating characteristic (ROC) curve analysis was used to estimate the overall discrimination ability. Net reclassification improvement (NRI) and integrated discrimination improvement (IDI) models were also analyzed.

Results: Pre-school children with PIE had significantly lower HRV measurements than healthy controls in time (Mean_RR, SDRR, RMSSD, pNN50) and frequency (VLF, LF, HF, LF/HF, TP) domains. For the MSE analysis, area 1_5 in awake state was lower, and areas 6_15 and 6_20 in sleep state were higher in PIE with a significant statistical difference. KWSE in the PIE group was also inferior to that in healthy controls. In ROC curve analysis, pNN50 had the greatest discriminatory power for PIE. Based on both NRI and IDI models, the combination of MSE indices (wake: area1_5 and sleep: area6_20) and KWSE ($m = 2$, $\tau = 1$, $\alpha = 0.16$) with traditional HRV measures had greater discriminatory power than any of the single HRV measures.

OPEN ACCESS

Edited by:
Lilei Yu,
Renmin Hospital of Wuhan University, China

Reviewed by:
Riccardo Pernice,
University of Palermo, Italy
Jinwei Tian,
The Second Affiliated Hospital of Harbin Medical University, China

****Correspondence:***
Luming Li
lilm@mail.tsinghua.edu.cn

Specialty section:
This article was submitted to Autonomic Neuroscience, a section of the journal Frontiers in Neurology

Received: *23 November 2020*
Accepted: *10 May 2021*
Published: *25 June 2021*

Citation:
Yang Z, Cheng T-Y, Deng J, Wang Z, Qin X, Fang X, Yuan Y, Hao H, Jiang Y, Liao J, Yin F, Chen Y, Zou L, Li B, Gao Y, Shu X, Huang S, Gao F, Liang J and Li L (2021) Impairment of Cardiac Autonomic Nerve Function in Pre-school Children With Intractable Epilepsy. Front. Neurol. 12:632370. doi: 10.3389/fneur.2021.632370

Significance: Impaired HRV and complexity were found in pre-school children with PIE. HRV, MSE, and KWSE could discriminate patients with PIE from subjects with normal cardiac complexity. These findings suggested that the MSE and KWSE methods may be helpful for assessing and understanding heart rate dynamics in younger children with epilepsy.

Keywords: pre-school children, intractable epilepsy, heart rate variability, multiscale entropy, symbolization entropy

INTRODUCTION

Epilepsy is a brain disorder affecting patients of all ages (1) with approximately 10.5 million children in the world suffering from uncontrolled seizures (1, 2), and 20–30% of these children are resistant to antiepileptic drugs (AEDs) and other clinical therapies (3). Sudden unexpected death in epilepsy (SUDEP) has been reported to account for 15 and 50% of all deaths in patients with epilepsy and drug-resistant epilepsy, respectively (4), and the regulation of the autonomic nervous system (ANS) has been highlighted (5). Specifically, alterations of the sympathetic and parasympathetic systems resulting in cardiac arrhythmia, apnea, or cerebral electrical shutdown have been linked to SUDEP (6, 7). Recurrent seizures have higher negative impact on physical growth, sleep, behavior, and mental development (such as depression, anxiety, psychosis, suicide) later in life, bringing heavy burdens to families and society (2, 3, 8–13). Apart from recurrent and unprovoked seizures, epilepsy also contributes to alterations of cardiac autonomic modulation, exhibiting an impairment of sympathetic and/or parasympathetic modulation of cardiac activity (14, 15). Children with intractable epilepsy demonstrate age-related seizure expression (2); thus, more attention should be paid to younger children, especially pre-school children, for their better future development. However, few studies have focused on the cardiac autonomic nerve system (CANS) of pre-school children with intractable epilepsy, and whether epilepsy and seizures impair the function of CANS in such younger age range is still unknown.

Heart rate variability (HRV) is considered one of the accurate biomarkers of the sympathovagal balance of the CANS by a noninvasive method. Generally, a high HRV reflects the sympathovagal balance or well-conditioned adaptability of CANS, and a low HRV relates to a sign of deficient and abnormal function of the ANS (16). HRV measurements have been effective and independent predictors for cardiovascular and neurological diseases (17, 18). Previous studies of autonomic modulation in children with epilepsy published different results, most of which indicate the impairment of CANS regulation considering HRV measurements in the time and frequency domain (14, 15, 19–26). In addition to 24-h long-term analysis, recent studies also focused on ictal or peri-ictal characters with the HRV method to investigate heart activity abnormalities or detect seizures (27–30). The inconsistency in the results, however, was probably owing to different designs of the experiments in sample size, epilepsy type, recording time, and analysis detail. Moreover, HRV index from 24-h Holter electrocardiogram (ECG) recording in pre-school children was still not covered in patients with intractable epilepsy and their healthy control subjects.

Heart rate signals have typical non-linear features because they are the results of the interaction of multiple physiological systems and are influenced by various internal and external factors (18). There are some limitations for traditional non-linear domain HRV measures to assess the complexity of heart rate dynamics (18). For example, classical entropy-based complexity measures quantify only the regularity of time series on a single scale without considering more scales from interaction and consolidative capability of time and space in CANS. Under the postulation that the healthy allow for responding to transient stressors for adaptation to the demands of an ever-changing environment, the multiscale entropy (MSE) method was proposed (31, 32). Diseased and/or aged systems are less adaptable, so the complexity of the human body should be reduced, which could be observed by MSE analysis but could not be observed using traditional HRV entropy. MSE has been extensively used and developed in diagnostics, classification, risk stratification, and prognosis for patients undergoing peritoneal dialysis as well as patients with diseases such as stroke, heart failure, primary aldosteronism, Alzheimer's disease, autism spectrum disorder, and Parkinson disease. Actually, MSE analysis is a kind of direct and fixed coarsening of RR intervals. Besides this, symbolization entropy is also a normal coarsening process to time series with adjustable control parameters for observing the effects of parameters and choosing the stable parameters. Kurths–Wessel symbolization entropy (KWSE) is a relatively easy symbolization method to implement and is closely related to heart rate signals, finally forming a four-symbol static time series transformation method (scope of recommendations for α: [0.03, 0.07] in original papers) (33–35). It has been used in the discrimination of elder, cardiac heart failure, and adult epilepsy from healthy people and seems to be a stable and reliable marker for cardiac complexity (36). However, MSE and KWSE analyses of heart rhythm dynamics in pre-school patients with intractable epilepsy have not yet been studied.

In our previous study, we looked into the difference of HRV and MSE features between adult patients with intractable epilepsy and healthy controls (37). Several indicators were found to have significant results. In this study, we aimed to investigate the variability and complexity of long-term ECG signals using not only HRV and MSE analysis, but also KWSE analysis in pre-school children with intractable epilepsy. Furthermore, the results of MSE and KWSE analysis were compared with traditional complexity measures.

MATERIALS AND METHODS

Participants

Pediatric patients with intractable epilepsy (PIE) as defined by the International League Against Epilepsy (38) were screened strictly based on the inclusion and exclusion criteria in the VNS-PIE clinical trial. A total of 11 centers participated in the VNS-PIE study. These included Peking University First Hospital (Principal Unit), Chinese PLA General Hospital, Shenzhen Children's Hospital, Qilu Hospital of Shandong University, Shandong Province Hospital, the First Hospital of Jilin University, the Second Affiliated Hospital of Xi'an Jiaotong University, Xiangya Hospital Centeral South University, the Children's Hospital Zhejiang University School of Medical, Fujian Medical University Union Hospital, and the Affiliated Hospital of Zunyi Medical College. Pediatric patients had undergone routine pre-surgical examinations, including clinical history, biochemical examination, long term video-electroencephalograph (EEG), imaging examination (magnetic resonance or MR), cognitive development testing (Gesell scale), and 24-h Holter ECG recordings. Inclusion criteria were as follows (1) age 3–6 years, (2) at least six seizures per month, (3) refractory epilepsy, (4) in good health except for epilepsy, (5) family members of patients can understand the method and sign the informed consent, and (6) patients with good compliance and can complete post-operative follow-up. Exclusion criteria were as follows: (1) results of MRI showed epilepsy was caused by intracranial space-occupying lesions; (2) tumor, cardiopulmonary anomaly, heart failure, progressive neurological diseases, asthma, mental disease, peptic ulcer, diabetes, poor health, and other contraindications toward surgery; (3) vagal nerve lesion or damage; (4) could not write the epilepsy diary; (5) participating in another clinical trial; (6) could not complete the operation; (7) could not complete the post-operative follow-up; or (8) could not complete the programming. Pediatric healthy control (PHC) subjects with matched age and gender were recruited into this study based on their clinical history, physical examination results, and 24-h Holter ECG results. This trial (VNS-PIE) was approved by the Clinical Trial Ethics Committee of Peking University First Hospital (Protocol Number: G112L31101; Date: 31/7/2017) and registered on ClinicalTrials.gov protocol system (Clinical Trials Identifier: NCT03062514). The parents of all the pediatric participants provided informed consent in written form before the start of the study. The observed variables of participants included demographic data, seizure type, epilepsy duration, etiology, seizure frequency, number of AEDs used, pre-surgical MRI findings, ictal scalp video-EEG characteristic and ECG recordings.

ECG Recording and Pre-processing

A 12-lead ambulatory ECG monitoring device (MIC-12H-3S; JincoMed, Beijing, China) with a sampling rate of 500 samples/s per channel was used to record a consecutive 24-h ECG in all participants. Wearing this Holter ECG device, participants (patients and healthy controls) were in freely moving conditions and normal daily style to avoid strenuous activities or restricted movement. Their parents were asked to keep a record of the children's main activity and observed seizures every hour, including the time, duration, and type of each activity and seizure. The chest lead V5 with stable and reliable signal quality was selected as the main analysis lead and the standard limb lead II as the secondary analysis lead. If the above two lead signals were missing or their signal-to-noise ratios were low, we selected other lead as an auxiliary analysis lead, which was recorded as a normal and stable waveform. The ECG segments with possible seizures along with the segments within at least 15 min before and from seizure onsets were discarded to avoid their potential effects on further analyses.

Based on Matlab (R2020a, Mathworks, Natick, MA, USA) and Kubios (Kubios Premium 3.4.1, University of Eastern Finland, Kuopio) softwares, the ECG fragments and abnormal QRS waves submerged by noise or motion artifacts were removed. The long-term RR interval time series were formed, whose abnormal R-wave markers were $<10\%$, and the length of each record was not <20 h. Then 4-h periods of RR intervals in the awake and sleep state were selected, respectively, by researchers for each recording according to the heart rate characteristics and activity recordings (39, 40).

Measures From RR Intervals

Traditional HRV measures always include time and frequency domain analysis according to the recommendations of the European Society of Cardiology and the North American Society of Pacing Electrophysiology (18). Mean RR was the mean RR interval values. SDRR was calculated as the standard deviation of RR intervals and taken to represent the overall variability of autonomic modulation. RMSSD was the root mean square of successive differences between successive RR intervals. pNN50 was calculated as the percentage of absolute differences in normal RR intervals >50 ms. RMSSD and pNN50 were regarded as the variability of parasympathetic nerve function on the heart rate. The frequency domain parameters, including high frequency (HF; 0.15–0.4 Hz), low frequency (LF; 0.04–0.15 Hz), and very low frequency (VLF; 0.003–0.04 Hz) power, were calculated by Fast Fourier transformation (FFT) algorithm. The total power (TP) was the sum of HF, LF, and VLF power, and the ratio of LF to HF (LF/HF) was also calculated. LF was taken to reflect the modulations of both the parasympathetic and sympathetic nervous systems, whereas HF primarily demonstrated the function of parasympathetic nerve. It was suggested that the VLF power appeared to be generated intrinsically by the heart itself (41).

Traditional non-linear HRV measures included ApEn (42) and SampEn (43) in this study. Instead of merely estimating the complexity of a time series with a single scale, the MSE method presents the meaningful structural richness of information embedded in multiple spatial and temporal scales (31, 32). In the analysis of MSE, we selected two 4-h periods of RR intervals in the quiet awake state and sleep state to reduce the variability of the circadian rhythm and physical activity. Similar processing can be found in previous research (37, 39, 40). The MSE method comprises two steps: (1) Coarse-graining process: the RR intervals were reconstructed as different time scales. For example, for a given RR interval, in which N is the number of time series,

the multiple coarse-graining time series $y_j^{(\tau)}$ was the average of n non-overlapping consecutive beats with an increasing scale factor τ.The equations were calculated according to Equation (1):

$$y_j^{(\tau)} = \frac{1}{\tau} \sum_{i=(j-1)\tau+1}^{j\tau} RR_i,\ 1 \le j \le N/\tau \quad (1)$$

(2) Quantified by sample entropy with parameters $m = 2$ and $r = 0.15$ * SDRR, where m was the embedding dimension, $\boldsymbol{r}$ was the size of the cell for coarse-graining the phase space, and SDRR was the standard deviation of the 4-h RR interval time series as defined in the paper in which the method was originally proposed (31, 32). The implementation of the parameters corresponded to normalizing the time series so that the sample entropy results depended only on the sequential ordering rather than the variance of the original time series. For each of the 4-h periods, including periods in the awake and sleep states, four different measures were calculated from the MSE profile: the area of entropy values of scales 1–5 (area 1_5), which quantified the complexity of RR dynamics in a short time scale; 6–15 (area 6_15) and 6–20 (area 6_20), which quantified the complexity of RR dynamics in long time scales; and the linear-fitted slope of scale 1–5 (k1), which characterized the modulation pattern in short scales (37, 39, 40). Such indices were proved to be efficient in our previous study discriminating adult patients with epilepsy and healthy controls (37). To avoid underestimation of entropy due to nonstationary artifacts, especially trends of RR intervals series, a detrending process was used on RR intervals before MSE analysis to adaptively extract the trends and subtract them (44, 45).

Besides the coarse graining on different scales in the MSE method, the symbolization of time series was also a coarse process by transforming the original sequence into a sequence containing only individual values, which showed fast, antinoise, and robust features in practical application. A static time series transformation method of four symbols determined KWSE with three steps (33–35). (1) In symbolization, the RR intervals were transformed to a symbolization series $S_i(RR_i)$ based on Equation (2):

$$S_i(RR_i) = \begin{cases} 0:\ \mu < RR_i \le (1+\alpha)\mu \\ 1:\ (1+\alpha)\mu < RR_i \le \infty \\ 2:\ (1-\alpha)\mu < RR_i \le \mu \\ 3:\ 0 < RR_i \le (1-\alpha)\mu \end{cases},\ 1 \le i \le N \quad (2)$$

where μ was the mean of the RR intervals series and α was the parameter to control the symbolization range. (2) Coding for the symbolization series, C_i was constructed by m points with τ delay based on Equation (3):

$$C_i = \sum_{j=1}^{m} 2^{m+1-j} S_{i+(j-1)\tau},\ 1 \le i \le N - m\tau \quad (3)$$

(3) With the Shannon entropy calculation, H was finally calculated by a classical Shannon entropy of C_i denoting the complexity of RR intervals based on Equation (4):

$$H = -\sum C_i\ C_i \quad (4)$$

Statistical Analysis

Continuous variables were presented as mean ± standard deviation (SD). Comparisons of continuous data between the PIE and control groups were made using the Mann–Whitney U-test. Differences between qualitative or categorical variables were assessed using the chi-square test or Fisher's exact test. To compare the ability of different Holter parameters to differentiate the PIE patients from the healthy control patients, a receiver operating characteristic curve (ROC) was constructed from the sensitivity and specificity with logistic regression models, and the area under the ROC curve (AUC) was used to estimate the overall discrimination ability. C-statistics were used to describe the discrimination of the models before and after adding non-linear parameters (46–48). Net reclassification improvement (NRI) and integrated discrimination improvement (IDI) were used to assess improvement of the discriminating power by using two different logistic regression models with 0.2 and 0.4 as the cutoff points, which are commonly used cutoff values (46, 48). All statistical analyses were performed using SPSS (Version 20, IBM Corp., Armonk, NY, USA) and Matlab (R2020a, Mathworks, Natick, MA, USA). Statistical significance was set at $p < 0.05$.

RESULTS

Demographics and Clinical Factors

A total of 93 patients with PIE and 46 healthy control participants were included in this study, according to the protocols. Among the 93 patients, based on their epileptic diary, 25 were reported to have possible seizures during the 24-h ECG recording, and 21 reported to have focal seizures lasting <60 s.

Demographic data and clinical factors of patients with PIE ($n = 93$, range 3.1–5.6 years old) and healthy controls ($n = 46$, range 3.0 to 5.5 years old) are presented in **Table 1**. Demographic data, including gender, age, and body mass index (BMI), showed no significant differences between patients and controls. However, there were significant statistical differences in each subitem of the Gesell scale, indicating that patients with PIE were undergoing general heavy mental and cognitive degradation. Other clinical factors included epilepsy duration, use of AEDs, seizure frequency, seizure type, and cerebral lesions. Twelve types of therapeutic AEDs were reported to be previously used, among which valproate was the most administered one, taken by 72 subjects. Detailed information of clinical and therapeutic characteristics of patients are also shown in **Table 1**.

ECG Signals Analysis

The measurements of traditional HRV analysis including time and frequency domain from long-term RR intervals were significantly lower in patients with PIE than that in healthy controls, whereas non-linear parameters (ApEn and SampEn) could not differentiate the two populations (**Table 2**). The result imply impairment of the function of CANS in PIE patients compared with healthy controls as expected.

The results of MSE are shown in **Figure 1** and **Table 2**. The profiles of MSE were different based on the wake/sleep state, which might show the influence of circadian rhythm and the state of the brain. In comparison to pediatric healthy controls, we

TABLE 1 | Demographic data and clinical data of the patients.

Characteristics	PIE ($n = 93$)	PHC ($n = 46$)	*P*-value
Male, no. (%)	60 (64.5)	27 (58.7)	0.50
Age (years)	4.5 ± 0.8	4.2 ± 0.8	0.09
Body mass index (kg/m^2)	15.9 ± 2.1	15.6 ± 1.9	0.31
Gesell scale			
Adaptability	25.5 ± 21.1	97.5 ± 7.3	<0.001
Gross motor	30.8 ± 19.4	93.7 ± 9.4	<0.001
Fine motor	27.2 ± 21.9	95.5 ± 7.2	<0.001
Language	24.6 ± 20.1	96.4 ± 9.5	<0.001
Individual and social interaction	26.9 ± 21.4	97.2 ± 9.5	<0.001
Epilepsy duration (months)	39.7 ± 13.4	N.A.	N.A.
No. of previous AEDs	5.4 ± 2.1	N.A.	N.A.
No. of present AEDs	2.9 ± 1.2	N.A.	N.A.
Seizures per month	370.3 ± 488.6	N.A.	N.A.
Seizure type, no. (%)			
Tonic seizure	38 (40.9)	N.A.	N.A.
Atypical absence	10 (10.8)	N.A.	N.A.
Atonic seizure	6 (6.5)	N.A.	N.A.
Myoclonic seizure	17 (18.3)	N.A.	N.A.
Spasm	45 (48.4)	N.A.	N.A.
Others	20 (21.5)	N.A.	N.A.
Cerebral lesions (MRI), no. (%)			
Temporal	2 (2.2)	N.A.	N.A.
Frontal	7 (7.5)	N.A.	N.A.
Parietal	12 (12.9)	N.A.	N.A.
Occipital	11 (11.8)	N.A.	N.A.
Diffusing or multiple lesions	10 (10.8)	N.A.	N.A.
Negative	57 (61.3)	N.A.	N.A.
Previous usage of AEDs, no. (%)			
Valproate	72 (77.4)	N.A.	N.A.
Topiramate	48 (51.6)	N.A.	N.A.
Levetiracetam	39 (41.9)	N.A.	N.A.
Clonazepam	33 (35.5)	N.A.	N.A.
Lamotrigine	24 (25.8)	N.A.	N.A.
Oxcarbazepine	16 (17.2)	N.A.	N.A.
Clobazam	15 (16.1)	N.A.	N.A.
Zonisamide	5 (5.4)	N.A.	N.A.
Vigabatrin	5 (5.4)	N.A.	N.A.
Carbamazepine	3 (3.2)	N.A.	N.A.
Phenobarbital	2 (2.2)	N.A.	N.A.
Rufinamide	1 (1.1)	N.A.	N.A.

Data were presented as mean value ± standard deviation or number (percentage). No. denotes "number." N.A. denotes "not available," and five patients' BMI were not available.

TABLE 2 | Traditional HRV and MSE measurements of PIE and PHC participants.

Measures	PIE ($n = 93$)	PHC ($n = 46$)	*P*-value
Mean_RR(ms)	580.4 ± 52.8	616.4 ± 58.7	0.003
SDRR(ms)	33.6 ± 21.8	45.1 ± 15.9	<0.001
RMSSD(ms)	36.7 ± 25.7	50.6 ± 23.3	<0.001
pNN50(%)	9.0 ± 8.8	19.0 ± 11.4	<0.001
VLF(ms^2)	105.3 ± 169.7	155.7 ± 77.3	<0.001
LF(ms^2)	482.8 ± 512.4	815.0 ± 452.4	<0.001
HF(ms^2)	714.4 ± 865.9	1428.9 ± 1235.3	<0.001
LF/HF(ms^2)	1.1 ± 0.8	0.8 ± 0.3	0.04
TP(ms^2)	1304.4 ± 1406.2	2401.7 ± 1683.5	<0.001
ApEn	1.42 ± 0.07	1.42 ± 0.05	0.58
SampEn	1.55 ± 0.15	1.53 ± 0.10	0.42
MSE			
Wake			
area1_5	4.43 ± 0.97	4.93 ± 1.05	0.02
area6_15	12.88 ± 2.30	13.75 ± 1.95	0.05
area6_20	20.41 ± 3.60	21.62 ± 2.98	0.08
k1	0.05 ± 0.06	0.06 ± 0.06	0.35
Sleep			
area1_5	5.34 ± 0.93	5.39 ± 0.95	0.66
area6_15	11.94 ± 2.01	11.09 ± 1.95	0.02
area6_20	18.48 ± 3.26	16.74 ± 3.09	0.003
k1	−0.05 ± 0.07	−0.07 ± 0.06	0.08

Data were presented as mean value ± standard deviation.

found the MSE of PIE patients in a scale of 3–9 in the wake state to be significantly lower as well as scale 10–20 in the sleep state significantly higher. Also, we found that, in PIE patients, area 1_5 in the wake state was significantly lower and areas 6_15 and 6_20 in the sleep state were significantly higher than the PHC group. No significant differences were found in other measures of MSE.

The significant results show the potential discriminating power of MSE measures between PIE patients and PHC, indicating the impairment in the complexity of CANS in PIE patients. Although, as we can observe from the results, some of the measures of MSE might not work as efficiently as traditional time and frequency domain HRV analysis to distinguish PIE and PHC participants.

The profile of KWSE is presented in **Figure 2**. The larger the m parameter, the higher the amplitude of the total KWSE curve. Also, no matter which of the six combinations of m (2, 3, 4) and τ (1, 2) selected, the entropy values between the two groups were significantly different when $\alpha \geq 0.12$, and especially, the p-value did not exceed 0.001 when α was between 0.14 and 0.61.

From the results above, we can also find that, in quantifying the complexity of the heart rate signals, the MSE and KWSE worked better than the traditional HRV non-linear parameters ApEn and SampEn. This provided evidence of potentially higher discriminating power when traditional HRV and MSE/KWSE are combined during the modeling.

ROC Curve Analysis

In the ROC curve analysis of a single variable, for traditional HRV parameters, pNN50 (AUC = 0.746) had the greatest discriminatory power for patients with PIE and healthy control subjects and complexity measures (**Figure 3**). In quantifying the complexity, the AUC of non-linear HRV parameters ApEn and SampEn were 0.536 and 0.505, respectively. For the MSE results,

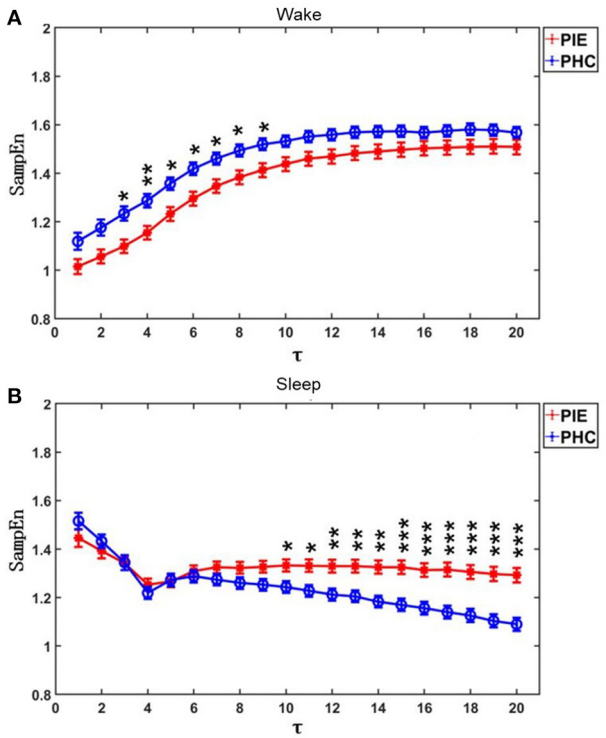

FIGURE 1 | MSE profiles for PIE and PHC. Data are shown as mean value and bars denoted the standard error ($SE = SD/\sqrt{n}$). **(A)** Participants were on wake state; **(B)** Participants were on sleep state. τ was the scales. *P*-value was calculated by Mann-Whitney *U*-test. $^{*}p < 0.05$; $^{**}p < 0.01$; $^{***}p < 0.001$.

in the wake state, the AUC of area1_5, area6_15, area6_20, and k1 were 0.568, 0.550, 0.546, and 0.528, respectively, and in the sleep state, the AUC of area1_5, area6_15, area6_20, and k1 were 0.504, 0.624, 0.648, and 0.603, respectively. The result of KWSE ($m = 2$, $\tau = 1$, $\alpha = 0.16$) was 0.783, which had the maximum distinguishing ability. This again showed that the MSE measures and KWSE overall had more discriminating power than the non-linear HRV when quantifying the complexity of the RR time series.

Then, we looked at the combination of one of the traditional HRV parameters and one of the heart rate complexity measures (MSE or KWSE). In this analysis, according to the profiles of MSE and KWSE exhibited in section ECG Signals Analysis, we selected MSE indices (wake: area1_5 and sleep: area6_20) and KWSE ($m = 2$, $\tau = 1$, $\alpha = 0.16$) to construct the model. As a result, we found remarkable improvement in the discriminating power as shown in **Table 3**. The results show that all of the AUCs of the combined models for each of the traditional HRV measure are over 0.783, larger than that of any single HRV measure alone. Among them, the HRV adding KWSE models always had larger AUC than that adding MSE models with the largest being 0.861 of pNN50+KWSE. In both the NRI and IDI indices, the results confirm that the combination of the traditional HRV and MSE/KWSE had greater discriminatory power than any of the single HRV measures with all the NRI and IDI values positive, and all p-values < 0.05. This result proved that the combination of the traditional HRV and MSE/KWSE was more efficient than single variable models, and the HRV+KWSE models seemed to be the most promising indices for the improvement of discrimination.

DISCUSSION

The main findings of this study were (1) the pre-school children with PIE had worse heart rhythm complexity than age- and gender-matched healthy control children, which was first studied to the best of our knowledge; (2) in all linear and non-linear measures based on heart rate, pNN50, VLF, and KWSE had the greatest discriminatory power to detect the patients undergoing PIE as a single parameter, and these were superior to the traditional non-linear measures; (3) the combination of traditional HRV measures and MSE/KWSE increased the discriminatory power to differentiate PIE from healthy controls, and the HRV+KWSE models had the most promising results. The demographics and clinical factors did not demonstrate significant impact on our results.

Traditional time and frequency domain analysis of HRV is a conventional and useful tool to evaluate the cardiac autonomic system and is commonly used to stratify the risk of patients with cardiovascular and neurological diseases (17, 18). Aging and disease have long been the main factors to be focused on for dynamic characteristics of heart rate (18). According to our results, we can not only find a major degradation in behavior and cognition based on the Gesell scale, but also observe a general impairment of the cardiac autonomic function by analyzing the RR time series. By the method of traditional HRV, the values of the time and frequency domain parameters of the pre-school PIE patients, including SDRR, RMSSD, pNN50, VLF, LF, and HF, are significantly lower than the paired healthy controls, reflecting prominent autonomic dysfunction in both the sympathetic and the vagal tone. This result is consistent with most of the previous studies on CANS functions of children with epilepsy, which indicate the impairment of CANS regulation with multiple decrease in HRV measurements in the time and frequency domain, such as HF, LF, RMSSD, and pNN50 (17, 19, 20, 22). We also noticed that the LF/HF result of the PIE group was significantly higher than the PHC group, indicating the imbalance of the CANS in patients. Several studies as well found the imbalance of sympathetic vagal with LF increase or LF/HF increase (23, 26, 49). However, some studies found no alterations on HRV measures (14, 24). The difference of these results may be owing to inconsistent sample size, epilepsy type, recording time, and analysis detail and so on. Still, few studies concern pre-school children with PIE even in the healthy state. Our result first offers evidence of the impairment of cardiac autonomic function in epilepsy patients of pre-school age group, which supports the extension of the previous conclusion to a wider age range.

Non-linear features are important to characterize and quantify the dynamic variation of physiological systems including CANS (18). Apart from traditional non-linear domain measures of HRV,

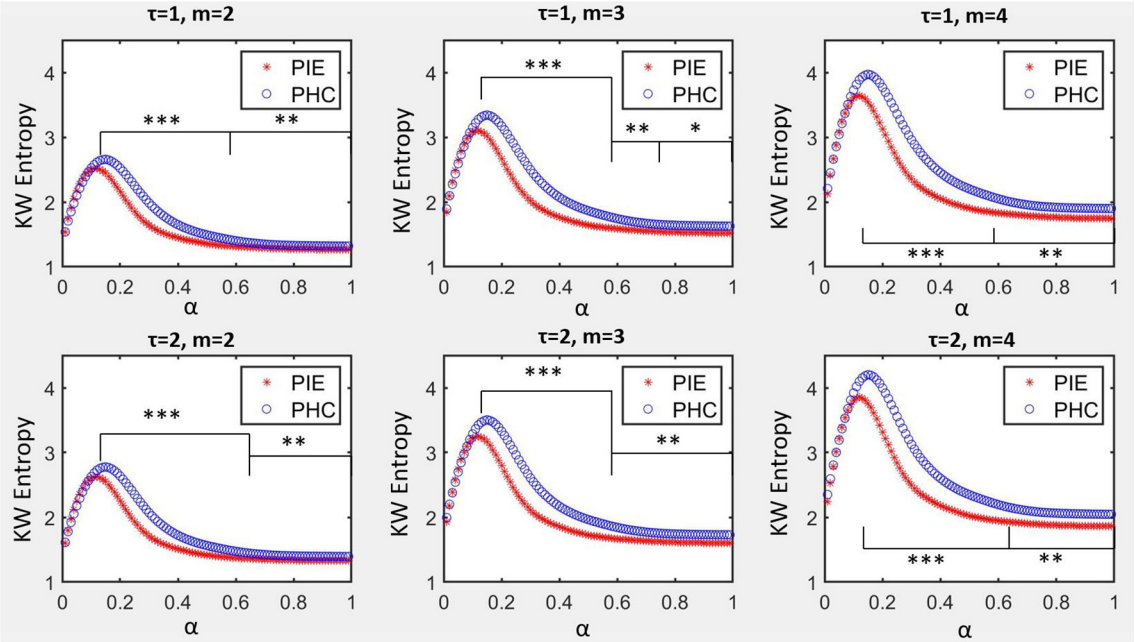

FIGURE 2 | KW entropy profiles for PIE and PHC. Data are shown as mean value. α was the parameter to control the symbolization range for symbolization series S_i, m was the size of word of coded series C_i, τ was the delay of coded series C_i. *p <0.05; **p <0.01; ***p <0.001.

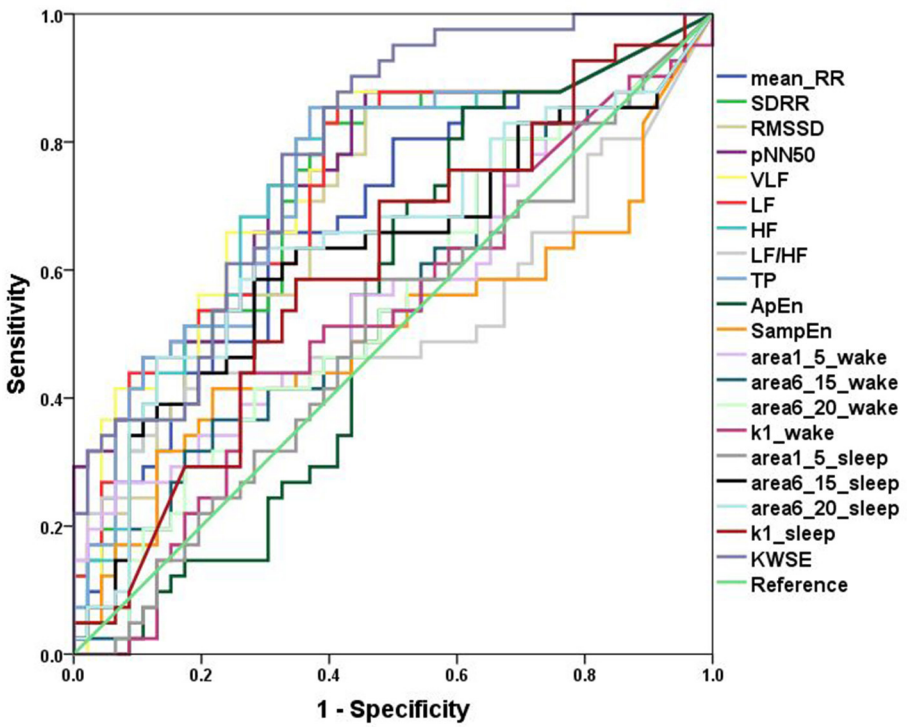

FIGURE 3 | ROC curves. Analysis of the discrimination power of the two groups by ROC curve analysis. TheAUC of Mean_RR, SDRR, RMSSD, pNN50, VLF, LF, HF, LF/HF, TP, ApEn, SampEn, area1_5_wake, area6_15_wake, area6_20_wake, k1_wake, area1_5_sleep, area6_15_ sleep, area6_20_ sleep, k1_ sleep, KWSE ($m = 2$, $\tau = 1$, $\alpha = 0.16$) were 0.680, 0.727, 0.706, 0.746, 0.743, 0.734, 0.732, 0.531, 0.736, 0.536,0.505, 0.568, 0.550, 0.546, 0.528, 0.504, 0.624, 0.648, 0.603, and 0.783, respectively.

TABLE 3 | AUC, NRI, and IDI models of traditional HRV parameters adding heart rate complexity parameters.

Measures		AUC	R square	NRI	NRI:*p*-value	IDI	IDI:*p*-value
SDRR		0.727	0.273				
	Wake:area1_5	0.781	0.418	0.451	0.002	0.142	0.001
	Sleep:area6_20	0.798	0.425	0.452	0.002	0.146	0.001
	KWSE*	0.814	0.428	0.488	0.001	0.152	0.001
RMSSD		0.706	0.226				
	Wake:area1_5	0.802	0.402	0.387	0.006	0.143	0.002
	Sleep:area6_20	0.798	0.394	0.409	0.003	0.107	0.009
	KWSE*	0.828	0.427	0.481	0.001	0.142	0.001
pNN50		0.746	0.234				
	Wake:area1_5	0.829	0.432	0.562	<0.001	0.155	< 0.001
	Sleep:area6_20	0.831	0.432	0.568	<0.001	0.159	< 0.001
	KWSE*	0.861	0.455	0.604	<0.001	0.167	< 0.001
VLF		0.743	0.231				
	Wake:area1_5	0.812	0.421	0.543	<0.001	0.147	< 0.001
	Sleep:area6_20	0.814	0.423	0.567	<0.001	0.139	0.001
	KWSE*	0.836	0.439	0.573	<0.001	0.161	< 0.001
LF		0.734	0.229				
	Wake:area1_5	0.825	0.428	0.341	0.004	0.122	0.004
	Sleep:area6_20	0.832	0.429	0.419	0.002	0.125	0.004
	KWSE*	0.841	0.443	0.498	0.001	0.149	0.001
HF		0.732	0.228				
	Wake:area1_5	0.819	0.417	0.507	<0.001	0.156	0.001
	Sleep:area6_20	0.823	0.424	0.517	<0.001	0.154	0.001
	KWSE*	0.843	0.429	0.533	<0.001	0.161	0.001
TP		0.736	0.231				
	Wake:area1_5	0.828	0.431	0.541	<0.001	0.162	< 0.001
	Sleep:area6_20	0.825	0.428	0.531	<0.001	0.161	< 0.001
	KWSE*	0.839	0.439	0.587	<0.001	0.185	< 0.001

*AUC, areas under the curve; NRI, net reclassification improvement; IDI, integrated discrimination improvement; MSE, multiscale entropy. KWSE, Kurths–Wessel symbol entropy. *$m = 2$, $\tau = 1$, $\alpha = 0.16$.*

the MSE and KWSE methods were also included in our analysis, which consider more scales of temporal and spatial interaction in CANS (31–35). From our data, although traditional non-linear domain HRV ApEn and SampEn failed to reveal the decrement of the complexity in the patients, the MSE and KWSE methods, however, successfully proved this alteration. Several scales and indices of MSE and KWSE of the PIE group showed significant differences from the PHC group. The decrease of complexity under free-running conditions reflected a declined ability of the systems to function in certain dynamical regimes, possibly due to dysregulation or impairment of autonomic control mechanisms. The results demonstrate the dysfunction of CANS in PIE and, in the meantime, proved the efficiency of the multiscale methods compared with the traditional single-scale methods, which matched our previous expectation. However, no previous study has reported the results of MSE and KWSE analysis in pre-school children with PIE. Recent studies of MSE on pediatric patients with epilepsy focused mainly on the EEG signals, which all showed that healthy controls had more complexity than epilepsy patients (50–54). Our result complemented this conclusion with the ECG signals and might provide new insights into cardiac complexity in epilepsy.

In the modeling of the discrimination of the patients and healthy controls, we also found that models including multiscale measures worked better than any single-index model. The largest AUC of the models increased from 0.783 with HRV indices alone to 0.861 with HRV and MSE/KWSE combined. Among them, we found that the HRV+KWSE seemed to work the most efficiently. The results show the effectiveness of the MSE/KWSE as auxiliary methods in the modeling of discrimination. Particularly, the KWSE method seemed to be the most promising method for the improvement of the models for pre-school children with epilepsy. In addition to the results, we also chose the parameters carefully to get the dynamic features on the heart rate. The original recommendation range for α in analysis of KWSE was not suitable for pre-school children in our data, and the interval [0.12, 0.99] had more stable discrimination power. We selected the set of parameters as $m = 2$, $\tau = 1$, $\alpha = 0.16$, to simplify the calculation while preserving the discriminating power. In short, this is the first modeling of the discrimination of PIE patients

and healthy controls of the pre-school age group based on ECG signals, and by the HRV with MSE/KWSE measures, the models exhibited enough efficiency.

There were also some limitations in our study: (1) Although the age range was focused and narrow, we recruited heterogeneous children with various epilepsy etiologies, epilepsy durations, kinds of AEDs, seizure frequency, seizure type, cerebral lesions, mental development, and so on. These factors may have potential impact on variability and complexity for CANS. For example, for studies focusing on specific syndromes, Hattori et al. (26) found that LF significantly improved from 10-min ECG in sleep state for children with West syndrome aged <1 year. Other studies focusing on Dravet syndrome found a total decline in multiple HRV indices on 24-h ECG (22, 55), and Delogu et al. (22) also found no significant results in all HRVs for patients with other syndromes. These results show that complicated factors that affect the results can be significant. (2) We only roughly deleted possible seizure episodes based on ECG data by visual inspection. Because the EEG data is considered as the gold standard of identification of the seizure episodes, there might remain undetected seizure episodes in our pre-processed ECG data. They might impact our results because some studies have published the effects of seizure episodes on heart rate and HRV (27–30). Further studies are needed to explore the impact of seizures on the CANS of pre-school children.

CONCLUSION

PIE in pre-school children is associated with diminished HRV, MSE, and KWSE measures, thereby reflecting the loss of sympathetic vagal balance and function of autonomic system on heart rate. More importantly, when modeling with traditional HRV measurements, the combinations with MSE and KWSE significantly improve the power to differentiate PIE from healthy subjects. These quantification methods of HRV could also be used in younger children and may provide new insights into the cardiac complexity in epilepsy.

DATA AVAILABILITY STATEMENT

The raw data supporting the conclusions of this article will be made available by the authors, without undue reservation.

ETHICS STATEMENT

The studies involving human participants were reviewed and approved by the Clinical Trial Ethics Committee of Peking University First Hospital. Written informed consent to participate in this study was provided by the participants' legal guardian/next of kin.

AUTHOR CONTRIBUTIONS

All authors listed have made a substantial, direct and intellectual contribution to the work, and approved it for publication.

FUNDING

This study was supported by the National Key Research and Development Program of China (2016YFC0105502), National Natural Science Foundation of China (81527901), and Shenzhen International Cooperative Research Project (GJHZ20180930110402104).

ACKNOWLEDGMENTS

The authors gratefully acknowledge all researchers in VNS-PIE trial in disease diagnosing, patient enrollment, examination conduct, data collecting, and professional suggestions in 11 hospitals.

REFERENCES

1. Moshé SL, Perucca E, Ryvlin P, Tomson T. Epilepsy: new advances. *Lancet.* (2015) 385:884–98. doi: 10.1016/S0140-6736(14)60456-6
2. Guerrini R. Epilepsy in children. *Lancet.* (2006) 367:499–524. doi: 10.1016/S0140-6736(06)68182-8
3. Fisher RS, van Emde Boas W, Blume W, Elger C, Genton P, Lee P, et al. Epileptic seizures and epilepsy: definitions proposed by the international league against epilepsy (ILAE) and the international bureau for epilepsy (IBE). *Epilepsia.* (2005) 46:470–2. doi: 10.1111/j.0013-9580.2005.66104.x
4. Tolstykh GP, Cavazos JE. Potential mechanisms of sudden unexpected death in epilepsy. *Epilepsy Behav.* (2013) 26:410–4. doi: 10.1016/j.yebeh.2012.09.017
5. Stollberger C, Finsterer J. Cardiorespiratory findings in sudden unexplained/unexpected death in epilepsy (SUDEP). *Epilepsy Res.* (2004) 59:51–60. doi: 10.1016/j.eplepsyres.2004.03.008
6. Devinsky O, Hesdorffer DC, Thurman DJ, Lhatoo S, Richerson G. Sudden unexpected death in epilepsy: epidemiology, mechanisms, and prevention. *Lancet Neurol.* (2016) 15:1075–88. doi: 10.1016/S1474-4422(16)30158-2
7. Tomson T, Nashef L, Ryvlin P. Sudden unexpected death in epilepsy: current knowledge and future directions. *Lancet Neurol.* (2008) 7:1021–31. doi: 10.1016/S1474-4422(08)70202-3
8. Helmstaedter C, Kurthen M, Lux S, Reuber M, Elger CE. Chronic epilepsy and cognition: a longitudinal study in temporal lobe epilepsy. *Annal Neurol.* (2003) 54:425–32. doi: 10.1002/ana.10692
9. Hirsch E, Schmitz B, Carreno M. Epilepsy, antiepileptic drugs (AEDs) and cognition. *Acta Neurol Scand.* (2003) 108:23–32. doi: 10.1034/j.1600-0404.108.s180.4.x
10. Jones JE, Siddarth P, Gurbani S, Shields WD, Caplan R. Cognition, academic achievement, language, and psychopathology in pediatric chronic epilepsy: short-term outcomes. *Epilepsy Behav.* (2010) 18:211–7. doi: 10.1016/j.yebeh.2010.03.015
11. Hansen BH, Alfstad KÅ, van Roy B, Henning O, Lossius MI. Sleep problems in children and adolescents with epilepsy: associations with psychiatric comorbidity. *Epilepsy Behav.* (2016) 62:14–9. doi: 10.1016/j.yebeh.2016.06.015
12. Austin Joan K, Caplan R. Behavioral and psychiatric comorbidities in pediatric epilepsy: toward an integrative model. *Epilepsia.* (2007) 48:1639–51. doi: 10.1111/j.1528-1167.2007.01154.x
13. Agrawal N, Govender S. Epilepsy and neuropsychiatric comorbidities. *Adv Psychiatric Treatment.* (2018) 17:44–53. doi: 10.1192/apt.bp.108.006510
14. Sevcencu C, Struijk JJ. Autonomic alterations and cardiac changes in epilepsy. *Epilepsia.* (2010). 51:725–37. doi: 10.1111/j.1528-1167.2009.02479.x

15. Lotufo PA, Valiengo L, Benseñor IM, Brunoni AR. A systematic review and meta-analysis of heart rate variability in epilepsy and antiepileptic drugs. *Epilepsia*. (2012) 53:272–82. doi: 10.1111/j.1528-1167.2011.03361.x
16. Evrengül H, Tanriverdi H, Dursunoglu D, Kaftan A, Kuru O, Unlu U, et al. Time and frequency domain analyses of heart rate variability in patients with epilepsy. *Epilepsy Res.* (2005) 63:131–9. doi: 10.1016/j.eplepsyres.2005.02.001
17. Hallioglu O, Okuyaz C, Mert E, Makharoblidze K. Effects of antiepileptic drug therapy on heart rate variability in children with epilepsy. *Epilepsy Res.* (2008) 79:49–54. doi: 10.1016/j.eplepsyres.2007.12.020
18. Malik M, Thomas Bigger J, John Camm A, Kleiger RE, Malliani A, Moss AJ, et al. Heart rate variability standards of measurement, physiological interpretation, and clinical use. *Eur Heart J*. (1996) 17:354–81. doi: 10.1093/oxfordjournals.eurheartj.a014868
19. Tomson T, Ericson M, Ihrman C, Lindblad LE. Heart rate variability in patients with epilepsy. *Epilepsy Res*. (1998) 30:77–83. doi: 10.1016/S0920-1211(97)00094-6
20. Harnod T, Yang C, Hsin Y, Shieh K, Wang P, Kuo TJS. Heart rate variability in children with refractory generalized epilepsy. (2008) 17:297–301. doi: 10.1016/j.seizure.2007.09.002
21. Hirfanoglu T, Serdaroglu A, Cetin I, Kurt G, Capraz I, Ekici F, et al. Effects of vagus nerve stimulation on heart rate variability in children with epilepsy. *Epilepsy Behav*. (2018) 81:33–40. doi: 10.1016/j.yebeh.2018.01.036
22. Delogu AB, Spinelli A, Battaglia D, Dravet C, De Nisco A, Saracino A, et al. Electrical and autonomic cardiac function in patients with dravet syndrome. *Epilepsia*. (2011) 52:55–8. doi: 10.1111/j.1528-1167.2011.03003.x
23. Varon CJPM. Interictal cardiorespiratory variability in temporal lobe and absence epilepsy in childhood. *Physiol Meas*. (2015) 36:845–56. doi: 10.1088/0967-3334/36/4/845
24. Assaf N, Weller B, Deutsh-Castel T, Cohen A, Tirosh EJ. The relationship between heart rate variability and epileptiform activity among children–a controlled study. *J Clin Neurophysiol.* (2008) 25:317–20. doi: 10.1097/WNP.0b013e318182ed2d
25. Yang TF, Wong TT, Chang KP, Kwan SY, Kuo TB. Power spectrum analysis of heart rate variability in children with epilepsy. *Childs Nerv Syst.* (2001) 17:602–6. doi: 10.1007/s003810100505
26. Hattori A, Hayano J, Fujimoto S, Ando N, Mizuno K, Kamei M, et al. Cardiac vagal activation by adrenocorticotropic hormone treatment in infants with west syndrome. *Tohoku J Exp Med.* (2007) 211:133–9. doi: 10.1620/tjem.211.133
27. Arbune AA, Jeppesen J, Conradsen I, Ryvlin P, Beniczky S. Peri-ictal heart rate variability parameters as surrogate markers of seizure severity. *Epilepsia*. (2020) 61:S55–60. doi: 10.1111/epi.16491
28. Giannakakis G, Tsiknakis M, Vorgia P. Focal epileptic seizures anticipation based on patterns of heart rate variability parameters. *Comput Meth Programs Biomed.* (2019) 178:123–32. doi: 10.1016/j.cmpb.2019.05.032
29. Jeppesen J, Fuglsang-Frederiksen A, Johansen P, Christensen J, Wustenhagen S, Tankisi H, et al. Seizure detection based on heart rate variability using a wearable electrocardiography device. *Epilepsia.* (2019) 60:2105–13. doi: 10.1111/epi.16343
30. Pernice R, Faes L, Kotiuchyi I, Stivala S, Busacca A, Popov A, et al. Time, frequency and information domain analysis of short-term heart rate variability before and after focal and generalized seizures in epileptic children. *Physiol Meas.* (2019) 40:074003. doi: 10.1088/1361-6579/ab16a3
31. Costa M, Goldberger AL, Peng CK. Multiscale entropy analysis of complex physiologic time series. *Phys Rev Lett.* (2002) 89:068102. doi: 10.1103/PhysRevLett.89.068102
32. Costa M, Goldberger AL, Peng CKJPRE. Multiscale entropy analysis of biological signals. *Phys Rev E Stat Nonlin Soft Matter Phys*. (2005) 71:021906. doi: 10.1103/PhysRevE.71.021906
33. Kurths J, Voss A, Saparin P, Witt A, Wessel N. Quantitative analysis of heart rate variability. *Chaos*. (1995) 5:88–94. doi: 10.1063/1.166090
34. Wessel N, Ziehmann C, Kurths J, Meyerfeldt U, Voss A. Short-term forecasting of life-threatening cardiac arrhythmias based on symbolic dynamics and finite-time growth rates. *Phys Rev E Stat Phys Plasmas Fluids Relat Interdiscip Topics*. (2000) 61:733–9. doi: 10.1103/PhysRevE.61.733
35. Wessel N, Malberg H, Bauernschmitt R, Kurths J. Nonlinear methods of cardiovascular physics and their clinical applicability. *Int J Bifurcat Chaos.* (2007) 17:3325–71. doi: 10.1142/S0218127407019093
36. Wen-Po Y, Tie-Bing L, Jia-Fei D, Jun W. Multiscale permutation entropy analysis of electroencephalogram. *Acta Phys Sinica Chin Ed.* (2014) 63:7498. doi: 10.7498/aps.63.078704
37. Liu H, Yang Z, Meng F, Guan Y, Ma Y, Liang S, et al. Impairment of heart rhythm complexity in patients with drug-resistant epilepsy: an assessment with multiscale entropy analysis. *Epilepsy Res.* (2017) 138:11–7. doi: 10.1016/j.eplepsyres.2017.10.002
38. Kwan P, Arzimanoglou A, Berg AT, Brodie MJ, Allen Hauser W, Mathern G, et al. Definition of drug resistant epilepsy: consensus proposal by the *ad hoc* task force of the iLAE commission on therapeutic strategies. *Epilepsia.* (2010) 51:1069–77. doi: 10.1111/j.1528-1167.2009.02397.x
39. Lin YH, Wu VC, Lo MT, Wu XM, Hung CS, Wu KD, et al. Reversible heart rhythm complexity impairment in patients with primary aldosteronism. *Sci Rep*. (2015) 5:11249. doi: 10.1038/srep11249
40. Lin Y-H, Lin C, Ho Y-H, Wu V, Lo M-T, Hung K-Y, et al. Heart rhythm complexity impairment in patients undergoing peritoneal dialysis. *Sci Rep*. (2016) 6:28202. doi: 10.1038/srep28202
41. McCraty R, Shaffer F. Heart rate variability: new perspectives on physiological mechanisms, assessment of self-regulatory capacity, and health risk. *Glob Adv Health Med*. (2015) 4:46–61. doi: 10.7453/gahmj.2014.073
42. Pincus SM. Approximate entropy as a measure of system complexity. *Proc Natl Acad Sci USA*. (1991) 88:2297. doi: 10.1073/pnas.88.6.2297
43. Richman J, Moorman J. Physiological time-Series analysis using approximate entropy and sample entropy. *Am J Physiol Heart Circulatory Physiol.* (2000) 278:H2039–49. doi: 10.1152/ajpheart.2000.278.6.H2039
44. Wu Z, Huang NE, Long SR, Peng C-K. On the trend, detrending, and variability of nonlinear and nonstationary time series. (2007) 104:14889–94. doi: 10.1073/pnas.0701020104
45. Lo MT, Novak V, Peng CK, Liu Y, Hu KJPRE. Nonlinear phase interaction between nonstationary signals: a comparison study of methods based on Hilbert-Huang and Fourier transforms. *Phys Rev E Stat Nonlin Soft Matter Phys*. (2009) 79:061924. doi: 10.1103/PhysRevE.79.061924
46. Steyerberg EW, Vickers AJ, Cook NR, Gerds T, Gonen M, Obuchowski N, et al. Assessing the performance of prediction models. *Epidemiology.* (2010) 21:128–38. doi: 10.1097/EDE.0b013e3181c30fb2
47. Pickering JW, Endre ZH. New metrics for assessing diagnostic potential of candidate biomarkers. *Clin J Am Soc Nephrol.* (2012) 7:1355–64. doi: 10.2215/CJN.09590911
48. Pencina MJ, D'Agostino RBJ, Vasan RS. Evaluating the added predictive ability of a new marker: from area under the ROC curve to reclassification and beyond. *Stat Med.* (2008). 27:157–72. doi: 10.1002/sim.2929
49. Ferri R, Curzi-Dascalova L, Arzimanoglou A, Bourgeois M, Beaud C, Nunes ML, et al. Heart rate variability during sleep in children with partial epilepsy. *J Sleep Res.* (2002) 11:153–60. doi: 10.1046/j.1365-2869.2002.00283.x
50. Chu YJ, Chang CF, Shieh JS, Lee WT. The potential application of multiscale entropy analysis of electroencephalography in children with neurological and neuropsychiatric disorders. *Entropy*. (2017) 19:13. doi: 10.3390/e19080428
51. Hussain L, Saeed S, Awan IA, Idris A. Multiscaled complexity analysis of EEG epileptic seizure using entropy-Based techniques. *Arch Neurosci.* (2018) 5:e61161. doi: 10.5812/archneurosci.61161
52. Zavala-Yoe R, Ramirez-Mendoza R, Cordero LM. Novel way to investigate evolution of children refractory epilepsy by complexity metrics in massive information. *Springerplus.* (2015) 4:437. doi: 10.1186/s40064-015-1173-6
53. Zavala-Yoe R, Ramirez-Mendoza RA, Cordero LM. Entropy measures to study and model long term simultaneous evolution of children in doose and lennox-gastaut syndromes. *J Integr Neurosci.* (2016) 15:205–21. doi: 10.1142/S0219635216500138
54. Weng W-C, Jiang GJA, Chang C-F, Lu W-Y, Lin C-Y, Lee W-T, et al. Complexity of multi-channel electroencephalogram signal analysis in childhood absence epilepsy. *PLoS ONE.* (2015) 10:e0134083. doi: 10.1371/journal.pone.0134083
55. Lyu SY, Nam SO, Lee Y-J, Kim G, Kim YA, Kong J, et al. Longitudinal change of cardiac electrical and autonomic function and potential risk factors in children with dravet syndrome. *Epilepsy Res.* (2019) 152:11–7. doi: 10.1016/j.eplepsyres.2019.02.018

Conflict of Interest: HH and LL reported personal fees from Beijing Pins Medical Co., outside the submitted work. The funder was not involved in the study design, collection, analysis, interpretation of data, the writing of this article or the decision to submit it for publication.

The remaining authors declare that the research was conducted in the absence of any commercial or financial relationships that could be construed as a potential conflict of interest.

frontiers in Physiology

ORIGINAL RESEARCH
published: 27 July 2021
doi: 10.3389/fphys.2021.642299

Irritant Inhalation Evokes P Wave Morphological Changes in Spontaneously Hypertensive Rats via Reflex Modulation of the Autonomic Nervous System

*J. Shane Hooper and Thomas E. Taylor-Clark**

Molecular Pharmacology and Physiology, Morsani College of Medicine, University of South Florida, Tampa, FL, United States

Irritant inhalation is associated with increased incidence of atrial fibrillation (AF) and stroke. Irritant inhalation acutely regulates cardiac function via autonomic reflexes. Increases in parasympathetic and sympathetic reflexes may increase atrial susceptibility to ectopic activity and the initiation of arrhythmia such as AF. Both age and hypertension are risk factors for AF. We have shown that irritant-evoked pulmonary–cardiac reflexes are remodeled in spontaneously hypertensive (SH) rats to include a sympathetic component in addition to the parasympathetic reflex observed in normotensive Wistar-Kyoto (WKY) rats. Here, we analyzed P wave morphology in 15-week old WKY and SH rats during inhalation of the transient receptor potential ankyrin 1 agonist allyl isothiocyanate (AITC). P Wave morphology was normal during vehicle inhalation but was variably modulated by AITC. AITC increased RR intervals (RRi), PR intervals, and the P Wave duration. In SH rats only, AITC inhalation increased the occurrence of negative P waves. The incidence of AITC-evoked negative P waves in SH rats was dependent on RRi, increasing during bradycardic and tachycardic cardiac cycles. Inhibition of both parasympathetic (using atropine) and sympathetic (using atenolol) components of the pulmonary–cardiac reflex decreased the incidence of negative P waves. Lastly, the probability of evoking a negative P Wave was increased by the occurrence of preceding negative P waves. We conclude that the remodeled irritant-evoked pulmonary–cardiac reflex in SH rats provides a substrate for altered P Wave morphologies. These are likely ectopic atrial beats that could provide a trigger for AF initiation in structurally remodeled atria.

Keywords: autonomic (vegetative) nervous system, TRPA1, irritant, ECG, P wave, ectopic beat, atrial fibrillation, hypertension

OPEN ACCESS

Edited by:
Vaughan G. Macefield, Baker Heart and Diabetes Institute, Australia

Reviewed by:
Luiz Eduardo Virgilio Silva, University of São Paulo, Brazil
Renata Maria Lataro, Federal University of Santa Catarina, Brazil

***Correspondence:**
Thomas E. Taylor-Clark
ttaylorclark@usf.edu

Specialty section:
This article was submitted to Autonomic Neuroscience, a section of the journal Frontiers in Physiology

Received: *15 December 2020*
Accepted: *06 July 2021*
Published: *27 July 2021*

Citation:
Hooper JS and Taylor-Clark TE (2021) Irritant Inhalation Evokes P Wave Morphological Changes in Spontaneously Hypertensive Rats via Reflex Modulation of the Autonomic Nervous System. Front. Physiol. 12:642299. doi: 10.3389/fphys.2021.642299

INTRODUCTION

Atrial conduction abnormalities may be caused by structural changes in the heart (e.g., hypertrophy, dilation, fibrosis) and by electrophysiological remodeling (e.g., ion channels, connexins) within cardiomyocytes (Nattel et al., 2000). Aberrant atrial conduction, particularly in the form of atrial fibrillation (AF) and atrial flutter, is a common cause of atrial

dysfunction accompanied by debilitating cardiac symptoms and an increased chance of developing arterial blood clots (resulting in stroke and pulmonary embolism) (Hald et al., 2018). There are multiple risk factors for the development of AF, including advanced age, hypertension, congestive heart failure, diabetes, and obesity (Benjamin et al., 1998). Although substantial work has investigated the tendency for episodes of AF to cause electrical or structural remodeling that promote the maintenance of AF ("AF begets AF") (Nattel et al., 2000), less is known about the direct trigger for the initiation of AF in clinical populations (Haïssaguerre et al., 1998; Hnatkova et al., 1998; O'Donnell et al., 2003; Rajawat et al., 2004; Ohkubo et al., 2008). Studies suggest that modulation of atrial conduction by the autonomic nervous system alters AF susceptibility in animal models (Shen and Zipes, 2014). Activation of both parasympathetic cholinergic pathways and sympathetic adrenergic pathways increases AF susceptibility, and simultaneous activation may be additive (Liu and Nattel, 1997; Oliveira et al., 2011; Shen et al., 2011).

Epidemiological studies have routinely shown that inhalation of air pollution, such as particulate matter (PM), is associated with cardiopulmonary morbidity and mortality, particularly in individuals with preexisting cardiovascular disease (CVD) (Pope et al., 2004; Brook et al., 2010). PM inhalation is also associated with increased incidence of stroke (Huang et al., 2019). Furthermore, in a controlled exposure study, PM inhalation increased the incidence of AF in an aged population with structural heart disease (Link et al., 2013). Inhalation of irritants and pollutants, including PM, causes changes in the autonomic control of heart rate and blood pressure, via reflexes initiated by sensory nerves innervating the airways (Taylor-Clark, 2020). Many of these irritants and pollutants activate a subset of nociceptive vagal sensory C-fibers via the gating of the transient receptor potential ankyrin 1 (TRPA1) ion channel (Bautista et al., 2005; Taylor-Clark et al., 2009; Taylor-Clark and Undem, 2010; Deering-Rice et al., 2011, 2019). In healthy animals, activation of airway vagal C-fibers causes a central reflex increase in parasympathetic drive to the heart, resulting in atropine-sensitive reflex bradycardia and hypotension (Coleridge and Coleridge, 1984; Hooper et al., 2016). Similarly, in healthy individuals, inhalation of PM evokes bradycardia (Devlin et al., 2003; Routledge et al., 2006; Peretz et al., 2008). Interestingly, PM is associated with tachycardia and hypertension in a number of clinical cohorts with preexisting CVD, including hypertension and a history of myocardial dysfunction (Peters et al., 2000; Devlin et al., 2003; Gold et al., 2005; Park et al., 2005; Chahine et al., 2007; Chuang et al., 2007). This suggests that PM-evoked modulation of cardiovascular function is remodeled by preexisting CVD. We recently showed evidence of a similar remodeling of irritant-evoked reflexes in spontaneously hypertensive (SH) rats: inhalation of irritants, including allyl isothiocyanate (AITC), the TRPA1 agonist, caused a complex brady-tachycardia accompanied by premature ventricular contractions (PVCs) in SH rats, but only bradycardia with no PVCs in the normotensive Wistar-Kyoto (WKY) rat (Hooper et al., 2019). The AITC-evoked tachycardic episodes and PVCs were blocked by β1 adrenoceptor inhibitor atenolol but not by atropine, indicating chronic hypertension remodeled irritant-evoked pulmonary–cardiac reflexes to include a *de novo* sympathetic component.

Given that (1) AF risk factors include preexisting CVD, (2) AF susceptibility is sensitive to autonomic balance, (3) inhalation of pollutants is associated with AF and stroke in susceptible individuals with preexisting CVD, and (4) preexisting CVD remodels irritant-evoked pulmonary–cardiac reflexes, we hypothesize that inhalation of AITC would cause greater atrial conduction abnormalities in SH rats compared to WKY rats. We have reanalyzed ECG data from our previous publication (Hooper et al., 2019) to study P Wave parameters. Here, we show that AITC inhalation increases the incidence of negative P waves in SH rats compared to WKY rats, and that this is dependent on the reflex activation of both parasympathetic and sympathetic drive to the heart. Negative P waves are likely ectopic atrial beats (Waldo et al., 1975), and ectopic atrial activity is considered a major trigger of paroxysmal AF (Haïssaguerre et al., 1998; O'Donnell et al., 2003; Rajawat et al., 2004; Ohkubo et al., 2008). Thus the remodeled irritant-evoked pulmonary–cardiac reflex in a model of chronic hypertension provides an electrical substrate that may be an additional risk factor in the initiation and maintenance of AF in susceptible populations.

MATERIALS AND METHODS

ECG Acquisition and Agonist Exposure

All animal studies were approved by the University of South Florida Institutional Animal Care and Use Committee (AAALAC #000434). This data is a reanalysis of experimental studies previously described (Hooper et al., 2019). Briefly, 15-week-old male SH and WKY rats, purchased from Charles River, were implanted with a radiotelemetric device [4ET, Data Sciences International (DSI)] through a midline incision in the abdomen under controlled anesthetic (1–5% isoflurane). A trocar was then used to tunnel through the right pectoral muscle layers allowing for the negative ECG lead to be fed rostrally through the trocar and secured by a single polyethylene suture. The positive ECG lead was implanted into the lower left flank using the same procedure giving the lead II ECG position. A total of 7–10 days following surgery, ECGs were recorded from freely moving rats contained in a plexiglass chamber ($4.5 \times 11''$) placed on top of the DSI receiver (RPC-1). The receiver was connected to a computer running Ponemah software via an A/D converter.

Electrocardiogram were recorded continuously for 30 min during sequential exposures to ambient air, nebulized vehicle [4% ethanol in phosphate buffered saline (PBS)] and AITC (4.3 mg/ml) made up in 4% ethanol and PBS (10 min each). Exposures were performed using a Trek S (PARI Respiratory Equipment) nebulizer (4 L/min), which produces 1–5 μm particles. In some cases, rats were pretreated with either the muscarinic inhibitor atropine (1 mg/kg, i.p.) or the β1 adrenoceptor inhibitor atenolol (0.5 mg/kg, i.p.) 1 h prior to the nebulized exposures. The half-life for atropine in the rat is between 45 and 100 min (Harrison et al., 1974). As such we expect little attenuation of atropine's effect after 60 min, consistent with the complete abolishment of AITC-evoked reflex-mediated

bradycardia in Sprague Dawley rats (Hooper et al., 2016). The half-life for atenolol in the rat is 24–35 h (Tabacova and Kimmel, 2002). We expect little decrease in atenolol's effect following 1 h. In total 15 WKY rats (9 control, 6 treated with atropine) and 25 SH rats (12 control, 9 treated with atropine, 4 treated with atenolol) were used in this study. All experiments were performed at the same time of day (0900–1100) to minimize physiological variation due to circadian rhythms.

Data Analysis

Data was recorded at 5000 Hz and the cardiac cycle, including P, QRS, and T waves, were resolved using the Ponemah P3Plus software. In particular the beginning and end of the P Wave (Pstart and Pend) were determined. The RR interval (RRi, in ms), PR interval (PRi, in ms, defined as the interval between the Pstart and R wave), P Wave duration (Pwidth, in ms, defined as the interval between the Pstart and Pend) data were analyzed. The P Wave amplitude/height (P-H, in mV) was calculated as the amplitude of the highest or lowest point during the P Wave from the Iso-electric line at Pstart. The P-H for a biphasic P Wave was calculated as the greater of the positive and negative amplitudes.

As movement can cause interference in the ECG signal leading to software P Wave misidentification, all cycles were individually assessed to ensure proper marking and any cycle with an indiscernible P Wave was excluded from the analysis. Based upon our need for correlating P Wave parameters with heart rate on a beat-to-beat basis, we have chosen to present heart rate in the form of the RRi parameter (Heart rate = (1000/RRi) $\times$ 60). Overall mean $\pm$ SEM ECG parameter data for each condition represents the mean of all measurable events within the first 4 min of exposure for each rat. Only the first 4 min of AITC exposure were analyzed because previous studies had identified some tachyphylaxis of the reflex modulation of the cardiac cycle (Hooper et al., 2016, 2019). The raw RRi and PRi data was previously published (Hooper et al., 2019). The AITC-evoked effect on each ECG parameter was calculated for each rat by subtracting the raw parameter during vehicle inhalation from the raw parameter during AITC inhalation. The probability of evoking a negative P Wave was calculated by dividing the number of cardiac cycles with a negative P Wave by the total number of cardiac cycles. The percentage of tachycardic and bradycardic cardiac cycles in a given exposure was calculated as the percentage of RRi that were <0.875 (tachycardic) and >1.125 (bradycardic) of the average RRi taken from the first 2 min of the vehicle exposure for each animal.

In some groups (control WKY rats, control SH rats, and rats pretreated with atenolol), the mean number of negative P waves in each consecutive "train" of negative P waves was calculated for each animal. A train was defined as a cluster of consecutive cardiac cycles with negative P waves. Thus an individual negative P Wave immediately preceded and followed by positive P waves was allocated a value of 1, and consecutive negative P waves were allocated the value of the sum of the total number of negative P waves occurring before a positive P Wave occurred. As such each train had $\geq$1 negative P waves. An average of this data produced the mean consecutive negative P Wave data for a given challenge of a single animal. To calculate the probability of a negative P Wave occurring based upon the number of preceding consecutive negative P waves, all of the P waves from a given challenge of a single animal were classified into either success or failure for a series of escalating criteria: (1) the occurrence of a negative P Wave occurring after a positive P Wave; then (2) the occurrence of a negative P Wave occurring after a single negative P Wave; then (3) the occurrence of a negative P Wave occurring after two consecutive negative P Wave; etc.). A sum was then taken of all successes (s) and failures (f) occurring during a given challenge for each criterion across all animals in the group. The probability was then calculated using the formula: s/(s + f).

Statistics

Data were compiled and analyzed using GraphPad software. Raw data of RRi, PRi, Pwidth, and P-H were found to have Gaussian distributions (Shapiro–Wilk test, $p > 0.05$), and were compared using ANOVA with Sidak's multiple comparisons. The AITC-evoked effect on RRi, PRi, Pwidth, and P-H were compared between WKY and SH rats using unpaired *T*-tests. Raw data of the % of cardiac cycles that were defined as bradycardic, tachycardic, or associated with a negative P Wave were compared with Kruskal–Wallis ANOVA with Dunn's multiple comparisons. The AITC-evoked effect on the % of cardiac cycles that were associated with a negative P Wave were compared between WKY and SH rats using the unpaired Mann–Whitney test. The Pearson correlation coefficient, *r*, was determined for the correlation between P Wave parameters (PRi, Pwidth, and P-H) and RRi. In all cases, $p < 0.05$ was considered significant.

Chemicals

Allyl isothiocyanate, atropine (free base), and atenolol were purchased from Sigma.

RESULTS

We had previously investigated the effect of inhalation of nebulized vehicle (4% ethanol in PBS) and AITC (4.3 mg/ml) on the cardiac cycle in conscious WKY and SH rats using electrocardiogram (ECG) radiotelemetry (Hooper et al., 2019). Here, we reanalyzed the data to explore in detail the effect of AITC inhalation on P Wave characteristics (**Figures 1–3**), as these can be indicators of atrial susceptibility to clinically relevant arrhythmia. During the inhalation of vehicle, the cardiac cycle and P Wave morphology were relatively stable (**Figures 1**, **2**). While the RRi of SH rats was significantly shorter than WKY rats during vehicle inhalation ($p < 0.05$), there were no significant differences in PRi, Pwidth, and P-H between the strains ($p > 0.05$) (**Figures 3A,C,E,G**). Inhalation of AITC caused appreciable changes in the cardiac cycle and P Wave morphology (**Figures 1**, **2**). In WKY rats, AITC induced a significant increase in RRi compared to vehicle ($p < 0.05$, **Figure 3A**). This AITC-evoked bradycardia was accompanied with an increase in PRi and Pwidth ($p < 0.05$, **Figures 3C,E**), although there was no significant effect on the P-H ($p > 0.05$, **Figure 3G**). In SH rats,

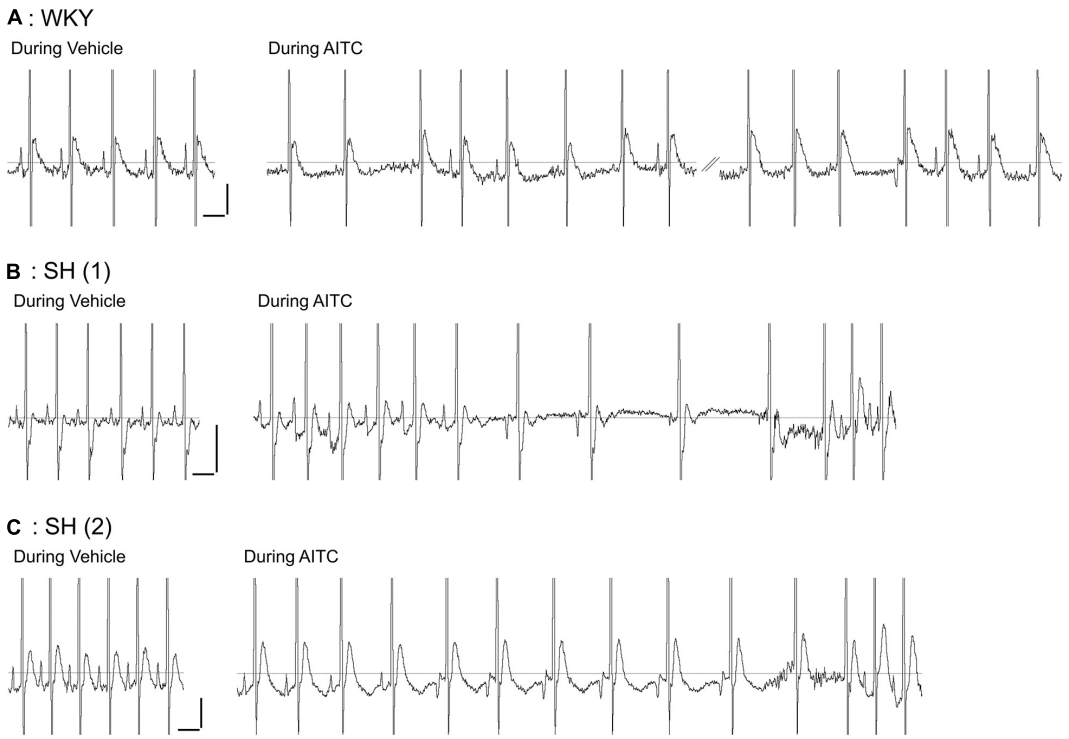

FIGURE 1 | Effect of allyl isothiocyanate (AITC) inhalation on ECG in conscious Wistar-Kyoto (WKY) and spontaneously hypertensive (SH) rats. Representative ECG for a single WKY rat **(A)** and two separate SH rats **(B,C)** during exposure to vehicle (4% ethanol) and AITC (4.3 mg/ml). Note the prominent and reproducible P Wave prior to the QRS complex in all three animals during vehicle inhalation. The trace during AITC inhalation by the WKY rat **(A)** was interrupted by a period of poor ECG recording (not shown). Horizontal scale bars denote 100 ms, vertical scale bars denote 0.1 mV.

AITC significantly increased RRi ($p < 0.05$, **Figure 3A**), although this effect was less than that observed in WKY rats ($p < 0.05$, **Figure 3B**). AITC also increased PRi ($p < 0.05$, **Figure 3C**) in SH rats, but had no effect on Pwidth ($p > 0.05$, **Figure 3E**). In contrast to WKY, AITC caused a significant decrease in P-H in SH rats ($p < 0.05$, **Figure 3G**). The substantial effect of AITC inhalation on the RRi was also reflected in changes in P Wave morphology: converting the simple monophasic positive P waves observed during vehicle inhalation into notched, biphasic, and even inverted (i.e., negative) P waves in some cardiac cycles during AITC inhalation (**Figures 1**, **2**). In particular, we found that AITC caused an increase in the % of cardiac cycles with negative P waves in SH rats ($p < 0.05$) but not in WKY rats ($p > 0.05$) (**Figures 3I,J**).

Given the disordered effect of AITC inhalation on RRi and P Wave morphology, we investigated the correlation of P Wave characteristics with RRi on a beat-to-beat basis. During AITC exposure, many RRi in WKY rats were substantial prolonged (i.e., bradycardic cardiac cycles) compared to vehicle (**Figure 4A**). Increased RRi in WKY rats was negatively correlated with P-H ($p < 0.05$, $r^2 = 0.11$), but few P-H values were actually negative (i.e., inverted). The AITC-evoked effect on RRi in WKY rats positively correlated with increases in Pwidth ($p < 0.05$, $r^2 = 0.27$, **Figure 4B**) and PRi ($p < 0.05$, $r^2 = 0.23$, **Figure 4C**). As seen previously in SH rats (Hooper et al., 2019), the distribution of RRi during AITC inhalation was complex: AITC increased the occurrence of both prolonged RRi (i.e., bradycardic cardiac cycles) and shortened RRi (i.e., tachycardic cardiac cycles) compared to vehicle (**Figure 4D**). Interestingly, AITC evoked negative P waves across the entire spectrum of RRi in the SH rats. Similar to WKY, the AITC-evoked effect on RRi in SH rats was positively correlated with Pwidth ($p < 0.05$, $r^2 = 0.29$, **Figure 4E**) and PRi ($p < 0.05$, $r^2 = 0.16$, **Figure 4F**).

In order to compare the incidence of negative P waves at different RRi we generated histograms of the number of cardiac cycles, the number of negative P waves and the probability of a P Wave being negative in relation to RRi. Furthermore, we added datasets from WKY and SH rats pretreated with atropine (1 mg/kg) and SH rats pretreated with atenolol (0.5 mg/kg), in order to determine the contribution of muscarinic receptors (i.e., parasympathetic activity) and β1 receptors (i.e., sympathetic activity), respectively, to the generation of negative P waves during vehicle and AITC inhalation. In WKY rats, few negative P waves were evoked during vehicle ($n = 134$) and, given the substantial number of cardiac cycles recorded ($n = 8220$) this indicated that vehicle has a very low probability of evoking a negative P Wave at any RRi (**Figure 5A**). During inhalation of AITC by WKY rats, the probability of evoking a negative P Wave appeared to increase for prolonged RRi (i.e., bradycardic cardiac cycles) (**Figure 5A**). In SH rats, few negative P waves were evoked during vehicle and so in general there was a very low probability of evoking a negative P Wave – although this probability

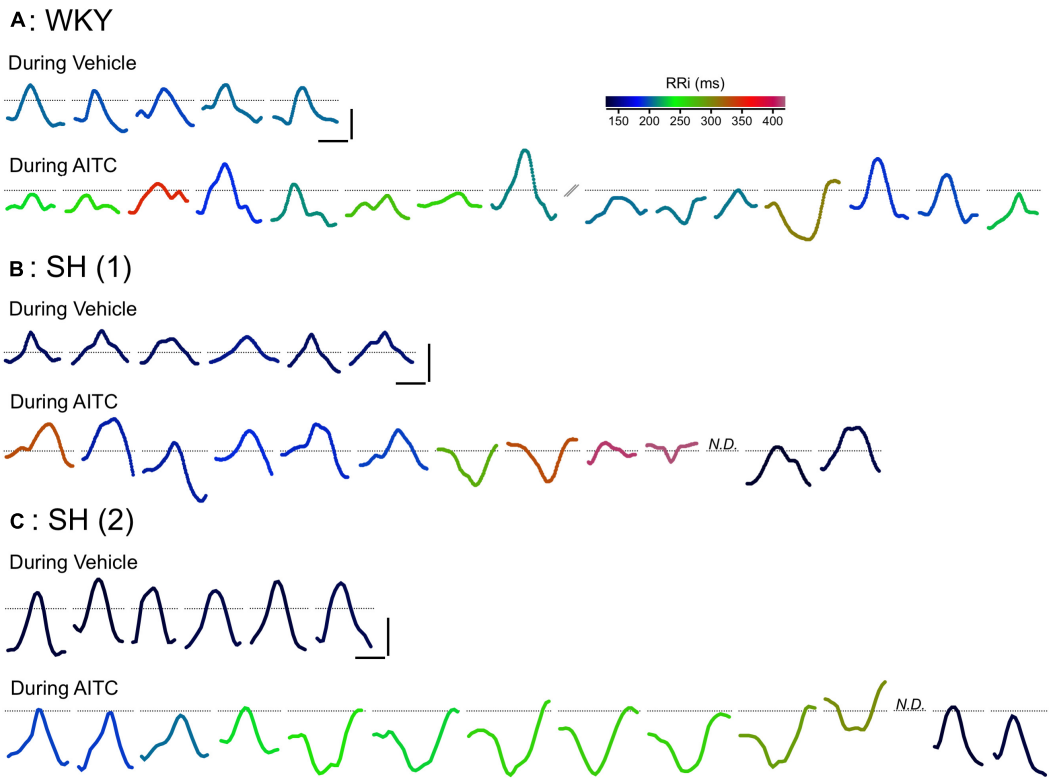

FIGURE 2 | Effect of AITC inhalation on P Wave morphology in conscious WKY and SH rats. Representative consecutive P waves for vehicle (4% ethanol) and AITC (4.3 mg/ml) inhalation shown in **Figure 1**: a single WKY rat **(A)** and two separate SH rats **(B,C)**. The consecutive P waves shown for AITC inhalation by the WKY rat **(A)** was interrupted by a period of poor ECG recording (not shown). In some cases, the P Wave could not be discerned (N.D.). Each P Wave is colored by a rainbow color range denoting the particular RRi of that cardiac cycle. Horizontal scale bars denote 10 ms, vertical scale bars denote 0.05 mV, dotted lines denote the location of 0 mV.

appeared to increase with the few RRi > 220 ms (**Figure 5B**). Interestingly, the probability of evoking a negative P Wave in SH rats exposed to AITC was highly dependent on the individual RRi – the probability was very low at "normal" RRi but increased robustly at RRi<120 and >220 ms. These data suggest that atrial conduction at resting RRi is normal in SH rats, but it is disturbed for RRi outside of the resting range. As shown previously (Hooper et al., 2019), atropine abolished AITC-evoked bradycardia in both WKY and SH, consistent with the established role of vagal parasympathetic signaling in irritant-evoked pulmonary–cardiac reflexes. Consequently, no negative P waves were observed during RRi >220 ms (**Figures 5C,D**). Previously, we had shown that atenolol did not prevent AITC-evoked bradycardia in SH rats (Hooper et al., 2019). Here we found that AITC-evoked RRi > 220 ms in SH rats pretreated with atenolol had a high probability of having a negative P Wave (**Figure 5E**). Given that atropine completely abolished AITC-evoked modulation of RRi in WKY (thus indicating the reflex was entirely mediated by parasympathetic/muscarinic signaling), there was little rationale for assessing the contribution of sympathetic signaling in mediating the AITC-evoked response in the original study (Hooper et al., 2019).

Resting heart rate varies within cohorts of both WKY and SH strains (assessed at the same age) (**Figure 3A**). Thus it is not possible to ascribe a certain absolute value of RRi as a threshold for either bradycardia or tachycardia. We therefore defined thresholds for bradycardic cardiac cycles and tachycardic cardiac cycles for each rat (see methods) and then calculated the probability of evoking a negative P Wave in these 2 categories (**Figure 6**). AITC caused a significant increase in the % of cardiac cycles that were bradycardic in control WKY and control SH rats ($p < 0.05$, **Figure 6A**). AITC-evoked bradycardic cardiac cycles were abolished by atropine in both WKY and SH rats ($p < 0.05$, **Figure 6A**). AITC also caused an increase in the % of cardiac cycles that were bradycardic in SH rats treated with atenolol ($p < 0.05$, **Figure 6A**), which was not significantly different to control SH rats ($p > 0.05$). Importantly, AITC robustly increased the % of bradycardic cardiac cycles that had negative P waves in control SH rats ($p < 0.05$, **Figure 6B**), but not in control WKY rats ($p > 0.05$). In addition, AITC increased the % of bradycardic cardiac cycles that had negative P waves in SH rats treated with atenolol ($p < 0.05$, **Figure 6B**). This AITC-evoked response in SH rats treated with atenolol appeared to be smaller in magnitude compared to control SH rats, but this did not reach significance ($p > 0.05$). The % of bradycardic beats that had negative P waves in the atropine-treated groups could not be calculated because atropine eliminated the bradycardic cardiac cycles.

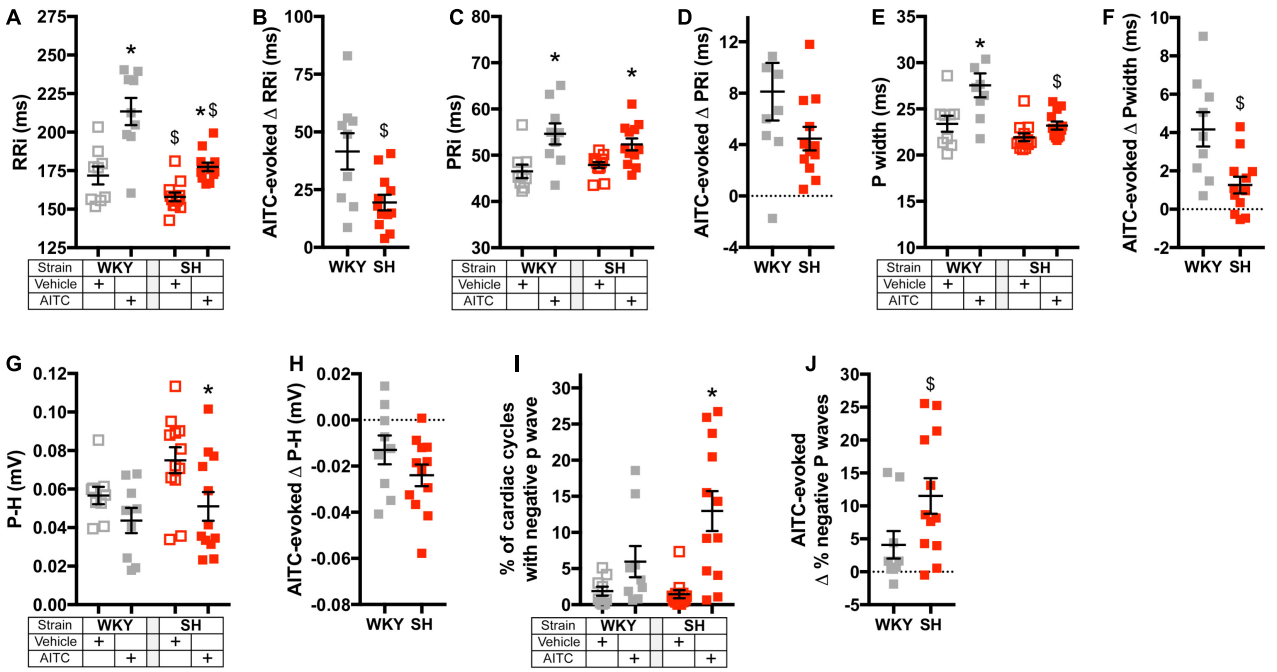

FIGURE 3 | Effect of AITC inhalation on heart rate and P Wave parameters in conscious WKY and SH rats. **(A,C,E,G,I)** Mean ± SEM of RRi **(A)**, PRi **(C)**, Pwidth **(E)**, P-H **(G)**, and the % of cardiac cycles with a negative P Wave **(I)** during inhalation of vehicle (open squares) and AITC (4.3 mg/ml, closed squares) in WKY rats (gray, $n = 9$) and SH rats (red, $n = 12$). The mean ± SEM of RRi **(A)** and PRi **(C)** were previously published (Hooper et al., 2019). **(B,D,F,H,J)** Mean ± SEM of the difference between vehicle- and AITC-evoked RRi **(B)**, PRi **(D)**, Pwidth **(F)**, P-H **(H),** and the % of cardiac cycles with a negative P Wave **(J)** in WKY rats (gray, $n = 9$) and SH rats (red, $n = 12$). In **(A,C,E,G)**, * denotes significant effect of AITC compared to vehicle ($p < 0.05$) and $ denotes significant difference between WKY and SH rats ($p < 0.05$), both assessed by ANOVA with Sidak's multiple comparisons. In **(B,D,F,H)**, $ denotes significant difference between WKY and SH rats ($p < 0.05$, unpaired *T*-test). In **(I)**, * denotes significant effect of AITC compared to vehicle ($p < 0.05$, Kruskal–Wallis ANOVA with Dunn's multiple comparisons). In **(J)**, $ denotes significant difference between WKY and SH rats ($p < 0.05$, unpaired Mann–Whitney test).

Allyl isothiocyanate caused an increase in the % of cardiac cycles that were tachycardic in control SH rats ($p < 0.05$, **Figure 6C**), but not in control WKY rats. AITC-evoked tachycardia in SH rats was abolished by atenolol ($p < 0.05$), but was unaffected by atropine, indicating that it is likely dependent on reflex sympathetic nerve activation. AITC caused an increase in the % of tachycardic cardiac cycles that had negative P waves in control SH rats ($p < 0.05$, **Figure 6D**), but not in control WKY rats. Interestingly, AITC failed to increase the % of tachycardic cardiac cycles that had negative P waves in SH rats treated with atropine ($p > 0.05$, **Figure 6D**), despite the numerous tachycardic cardiac cycles evoked in these animals. The % of tachycardic beats that had negative P waves in the atenolol-treated SH rats could not be calculated because atenolol eliminated the tachycardic cardiac cycles. Overall, the data suggests that SH rats have a greater susceptibility to evoke negative P waves in cardiac cycles with "non-normal" RRi than WKY rats, and that this is sensitive to autonomic blockade of both the parasympathetic and sympathetic control of the heart.

Analysis of individual ECG records showed a tendency of negative P waves to cluster (**Figures 1**, **2**). We calculated the mean number of negative P waves in each consecutive "train" of negative P waves. This was approximately one for all groups during vehicle inhalation – i.e., negative P waves were only found singularly – with the exception of atropine-treated WKY and SH rats which often had no negative P waves at all (**Figure 7A**). In control SH rats, AITC inhalation evoked a significant increase in the mean number of negative P waves in each consecutive "train" ($p < 0.05$, **Figure 7A**). AITC failed to increase the mean number of negative P waves in each consecutive "train" in the other groups ($p > 0.05$). Analysis of the probability that a given P Wave was negative in control SH rats during treatment with AITC showed that the probability rose from 0.08 ± 0.02 immediately following a single positive P Wave to 0.33 ± 0.06 immediately following a single negative P Wave (**Figure 7B**). Thus, the probability of AITC evoking a negative P Wave in control SH rats was significantly increased by the number of preceding negative P waves ($p < 0.05$, **Figure 7B**).

DISCUSSION

Airborne pollutants such as PM, ozone, diisocyanates, and acrolein trigger acute cardiopulmonary responses via the TRPA1-mediated activation of nociceptive sensory nerves innervating the airways (Bautista et al., 2005; Taylor-Clark et al., 2009; Taylor-Clark and Undem, 2010; Deering-Rice et al., 2011, 2019; Taylor-Clark, 2020). Activation of nociceptive airway sensory nerves causes a vagal–vagal central reflex-mediated bradycardia (Coleridge and Coleridge, 1984; Hooper et al., 2016). We

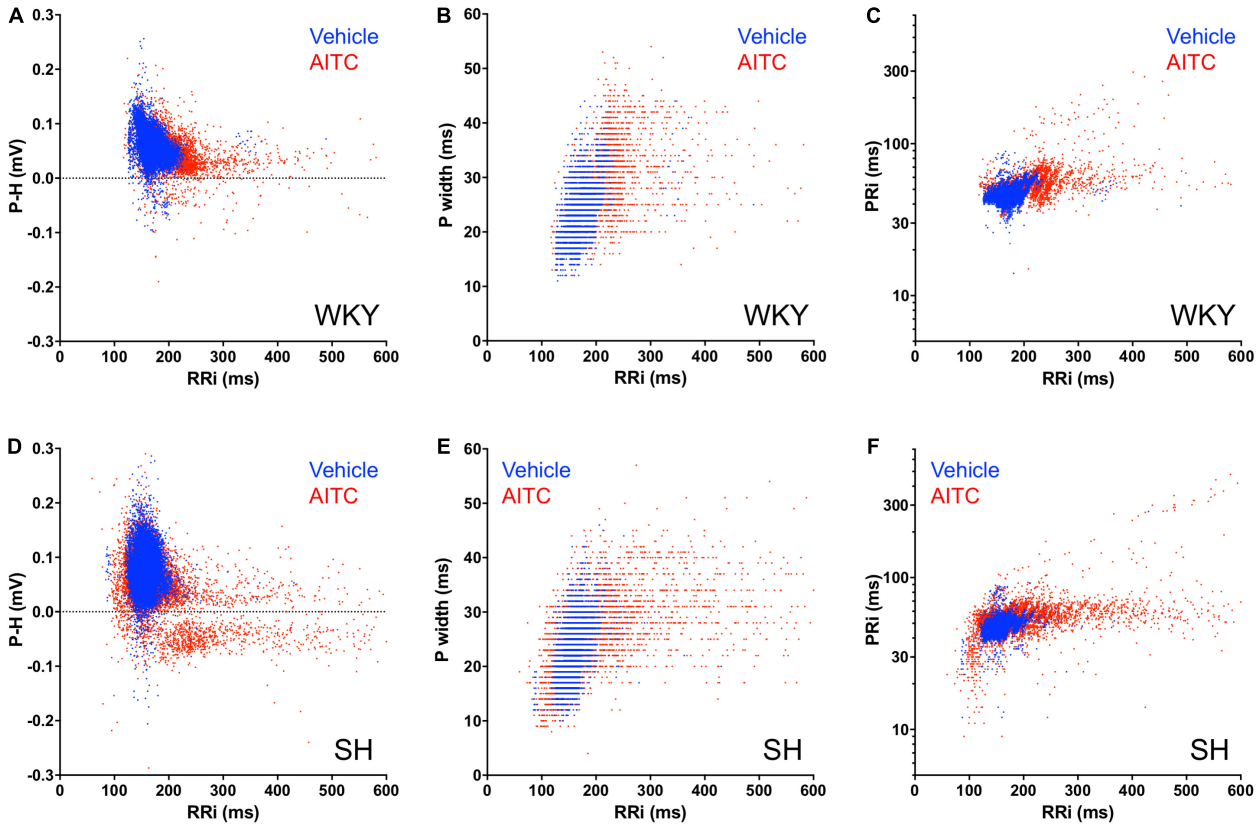

FIGURE 4 | Correlation of RRi with P Wave parameters for individual cardiac cycles during AITC and vehicle inhalation. Each cardiac cycle is represented by either a blue dot (during vehicle inhalation) or a red dot (during AITC inhalation). **(A,D)** Correlation of RRi with P-H. **(B,E)** Correlation of RRi with P width. **(C,F)** Correlation of RRi with PRi. **(A–C)** Events in WKY rats (n = 9 animals, 8220 cycles during vehicle, 4224 cycles during AITC). **(D–F)** Events in SH rats (n = 12 animals, 11,745 cycles during vehicle, 9558 cycles during AITC).

have previously shown that this irritant-evoked pulmonary–cardiac reflex is remodeled in hypertensive rats such that, in addition to the atropine-sensitive reflex bradycardia, there is an additional *de novo* atenolol-sensitive reflex tachycardia with accompanying PVCs (Hooper et al., 2019). Here, we have found that hypertensive rats are also more susceptible to atrial conduction abnormalities evoked by nociceptive pulmonary–cardiac reflexes, and this is dependent on the activation of both parasympathetic and sympathetic signaling.

P Wave polarity and morphology is an indicator of atrial electrical conduction. If initiated at the sinoatrial node, P waves (in lead II position) are positive in direction without major notches (Waldo et al., 1975). Gross deviations from this shape suggests ectopic P Wave initiation, the source of which can be identified in 12-lead ECG studies of the human heart (Waldo et al., 1977; O'Donnell et al., 2003; Rajawat et al., 2004; Ohkubo et al., 2008; Censi et al., 2016). For example, ectopic activity originating near the pulmonary veins (in the left atria) can cause notched or negative P waves in lead II (Waldo et al., 1977; Rajawat et al., 2004; Ohkubo et al., 2008). Ectopic atrial activity is observed in all AF patients, with many unique P waves originating from the pulmonary veins (Haïssaguerre et al., 1998; O'Donnell et al., 2003; Rajawat et al., 2004; Ohkubo et al., 2008). The importance of these ectopic P waves is shown by the observation that ablation of regions surrounding the pulmonary vein can eliminate the ectopic beats and reduce AF (Haïssaguerre et al., 1998). The tendency to evoke ectopic P waves is negatively correlated with the effective refractory period (ERP) of atrial tissue, which is shortest near the pulmonary veins (Oliveira et al., 2011; Fan et al., 2019). There are multiple factors that promote aberrant atrial conduction including atrial hypertrophy and fibrosis (structural changes) and by changes in intrinsic electrical components (e.g., ion channels, connexins) within cardiomyocytes (Nattel et al., 2000). Conditions which promote these factors, such as age, congestive heart failure, hypertension, and diabetes are risk factors for AF (Benjamin et al., 1998). Furthermore, it is likely that structural changes induce electrical remodeling and vice versa. This complexity culminates in the concept that "AF begets AF" (Nattel et al., 2000), which can be seen in experimentally paced animals (Hayashi et al., 2002; Ogawa et al., 2009; Oliveira et al., 2011) and in the progression of clinical AF from paroxysmal to persistent AF in some patients (O'Donnell et al., 2003). AF is associated with a progressive decrease in ERP (Hayashi et al., 2002; Anyukhovsky et al., 2005; Fan et al., 2019), which provides a substrate for re-entry – promoting AF maintenance or further AF initiations.

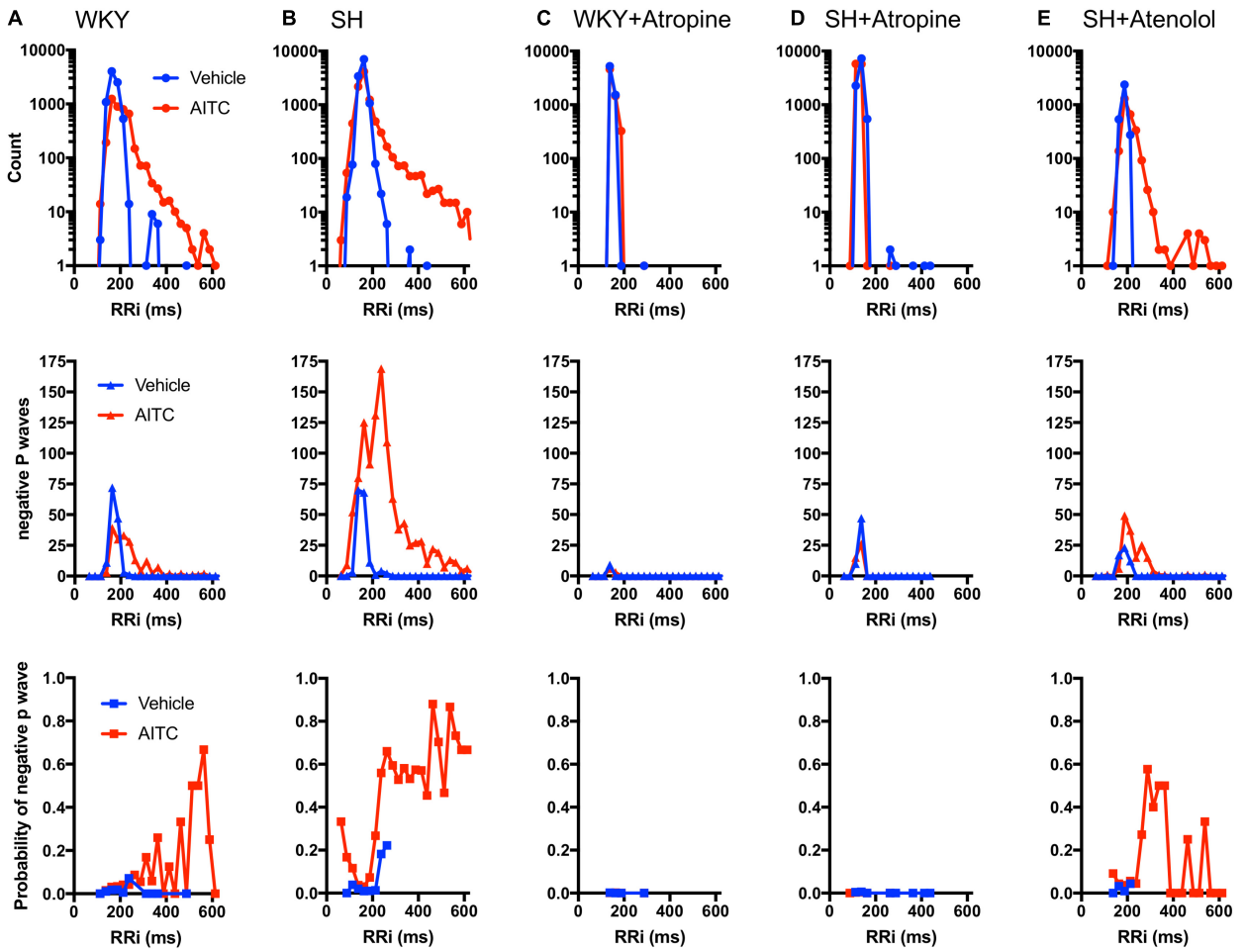

FIGURE 5 | Correlation of RRi with incidence of negative P waves during AITC and vehicle inhalation. Each cardiac cycle from WKY rats (**A**, *n* = 9 animals, 8220 cycles during vehicle, 4224 cycles during AITC), SH rats (**B**, *n* = 12 animals, 11,745 cycles during vehicle, 9558 cycles during AITC), WKY rats pretreated with 1 mg/kg atropine **(C**, 6 animals, 6771 cycles during vehicle, 6363 cycles during AITC), SH rats pretreated with 1 mg/kg atropine (**D**, 9 animals, 10,104 cycles during vehicle, 11,511 cycles during AITC), and SH rats pretreated with 0.5 mg/kg atenolol **(E**, *n* = 4 animals, 3185 cycles during vehicle, 2601 cycles during AITC) was grouped by RRi into 25 ms bins. For each RRi bin during vehicle (blue) and AITC (red) inhalation the number of cardiac cycles recorded (top), the number of cycles with negative P waves (middle) and the probability of a given cycle having a negative P Wave (bottom) is shown.

Identifying the source of ectopic P waves in the less characterized rat heart with a single pair of leads (lead II) is not possible. Nevertheless, our data demonstrates a profound change in P Wave morphology in both WKY and SH rats during inhalation of AITC compared to vehicle: during vehicle inhalation, P waves are positive, and regularly shaped; whereas AITC causes variable changes in some P waves, decreasing their amplitude, increasing the PRi, introducing notches and causing inversions (negative P waves) (see **Figures 1**, **2**). The decreased amplitude and increased PRi is consistent with the slowing of atrial conduction, likely due to the actions of acetylcholine on atrial M2 muscarinic receptors following increases in reflex parasympathetic activity (Hooper et al., 2019). Notched or negative P waves are likely ectopic atrial beats (Waldo et al., 1975), and this is consistent with heterogeneity of conduction throughout the rat atria and pacemaker activity near the rat pulmonary vein (Masani, 1986; Maupoil et al., 2007; Fan et al., 2019; Logantha et al., 2019). AITC inhalation caused an increase in negative P waves in SH rats but not WKY rats, despite the observation that AITC-evoked increases in PRi were similar between the strains and AITC-evoked increases in RRi and Pwidth were greater in the WKY rat (**Figures 3**, **4**). The probability of a P wave being negative in SH rats was highly dependent on RRi – the probability was negligibly low at heart rates consistent with sinus rhythm but increased dramatically for bradycardic and tachycardic cardiac cycles (**Figure 5**).

Spontaneously hypertensive rats have decreased ERP compared to WKY rats, and there is greater heterogeneity of ERP across the atria in SH rats (Lau et al., 2013). Thus SH atria are intrinsically arrhythmogenic. However, our data suggest that in addition to this intrinsic susceptibility, the increased number of negative P waves evoked by AITC in SH rats is dependent on the aberrant remodeled pulmonary–cardiac reflex, which includes both atropine-sensitive and atenolol-sensitive components.

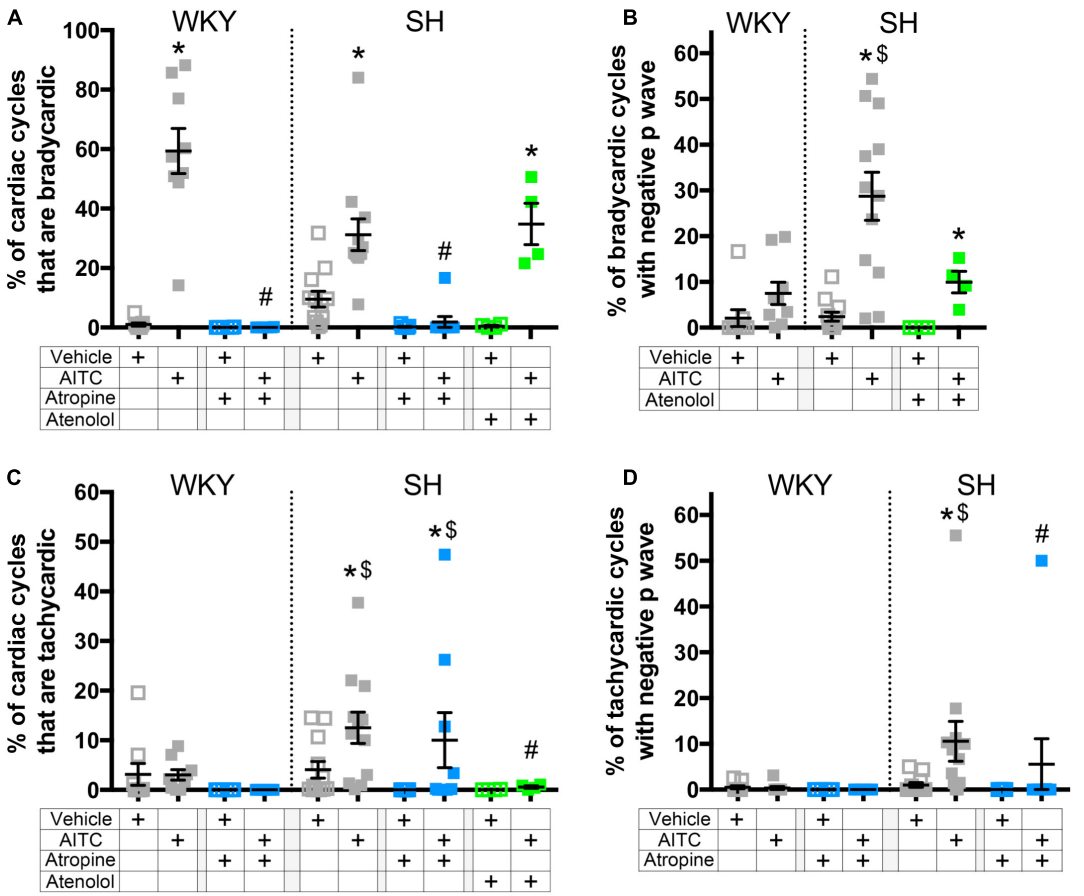

FIGURE 6 | The effect of AITC inhalation on the incidence of negative P waves during bradycardia and tachycardia in conscious WKY and SH rats. **(A)** Mean ± SEM of the % of cardiac cycles which were classified as bradycardic. **(B)** Mean ± SEM of the % of bradycardic cardiac cycles with a negative P Wave. **(C)** Mean ± SEM of the % of cardiac cycles which were classified as tachycardic. **(D)** Mean ± SEM of the % of tachycardic cardiac cycles with a negative P Wave. Data was recorded during vehicle (open squares) and AITC (4.3 mg/ml, closed squares) inhalation in control WKY and SH rats (gray, $n = 9$ and 12, respectively), WKY and SH rats pretreated with 1 mg/kg atropine (blue, $n = 6$ and 9, respectively), and SH rats pretreated with 0.5 mg/kg atenolol (green, $n = 4$). The symbol * denotes significant effect of AITC compared to vehicle ($p < 0.05$), $ denotes significant difference between WKY and SH rats ($p < 0.05$), and # denotes significant effect of autonomic drugs compared to control ($p < 0.05$), each assessed in Kruskal–Wallis ANOVA with Dunn's multiple comparisons.

Atropine had no effect on AITC-evoked tachycardia in the SH rat (**Figure 6C**), but abolished the negative P waves associated with that tachycardia (**Figure 6D**). Similarly, atenolol had no effect on AITC-evoked bradycardia in SH rats (**Figure 6A**), but prevented consecutive negative P waves from forming (**Figure 7A**). There was also a trend for atenolol to decrease the % of negative P waves associated with AITC-evoked bradycardia, but this failed to reach significance (**Figure 6B**). Overall, the data indicate that both parasympathetic and sympathetic reflexes contributed to the initiation of ectopic P waves during irritant inhalation. Despite the current observations that the AITC-evoked changes in RRi and P Wave polarity are abolished by atropine and/or atenolol in WKY and SH rats, we cannot definitely rule out a direct effect of AITC on the atrial tissue. Further inhalation studies with other nociceptor stimulants may provide clarity on this issue.

What can explain this reflex modulation of P Wave polarity? Vagal nerve stimulation causes atropine-sensitive bradycardia and alters the morphology of P waves (Ninomiya, 1966). Outside of the sinoatrial node, muscarinic signaling increases I_{KACh} currents, resulting in decreased action potential duration (Chen et al., 2014). Furthermore, this effect is heterogeneous (Ninomiya, 1966; Liu and Nattel, 1997), thus parasympathetic signaling reduces atrial ERP in a spatially and temporally heterogeneous manner, and consequently increases the susceptibility and duration of experimentally induced AF (Liu and Nattel, 1997; Oliveira et al., 2011). Stimulation of sympathetic signaling to the heart also decreases atrial ERP (Liu and Nattel, 1997), principally by modulating cardiomyocyte Ca^{2+} handling (Chen et al., 2014). However, this effect is not spatially heterogeneous, and thus sympathetic stimulation alone only marginally increases susceptibility to experimentally induced AF (Liu and Nattel, 1997). Nevertheless, there is evidence that coactivation of parasympathetic and sympathetic activity correlates with atrial arrhythmia and AF susceptibility (Shen et al., 2011). Furthermore, stellate ganglion ablation

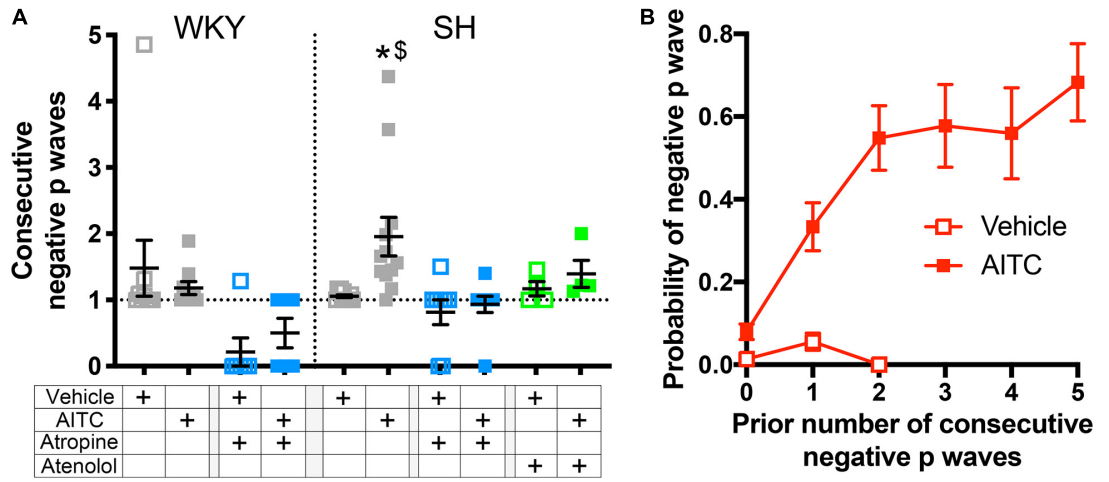

FIGURE 7 | Allyl isothiocyanate inhalation increases the probability of consecutive negative P waves in SH rats. **(A)** Mean ± SEM of the average number of negative P waves in each consecutive "train" of negative P waves during vehicle (open squares) and AITC (4.3 mg/ml, closed squares) inhalation in control WKY and SH rats (gray, $n = 9$ and 12, respectively), WKY and SH rats pretreated with 1 mg/kg atropine (blue, $n = 6$ and 9, respectively), and SH rats pretreated with 0.5 mg/kg atenolol (green, $n = 4$). The symbol * denotes significant effect of AITC compared to vehicle ($p < 0.05$) and $ denotes significant difference between WKY and SH rats ($p < 0.05$), both assessed in Kruskal–Wallis ANOVA with Dunn's multiple comparisons. **(B)** Mean ± SEM the probability of a given cycle having a negative P Wave in control SH rats ($n = 12$) during vehicle (open squares) and AITC (4.3 mg/ml, closed squares) as a function of the prior number of consecutive negative P waves.

reduced experimentally induced AF (Ogawa et al., 2009; Shelton et al., 2018). This suggests that an increase in sympathetic signaling to the heart can also contribute to atrial conduction dysfunction. Here, we have shown that AITC inhalation in the SH rat increases the probability of negative P Wave initiation, and this appears dependent on both parasympathetic and sympathetic signaling. Although the current data is consistent with a role of autonomic reflexes in the modulation of the atrial ERP, further studies are required to directly measure the ERP in the SH heart during AITC-evoked reflex modulation.

Although AITC inhalation induced a significant increase in ectopic P waves in SH rats, we wish to emphasize that we found no evidence of AF. This may be due to the age of the rats (15 weeks) used in this study. Tachypacing-induced atrial tachyarrhythmia were significantly increased in 11 month old SH rats compared to age-mated WKY rats or 3 month old SH rats (Choisy et al., 2007), and 55 week old SH rats have spontaneous premature atrial contractions and atrial tachycardia unlike WKY rats or 14 week old SH rats (Scridon et al., 2012). Aging leads to increased cardiac fibrosis and hypertrophy in the SH rat (Choisy et al., 2007; Lau et al., 2013), which was associated with P Wave abnormalities, ventricular arrhythmia, and heart failure at >12 months (Pfeffer et al., 1976; Dunn et al., 1978). Despite the lack of AF, AITC-evoked negative P waves in SH rats were clustered in consecutive "trains," with the probability of a negative P Wave increasing dramatically with the occurrence of preceding negative P waves. This may have occurred because the electrical conditions conducive to increased ectopic atrial activity (decreased atrial ERP with spatially and temporally heterogeneity) occurred over a period longer than an individual cardiac cycle. Such a hypothesis would be consistent with the importance of sympathetic signaling in these responses which modulates cardiac rhythms over slower cycles than the beat-to-beat modulation of parasympathetic signaling (Thoren et al., 1979; Chen et al., 2014). Nevertheless, we cannot discount the additional possibility that the occurrence of a negative P Wave itself increased the probability of a subsequent negative P Wave. This may reflect early stages of electrical and structural remodeling in the SH (Dunn et al., 1978), and is consistent with reports that, in some clinical populations, ectopic atrial beats, especially originating from the pulmonary veins (negative P Wave in lead II), can initiate AF (Haïssaguerre et al., 1998; O'Donnell et al., 2003; Rajawat et al., 2004; Ohkubo et al., 2008).

In conclusion, we have shown that the remodeled irritant-evoked pulmonary–cardiac reflex (composed of both parasympathetic and sympathetic components) in the SH rat provides an electrical substrate that induces negative P waves. These ectopic P waves could trigger AF initiation in structurally remodeled atria. Inhalation of the selective TRPA1 agonist AITC activates the same neural pathways as air pollution. Air pollution has previously been shown to increase the incidence of AF in an aged population with structural heart disease (57% of whom also had hypertension) (Link et al., 2013). Thus the remodeling of pollution-sensitive pulmonary–cardiac reflexes may be an additional risk factor in the initiation and maintenance of AF in susceptible populations.

DATA AVAILABILITY STATEMENT

The raw data supporting the conclusions of this article will be made available by the authors, without undue reservation.

ETHICS STATEMENT

The animal study was reviewed and approved by University of South Florida Institutional Animal Care and Use Committee (AAALAC #000434).

AUTHOR CONTRIBUTIONS

TT-C developed the hypothesis. JH performed all the experiments and analyzed all the raw data. JH and TT-C completed the analysis and wrote the manuscript. Both authors contributed to the article and approved the submitted version.

FUNDING

This work was funded by the American Heart Association (16GRNT31460004) and the National Heart Lung and Blood Institute (R56HL141330 and R01HL152219).

ACKNOWLEDGMENTS

We wish to gratefully thank Sami Noujaim (University of South Florida) for his advisory and editorial contributions to this manuscript.

REFERENCES

Anyukhovsky, E. P., Sosunov, E. A., Chandra, P., Rosen, T. S., Boyden, P. A., Danilo, P. Jr., et al. (2005). Age-associated changes in electrophysiologic remodeling: a potential contributor to initiation of atrial fibrillation. *Cardiovasc. Res.* 66, 353–363. doi: 10.1016/j.cardiores.2004.10.033

Bautista, D. M., Movahed, P., Hinman, A., Axelsson, H. E., Sterner, O., Hogestatt, E. D., et al. (2005). Pungent products from garlic activate the sensory ion channel TRPA1. *Proc. Natl. Acad. Sci. U.S.A.* 102, 12248–12252. doi: 10.1073/pnas.0505356102

Benjamin, E. J., Wolf, P. A., D'agostino, R. B., Silbershatz, H., Kannel, W. B., and Levy, D. (1998). Impact of atrial fibrillation on the risk of death: the framingham heart study. *Circulation* 98, 946–952. doi: 10.1161/01.cir.98.10.946

Brook, R. D., Rajagopalan, S., Pope, C. A. III, Brook, J. R., Bhatnagar, A., Diez-Roux, A. V., et al. (2010). Particulate matter air pollution and cardiovascular disease: an update to the scientific statement from the American heart association. *Circulation* 121, 2331–2378. doi: 10.1161/cir.0b013e3181dbece1

Censi, F., Corazza, I., Reggiani, E., Calcagnini, G., Mattei, E., Triventi, M., et al. (2016). P-wave variability and atrial fibrillation. *Sci. Rep.* 6:26799.

Chahine, T., Baccarelli, A., Litonjua, A., Wright, R. O., Suh, H., Gold, D. R., et al. (2007). Particulate air pollution, oxidative stress genes, and heart rate variability in an elderly cohort. *Environ. Health Perspect.* 115, 1617–1622. doi: 10.1289/ehp.10318

Chen, P. S., Chen, L. S., Fishbein, M. C., Lin, S. F., and Nattel, S. (2014). Role of the autonomic nervous system in atrial fibrillation: pathophysiology and therapy. *Circ. Res.* 114, 1500–1515. doi: 10.1161/circresaha.114.303772

Choisy, S. C., Arberry, L. A., Hancox, J. C., and James, A. F. (2007). Increased susceptibility to atrial tachyarrhythmia in spontaneously hypertensive rat hearts. *Hypertension* 49, 498–505. doi: 10.1161/01.hyp.0000257123.95372.ab

Chuang, K. J., Chan, C. C., Su, T. C., Lin, L. Y., and Lee, C. T. (2007). Associations between particulate sulfate and organic carbon exposures and heart rate variability in patients with or at risk for cardiovascular diseases. *J. Occup. Environ. Med.* 49, 610–617. doi: 10.1097/jom.0b013e318058205b

Coleridge, J. C., and Coleridge, H. M. (1984). Afferent vagal C fibre innervation of the lungs and airways and its functional significance. *Rev. Physiol. Biochem. Pharmacol.* 99, 1–110. doi: 10.1007/bfb0027715

Deering-Rice, C. E., Memon, T., Lu, Z., Romero, E. G., Cox, J., Taylor-Clark, T., et al. (2019). Differential activation of TRPA1 by diesel exhaust particles: relationships between chemical composition, potency, and lung toxicity. *Chem. Res. Toxicol.* 32, 1040–1050. doi: 10.1021/acs.chemrestox.8b00375

Deering-Rice, C. E., Romero, E. G., Shapiro, D., Hughen, R. W., Light, A. R., Yost, G. S., et al. (2011). Electrophilic components of diesel exhaust particles (DEP) activate transient receptor potential ankyrin-1 (TRPA1): a probable mechanism of acute pulmonary toxicity for DEP. *Chem. Res. Toxicol.* 24, 950–959. doi: 10.1021/tx200123z

Devlin, R. B., Ghio, A. J., Kehrl, H., Sanders, G., and Cascio, W. (2003). Elderly humans exposed to concentrated air pollution particles have decreased heart rate variability. *Eur. Respir. J. Suppl.* 40, 76s–80s.

Dunn, F. G., Pfeffer, M. A., and Frohlich, E. D. (1978). ECG alterations with progressive left ventricular hypertrophy in spontaneous hypertension. *Clin. Exp. Hypertens.* 1, 67–86. doi: 10.3109/10641967809068596

Fan, B., Wang, H., Wu, T., Li, Y., Lin, Z., Li, M., et al. (2019). Electrophysiological measurement of rat atrial epicardium using a novel stereotaxic apparatus. *Int. Heart J.* 60, 400–410. doi: 10.1536/ihj.18-215

Gold, D. R., Litonjua, A. A., Zanobetti, A., Coull, B. A., Schwartz, J., Maccallum, G., et al. (2005). Air pollution and ST-segment depression in elderly subjects. *Environ. Health Perspect.* 113, 883–887. doi: 10.1289/ehp.7737

Haïssaguerre, M., Jaïs, P., Shah, D. C., Takahashi, A., Hocini, M., Quiniou, G., et al. (1998). Spontaneous initiation of atrial fibrillation by ectopic beats originating in the pulmonary veins. *N. Engl. J. Med.* 339, 659–666. doi: 10.1056/nejm199809033391003

Hald, E. M., Rinde, L. B., Løchen, M. L., Mathiesen, E. B., Wilsgaard, T., Njølstad, I., et al. (2018). Atrial fibrillation and cause-specific risks of pulmonary embolism and ischemic stroke. *J. Am. Heart Assoc.* 7:e006502.

Harrison, S. D. Jr., Bosin, T. R., and Maickel, R. P. (1974). Physiological disposition of atropine in the rat. *Pharmacol. Biochem. Behav.* 2, 843–845. doi: 10.1016/0091-3057(74)90120-8

Hayashi, H., Wang, C., Miyauchi, Y., Omichi, C., Pak, H. N., Zhou, S., et al. (2002). Aging-related increase to inducible atrial fibrillation in the rat model. *J. Cardiovasc. Electrophysiol.* 13, 801–808. doi: 10.1046/j.1540-8167.2002.00801.x

Hnatkova, K., Waktare, J. E., Murgatroyd, F. D., Guo, X., Baiyan, X., Camm, A. J., et al. (1998). Analysis of the cardiac rhythm preceding episodes of paroxysmal atrial fibrillation. *Am. Heart J.* 135, 1010–1019. doi: 10.1016/s0002-8703(98)70066-3

Hooper, J. S., Hadley, S. H., Morris, K. F., Breslin, J. W., Dean, J. B., and Taylor-Clark, T. E. (2016). Characterization of cardiovascular reflexes evoked by airway stimulation with allylisothiocyanate, capsaicin, and ATP in sprague-dawley rats. *J. Appl. Physiol.* 120, 580–591. doi: 10.1152/japplphysiol.00944.2015

Hooper, J. S., Stanford, K. R., Alencar, P. A., Alves, N. G., Breslin, J. W., Dean, J. B., et al. (2019). Nociceptive pulmonary-cardiac reflexes are altered in the spontaneously hypertensive rat. *J. Physiol.* 597, 3255–3279. doi: 10.1113/jp278085

Huang, K., Liang, F., Yang, X., Liu, F., Li, J., Xiao, Q., et al. (2019). Long term exposure to ambient fine particulate matter and incidence of stroke: prospective cohort study from the China-PAR project. *BMJ* 367:l6720. doi: 10.1136/bmj.l6720

Lau, D. H., Shipp, N. J., Kelly, D. J., Thanigaimani, S., Neo, M., Kuklik, P., et al. (2013). Atrial arrhythmia in ageing spontaneously hypertensive rats: unraveling the substrate in hypertension and ageing. *PLoS One* 8:e72416. doi: 10.1371/journal.pone.0072416

Link, M. S., Luttmann-Gibson, H., Schwartz, J., Mittleman, M. A., Wessler, B., Gold, D. R., et al. (2013). Acute exposure to air pollution triggers atrial fibrillation. *J. Am. Coll. Cardiol.* 62, 816–825. doi: 10.1016/j.jacc.2013.05.043

Liu, L., and Nattel, S. (1997). Differing sympathetic and vagal effects on atrial fibrillation in dogs: role of refractoriness heterogeneity. *Am. J. Physiol.* 273, H805–H816.

Logantha, S., Kharche, S. R., Zhang, Y., Atkinson, A. J., Hao, G., Boyett, M. R., et al. (2019). Sinus node-like pacemaker mechanisms regulate ectopic pacemaker activity in the adult rat atrioventricular ring. *Sci. Rep.* 9:11781.

Masani, F. (1986). Node-like cells in the myocardial layer of the pulmonary vein of rats: an ultrastructural study. *J. Anat.* 145, 133–142.

Maupoil, V., Bronquard, C., Freslon, J. L., Cosnay, P., and Findlay, I. (2007). Ectopic activity in the rat pulmonary vein can arise from simultaneous activation of alpha1- and beta1-adrenoceptors. *Br. J. Pharmacol.* 150, 899–905. doi: 10.1038/sj.bjp.0707177

Nattel, S., Li, D., and Yue, L. (2000). Basic mechanisms of atrial fibrillation–very new insights into very old ideas. *Annu. Rev. Physiol.* 62, 51–77. doi: 10.1146/annurev.physiol.62.1.51

Ninomiya, I. (1966). Direct evidence of nonuniform distribution of vagal effects on dog atria. *Circ. Res.* 19, 576–583. doi: 10.1161/01.res.19.3.576

O'Donnell, D., Bourke, J. P., and Furniss, S. S. (2003). P Wave morphology during spontaneous and paced pulmonary vein activity: differences between patients with atrial fibrillation and normal controls. *J. Electrocardiol.* 36, 33–40. doi: 10.1054/jelc.2003.50011

Ogawa, M., Tan, A. Y., Song, J., Kobayashi, K., Fishbein, M. C., Lin, S. F., et al. (2009). Cryoablation of stellate ganglia and atrial arrhythmia in ambulatory dogs with pacing-induced heart failure. *Heart Rhythm* 6, 1772–1779. doi: 10.1016/j.hrthm.2009.08.011

Ohkubo, K., Watanabe, I., Yamada, T., Okumura, Y., Hashimoto, K., Ashino, S., et al. (2008). P Wave morphology of an arrhythmogenic focus in patients with atrial fibrillation originating from a pulmonary vein or the superior vena cava. *Circ. J.* 72, 1650–1657. doi: 10.1253/circj.cj-08-0099

Oliveira, M., Da Silva, M. N., Geraldes, V., Xavier, R., Laranjo, S., Silva, V., et al. (2011). Acute vagal modulation of electrophysiology of the atrial and pulmonary veins increases vulnerability to atrial fibrillation. *Exp. Physiol.* 96, 125–133. doi: 10.1113/expphysiol.2010.053280

Park, S. K., O'neill, M. S., Vokonas, P. S., Sparrow, D., and Schwartz, J. (2005). Effects of air pollution on heart rate variability: the VA normative aging study. *Environ. Health Perspect.* 113, 304–309. doi: 10.1289/ehp.7447

Peretz, A., Kaufman, J. D., Trenga, C. A., Allen, J., Carlsten, C., Aulet, M. R., et al. (2008). Effects of diesel exhaust inhalation on heart rate variability in human volunteers. *Environ. Res.* 107, 178–184. doi: 10.1016/j.envres.2008.01.012

Peters, A., Liu, E., Verrier, R. L., Schwartz, J., Gold, D. R., Mittleman, M., et al. (2000). Air pollution and incidence of cardiac arrhythmia. *Epidemiology* 11, 11–17. doi: 10.1097/00001648-200001000-00005

Pfeffer, M. A., Pfeffer, J. M., and Frohlich, E. D. (1976). Pumping ability of the hypertrophying left ventricle of the spontaneously hypertensive rat. *Circ. Res.* 38, 423–429. doi: 10.1161/01.res.38.5.423

Pope, C. A. III, Burnett, R. T., Thurston, G. D., Thun, M. J., Calle, E. E., Krewski, D., et al. (2004). Cardiovascular mortality and long-term exposure to particulate air pollution: epidemiological evidence of general pathophysiological pathways of disease. *Circulation* 109, 71–77. doi: 10.1161/01.cir.0000108927.80044.7f

Rajawat, Y. S., Gerstenfeld, E. P., Patel, V. V., Dixit, S., Callans, D. J., and Marchlinski, F. E. (2004). ECG criteria for localizing the pulmonary vein origin of spontaneous atrial premature complexes: validation using intracardiac recordings. *Pacing Clin. Electrophysiol.* 27, 182–188. doi: 10.1111/j.1540-8159.2004.00408.x

Routledge, H. C., Manney, S., Harrison, R. M., Ayres, J. G., and Townend, J. N. (2006). Effect of inhaled sulphur dioxide and carbon particles on heart rate variability and markers of inflammation and coagulation in human subjects. *Heart* 92, 220–227. doi: 10.1136/hrt.2004.051672

Scridon, A., Gallet, C., Arisha, M. M., Oréa, V., Chapuis, B., Li, N., et al. (2012). Unprovoked atrial tachyarrhythmias in aging spontaneously hypertensive rats: the role of the autonomic nervous system. *Am. J. Physiol. Heart Circ. Physiol.* 303, H386–H392.

Shelton, R. S., Ogawa, M., Lin, H., Shen, C., Wong, J., Lin, S. F., et al. (2018). Effects of stellate ganglion cryoablation on subcutaneous nerve activity and atrial tachyarrhythmias in a canine model of pacing-induced heart failure. *JACC Clin. Electrophysiol.* 4, 686–695. doi: 10.1016/j.jacep.2018.02.003

Shen, M. J., Choi, E. K., Tan, A. Y., Han, S., Shinohara, T., Maruyama, M., et al. (2011). Patterns of baseline autonomic nerve activity and the development of pacing-induced sustained atrial fibrillation. *Heart Rhythm* 8, 583–589. doi: 10.1016/j.hrthm.2010.11.040

Shen, M. J., and Zipes, D. P. (2014). Role of the autonomic nervous system in modulating cardiac arrhythmias. *Circ. Res.* 114, 1004–1021. doi: 10.1161/circresaha.113.302549

Tabacova, S. A., and Kimmel, C. A. (2002). Atenolol: pharmacokinetic/dynamic aspects of comparative developmental toxicity. *Reprod. Toxicol.* 16, 1–7. doi: 10.1016/s0890-6238(01)00193-9

Taylor-Clark, T. E. (2020). Air pollution-induced autonomic modulation. *Physiology* 35, 363–374. doi: 10.1152/physiol.00017.2020

Taylor-Clark, T. E., Kiros, F., Carr, M. J., and Mcalexander, M. A. (2009). Transient receptor potential ankyrin 1 mediates toluene diisocyanate-evoked respiratory irritation. *Am. J. Respir. Cell Mol. Biol.* 40, 756–762. doi: 10.1165/rcmb.2008-0292oc

Taylor-Clark, T. E., and Undem, B. J. (2010). Ozone activates airway nerves via the selective stimulation of TRPA1 ion channels. *J. Physiol.* 588, 423–433. doi: 10.1113/jphysiol.2009.183301

Thoren, P., Noresson, E., and Ricksten, S. E. (1979). Cardiac reflexes in normotensive and spontaneously hypertensive rats. *Am. J. Cardiol.* 44, 884–888. doi: 10.1016/0002-9149(79)90218-2

Waldo, A. L., Maclean, A. H., Karp, R. B., Kouchoukos, N. T., and James, T. N. (1977). Sequence of retrograde atrial activation of the human heart. correlation with P Wave polarity. *Br. Heart J.* 39, 634–640. doi: 10.1136/hrt.39.6.634

Waldo, A. L., Vitikainen, K. J., and Hoffman, B. F. (1975). The sequence of retrograde atrial activation in the canine heart. correlation with positive and negative retrograde P waves. *Circ. Res.* 37, 156–163. doi: 10.1161/01.res.37.2.156

Conflict of Interest: The authors declare that the research was conducted in the absence of any commercial or financial relationships that could be construed as a potential conflict of interest.

Publisher's Note: All claims expressed in this article are solely those of the authors and do not necessarily represent those of their affiliated organizations, or those of the publisher, the editors and the reviewers. Any product that may be evaluated in this article, or claim that may be made by its manufacturer, is not guaranteed or endorsed by the publisher.

frontiers in Neuroscience

ORIGINAL RESEARCH
published: 31 August 2021
doi: 10.3389/fnins.2021.669535

Oscillatory Pattern of Sympathetic Nerve Bursts Is Associated With Baroreflex Function in Heart Failure Patients With Reduced Ejection Fraction

Edgar Toschi-Dias[1,2,3], Nicola Montano[2,3], Eleonora Tobaldini[2,3], Patrícia F. Trevizan[1], Raphaela V. Groehs[1], Ligia M. Antunes-Correa[1], Thais S. Nobre[1], Denise M. Lobo[1], Allan R. K. Sales[1], Linda M. Ueno-Pardi[1], Luciana D. N. J. de Matos[1], Patrícia A. Oliveira[1], Ana Maria F. W. Braga[1], Maria Janieire N. N. Alves[1], Carlos E. Negrão[1,4] and Maria Urbana P. B. Rondon[4]*

[1] Instituto do Coração (InCor), Hospital das Clinicas HCFMUSP, Faculdade de Medicina, Universidade de São Paulo, São Paulo, Brazil, [2] Department of Internal Medicine, Fondazione IRCSS Ca' Granda, Ospedale Maggiore Policlínico, Milan, Italy, [3] Department of Clinical Sciences and Community Health, University of Milan, Milan, Italy, [4] School of Physical Education and Sport, University of São Paulo, São Paulo, Brazil

OPEN ACCESS

Edited by:
Lilei Yu,
Renmin Hospital of Wuhan University, China

Reviewed by:
Charlotte W. Usselman,
McGill University, Canada
Vlasta Bari,
IRCCS Policlinico San Donato, Italy

***Correspondence:**
Edgar Toschi-Dias
edgar.dias@metodista.br

Specialty section:
This article was submitted to Autonomic Neuroscience, a section of the journal Frontiers in Neuroscience

Received: 19 February 2021
Accepted: 13 July 2021
Published: 31 August 2021

Citation:
Toschi-Dias E, Montano N, Tobaldini E, Trevizan PF, Groehs RV, Antunes-Correa LM, Nobre TS, Lobo DM, Sales ARK, Ueno-Pardi LM, de Matos LDNJ, Oliveira PA, Braga AMFW, Alves MJNN, Negrão CE and Rondon MUPB (2021) Oscillatory Pattern of Sympathetic Nerve Bursts Is Associated With Baroreflex Function in Heart Failure Patients With Reduced Ejection Fraction. Front. Neurosci. 15:669535. doi: 10.3389/fnins.2021.669535

Sympathetic hyperactivation and baroreflex dysfunction are hallmarks of heart failure with reduced ejection fraction (HFrEF). However, it is unknown whether the progressive loss of phasic activity of sympathetic nerve bursts is associated with baroreflex dysfunction in HFrEF patients. Therefore, we investigated the association between the oscillatory pattern of muscle sympathetic nerve activity (LF_{MSNA}/HF_{MSNA}) and the gain and coupling of the sympathetic baroreflex function in HFrEF patients. In a sample of 139 HFrEF patients, two groups were selected according to the level of LF_{MSNA}/HF_{MSNA} index: (1) Lower LF_{MSNA}/HF_{MSNA} (lower terciles, $n = 46$, aged 53 ± 1 y) and (2) Higher LF_{MSNA}/HF_{MSNA} (upper terciles, $n = 47$, aged 52 ± 2 y). Heart rate (ECG), arterial pressure (oscillometric method), and muscle sympathetic nerve activity (microneurography) were recorded for 10 min in patients while resting. Spectral analysis of muscle sympathetic nerve activity was conducted to assess the LF_{MSNA}/HF_{MSNA}, and cross-spectral analysis between diastolic arterial pressure, and muscle sympathetic nerve activity was conducted to assess the sympathetic baroreflex function. HFrEF patients with lower LF_{MSNA}/HF_{MSNA} had reduced left ventricular ejection fraction (26 ± 1 vs. 29 ± 1%, $P = 0.03$), gain (0.15 ± 0.03 vs. 0.30 ± 0.04 a.u./mmHg, $P < 0.001$) and coupling of sympathetic baroreflex function (0.26 ± 0.03 vs. 0.56 ± 0.04%, $P < 0.001$) and increased muscle sympathetic nerve activity (48 ± 2 vs. 41 ± 2 bursts/min, $P < 0.01$) and heart rate (71 ± 2 vs. 61 ± 2 bpm, $P < 0.001$) compared with HFrEF patients with higher LF_{MSNA}/HF_{MSNA}. Further analysis showed an association between the LF_{MSNA}/HF_{MSNA} with coupling of sympathetic baroreflex function ($R = 0.56$,

$P < 0.001$) and left ventricular ejection fraction ($R = 0.23$, $P = 0.02$). In conclusion, there is a direct association between LF_{MSNA}/HF_{MSNA} and sympathetic baroreflex function and muscle sympathetic nerve activity in HFrEF patients. This finding has clinical implications, because left ventricular ejection fraction is less in the HFrEF patients with lower LF_{MSNA}/HF_{MSNA}.

Keywords: heart failure, oscillatory pattern, sympathetic nervous system, baroreflex control, cardiovascular variabilities

INTRODUCTION

Heart failure is a complex syndrome and considered the leading cause of hospitalization in patients over the age of 60 years, which accounts for about 30–40% of the mortality of these patients (Ponikowski et al., 2016). According to cardiac function, heart failure (HF) patients are currently classified as follows: (i) with preserved ejection fraction, (ii) with mid-range ejection fraction; and (iii) with reduced ejection fraction (HFrEF). It is also known that neurohumoral excitation is a hallmark of HFrEF and an independent predictor of mortality in patients suffering with this syndrome (Barretto et al., 2009).

HFrEF patients have increased sympathetic activity as shown by the enhanced sympathetic nerve discharges (Barretto et al., 2009; Triposkiadis et al., 2009), and a progressive loss of phasic activity of sympathetic nerve bursts (van de Borne et al., 1997). It is known that the sympathetic nervous system influence on cardiovascular control depends not only on its tonic but also its phasic activity (i.e., modulation). Thus, both the frequency and the intensity of the sympathetic nerve discharge determine a pattern of oscillation that influences the efficiency of sympathetic effector response (Toschi-Dias et al., 2013). This modulation of sympathetic nerve bursts may be evaluated by the balance between the spectral components of low (LF) and high frequency (HF) sympathetic nerve activity and represents the intrinsic behavior of sympathetic nervous system functioning (van de Borne et al., 1997; Toschi-Dias et al., 2013).

In healthy individuals, spontaneous fluctuations in heart rate (HR), blood pressure (BP), and muscle sympathetic nerve activity (MSNA) are strongly coupling in the LF band both at rest and during physiological maneuvers (e.g., orthostatic stress) (Malliani et al., 1991; Stauss et al., 1998; Furlan et al., 2000). Based on neuromodulation approaches, Stauss et al. (1998) demonstrated that vascular tonus is modulated by sympathetic nerve stimulations in the frequency range between 0.07 and 0.10 Hz in healthy subjects. However, sympathetic nerve stimulation reduced blood flow when the stimulation frequency was in the HF range (i.e., > 0.20 Hz). These findings indicate that peripheral sympathetic transmission to the vascular bed of humans acts as a low-pass filter with a cut-off frequency above 0.10 Hz (Stauss et al., 1998).

On the other hand, the increase of burst frequency with a shift from LF fluctuations toward HF bands (∼0.20 Hz) are linked with a marked reduction in the linear relationship between systolic arterial pressure (SAP) and MSNA oscillation in the presyncope phase during a tilt test maneuver (Kamiya et al., 2005; Barbic et al., 2015). These data demonstrate the physiological relevance of spectral density and coupling between cardiovascular variability parameters, because to induce an optimal vasomotor response, the tonic and phasic activities of the sympathetic firings must occur at ∼0.10 Hz for appropriate vasoconstriction (Pagani et al., 1997; Stauss et al., 1998; Furlan et al., 2000; Kamiya et al., 2005; Barbic et al., 2015).

A neural mechanism of interest is the baroreflex control, which exerts a major inhibitory influence on sympathetic outflow (Joyner et al., 2010). This autonomic reflex control modulates, at least in part, the tonus and the oscillatory pattern of MSNA (LF_{MSNA}/HF_{MSNA}) (Groehs et al., 2015). The effectiveness of the sympathetic baroreflex depends on its magnitude and coupling responses (Sunagawa et al., 2001). Curiously, baroreflex dysfunction is also a hallmark of HFrEF. The clinical implication of this knowledge is based on the fact that both baroreflex dysfunction and increased MSNA are associated with a poor prognosis in patients with HFrEF sympathetic nerve discharges (Grassi et al., 2004; Barretto et al., 2009), and a progressive loss of phasic activity of sympathetic nerve bursts. However, it is unknown whether a lower LF_{MSNA}/HF_{MSNA} can potentiate the sympathetic baroreflex dysfunction in HFrEF patients. In the present study, we tested the hypothesis that HFrEF patients with lower LF_{MSNA}/HF_{MSNA} would have an exacerbated hyperadrenergic state compared with HFrEF patients with higher LF_{MSNA}/HF_{MSNA}. In addition, we sought to determine whether there would be an association between LF_{MSNA}/HF_{MSNA} and the gain and coupling of sympathetic baroreflex function in these patients.

MATERIALS AND METHODS

This study was approved by the Scientific Commission of the Heart Institute (InCor), University of São Paulo Medical School (#3946/13/071) and Human Subject Protection Committee of the Clinical Hospital, University of São Paulo, Medical School (# 22255213.2.0000.0068). Signed informed consent was obtained from all patients during the screening visit.

Subjects

Patients were selected from a database of randomized studies performed at the Unit of Cardiovascular Rehabilitation and Exercise Physiology of the Heart Institute (InCor), University of São Paulo Medical School. Initially, 139 HFrEF patients, age ranging from 30 to 65 years, New York Heart Association functional class II to III, left ventricular ejection fraction (LVEF) < 40%, and peak oxygen uptake

(VO_2) < 20 ml.kg^{-1}.min^{-1} were included in the study. The exclusion criteria were recent myocardial infarction or unstable angina (<3 months), HFrEF duration (<3 months), and permanent pacemaker dependence. According to the level of the LF_{MSNA}/HF_{MSNA} index, patients were placed into two groups: (1) Lower LF_{MSNA}/HF_{MSNA} (lower terciles < 0.46, n = 46, aged 53 ± 1 y) and (2) Higher LF_{MSNA}/HF_{MSNA} (upper terciles > 1.24, n = 47, aged 52 ± 2 y).

Cardiac Function

According to international guidelines, LVEF was evaluated with two-dimensional echocardiography according to the Simpson method (IE33, Philips Medical Systems, Andover, MA) (Ponikowski et al., 2016).

Functional Capacity

To assess functional capacity, all patients underwent cardiopulmonary exercise testing as previously described (Martinez et al., 2011) on a braked cycle ergometer, using a ramp protocol with work rate increments of 10, 15, or 20 W every minute at 60 rpm up to exhaustion. Peak value of oxygen uptake (VO_2 peak) was averaged from the last 30 s interval and was considered the maximal exercise capacity (Martinez et al., 2011).

Muscle Sympathetic Nerve Activity

MSNA was recorded from the peroneal nerve using the microneurography technique (Vallbo et al., 1979; Toschi-Dias et al., 2013). In brief, multiunit postganglionic muscle sympathetic nerve recordings were made using a tungsten microelectrode (tip diameter 5–15 μm). The signals were amplified by a factor of 50–100K and band-pass filtered (0.7–2 KHz). For recordings and analysis, nerve activity was rectified and integrated with time constant at 0.1 s to obtain a mean voltage display of MSNA. In the present study, the tonic activity of the MSNA was evaluated through a time-domain analysis and expressed as burst frequency (i.e., bursts/min) and burst incidence (i.e., burst per 100 heartbeats) (Vallbo et al., 1979; Toschi-Dias et al., 2013). The phasic activity of MSNA was evaluated by a frequency domain analysis (i.e., power spectrum analysis of MSNA variability) and refers solely to the oscillatory pattern of the post-ganglionic sympathetic firing (Toschi-Dias et al., 2013).

Arterial Pressure, HR, and Respiratory Rate

Arterial pressure was monitored non-invasively by a finger photoplethysmography device (Finapres 2,300, Ohmeda, Englewood, CO) on a beat-to-beat basis. Simultaneously, HR was monitored through lead II of the ECG and respiratory rate was monitored with a piezoelectric thoracic belt (Pneumotrace II, model 1132, UFI, CA) placed around the upper abdomen.

Experimental Protocol

On the day of the experiment, all patients abstained from caffeine or other types of stimulants for 12 h. The protocol experiment was performed at approximately 8:00 AM, with the patients in a supine position in a quiet air-conditioned room (22–24°C). After obtaining an adequate sympathetic nerve recording site in the leg and after stabilization of the autonomic and cardiovascular variables, baseline recordings of arterial pressure, HR, MSNA, and respiratory rate were taken for 10 min.

Autonomic Control

After synchronization among signals, specific software (HeartScope II; AMPS-LLC, NY) was used by a trained investigator (ET-D) to process the MSNA, ECG, arterial pressure, and respiratory activity signals and to extract the time series of MSNA, R-R interval (RRi), systolic and diastolic arterial pressure (SAP and DAP, respectively), and respiration on a beat-to-beat basis. The sympathetic bursts were sampled once per cardiac cycle synchronously with the peak of the R-wave of ECG and automatically detected considering an amplitude threshold of 30% of baseline and rejection ratio of 3%. The maximum and minimum values of arterial pressure inside the i-th heart period were defined as SAP and DAP values, respectively, where i is the cardiac beat counter. Thereafter, the beat-to-beat variability of MSNA, RRi, systolic and diastolic arterial pressure (SAP and DAP, respectively), and respiratory activity were analyzed by an autoregressive frequency domain approach. On stationary segments of 200–300 beats, autoregressive spectral decomposition of times series were calculated based on the Levinson–Durbin recursion with the order of the model chosen according to Akaike's criterion. This procedure automatically quantifies the center frequency and the power spectral density of oscillatory components in very low (VLF: 0.003–0.04 Hz), low (LF: 0.04–0.15 Hz), and high frequency (HF: 0.15–0.40 Hz) ranges in absolute (abs.) values as well as in normalized units (n.u.). However, only the normalized units were used of the LF and HF components of RRi and MSNA variability due to the variances in data. According to the international guidelines, the RRi spectral component quantified in the LF band representing cardiac sympathetic modulation predominance, and the HF band synchronized with respiration, representing cardiac parasympathetic modulation (Malliani et al., 1991; Montano et al., 1994; Task Force, 1996). Spectral densities of SAP and DAP variability were quantified only in the LF band, indexes of the vasomotor sympathetic modulation (Malliani et al., 1991), because the quantified oscillatory component in the HF band did not represent an autonomic index (Bertram et al., 2000). Finally, due to central medullary sympathetic premotor oscillatory circuits and/or baroreflex resonance, the spectral density in the LF range of MSNA variability reflects the profile of oscillation of sympathetic modulation associated with 0.10-Hz rhythm, whereas spectral density in HF range reflects the marked influence of the central respiratory drive on medullary sympathetic premotor neurons (Malliani et al., 1991; Furlan et al., 2000; Montano et al., 2009). Furthermore, the LF/HF ratio of RRi and MSNA were calculated for estimation of the cardiac sympatho-vagal balance (LF_{RRi}/HF_{RRi}) and oscillatory pattern of MSNA (LF_{MSNA}/HF_{MSNA}), respectively (Martinez et al., 2011; Toschi-Dias et al., 2013; Groehs et al., 2015).

SYMPATHETIC BAROREFLEX CONTROL

To evaluate sympathetic baroreflex function, transfer function analysis by means of the bivariate autoregressive model was used with model order fixed to 10. As previously described in detail (Pinna et al., 2002; Bari et al., 2019), this procedure enables quantification of the gain, phase shift, and coherence of transfer function between two signals (e.g., MSNA and DAP) in a frequency range. Briefly, the transfer function was estimated as the ratio of the cross-spectrum computed from input signal (i.e., DAP) to the output signal (i.e., MSNA) to the power spectrum of the input signal. Thus, the gain of sympathetic baroreflex function measures the intensity of the response of the MSNA per unit of spontaneous change of the DAP, being expressed in a.u./mmHg (Pinna et al., 2002; Toschi-Dias et al., 2013; Bari et al., 2019). The phase shift estimated the delay between the oscillations in both variability signals (the SAP changes precede MSNA changes) and was accepted when it was between 0 and -π (radians). The squared coherence function of MSNA and DAP signals was estimated as a ratio of the squared cross-spectrum modulus to the product of the densities spectra of the input and output signals. This function ranged between 0 and 1, with 0 indicating null correlation and 1 maximum correlation. In the present study, the squared coherence index represents the level of neurovascular coupling between MSNA and DAP. The phase shift measures the time lag or lead between the signals. We calculated these indices of the transfer function in the frequency where the coherence peaked at the maximum value within the LF range (Pinna et al., 2002; Toschi-Dias et al., 2013; Bari et al., 2019).

Statistical Analysis

The data are presented as mean ± standard error. A chi-square (χ^2) test was used to assess categorical data differences. For each continuous or discrete variable, Lèvene and Kolmogorov–Smirnov tests were used to assess the homogeneity and normality of distribution, respectively. Demographic data and baseline physical characteristics and hemodynamic and autonomic data were compared using Student's *t*-tests or Mann–Whitney tests when appropriate. Spearman correlation was used to test the association between LF_{MSNA}/HF_{MSNA}, LVEF, VO_2, gain and coherence of sympathetic baroreflex function. Probability values of $P < 0.05$ were considered statistically significant.

RESULTS

Baseline characteristics of patients with HFrEF are shown in **Table 1**. Age, body mass index (BMI), sex, mean BP, and HFrEF etiology were similar between groups. However, LVEF and VO_2 were significantly lower and HR and proportion of patients using anticoagulant were significantly higher in the group with lower LF_{MSNA}/HF_{MSNA} compared with the group with higher LF_{MSNA}/HF_{MSNA}.

Spectral parameters of MSNA, RR-interval, SAP, and DAP of HFrEF patients with a lower and higher oscillatory pattern of MSNA are shown in **Table 2**. The loss of the physiological autonomic modulatory pattern characterized by a paradoxical decrease of LF component in the lower LF_{MSNA}/HF_{MSNA} group was observed in the RRi, SAP, and DAP variability. Furthermore, the lower LF_{MSNA}/HF_{MSNA} group had a decreased variance of and sympatho-vagal balance (LF/HF) than the higher LF_{MSNA}/HF_{MSNA} group had (**Table 2**). However, the oscillatory component in HF band of RRi and variance of MSNA, SAP, and DAP were similar between groups (**Table 2**).

In addition, significantly higher levels in burst frequency (**Figure 1A**) but not in burst incidence of MSNA (**Figure 1B**) occurred in the lower LF_{MSNA}/HF_{MSNA} group compared with the higher LF_{MSNA}/HF_{MSNA} group.

The sympathetic baroreflex function is shown in **Figure 2**. HFrEF patients with lower LF_{MSNA}/HF_{MSNA} had reduced gain and coherence of sympathetic baroreflex function than that observed in patients with higher LF_{MSNA}/HF_{MSNA}. Further analysis showed that LF_{MSNA}/HF_{MSNA} was directly associated with LVEF, gain and coherence of sympathetic baroreflex function, and was inversely associated with HR and MSNA burst frequency (**Table 3**), yet MSNA burst frequency was significantly associated with HR and inversely associated with gain and coherence of sympathetic baroreflex function (**Table 3**).

TABLE 1 | Baseline characteristics of HfrEF patients with lower and higher oscillatory pattern of MSNA.

	Lower LF_{MSNA}/HF_{MSNA}	Higher LF_{MSNA}/HF_{MSNA}	*P*
N	46	47	
Age, y	53 ± 1	52 ± 2	0.91
BMI, kg/m^2	26 ± 1	27 ± 1	0.32
Sex			
Male, n (%)	33 (72)	38 (81)	0.30
Female, n (%)	13 (28)	9 (19)	
LVEF,%	26 ± 1	29 ± 1	0.03
VO_2 peak, ml.kg^{-1}.min^{-1}	16 ± 1	18 ± 1	0.03
MAP, mmHg	89 ± 2	86 ± 2	0.89
HR, bpm	72 ± 2	63 ± 2	< 0.001
HFrEF etiology			
Idiopathic, n (%)	21 (46)	18 (38)	0.47
Ischaemic, n (%)	14 (30)	15 (32)	0.88
Hypertensive, n (%)	4 (9)	8 (17)	0.23
Chagasic, n (%)	7 (15)	6 (13)	0.73
Medications			
β-Blocker, n (%)	44 (96)	45 (96)	0.98
ACEI/ARA, n (%)	44 (96)	44 (94)	0.66
Diuretics, n (%)	42 (91)	46 (98)	0.16
Anticoagulant, n (%)	17 (36)	7 (15)	0.02
Digitalis, n (%)	9 (20)	10 (22)	0.84
Statins, n (%)	19 (41)	22 (47)	0.59

Values are means ± SE; HFrEF, heart failure with reduced ejection fraction; LF_{MSNA}/HF_{MSNA}, oscillatory pattern of MSNA; BMI, body mass index; LVEF, left ventricular ejection fraction; VO_2 peak, oxygen uptake at peak exercise, MBP, mean arterial pressure, HR, heart rate; HFrEF, chronic heart failure; ACEI/ARA, angiotensin-converting enzyme inhibitors/angiotensin II receptor antagonist.

TABLE 2 | Spectral parameters of MSNA, RR-interval, SAP, and DAP of HFrEF patients with lower and higher oscillatory pattern of MSNA.

	Lower LF_{MSNA}/HF_{MSNA}	Higher LF_{MSNA}/HF_{MSNA}	*P*
MSNA			
Variance, a.u.^{2}	0.17 ± 0.02	0.19 ± 0.02	0.49
LF n.u.,%	20 ± 1	70 ± 2	<0.01
HF n.u.,%	72 ± 2	28 ± 2	<0.01
LF/HF	0.3 ± 0.1	4.6 ± 0.9	<0.01
R-R interval			
Variance, ms^2	1828 ± 241	3628 ± 796	0.04
LF n.u.,%	15 ± 2	30 ± 4	<0.01
HF n.u.,%	53 ± 3	49 ± 3	0.44
LF/HF	0.3 ± 0.1	1.4 ± 0.4	<0.01
Systolic arterial pressure			
Variance, mmHg^2	19 ± 3	23 ± 3	0.26
LF abs., mmHg^2	1.5 ± 0.3	4.8 ± 0.8	<0.001
Diastolic arterial pressure			
Variance, mmHg^2	7.1 ± 0.8	8.4 ± 1.0	0.32
LF abs., mmHg^2	0.5 ± 0.1	1.7 ± 0.4	<0.001

Values are mean ± SE; HFrEF, heart failure with reduced ejection fraction; MSNA, muscle sympathetic nerve activity; SAP, systolic arterial pressure; DAP, diastolic arterial pressure; LF_{MSNA}/HF_{MSNA}, oscillatory pattern of MSNA; LF, low frequency; HF, high frequency; LF/HF, sympatho-vagal balance.

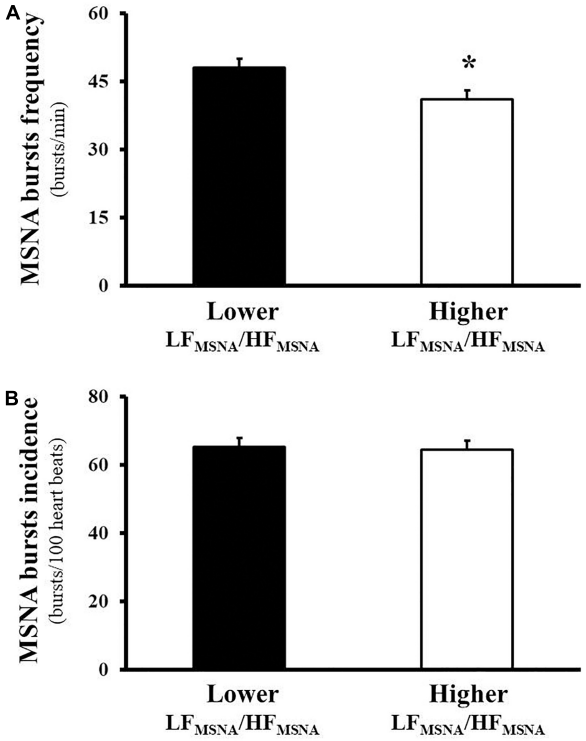

FIGURE 1 | Muscle sympathetic nerve activity (MSNA), assessed directly by the microneurography technique, in heart failure patients with reduced ejection fraction. The tonic activity of the MSNA reveals higher levels in burst frequency (bursts/min, **A**) but not in burst incidence (bursts/100 heart beats, **B**) in the Lower LF_{MSNA}/HF_{MSNA} group compared with the Higher LF_{MSNA}/HF_{MSNA} group.

DISCUSSION

The main and new findings of the present study were that the oscillatory pattern of MSNA was directly associated with gain and coupling of the sympathetic baroreflex function and inversely associated with MSNA burst frequency in patients with HFrEF. Indeed, our data showed that patients with HFrEF and lower LF_{MSNA}/HF_{MSNA} had higher levels of burst frequency and reduced cardiac function, functional capacity, gain and coupling of sympathetic baroreflex function.

In the present study, we aimed to investigate a candidate mechanism underlying the loss of rhythm of the MSNA in HFrEF patients. In this sense, we thought that the reduced gain and coupling of the sympathetic baroreflex function would be involved in this autonomic dysfunction in these patients. Accumulated evidence shows that sympathetic baroreflex plays an important role in the modulation of sympathetic nervous activity (van de Borne et al., 1997; Toschi-Dias et al., 2013). During the cardiac cycle, when blood pressure increases, the activation of arterial baroreceptors located in the aortic arch and in the carotid sinus reflexively restrains the sympathetic efferent outflow. In contrast, during the reduction in arterial pressure when arterial baroreceptors are deactivated the sympathetic activity increases reflexively (Toschi-Dias et al., 2017).

In humans, due to the resonance loop generated in negative feedback mechanisms such as the baroreceptor reflex arc, this rhythm occurs in a modulation range of 0.10 Hz and is produced mainly by the time constant and delays in the local and neuronal phenomena of a closed system (Burgess et al., 2003; Julien, 2006). This autonomic control can be drastically altered in cardiovascular disease. For example, the gain in sympathetic baroreflex is significantly reduced in patients with HFrEF (Grassi et al., 2004), hypertension (Laterza et al., 2007) and myocardial infarction (Martinez et al., 2011). To our knowledge, this is the first time that one of the mechanisms related to the loss of the intrinsic rhythm of sympathetic nervous activity has been demonstrated in patients with HFrEF. In fact, the coupling of the sympathetic baroreflex function is reduced in patients with HFrEF and lower LF_{MSNA}/HF_{MSNA}.

To the best of our knowledge, few studies have evaluated the phasic activity of neural sympathetic discharge (Pagani et al., 1997; van de Borne et al., 1997; Furlan et al., 2000; Barbic et al., 2015). Most of these studies explore only the oscillatory component in the LF range. Because the MSNA signal acquisition is performed before the adrenergic synapse, the interpretation of the rhythms from the relationship between the spectral components reveals the intrinsic behavior of the sympathetic nervous system. It has been documented that the increase in the LF component of signals involved in cardiovascular variability during physiological stress is the hallmark of phasic sympathetic activity of an effector organ (Furlan et al., 2000; Barbic et al., 2015). Based on the response of oscillatory components during orthostatic stress, an increase of the adrenergic tonic activity is accompanied by a proportional modification of their LF rhythmic pattern of sympathetic firing, RRi, and SAP in healthy subjects.

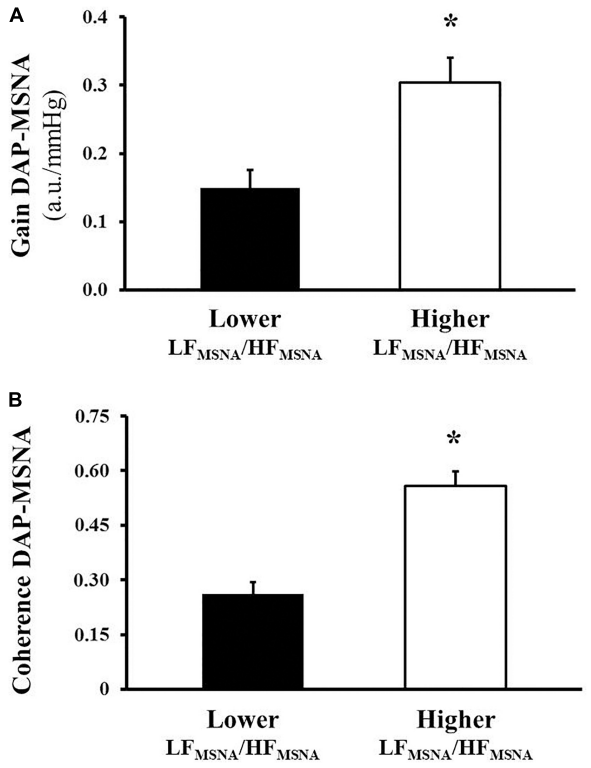

FIGURE 2 | Sympathetic baroreflex function of muscle sympathetic nerve activity (MSNA), assessed by the transfer function technique using bivariate autoregressive spectral analysis, in heart failure patients with reduced ejection fraction. The levels of gain are expressed in arbitrary unit/mm of mercury (u.a./mmHg, **A**) and coherence in percentage **(B)**. *$P < 0.01$ vs. Group with higher oscillatory pattern of MSNA.

As mentioned earlier, tonic and phasic activities of the sympathetic firings at rest and during physiological stress occur predominantly at ∼0.10 Hz to ensure appropriate vasoconstriction to organism demand (Pagani et al., 1997; Furlan et al., 2000; Barbic et al., 2015). However, the loss of oscillatory patterns of MSNA, characterized by an increase in burst frequency with the shift from LF range fluctuations toward the HF range, may be observed through the relation of the spectral components of the neural sympathetic discharges in HFrEF patients (van de Borne et al., 1997). This paradoxical phenomenon reveals the saturation of the sympathetic nervous system and is linked to a marked reduction in the gain and coupling of sympathetic baroreflex function. We can speculate that in cardiac dysfunction, as observed in HFrEF patients, some excitatory reflex mechanisms, such as chemoreflex control and cardiac sympathetic afferent reflex, can buffer the baroreflex control leading to a progressive loss in the central autonomic rhythm (Toschi-Dias et al., 2017). Further studies will be necessary to confirm this hypothesis.

Our findings have clinical implications because LF_{MSNA}/HF_{MSNA} was also positively associated with LVEF and inversely associated with heart rate. There is a consensus that LVEF is an independent predictor of cardiovascular death, hospitalization, and all-cause mortality (Lewis et al., 2003).

TABLE 3 | Relationship between oscillatory pattern of MSNA and burst frequency with functional and hemodynamic characteristics and sympathetic baroreflex function in HFrEF patients.

***N* = 93 patients**	**LF_{MSNA}/HF_{MSNA}**	**Burst frequency**
LVEF	0.23*	−0.13
VO_2 peak	0.18	−0.02
HR	−0.46*	0.37*
Gain DAP-MSNA	0.42*	−0.28*
Coherence DAP-MSNA	0.56*	−0.28*
Burst frequency	−0.28*	. . .

*Spearman rank correlation coefficients. HFrEF, heart failure with reduced ejection fraction; LF_{MSNA}/HF_{MSNA}, oscillatory pattern of muscle sympathetic nerve activity; MSNA, muscle sympathetic nerve activity; LVEF, left ventricular ejection fraction; VO_2 peak, peak oxygen uptake; HR, heart rate; DAP, diastolic arterial pressure. *$P < 0.05$.*

Interestingly, it has been demonstrated that patients with HFrEF with an absence of the LF component of MSNA have reduced LVEF and increased hyperadrenergic state (van de Borne et al., 1997). Our findings confirm these observations. We found that the loss of intrinsic rhythm of the MSNA is associated with a worsening in the cardiac systolic function in patients with HFrEF.

The present study extends the knowledge about the influence of the oscillatory pattern of the MSNA on the clinical condition of these patients. These data reveal, for the first time, that HFrEF patients with lower LF_{MSNA}/HF_{MSNA} have decreased functional capacity. This finding has clinical implications that should be taken into consideration in medical practice, because it is well established that VO_2 peak is a prognostic index due to its strong and independent association with clinical outcomes in HFrEF patients (Keteyian et al., 2016). In addition, we demonstrated, in a large population, a positive association between LF_{MSNA}/HF_{MSNA} and the levels of MSNA. In addition, we (Barretto et al., 2009) and others (Benedict et al., 1996; Stanek et al., 2001) demonstrated that MSNA and catecholamine levels are independent predictors of mortality in HFrEF patients.

Likewise, of clinical interest, we found that HFrEF patients with lower LF_{MSNA}/HF_{MSNA} have increased HR at rest. These data are important because an elevated HR is also considered a prognostic index of mortality (Poole-Wilson et al., 2002, 2003; Kotecha et al., 2017). Our data also suggest that patients with HFrEF under optimized clinical treatment have increased cardiovascular risk in the presence of a decreased MSNA oscillatory pattern.

Our study has some limitations that need to be addressed. First, the experimental protocol considers only recordings obtained with the patient in the resting position to evaluate autonomic nervous system in HFrEF patients. Some authors have suggested that the autonomic nervous system needs to be evaluated both at rest and during physiological maneuvers to examine the complexities of neural regulation. Therefore, it is difficult to generalize our findings to HFrEF patients during a physiological challenge (e.g., exercise, mental stress, and orthostatic maneuvers). Second, even considering that female participants in the present study were a smaller proportion (28 and 19% for the lower and higher LF_{MSNA}/HF_{MSNA} groups, respectively), someone could argue about the influence of

the menstrual cycle of these women on our results. We did not control the menstrual cycle and the use of hormonal contraceptives or hormone replacement therapy of the women participating in our study. However, because few women were under 50 years of age (i.e., mean age for the end of the reproductive period) our sample was mainly composed of postmenopausal women, who were similarly distributed between the groups. Thus, it is unlikely that menopause, the use of hormonal contraceptives, or hormone replacement therapy could be a confounding variable in the present study. Finally, considering our strategy for the composition of the HFrEF groups, it is possible that some differences in autonomic control markers could be expected due to the interdependence of cardiovascular parameters. Further analysis will be needed in future studies to address this issue.

In conclusion, HFrEF patients with a lower oscillatory pattern of MSNA have a worsening clinical condition as evidenced by the reduced cardiac function and functional capacity, exacerbated resting sympathetic activity, higher resting heart rate, and baroreflex dysfunction when compared with HFrEF patients with a higher oscillatory pattern of MSNA. In addition, there is a direct association between the LF_{MSNA}/HF_{MSNA} index and the gain and coupling of sympathetic baroreflex function and the MSNA in HFrEF patients.

DATA AVAILABILITY STATEMENT

The data, analytic methods, and study materials are available to other researchers at the Heart Institute (InCor) do Hospital das Clínicas da Faculdade de Medicina da Universidade de São Paulo, with Dra. Rondon (urbana@usp.br) or Dr Toschi-Dias (edgar.dias@metodista.br).

ETHICS STATEMENT

The studies involving human participants were reviewed and approved by the Scientific Commission of the Heart Institute (InCor), University of São Paulo Medical School (#3846/13/071) and Human Subject Protection Committee of the Clinical Hospital, University of São Paulo, Medical School (# 22255213.2.0000.0068). The patients/participants provided their written informed consent to participate in this study.

AUTHOR CONTRIBUTIONS

ET-D, NM, ET, and MR conceived and designed the research. ET-D, PT, RG, LA-C, TN, DL, AS, LU-P, LM, PO, AB, MA, CN, and MR performed the experiments. ET-D, ET, and NM analyzed the data. ET-D, NM, ET, CN, and MR interpreted the results of the experiments, and edited and revised the manuscript. ET-D and MR prepared the figures. ET-D and ET drafted the manuscript. All authors read and approved the final version of the manuscript.

FUNDING

This study was supported by the Fundação de Amparo à Pesquisa do Estado de São Paulo (FAPESP, # 2010/50048-1 and # 2015/22814-5) and in part, by the Fundação Zerbini and Coordenação de Aperfeiçoamento de Pessoal de Nível Superior (CAPES). ET-D was supported by FAPESP (2013/07651-7 and 2015/17642-0). CN and MR were supported by CNPq (# 303573/2015-5 and # 313152/2020-9, respectively).

REFERENCES

Barbic, F., Heusser, K., Marchi, A., Zamunér, A. R., Gauger, P., Tank, J., et al. (2015). Cardiovascular parameters and neural sympathetic discharge variability before orthostatic syncope: role of sympathetic baroreflex control to the vessels. *Physiol. Meas.* 36, 633–641. doi: 10.1088/0967-3334/36/4/633

Bari, V., Vaini, E., Pistuddi, V., Fantinato, A., Cairo, B., De Maria, B., et al. (2019). Comparison of causal and non-causal strategies for the assessment of baroreflex sensitivity in predicting acute kidney dysfunction after coronary artery bypass grafting. *Front. Physiol.* 10:1319. doi: 10.3389/fphys.2019.01319

Barretto, A. C., Santos, A. C., Munhoz, R., Rondon, M. U., Franco, F. G., Trombetta, I. C., et al. (2009). Increased muscle sympathetic nerve activity predicts mortality in heart failure patients. *Int. J. Cardiol.* 135, 302–307. doi: 10.1016/j.ijcard.2008.03.056

Benedict, C. R., Shelton, B., Johnstone, D. E., Francis, G., Greenberg, B., Konstam, M., et al. (1996). Prognostic significance of plasma norepinephrine in patients with asymptomatic left ventricular dysfunction. SOLVD investigators. *Circulation* 94, 690–697. doi: 10.1161/01.cir.94.4.690

Bertram, D., Barrès, C., Cheng, Y., and Julien, C. (2000). Norepinephrine reuptake, baroreflex dynamics, and arterial pressure variability in rats. *Am. J. Physiol. Regul. Integr. Comp. Physiol.* 279, R1257–R1267. doi: 10.1152/ajpregu.2000.279.4.R1257

Burgess, D. E., Randall, D. C., Speakman, R. O., and Brown, D. R. (2003). Coupling of sympathetic nerve traffic and BP at very low frequencies is mediated by large-amplitude events. *Am. J. Physiol. Regul. Integr. Comp. Physiol.* 284, R802–R810. doi: 10.1152/ajpregu.00002.2002

Task Force (1996). Heart rate variability: standards measurements, physiological interpretation, and clinical use. Task Force of the European Society of Cardiology & the North American Society of Pacing Electrophysiology. *Circulation* 93, 1043–1065.

Furlan, R., Porta, A., Costa, F., Tank, J., Baker, L., Schiavi, R., et al. (2000). Oscillatory patterns in sympathetic neural discharge and cardiovascular variables during orthostatic stimulus. *Circulation* 101, 886–892. doi: 10.1161/01.cir.101.8.886

Grassi, G., Seravalle, G., Dell'Oro, R., Facchini, A., Ilardo, V., and Mancia, G. (2004). Sympathetic and baroreflex function in hypertensive or heart failure patients with ventricular arrhythmias. *J. Hypertens.* 22, 1747–1753. doi: 10.1097/00004872-200409000-00019

Groehs, R. V., Toschi-Dias, E., Antunes-Correa, L. M., Trevizan, P. F., Rondon, M. U., Oliveira, P., et al. (2015). Exercise training prevents the deterioration in the arterial baroreflex control of sympathetic nerve activity in chronic heart failure patients. *Am. J. Physiol. Heart Circ. Physiol.* 308, H1096–H1102. doi: 10.1152/ajpheart.00723.2014

Joyner, M. J., Charkoudian, N., and Wallin, B. G. (2010). Sympathetic nervous system and blood pressure in humans:individualized patterns of regulation and their implications. *Hypertension* 56, 10–16. doi: 10.1161/HYPERTENSIONAHA.109.140186

Julien, C. (2006). The enigma of Mayer waves: facts and models. *Cardiovasc. Res.* 70, 12–21. doi: 10.1016/j.cardiores.2005.11.008

Kamiya, A., Hayano, J., Kawada, T., Michikami, D., Yamamoto, K., Ariumi, H., et al. (2005). Low-frequency oscillation of sympathetic nerve activity decreases during development of tilt-induced syncope preceding sympathetic withdrawal

and bradycardia. *Am. J. Physiol. Heart Circ. Physiol.* 289, H1758–H1769. doi: 10.1152/ajpheart.01027.2004

Keteyian, S. J., Patel, M., Kraus, W. E., Brawner, C. A., McConnell, T. R., Piña, I. L., et al. (2016). Variables measured during cardiopulmonary exercise testing as predictors of mortality in chronic systolic heart failure. *J. Am. Coll. Cardiol.* 67, 780–789. doi: 10.1016/j.jacc.2015.11.050

Kotecha, D., Flather, M. D., Altman, D. G., Holmes, J., Rosano, G., Wikstrand, J., et al. (2017). Heart rate and rhythm and the benefit of beta-blockers in patients with heart failure. *J. Am. Coll. Cardiol.* 69, 2885–2896.

Laterza, M. C., de Matos, L. D., Trombetta, I. C., Braga, A. M., Roveda, F., Alves, M. J., et al. (2007). Exercise training restores baroreflex sensitivity in never-treated hypertensive patients. *Hypertension* 49, 1298–1306. doi: 10.1161/HYPERTENSIONAHA.106.085548

Lewis, E. F., Moye, L. A., Rouleau, J. L., Sacks, F. M., Arnold, J. M., Warnica, J. W., et al. (2003). Predictors of late development of heart failure in stable survivors of myocardial infarction: the CARE study. *J. Am. Coll. Cardiol.* 42, 1446–1453. doi: 10.1016/s0735-1097(03)01057-x

Malliani, A., Pagani, M., Lombardi, F., and Cerutti, S. (1991). Cardiovascular neural regulation explored in the frequency domain. *Circulation* 84, 482–492. doi: 10.1161/01.cir.84.2.482

Martinez, D. G., Nicolau, J. C., Lage, R. L., Toschi-Dias, E., de Matos, L. D., Alves, M. J., et al. (2011). Effects of long-term exercise training on autonomic control in myocardial infarction patients. *Hypertension* 58, 1049–1056. doi: 10.1161/HYPERTENSIONAHA.111.176644

Montano, N., Furlan, R., Guzzetti, S., McAllen, R. M., and Julien, C. (2009). Analysis of sympathetic neural discharge in rats and humans. *Philos. Trans. A Math. Phys. Eng. Sci.* 367, 1265–1282. doi: 10.1098/rsta.2008.0285

Montano, N., Ruscone, T. G., Porta, A., Lombardi, F., Pagani, M., and Malliani, A. (1994). Power spectrum analysis of heart rate variability to assess the changes in sympathovagal balance during graded orthostatic tilt. *Circulation* 90, 1826–1831. doi: 10.1161/01.cir.90.4.1826

Pagani, M., Montano, N., Porta, A., Malliani, A., Abboud, F., Birkett, C., et al. (1997). Relationship between spectral components of cardiovascular variabilities and direct measures of muscle sympathetic nerve activity in humans. *Circulation* 95, 1441–1448. doi: 10.1161/01.cir.95.6.1441

Pinna, G. D., Maestri, R., Raczak, G., and La Rovere, M. T. (2002). Measuring baroreflex sensitivity from the gain function between arterial pressure and heart period. *Clin. Sci. (Lond).* 103, 81–88. doi: 10.1042/cs1030081

Ponikowski, P., Voors, A. A., Anker, S. D., Bueno, H., Cleland, J. G., Coats, A. J., et al. (2016). 2016 ESC Guidelines for the diagnosis and treatment of acute and chronic heart failure: the task force for the diagnosis and treatment of acute and chronic heart failure of the European Society of Cardiology (ESC). Developed with the special contribution of the Heart Failure Association (HFA) of the ESC. *Eur. J. Heart Fail.* 18, 891–975. doi: 10.1002/ejhf.592

Poole-Wilson, P. A., Cleland, J. G., Di Lenarda, A., Hanrath, P., Komajda, M., Metra, M. J., et al. (2002). Rationale and design of the carvedilol or metoprolol European trial in patients with chronic heart failure: COMET. *Eur. J. Heart Fail.* 4, 321–329. doi: 10.1016/s1388-9842(02)00025-9

Poole-Wilson, P. A., Swedberg, K., Cleland, J. G., Di Lenarda, A., Hanrath, P., Komajda, M., et al. (2003). Comparison of carvedilol and metoprolol on clinical outcomes in patients with chronic heart failure in the Carvedilol or Metoprolol European Trial (COMET): randomised controlled trial. *Lancet* 362, 7–13. doi: 10.1016/S0140-6736(03)13800-7

Stanek, B., Frey, B., Hülsmann, M., Berger, R., Sturm, B., Strametz-Juranek, J., et al. (2001). Prognostic evaluation of neurohumoral plasma levels before and during beta-blocker therapy in advanced left ventricular dysfunction. *J. Am. Coll. Cardiol.* 38, 436–442. doi: 10.1016/s0735-1097(01)01383-3

Stauss, H. M., Anderson, E. A., Haynes, W. G., and Kregel, K. C. (1998). Frequency response characteristics of sympathetically mediated vasomotor waves in humans. *Am. J. Physiol.* 274, H1277–H1283. doi: 10.1152/ajpheart.1998.274.4.H1277

Sunagawa, K., Sato, T., and Kawada, T. (2001). Integrative sympathetic baroreflex regulation of arterial pressure. *Ann. N. Y. Acad. Sci.* 940, 314–323. doi: 10.1111/j.1749-6632.2001.tb03687.x

Toschi-Dias, E., Rondon, M. U. P. B., Cogliati, C., Paolocci, N., Tobaldini, E., and Montano, N. (2017). Contribution of autonomic reflexes to the hyperadrenergic state in heart failure. *Front. Neurosci.* 11:162. doi: 10.3389/fnins.2017.00162

Toschi-Dias, E., Trombetta, I. C., Dias da Silva, V. J., Maki-Nunes, C., Cepeda, F. X., Alves, M. J., et al. (2013). Time delay of baroreflex control and oscillatory pattern of sympathetic activity in patients with metabolic syndrome and obstructive sleep apnea. *Am. J. Physiol. Heart Circ. Physiol.* 304, H1038–H1044. doi: 10.1152/ajpheart.00848.2012

Triposkiadis, F., Karayannis, G., Giamouzis, G., Skoularigis, J., Louridas, G., and Butler, J. (2009). The sympathetic nervous system in heart failure physiology, pathophysiology, and clinical implications. *J. Am. Coll. Cardiol.* 54, 1747–1762. doi: 10.1016/j.jacc.2009.05.015

Vallbo, A. B., Hagbarth, K. E., Torebjork, H. E., and Wallin, B. G. (1979). Somatosensory, proprioceptive, and sympathetic activity in human peripheral nerves. *Physiol. Rev.* 59, 919–957. doi: 10.1152/physrev.1979.59.4.919

van de Borne, P., Montano, N., Pagani, M., Oren, R., and Somers, V. K. (1997). Absence of low-frequency variability of sympathetic nerve activity in severe heart failure. *Circulation* 95, 449–454. doi: 10.1161/01.cir.95.6.1449

Conflict of Interest: The authors declare that the research was conducted in the absence of any commercial or financial relationships that could be construed as a potential conflict of interest.

frontiers in Neuroscience

ORIGINAL RESEARCH
published: 13 September 2021
doi: 10.3389/fnins.2021.690919

Central Administration of Hydrogen Sulfide Donor NaHS Reduces Iba1-Positive Cells in the PVN and Attenuates Rodent Angiotensin II Hypertension

*Basak Donertas Ayaz[1,2], Aline C. Oliveira[3], Wendi L. Malphurs[1], Ty Redler[1], Alan Moreira de Araujo[4], Ravindra K. Sharma[3], Basar Sirmagul[2] and Jasenka Zubcevic[1,5]**

[1] Department of Physiological Sciences, College of Veterinary Medicine, University of Florida, Gainesville, FL, United States, [2] Department of Pharmacology, College of Medicine, Eskisehir Osmangazi University, Eskisehir, Turkey, [3] Department of Physiology and Functional Genomics, College of Medicine, University of Florida, Gainesville, FL, United States, [4] Department of Pharmacodynamics, College of Pharmacy, University of Florida, Gainesville, FL, United States, [5] Department of Physiology and Pharmacology, Center for Hypertension and Precision Medicine, College of Medicine, University of Toledo, Toledo, OH, United States

OPEN ACCESS

Edited by:
Yan Yao,
State Key Laboratory of Cardiovascular Disease, Fuwai Hospital, Chinese Academy of Medical Sciences, China

Reviewed by:
Barbara Falquetto,
University of São Paulo, Brazil
Renata Maria Lataro,
Federal University of Santa Catarina, Brazil

***Correspondence:**
Jasenka Zubcevic
Jasenka.Zubcevic@utoledo.edu

Specialty section:
This article was submitted to Autonomic Neuroscience, a section of the journal Frontiers in Neuroscience

Received: 04 April 2021
Accepted: 10 August 2021
Published: 13 September 2021

Citation:
Donertas Ayaz B, Oliveira AC, Malphurs WL, Redler T, de Araujo AM, Sharma RK, Sirmagul B and Zubcevic J (2021) Central Administration of Hydrogen Sulfide Donor NaHS Reduces Iba1-Positive Cells in the PVN and Attenuates Rodent Angiotensin II Hypertension. Front. Neurosci. 15:690919. doi: 10.3389/fnins.2021.690919

Hydrogen sulfide (H_2S) is a gaseous signaling molecule with neuromodulatory, anti-inflammatory, and anti-hypertensive effects. Here, we investigate whether chronic intracerebroventricular (ICV) infusion of sodium hydrosulfide (NaHS), an H_2S donor, can alleviate angiotensin II (Ang II)–induced hypertension (HTN), improve autonomic function, and impact microglia in the paraventricular nucleus (PVN) of the hypothalamus, a brain region associated with autonomic control of blood pressure (BP) and neuroinflammation in HTN. Chronic delivery of Ang II (200 ng/kg/min, subcutaneous) for 4 weeks produced a typical increase in BP and sympathetic drive and elevated the number of ionized calcium binding adaptor molecule 1–positive ($Iba1^+$) cells in the PVN of male, Sprague–Dawley rats. ICV co-infusion of NaHS (at 30 and/or 60 nmol/h) significantly attenuated these effects of Ang II. Ang II also increased the abundance of cecal *Deltaproteobacteria* and *Desulfovibrionales*, among others, which was prevented by ICV NaHS co-infusion at 30 and 60 nmol/h. We observed no differences in circulating H_2S between the groups. Our results suggest that central H_2S may alleviate rodent HTN independently from circulating H_2S via effects on autonomic nervous system and PVN microglia.

Keywords: hydrogen sulfide, hypertension, microglia, neuroinflammation, paraventricular nucleus, microbiota, angiotensin

INTRODUCTION

Uncontrolled, treatment-resistant hypertension (HTN) develops in part due to aberrant autonomic mechanisms characterized by hyperactivity of the sympathetic nervous system (Tsioufis et al., 2011) and impairment of cardiac vagal modulation (Mancia and Grassi, 2014). The paraventricular nucleus (PVN) of the hypothalamus is an important hub integrating a variety of central and peripheral signals in regulation of autonomic pathways for cardiovascular homeostasis

(Badoer, 2001; Coote, 2005). Neuroinflammation of PVN, marked by microglia activation and increased microglial cell number (Shi et al., 2010; Santisteban et al., 2015; Sharma et al., 2019), has been associated with sympathetic over-activity and fluid imbalance in rodent HTN, suggesting that microglia may exert effects on autonomic regulation of blood pressure (BP). Microglia are the resident immune cells of the brain involved in the regular maintenance of the neural environment and pruning of synapses, and aberrant pruning and exacerbated neuroinflammation involving activated microglia are implicated in the various neuropathologies (Paolicelli and Ferretti, 2017; Sakai, 2020; Geloso and D'Ambrosi, 2021). Consequently, significant research to date has attempted to understand the role of microglia in many inflammatory conditions including in HTN.

Hydrogen sulfide (H_2S) is an endogenous signaling molecule produced by the gut bacteria and the host (Kimura, 2014; Donertas Ayaz and Zubcevic, 2020). Impairment in H_2S homeostasis has been implicated in development of HTN (Zhong et al., 2003; Yan et al., 2004; Yang et al., 2008; Huang et al., 2015) and studies using H_2S donors have alluded to a therapeutic potential of H_2S in HTN. To date, the BP-lowering effects of H_2S have been primarily attributed to direct vascular effects in various animal models of HTN (d'Emmanuele di Villa Bianca et al., 2015; Xue et al., 2015; Ni et al., 2018; Xiao et al., 2018; Li et al., 2019b; Zhu et al., 2021). However, the central effects of H_2S cannot be discounted, as H_2S-producing enzymes are present in the brain (Abe and Kimura, 1996). Moreover, H_2S is a gaseous molecule that reportedly crosses the blood–brain barrier, which may affect the central nervous system (CNS) directly (Che et al., 2018). However, a few studies to date have investigated central effects of H_2S in HTN (Streeter et al., 2011; Yu et al., 2015; Liang et al., 2017) while precise mechanisms of central BP-lowering effects of H_2S remain unknown.

Hydrogen sulfide is a neuromodulator with neuroprotective effects (Zhang and Bian, 2014). It can freely cross the cell membrane to regulate several intracellular signaling processes (Zhang and Bian, 2014). Recent studies showed that H_2S can attenuate glial-mediated neuroinflammation (Xuan et al., 2012; Lee et al., 2013, 2016), and that the PVN is a site of action of H_2S (Liang et al., 2017). Treatment with H_2S donors *in vitro* can decrease pro-inflammatory cytokines in glial cells (Lee et al., 2016), while intraperitoneal injection of sodium hydrosulfide (NaHS), an H_2S donor, lowers pro-inflammatory cytokines and gliosis in the hippocampus (Xuan et al., 2012). Thus, the first objective of this study was to test whether chronic, intracerebroventricular (ICV) infusion of NaHS may alleviate rodent angiotensin II (Ang II)–induced HTN and reduce microglia cell counts in the PVN. Rodent and human HTN have also been linked with gut dysbiosis (Yang et al., 2015; Li et al., 2017; Yan et al., 2017) and inhibition of microglial activity in the PVN can rebalance the gut microbiota in HTN (Sharma et al., 2019). Thus, we further hypothesized that central NaHS administration may attenuate Ang II-induced gut dysbiosis.

The present study shows that chronic ICV infusion of NaHS attenuated Ang II-induced increase in microglial cells in the PVN, alleviated Ang II-dependent autonomic dysfunction, and reduced BP. Lastly, ICV infusion of NaHS prevented Ang II-dependent elevation in several cecal bacterial taxa, including but not limited to the sulfate-reducing *Desulfovibrionales*. No change in circulating H_2S levels was observed in any of the treatment groups. Thus, H_2S may have direct central neuromodulating and neuroimmune effects that are beneficial for cardiovascular homeostasis, and thus presents a viable anti-hypertensive target.

MATERIALS AND METHODS

All experimental procedures were approved by the University of Florida Institutional Animal Care and Use Committee and complied with the standards stated in the National Institutes of Health Guide for the Care and Use of Laboratory Animals.

Animals

Eight-week-old, male, Sprague–Dawley (SD) rats (n = 31) were purchased from Charles River Laboratories (United States) and housed individually in a temperature-controlled room (22 ± 1°C) of University of Florida Animal Care Service Facility with a 12:12-h light–dark cycle with food and water *ad libitum*.

Experimental Procedures

NaHS and Angiotensin II Delivery, BP Measurement, and Variability Analysis of Systolic BP and Heart Rate

A schematic of the timeline used is shown in **Figure 1**. BP and heart rate (HR) measurements were performed in conscious freely moving rats using radio-telemetry transmitters (HD-S10 model, DSI, Saint Paul, MN, United States, Ponemah software v.6.11). Telemetry transmitters were implanted into the descending abdominal aorta of all rats as previously described (Huetteman and Bogie, 2009). After 7 days of recovery, baseline measurements were taken for 48 h. Then, an ICV brain cannula (ALZET, Durect Corp., Cupertino, CA, United States, Brain Infusion Kit 1 3–5 mm) was implanted into left cerebral ventricle in all rats (coordinates: 1.3 mm anterior–posterior from bregma, 1.50 medial–lateral, and 4.50 dorsal–ventral from skull surface, Paxinos and Watson Rat Brain Atlas) to deliver either NaHS (30 and 60 nmol/h in separate groups of rats; Sigma-Aldrich, United States, CAS Number 207683-19-0) or vehicle phosphate-buffered saline (PBS, 1 × without calcium and magnesium; CORNING Cellgro) for 4 weeks. ICV cannulas were connected to subcutaneous (SC) osmotic minipumps (ALZET, Durect Corp., model 2004, rate of infusion 0.25–0.28 μl per hour). A separate SC osmotic minipump was implanted as well to deliver either Ang II (200 ng/kg/min in normal saline; Bachem, Torrance, CA, United States) or vehicle (normal saline) for 4 weeks. Thus, animals were divided in the following groups: (1) Control (n = 4, ICV PBS and SC normal saline); (2) Ang II (n = 5, ICV PBS + SC Ang II); (3) 30 nmol/h NaHS (n = 4, ICV 30 nmol/h NaHS + SC PBS); (4) 60 nmol/h NaHS (n = 4, ICV 60 nmol/h NaHS + SC PBS); (5) 30 nmol/h NaHS + Ang II (n = 7, ICV 30 nmol/h NaHS + SC Ang II); (6) 60 nmol/h NaHS + Ang II (n = 7, ICV 60 nmol/h NaHS + SC Ang II). After 7 days of recovery, BP and HR measurements were performed once a week for 48 h for 4 weeks. Mean arterial pressure (MAP),

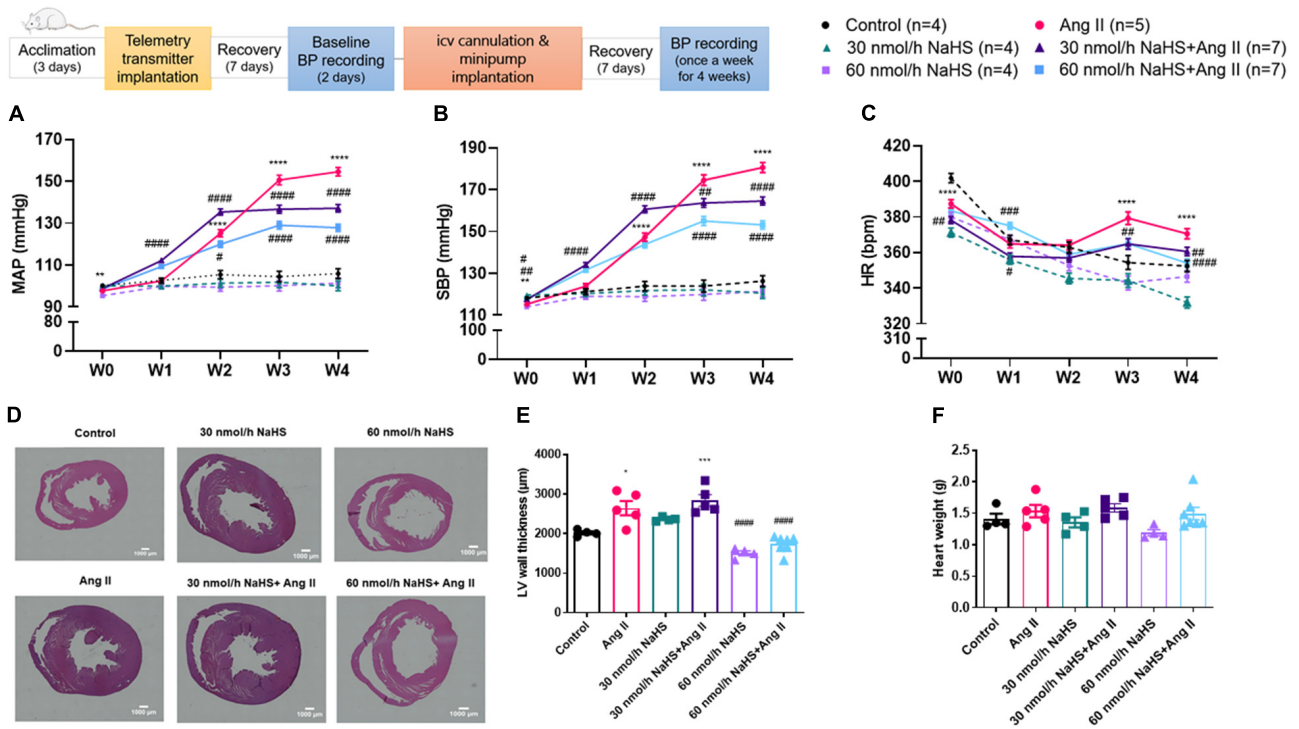

FIGURE 1 | Schematic representation of study design (ICV: intracerebroventricular; BP: blood pressure). Chronic ICV infusion of NaHS attenuated angiotensin (Ang) II–induced increase in **(A)** mean arterial pressure (MAP) and **(B)** systolic blood pressure (SBP) in Sprague–Dawley rats. **(C)** Ang II effect on heart rate (HR). Data was analyzed by Kruskal–Wallis *H* test followed by Tukey's multiple comparisons test and presented as mean ± SEM. $^{****}p < 0.0001$, $^{***}p < 0.001$, $^{**}p < 0.01$, $^{*}p < 0.05$ control vs. Ang II. $^{\#\#\#\#}p < 0.0001$, $^{\#\#\#}p < 0.001$, $^{\#\#}p < 0.01$, $^{\#}p < 0.05$ Ang II vs. NaHS/Ang II-treated rats. In panels **(D–E)**, Ang II-induced left ventricular (LV) hypertrophy as measured by LV thickness was attenuated by 60 nmol/h but not 30 nmol/h NaHS ICV infusion. In panel **(D)**, representative images of H&E stain in ventricular sections of experimental groups (magnification: ×4, scale bar = 1000 μm). In panel **(E)**, LV wall thickness (μm) and **(F)** heart weight (g). Data were analyzed by one-way ANOVA followed by Tukey's multiple comparisons test and presented as mean ± SEM. $^{***}p < 0.001$, $^{*}p < 0.05$ Control vs. all other groups. $^{\#\#\#\#}p < 0.0001$ Ang II vs. all other groups.

systolic blood pressure (SBP), and HR were automatically derived from the Ponemah software (DSI, Ponemah software v.6.11). Variations in SBP and inter-beat interval (IBI) were computed to assess cardiovascular autonomic modulation using Ponemah's variability analysis module. Variations have been categorized into three frequency bands [very low frequency (VLF) at 0–0.26 Hz, low frequency (LF) at 0.26–0.76 Hz, and high frequency (HF) at 0.76–3.3 Hz (Tayler et al., 2018)] using Fast Fourier transform, and these bands were automatically derived from Ponemah software. To assess variability of SBP, total power of SBP (TP_{SBP}), an index of global variability, and LF of SBP (LF_{SBP}), reflecting vasomotor sympathetic modulation (deBoer et al., 1987; Madwed et al., 1989), were derived. For assessment of HR variability, total power of IBI (TP_{IBI}), VLF of IBI (VLF_{IBI}), reportedly related to changes in the renin–angiotensin system and thermoregulation (Taylor et al., 1998; Pumprla et al., 2002) and parasympathetic modulation (Taylor et al., 1998), LF of IBI (LF_{IBI}), which reportedly contains both vagal and cardiac sympathetic components (Shaffer and Ginsberg, 2017), HF of IBI (HF_{IBI}), reflecting cardiac parasympathetic modulation (Pagani et al., 1986), normalized LF of IBI, representing the relative value of LF_{IBI} power component in comparison to the TP, normalized HF of IBI, representing the relative value of HF_{IBI} power component in comparison to the TP, and LF/HF of the IBI (LH/HF_{IBI}), an index of cardiac autonomic balance (Montano et al., 1994), were derived. For these analyses, the averaged SBP and HR variability data was collected for 5 min of every hour for 48 h.

Tissue and Cecal Content Collection

At study endpoint, rats were euthanized using 4% isoflurane in 95:5 O_2/CO_2. Whole cecal content was collected from all rats and stored at −80°C until analysis. Whole brains were post-fixed in fresh 2% paraformaldehyde (PFA) at 4°C overnight, then transferred to 30% sucrose solution at 4°C for cryoprotection. Brains were then placed in OCT (Tissue-Tek; Sakura Finetek, Torrance, CA, United States) and frozen at −80°C until sectioning. Whole hearts were collected and post-fixed in fresh 2% PFA at 4°C for 48 h, after which they were transferred to 70% ethanol and stored at 4°C until infiltration process.

Histology

Before the infiltration process, PFA-fixed hearts were cut transversely into three pieces. On the dorsal aspect of the heart, the first cut was made right below the pulmonary artery, and the second cut was made 5 mm below the first cut. The middle

TABLE 1 | Changes in blood pressure and heart rate in response to subcutaneous Angiotensin II and intracerebroventricular NaHS infusion.

Parameter	Weeks	Control (n = 4) (*)	Ang II (n = 5) (#)	30 nmol/h NaHS (n = 4)	30 nmol/h NaHS + Ang II (n = 7) (∧)	60 nmol/h NaHS (n = 4)	60 nmol/h NaHS + Ang II (n = 7)
MAP (mmHg)	0	100.25 ± 0.59	97.72 ± 0.53**	100.03 ± 0.59##	98.78 ± 0.45*	95.30 ± 0.59****, ##	98.59 ± 0.45*
	1	102.70 ± 1.19ϕ	102.44 ± 1.06ϕϕϕϕ	99.87 ± 1.19	112.09 ± 0.90ϕϕϕϕ, ****, ####	99.81 ± 1.19ϕϕϕϕ	109.30 ± 0.90ϕϕϕϕ, ****, ####, ∧
	2	105.39 ± 1.98ϕ	125.17 ± 1.77ϕϕϕϕ, ****	101.29 ± 1.98####	135.32 ± 1.50ϕϕϕϕ, ****, ####	99.39 ± 1.98ϕ, *, ####	119.96 ± 1.50ϕϕϕϕ, ****, #, ∧∧∧∧
	3	104.44 ± 2.54	150.62 ± 2.27ϕϕϕϕ, ****	101.80 ± 2.54####	136.70 ± 1.92ϕϕϕϕ, ****, ####	100.14 ± 2.54####	129.04 ± 1.92ϕϕϕϕ, ****, ####, ∧∧
	4	105.91 ± 2.35ϕ	154.54 ± 2.10ϕϕϕϕ, ****	100.06 ± 2.35####	137.16 ± 1.78ϕϕϕϕ, ****, ####	101.38 ± 2.35ϕ, ####	127.80 ± 1.78ϕϕϕϕ, ****, ####,∧∧∧
SBP (mmHg)	0	118.15 ± 0.76	115.24 ± 0.68**	119.67 ± 0.76####	117.50 ± 0.57#	114.10 ± 0.76***	117.58 ± 0.57##
	1	121.27 ± 1.46ϕ	123.83 ± 1.30ϕϕϕϕ	120.32 ± 1.46	134.02 ± 1.10ϕϕϕϕ, ****, ####	119.00 ± 1.46ϕϕϕϕ, #	131.67 ± 1.10ϕϕϕϕ, ****, ####
	2	123.95 ± 2.23ϕϕ	147.29 ± 1.99ϕϕϕϕ, ****	121.76 ± 2.23####	160.59 ± 1.68ϕϕϕϕ, ****, ####	118.91 ± 2.23ϕ, ####	143.82 ± 1.68ϕϕϕϕ, ****, ∧∧∧∧
	3	123.92 ± 2.84ϕ	174.48 ± 2.54ϕϕϕϕ, ****	122.09 ± 2.84####	163.64 ± 2.15ϕϕϕϕ, ****, ##	119.90 ± 2.84ϕ, ####	154.98 ± 2.15ϕϕϕϕ, ****, ####, ∧∧
	4	126.27 ± 2.65ϕϕ	180.53 ± 2.37ϕϕϕϕ, ****	120.50 ± 2.65####	164.57 ± 2.00ϕϕϕϕ, ****, ####	121.37 ± 2.65ϕϕ, ####	153.13 ± 2.00ϕϕϕϕ, ****, ####, ∧∧∧∧
HR (bpm)	0	401.86 ± 2.62	387.45 ± 2.35****	371.19 ± 2.62****, ####	378.20 ± 1.98****, ##	379.99 ± 2.62****, #	383.46 ± 1.98****
	1	367.12 ± 2.58ϕϕϕϕ	364.86 ± 2.31ϕϕϕϕ	355.97 ± 2.58ϕϕϕϕ, **, #	357.91 ± 1.95ϕϕϕϕ, **, #	367.14 ± 2.58ϕϕϕϕ	375.04 ± 1.95ϕϕϕ, *, ###, ∧∧∧∧
	2	362.90 ± 3.00ϕϕϕϕ	364.13 ± 2.69ϕϕϕϕ	345.38 ± 3.00ϕϕϕϕ, ****, ####	356.93 ± 2.27ϕϕϕϕ	352.66 ± 3.00ϕϕϕϕ, *, ##	358.98 ± 2.27ϕϕϕϕ
	3	354.31 ± 3.93ϕϕϕϕ	379.33 ± 3.52ϕ, ****	344.26 ± 3.93ϕϕϕϕ, ####	364.89 ± 2.97ϕϕϕϕ, *, ##	342.88 ± 3.93ϕϕϕϕ, *, ####	364.99 ± 2.97ϕϕϕϕ, *, ##
	4	352.36 ± 3.23ϕϕϕϕ	370.59 ± 2.89ϕϕϕϕ, ****	331.86 ± 3.23ϕϕϕϕ, ****, ####	360.60 ± 2.44ϕϕϕϕ, *, ##	346.50 ± 3.23ϕϕϕϕ, ####	354.02 ± 2.44ϕϕϕϕ, ####

Ang II, Angiotensin II; MAP, mean arterial pressure; SBP, systolic blood pressure; HR, heart rate.
Data was analyzed by Kruskal–Wallis H test followed by Tukey's multiple comparisons test and presented as mean ± SEM.
$^{\phi\phi\phi\phi}p < 0.0001$, $^{\phi\phi\phi}p < 0.001$, $^{\phi\phi}p < 0.01$, $^{\phi}p < 0.05$ *vs. Baseline.*
$^{****}p < 0.0001$, $^{***}p < 0.001$, $^{**}p < 0.01$, $^{*}p < 0.05$ *Control vs. all other groups.*
$^{\#\#\#\#}p < 0.0001$, $^{\#\#\#}p < 0.001$, $^{\#\#}p < 0.01$, $^{\#}p < 0.05$ *Ang II vs. NaHS-treated groups.*
$\wedge\wedge\wedge\wedge p < 0.0001$, $\wedge\wedge\wedge p < 0.001$, $\wedge\wedge p < 0.01$, $\wedge p < 0.05$ *30 nmol/h NaHS/Ang II vs. 60 nmol/h NaHS/Ang II.*

section was then embedded in paraffin using the Tissue-Tek VIP 5 vacuum infiltration processor (Sakura Finetek, United States) and cross-sectioned at 4-μm thickness using a microtome (Accu-Cut SRM 200; Sakura Finetek, United States). Sections with knife trace and/or folding were excluded and one representative slide per rat was stained with H&E using Leica's ST5020 automated multi-stainer in accordance with the manufacturer's protocol. Slides were imaged on a Keyence microscope (BZ-X810) under equal conditions and scanned and stitched using × 4 objective. The cross-sectional thickness of the left ventricular (LV) wall was measured from four different areas for one section/rat with ImageJ software, and the results were averaged.

Immunohistochemistry

Coronal sections of the hypothalamic PVN (40 μm in thickness; taken at −0.72 mm to −1.92 mm from Bregma, Paxinos and Watson Rat Brain Atlas) were obtained using a cryostat (MICROM HM 505 E; GMI, Ramsey, MN, United States). PVN sections were mounted on superfrost plus slides (Fisher). Slides were stored at −20°C until immunohistochemistry (IHC). Ionized calcium binding adaptor molecule-1 (Iba1) is the most widely used microglia marker of a protein that participates in membrane ruffling and phagocytosis in activated microglia, and elevated level of Iba1 refers to microglia activation (Ohsawa et al., 2004; Jurga et al., 2020). IHC and quantification of Iba1–positive ($Iba1^+$) cells in the PVN were performed as previously described (Oliveira et al., 2018; Sharma et al., 2018). Briefly, non-specific binding was blocked with 10% goat serum and Triton X-100 (0.3% in PBS) followed by incubation with rabbit anti-Iba1 primary antibody (1:500; Wako, Richmond, VA, United States) at 4°C overnight. After this, slides were incubated with Alexa Fluor 488–labeled anti-rabbit secondary antibody (1:500; Invitrogen, Carlsbad, CA, United States) for 1 h at room temperature. Slides were cover-slipped using Vectashield mounting media (Vector Labs, Burlingame, CA, United States). Images were taken using a Keyence microscope (BZ-X810) under ×20 objective. For every rat, a stack of 15 PVN images 2 μm apart was compressed to a single image using BZ-X800 Viewer and were analyzed using Fiji-ImageJ cell counter.

Analysis of Cecal Bacterial Communities by 16S rRNA Gene Sequencing

Cecal fecal microbial DNA was extracted using MO BIO's PowerMag Soil DNA Isolation Kit (catalog no. 27100-4-EP) as per manufacturer's instructions. Bacterial 16S rRNA genes were amplified using primers targeting the V4 region (515F 5′-GTGCCAGCMGCCGCGGTAA-3′ and 806R 5′-GGACTACHVGGGTWTCTAAT-3′), as previously described (Kozich et al., 2013). PCR amplicons were then sequenced in an Illumina MiSeq using the 300-bp paired-end kit (v.3). Sequences were denoised, taxonomically classified using Greengenes (v. 13_8), and clustered into 97% similarity operational taxonomic units (OTUs) with the mothur software (v. 1.39.5) (Schloss et al., 2009). OTUs that were considered putative contaminants were removed if their mean abundance in controls reached or exceeded 25% of their mean abundance in specimens. OTUs were then classified into taxonomic assignments. Assigned taxonomy were organized into an OTU table. Sequencing data are avaliable in the **Supplementary Material**.

Measurement of Plasma H_2S Levels

Hydrogen sulfide concentration in plasma was assayed spectrophotometrically as described previously (Zhuo et al., 2009). Briefly, 75 μl plasma mixed with 250 μl 1% (w/v) zinc acetate (zinc acetate, anhydrous, 99.9+%; Alfa Aesar, Fisher, United States, CAS Number 557-34-6) and 425 μl distilled water. Then, 20 mM *N*-dimethyl-*p*-phenylenediamine oxalate (Fisher, United States, CAS Number 207683-19-0 CAS 62778-12-5) in 7.2 μM HCI (133 μI) (Fisher, United States, CAS Number 7647-01-0, 7732-18-5) and 30 mM iron trichloride ($FeCl_3$) (iron (III) chloride, anhydrous, 98%; Alfa Aesar Fisher, United States, CAS Number 7705-08-0) in 1.2 μM HCI (133 μI) were added and incubated for 10 min at room temperature. Protein in the plasma was removed by adding 250 μl of 50% trichloroacetic acid [Trichloroacetic Acid (Crystalline/Certified); Fisher, United States, CAS Number 76-03-9] to the reaction mixture and pelleted by centrifugation at 12,000 × *g* for 15 min. Then 300 μl of samples were put into each well and absorbance of the solution was read with a spectrophotometer (BioTek Synergy Mx) at 670 nm in a 96-well plate (Fisher). All samples were assayed in duplicate and blank subtracted absorbance values were averaged.

Data Presentation, Bioinformatics, and Statistical Analysis

Significant differences in BP and variability data were analyzed using IBM SPSS Statistics version 21.0 via Kruskal–Wallis *H* test followed by Tukey's multiple comparisons test and were presented using GraphPad Prism version 9.0. Significant differences in LV thickness, the number of $Iba1^+$ microglial cells, H_2S plasma assay, Shannon diversity index, and *Firmicutes*/*Bacteroidetes* (F/B) ratio were determined using GraphPad Prism version 9.0 with one-way ANOVA followed by Tukey's multiple comparisons test or Kruskal–Wallis test where appropriate. Normality of distribution was tested using the Shapiro–Wilk test. A p value < 0.05 was considered statistically significant. Data are presented as mean ± SEM. Shannon diversity index is presented as minimum to maximum with a median.

Statistical analyses of cecal bacterial communities were conducted in R. Diversity within a sample is referred to as alpha diversity, and diversity between samples is referred to as beta diversity. Alpha diversity was estimated with the Shannon index on raw OTU abundance tables after filtering out contaminants. The significance of diversity differences was tested with ANOVA. To estimate beta diversity, OTUs occurring with a count of less than 3 in at least 10% of the samples were excluded and then computed using Bray–Curtis indices. Beta diversity, emphasizing differences across samples, was visualized using principal coordinate analysis (PCoA) ordination. Variation in community structure was assessed with permutational multivariate analyses of variance (PERMANOVA) with treatment group as the main fixed factor and using 9,999 permutations for significance testing. A p value < 0.05 was considered statistically significant. F/B ratio

TABLE 2 | Changes in autonomic variables in response to subcutaneous Angiotensin II and intracerebroventricular NaHS infusion.

Parameter	Weeks	Control (n = 4) (*)	Ang II (n = 5) (#)	30 nmol/h NaHS (n = 4)	30 nmol/h NaHS + Ang II (n = 7) (∧)	60 nmol/h NaHS (n = 4)	60 nmol/h NaHS + Ang II (n = 7)
LF of SBP ($mmHg^2$)	0	1.35 ± 0.06	$1.70 \pm 0.05^{****}$	$1.42 \pm 0.06^{\#\#\#}$	$1.44 \pm 0.04^{\#\#\#}$	$1.24 \pm 0.06^{\#\#\#\#}$	$1.24 \pm 0.04^{\#\#\#\#, \wedge\wedge}$
	1	$2.31 \pm 0.16^{\phi\phi\phi\phi}$	$1.57 \pm 0.14^{***}$	$1.35 \pm 0.16^{****}$	$1.58 \pm 0.12^{***}$	$1.89 \pm 0.16^{\phi\phi\phi\phi}$	$1.66 \pm 0.12^{\phi\phi\phi, **}$
	2	$1.75 \pm 0.14^{\phi\phi}$	$2.62 \pm 0.12^{\phi\phi\phi\phi, ****}$	$1.37 \pm 0.14^{*, \#\#\#\#}$	$1.98 \pm 0.10^{\phi\phi\phi\phi, \#\#\#\#}$	$1.74 \pm 0.14^{\phi\phi\phi\phi, \#\#\#\#}$	$1.76 \pm 0.10^{\phi\phi\phi\phi, \#\#\#\#}$
	3	1.51 ± 0.17	$2.66 \pm 0.15^{\phi\phi\phi\phi, ****}$	$1.29 \pm 0.17^{\#\#\#\#}$	$2.24 \pm 0.13^{\phi\phi\phi\phi, **, \#}$	$1.61 \pm 0.17^{\phi, \#\#\#\#}$	$2.10 \pm 0.13^{\phi\phi\phi\phi, **, \#\#}$
	4	1.59 ± 0.13	$2.51 \pm 0.11^{\phi\phi\phi\phi, ****}$	$1.31 \pm 0.13^{\#\#\#\#}$	$2.03 \pm 0.10^{\phi\phi\phi\phi, **, \#\#}$	$1.83 \pm 0.13^{\phi\phi\phi\phi, \#\#\#\#}$	$1.87 \pm 0.10^{\phi\phi\phi\phi, \#\#\#\#}$
Total Power of SBP	0	6.22 ± 0.25	6.27 ± 0.23	6.66 ± 0.25	$6.99 \pm 0.19^{*, \#}$	$4.27 \pm 0.25^{****, \#\#\#\#}$	$5.74 \pm 0.19^{\wedge\wedge\wedge\wedge}$
	1	$10.16 \pm 0.62^{\phi\phi\phi\phi}$	$6.84 \pm 0.56^{****}$	$5.85 \pm 0.62^{****}$	$8.45 \pm 0.47^{\phi\phi, *, \#}$	$7.42 \pm 0.62^{\phi\phi\phi\phi, **}$	$8.27 \pm 0.47^{\phi\phi\phi\phi, *}$
	2	7.49 ± 0.65	$12.03 \pm 0.58^{\phi\phi\phi\phi, ****}$	$5.93 \pm 0.65^{\#\#\#\#}$	$12.17 \pm 0.49^{\phi\phi\phi\phi, ****}$	$6.12 \pm 0.65^{\phi\phi, \#\#\#\#}$	$9.89 \pm 0.49^{\phi\phi\phi\phi, **, \#\#, \wedge\wedge}$
	3	7.42 ± 0.75	$13.46 \pm 0.67^{\phi\phi\phi\phi, ****}$	$5.82 \pm 0.75^{\#\#\#\#}$	$11.74 \pm 0.56^{\phi\phi\phi\phi, ****}$	$6.55 \pm 0.75^{\phi\phi, \#\#\#\#}$	$10.84 \pm 0.56^{\phi\phi\phi\phi, ***, \#\#}$
	4	7.10 ± 0.60	$12.55 \pm 0.54^{\phi\phi\phi\phi, ****}$	$5.63 \pm 0.60^{\#\#\#\#}$	$11.18 \pm 0.45^{\phi\phi\phi\phi, ****}$	$7.16 \pm 0.60^{\phi\phi\phi\phi, \#\#\#\#}$	$9.89 \pm 0.45^{\phi\phi\phi\phi, ***, \#\#\#, \wedge}$
VLF of IBI (ms^2)	0	3.20 ± 0.50	4.07 ± 0.45	3.60 ± 0.50	$4.49 \pm 0.38^{*}$	2.98 ± 0.50	$3.18 \pm 0.38\wedge$
	1	$5.76 \pm 0.32^{\phi\phi\phi\phi}$	$4.35 \pm 0.28^{***}$	$3.96 \pm 0.32^{****}$	$4.85 \pm 0.24^{*}$	$4.13 \pm 0.32^{\phi, ***}$	$4.14 \pm 0.24^{\phi, ****, \wedge}$
	2	$5.33 \pm 0.39^{\phi\phi\phi}$	4.75 ± 0.35	4.71 ± 0.39	$5.80 \pm 0.30^{\phi\phi, \#}$	$4.65 \pm 0.39^{\phi\phi}$	$5.02 \pm 0.30^{\phi\phi\phi\phi}$
	3	$7.10 \pm 0.36^{\phi\phi\phi\phi}$	$4.06 \pm 0.32^{****}$	$4.25 \pm 0.36^{****}$	$4.35 \pm 0.27^{****}$	$5.29 \pm 0.36^{\phi\phi\phi\phi, ***, \#}$	$4.90 \pm 0.27^{\phi\phi\phi\phi, ****, \#}$
	4	$7.17 \pm 0.40^{\phi\phi\phi\phi}$	$4.20 \pm 0.35^{****}$	$3.90 \pm 0.40^{****}$	$4.23 \pm 0.30^{****}$	$5.59 \pm 0.40^{\phi\phi\phi\phi, **, \#\#}$	$4.72 \pm 0.30^{\phi\phi\phi, ****}$
LF of IBI (ms^2)	0	0.79 ± 0.32	1.20 ± 0.29	0.79 ± 0.32	1.53 ± 0.24	0.85 ± 0.32	0.88 ± 0.24
	1	1.32 ± 0.11	1.16 ± 0.10	$0.99 \pm 0.11^{*}$	1.23 ± 0.08	1.18 ± 0.11	$0.93 \pm 0.08^{**, \wedge}$
	2	1.51 ± 0.16	$1.01 \pm 0.14^{*}$	$1.22 \pm 0.16^{\#}$	$1.54 \pm 0.12^{\#\#}$	1.38 ± 0.16	1.27 ± 0.12
	3	$1.57 \pm 0.13^{\phi}$	1.36 ± 0.12	$0.95 \pm 0.13^{**}$	1.34 ± 0.10	$1.12 \pm 0.13^{*}$	$1.04 \pm 0.10^{**, \#, \wedge}$
	4	$1.83 \pm 0.15^{\phi\phi}$	$1.13 \pm 0.13^{***}$	$0.82 \pm 0.15^{****}$	$1.42 \pm 0.11^{*}$	$1.28 \pm 0.15^{**}$	$0.90 \pm 0.11^{****, \wedge\wedge\wedge}$
HF of IBI (ms^2)	0	4.38 ± 0.34	$3.10 \pm 0.30^{**}$	$1.97 \pm 0.34^{****, \#}$	$2.11 \pm 0.25^{****, \#}$	$1.81 \pm 0.34^{****, \#\#}$	$2.71 \pm 0.25^{****, \#\#}$
	1	5.01 ± 0.46	$3.36 \pm 0.41^{**}$	$4.28 \pm 0.46^{\phi\phi\phi\phi}$	$3.81 \pm 0.34^{\phi\phi\phi\phi, *}$	$3.24 \pm 0.46^{\phi\phi, **}$	$2.26 \pm 0.34^{****, \#, \wedge\wedge}$
	2	$5.87 \pm 0.53^{\phi\phi}$	$3.61 \pm 0.48^{**}$	$5.36 \pm 0.53^{\phi\phi\phi\phi, \#}$	$4.50 \pm 0.40^{\phi\phi\phi\phi, *}$	$3.58 \pm 0.53^{\phi\phi, **}$	$4.39 \pm 0.40^{\phi\phi\phi\phi, *}$
	3	$7.08 \pm 0.58^{\phi\phi\phi\phi}$	$4.34 \pm 0.52^{\phi, ***}$	$6.78 \pm 0.58^{\phi\phi\phi\phi, \#\#}$	$3.52 \pm 0.44^{\phi\phi, ****}$	$3.25 \pm 0.58^{\phi\phi, ****}$	$3.48 \pm 0.44^{****}$
	4	$7.25 \pm 0.40^{\phi\phi\phi\phi}$	$3.82 \pm 0.36^{****}$	$3.50 \pm 0.40^{\phi\phi\phi, ****}$	$3.63 \pm 0.30^{\phi\phi\phi\phi, ****}$	$3.33 \pm 0.40^{\phi\phi\phi, ****}$	$3.39 \pm 0.30^{\phi, ****}$
LF/HF of IBI	0	$0.43 \pm 0.0.03$	$0.58 \pm 0.03^{***}$	$0.47 \pm 0.03^{\#\#}$	$0.49 \pm 0.02^{\#}$	$0.57 \pm 0.03^{**}$	$0.44 \pm 0.02^{\#\#\#\#}$
	1	0.40 ± 0.03	$0.52 \pm 0.03^{\phi, **}$	0.46 ± 0.03	$0.44 \pm 0.02^{\phi, \#}$	$0.55 \pm 0.03^{***}$	$0.54 \pm 0.02^{\phi\phi\phi\phi, ***, \wedge\wedge}$
	2	0.39 ± 0.03	$0.39 \pm 0.02^{\phi\phi\phi\phi}$	0.43 ± 0.03	$0.41 \pm 0.02^{\phi\phi}$	$0.58 \pm 0.03^{****, \#\#\#\#}$	0.43 ± 0.02
	3	0.40 ± 0.03	$0.31 \pm 0.02^{\phi\phi\phi\phi, **}$	$0.36 \pm 0.03^{\phi\phi\phi}$	$0.40 \pm 0.02^{\phi\phi\phi, \#\#}$	$0.56 \pm 0.03^{****, \#\#\#\#}$	$0.40 \pm 0.02^{\#\#}$
	4	0.39 ± 0.03	$0.33 \pm 0.02^{\phi\phi\phi\phi}$	$0.36 \pm 0.03^{\phi\phi\phi}$	$0.39 \pm 0.02^{\phi\phi\phi\phi}$	$0.56 \pm 0.03^{****, \#\#\#\#}$	$0.39 \pm 0.02^{\#}$
Normalized LF of IBI	0	0.26 ± 0.01	$0.31 \pm 0.01^{***}$	$0.28 \pm 0.01^{*, \#}$	0.30 ± 0.01	$0.32 \pm 0.01^{****}$	$0.26 \pm 0.01^{\#\#\#, \wedge\wedge}$
	1	0.25 ± 0.01	$0.28 \pm 0.01^{\phi, *}$	0.27 ± 0.01	$0.27 \pm 0.01^{\phi\phi\phi}$	$0.30 \pm 0.01^{***}$	$0.31 \pm 0.01^{\phi\phi\phi\phi, ****, \wedge\wedge\wedge}$
	2	0.24 ± 0.01	$0.23 \pm 0.01^{\phi\phi\phi\phi}$	0.26 ± 0.01	$0.25 \pm 0.01^{\phi\phi\phi\phi}$	$0.32 \pm 0.01^{****, \#\#\#\#}$	$0.26 \pm 0.01^{\#}$
	3	0.24 ± 0.01	$0.20 \pm 0.01^{\phi\phi\phi\phi, ***}$	$0.23 \pm 0.01^{\phi\phi\phi, \#}$	$0.25 \pm 0.01^{\phi\phi\phi\phi, \#\#\#\#}$	$0.31 \pm 0.01^{****, \#\#\#\#}$	$0.24 \pm 0.01^{\phi, \#\#\#}$
	4	0.24 ± 0.01	$0.21 \pm 0.01^{\phi\phi\phi\phi, *}$	$0.23 \pm 0.01^{\phi\phi\phi\phi}$	$0.25 \pm 0.01^{\phi\phi\phi\phi, \#\#}$	$0.32 \pm 0.01^{****, \#\#\#\#}$	$0.24 \pm 0.01^{\phi\phi, \#}$

(Continued)

TABLE 2 | Continued

Parameter	Weeks	Control ($n = 4$) (*)	Ang II ($n = 5$) (#)	30 nmol/h NaHS ($n = 4$)	30 nmol/h NaHS + Ang II ($n = 7$) (^)	60 nmol/h NaHS ($n = 4$)	60 nmol/h NaHS + Ang II ($n = 7$)
Normalized HF of IBI	0	0.74 ± 0.01	0.69 ± 0.01***	0.72 ± 0.01$^{\#}$	0.70 ± 0.01**	0.68 ± 0.01****	0.74 ± 0.01$^{\#\#\#}$, $^{\wedge\wedge}$
	1	0.75 ± 0.01	0.72 ± 0.01$^{\phi}$, *	0.73 ± 0.01	0.73 ± 0.01$^{\phi\phi\phi}$	0.70 ± 0.01***	0.69 ± 0.01$^{\phi\phi\phi\phi}$, ****, $^{\wedge\wedge\wedge}$
	2	0.76 ± 0.01	0.77 ± 0.01$^{\phi\phi\phi\phi}$	0.74 ± 0.01	0.75 ± 0.01$^{\phi\phi\phi\phi}$	0.68 ± 0.01****, $^{\#\#\#\#}$	0.74 ± 0.01$^{\#}$
	3	0.76 ± 0.01	0.80 ± 0.01$^{\phi\phi\phi\phi}$, ***	0.77 ± 0.01$^{\phi\phi\phi\phi}$, $^{\#}$	0.75 ± 0.01$^{\phi\phi\phi\phi}$, $^{\#\#\#\#}$	0.69 ± 0.01****, $^{\#\#\#\#}$	0.76 ± 0.01$^{\phi}$, $^{\#\#\#\#}$
	4	0.76 ± 0.01	0.79 ± 0.01$^{\phi\phi\phi\phi}$, *	0.77 ± 0.01$^{\phi\phi\phi\phi}$	0.75 ± 0.01$^{\phi\phi\phi\phi}$, $^{\#\#}$	0.68 ± 0.01****, $^{\#\#\#\#}$	0.76 ± 0.01$^{\phi\phi}$, $^{\#}$
Total Power of IBI	0	8.36 ± 0.93	8.38 ± 0.83	6.35 ± 0.93	8.13 ± 0.70	5.65 ± 0.93*, $^{\#}$	6.77 ± 0.70
	1	12.10 ± 0.69$^{\phi\phi\phi}$	9.61 ± 0.62**	9.23 ± 0.69$^{\phi\phi}$, **	9.89 ± 0.52$^{\phi}$, *	8.54 ± 0.69$^{\phi\phi}$, ***	7.91 ± 0.52****, $^{\#}$, $^{\wedge\wedge}$
	2	12.71 ± 0.89$^{\phi\phi\phi}$	9.37 ± 0.79**	11.29 ± 0.89$^{\phi\phi\phi\phi}$	11.85 ± 0.67$^{\phi\phi\phi\phi}$, $^{\#}$	9.61 ± 0.89$^{\phi\phi\phi}$, *	10.69 ± 0.67$^{\phi\phi\phi\phi}$
	3	15.75 ± 0.87$^{\phi\phi\phi\phi}$	9.76 ± 0.78****	11.98 ± 0.87$^{\phi\phi\phi\phi}$, **	9.22 ± 0.66****	9.66 ± 0.87$^{\phi\phi\phi}$, ****	9.43 ± 0.66$^{\phi\phi}$, ****
	4	16.25 ± 0.77$^{\phi\phi\phi\phi}$	9.15 ± 0.69****	8.22 ± 0.77****	9.28 ± 0.58****	10.20 ± 0.77$^{\phi\phi\phi\phi}$, ****	9.00 ± 0.58$^{\phi\phi}$, ****

Ang II, Angiotensin II; LF, low frequency; VLF, very low frequency; HF, high frequency; SBP, systolic blood pressure; IBI, inter-beat-interval.
Data was analyzed by Kruskal–Wallis H test followed by Tukey's multiple comparisons test and presented as mean ± SEM.
$^{\phi\phi\phi\phi}p < 0.0001$, $^{\phi\phi}p < 0.001$, $^{\phi}p < 0.01$, $^{\phi}p < 0.05$ *vs. Baseline.*
$^{****}p < 0.0001$, $^{***}p < 0.001$, $^{**}p < 0.01$, $^{*}p < 0.05$ *Control vs. all other groups.*
$^{\#\#\#\#}p < 0.0001$, $^{\#\#\#}p < 0.001$, $^{\#\#}p < 0.01$, $^{\#}p < 0.05$ *Ang II vs. NaHS-treated groups.*
$^{\wedge\wedge\wedge\wedge}p < 0.0001$, $^{\wedge\wedge\wedge}p < 0.001$, $^{\wedge\wedge}p < 0.01$, $^{\wedge}p < 0.05$ *30 nmol/h NaHS/Ang II vs. 60 nmol/h NaHS/Ang II.*

was calculated by dividing the abundance ratio (percentage of each species in total number of species identified) of *Firmicutes* with that of the *Bacteroidetes*.

Operational taxonomic units were aggregated into each taxonomic rank and plotted the relative abundance (how common or rare an OTU is relative to other OTUs in the same community) of the most abundant ones. Data are presented as mean ± SEM. Linear discriminant analysis effect size (LEfSe) was also employed to identify species that were differentially distributed between different samples[1]. The threshold of the linear discriminant analysis score was 2.0 and alpha value for the Kruskal–Wallis test and Wilcoxon test was 0.05.

RESULTS

Central Administration of NaHS Attenuated Angiotensin II–Induced Changes in BP, Heart Rate, and Left Ventricular Wall Thickness

Table 1 summarizes all significant differences between groups and times of treatment. Chronic SC Ang II infusion significantly elevated MAP and SBP starting at week 2 (W2), and these remained elevated through week 4 (W4) of infusion compared with the control groups (**Figures 1A,B**). Chronic, concomitant ICV infusion of 30 and 60 nmol/h NAHS dose-dependently (**Table 1**) attenuated Ang II-induced increase in MAP and SBP (**Figures 1A,B**). HR significantly decreased in all groups over time compared with baseline (W0) (**Table 1**). However, this time-dependent decrease in HR was significantly dampened by Ang II infusion when compared with control and NaHS/Ang II groups (**Figure 1C**).

In line with BP increase, Ang II infusion caused a significant increase in the LV wall thickness (**Figures 1D,E**) compared with the control and 60 nmol/h NaHS groups (Ang II: 2,643 ± 179.6 vs. control: 2,016 ± 40.9 μm, $p < 0.05$ and vs. 60 nmol/h NaHS: 1,500 ± 64.0 μm, 60 nmol/h NaHS/Ang II: 1,728 ± 79.4 μm, $p < 0.0001$). The Ang II-induced LV thickness was attenuated by 60 nmol/h NaHS ICV but not 30 nmol/h NaHS ICV co-treatment (**Figures 1D,E**, Ang II: 2,643 ± 179.6 vs. 60 nmol/h NaHS/Ang II: 1,728 ± 79.4 μm, $p < 0.0001$). No significant difference was found in heart weights between the groups (**Figure 1F**).

Central Effects of NaHS on Angiotensin II–Induced Imbalance in Autonomic Variables

Table 2 summarizes the statistical significance in derived autonomic variables between groups and times of treatment. Spectral analysis of SBP variability showed that Ang II infusion significantly increased TP_{SBP} and LF_{SBP} starting at W2 compared with control groups, and that ICV NaHS co-treatment significantly attenuated this increase at 60 nmol/h for TP_{SBP} and at 30 and 60 nmol/h for LF_{SBP} (**Table 2** and **Figure 2A**).

[1]https://huttenhower.sph.harvard.edu/galaxy

Spectral analysis of HR variability showed that VLF_{IBI} significantly increased with time in the control but not in the Ang II group (**Table 2**), suggesting that Ang II attenuated the time-dependent increase in this variable. Co-infusion of NaHS with Ang II partially corrected the Ang II-induced changes in VLF_{IBI} at W2 in the 30 nmol/h NaHS/Ang II group and at W3 in the 60 nmol/h NaHS/Ang II group (**Figure 2B**). However, at W4, VLF_{IBI} of all groups was significantly lower than control. Similarly, LF_{IBI} increased with time in the control group but not in the Ang II group (**Table 2** and **Figure 2C**). Co-infusion of NaHS with Ang II partially corrected the Ang II-induced changes in LF_{IBI} but only at W2 in the 30 nmol/h NaHS/Ang II group, while LF_{IBI} was significantly lower at W3 in the 60 nmol/h NaHS/Ang II group (**Figure 2C**). HF_{IBI} was significantly increased in all groups with time except in the Ang II group (**Table 2**). However, at W4, the control group showed significantly higher HF_{IBI} compared with all groups, and no significant differences were found between the Ang II and NaHS/Ang II groups (**Table 2** and **Figure 2D**). A decrease in LF/HF_{IBI}, an index of cardiac autonomic modulation, was also observed in the Ang II and 30 nmol/h NaHS/Ang II group, with no change in 60 nmol/h NaHS/Ang II group (**Table 2** and **Figure 2G**). TP_{IBI} was significantly increased in the control, 60 nmol/h NaHS control, and 60 nmol/h NaHS/Ang II groups with time, whereas this variable was not significantly altered with Ang II (**Table 2**). Analysis of normalized values shows that both the Ang II infusion alone and co-infusions of ICV NaHS with Ang II significantly reduced nLF_{IBI} (**Figure 2E**) and increased nHF_{IBI} (**Figure 2F**) with time. The nLF_{IBI} and nHF_{IBI} and LF/HF_{IBI} remained unchanged in the control and 60 nmol/h NaHS control group, while 30 nmol/h NaHS control group produced a significantly reduced nLF_{IBI} and increased nHF_{IBI} with time, resulting in decreased LF/HF_{IBI} in this group (**Table 2**). These data suggest that ICV NaHS can affect Ang II-dependent changes in autonomic variables.

Central Effects of NaHS on Angiotensin II–Induced Elevation in Iba1$^+$ Cells in the PVN

As NaHS is an anti-inflammatory agent (Li et al., 2008; Sidhapuriwala et al., 2009; Aslami et al., 2013), and as microglial cell numbers are reportedly increased in the PVN in rodent Ang II HTN (Shi et al., 2010; Shen et al., 2015), we investigated if ICV NaHS administration would reduce the numbers of Iba1$^+$ cells in the PVN in rodent Ang II HTN. We observed a significant increase in the number of Iba1$^+$ cells in the PVN of Ang II-infused rats (per 300 μm^2 area of PVN) compared with the control group (**Figures 3A,B**: Ang II: 49.6 $\pm$ 1.9 vs. control: 23.7 $\pm$ 2.3, $p < 0.0001$). Co-infusion of both 30 and 60 nmol/h NaHS resulted in significantly less Iba1$^+$ cells compared with the Ang II group (**Figures 3A,B**: Ang II: 49.6 $\pm$ 1.9 vs. 30 nmol/h NaHS/Ang II: 28.5 $\pm$ 2.7, $p < 0.001$; vs. 60 nmol/h NaHS/Ang II: 34.5 $\pm$ 2.0, $p < 0.05$). These data suggest that ICV NaHS can attenuate Ang II-induced increase in microglial cells in the PVN of rats.

Alterations in Cecal Microbial Composition in Rodents With Angiotensin II HTN and After Central Administration of NaHS

Considering the association between gut dysbiosis and rodent and human HTN (Yang et al., 2015; Adnan et al., 2017; Li et al., 2017), we investigated the abundance and diversity of gut microbial species in all groups. Alpha diversity (Shannon index) is a measure of richness (how many OTUs) and evenness (how evenly distributed these OTUS are) in a sample (Willis, 2019). We observed no significant differences in alpha diversity (Shannon index) in any of the treatment groups except in the 60 nmol/h NaHS/Ang II group when compared with all other groups but not the 60 nmol/h NaHS group (**Figure 4A**: 60 nmol/h NaHS/Ang II: 3.9 $\pm$ 0.3 vs. control: 5.2 $\pm$ 0.2, $p < 0.05$; vs. 30 nmol/h NaHS: 5.6 $\pm$ 0.1, $p < 0.01$; vs. Ang II: 5.5 $\pm$ 0.1, $p < 0.01$; vs. 30 nmol/h NaHS/Ang II: 5.0 $\pm$ 0.4, $p < 0.05$). This suggested a difference in richness (number of taxa) and/or evenness (the relative abundances of those taxa) in cecal fecal bacterial samples from the 60 nmol/h NaHS/Ang II group, and to a certain extent the 60 nmol/h NaHS group compared with all other groups. However, PCoA analysis (**Figure 4B**) showed no apparent clustering between the groups. In addition, *Firmicutes*, *Bacteroidetes*, and *Verrucomicrobia* were the most abundant bacterial phyla in all groups; however, abundance in these phyla was not significantly different between the groups (**Figure 4C**). In addition, we observed no difference in the F/B ratios between the treatment groups (**Figure 4D**).

Central Administration of NaHS Diminished Angiotensin II Effects on the Abundance of Cecal *Desulfovibrionales*, *Deltaproteobacterium*, and *Dehalobacterium*

LEfSe analysis of specific bacterial taxa demonstrated a significant increase in the abundance of, among others, *Desulfovibrionales*, *Deltaproteobacterium*, and *Dehalobacterium* in the Ang II group (in purple) compared with all other groups (**Figure 4E**). The observed increase in abundance of sulfate-reducing *Desulfovibrionales* after Ang II infusion suggested that the production of bacterial derived H_2S may be altered in the Ang II group, and that this can be corrected with ICV NaHS treatment. In addition, we observed higher abundance of *Parabacteroides* in the control group (in blue) compared with all other groups, higher abundance of *Staphylococcus* and *Bacillales* in the 30 nmol/h NaHS/Ang II group (in green), and *Ruminococcaceae*, among others, in the 30 nmol/h NaHS group (in red) compared with all other groups including the control group (in blue, **Figure 4E**).

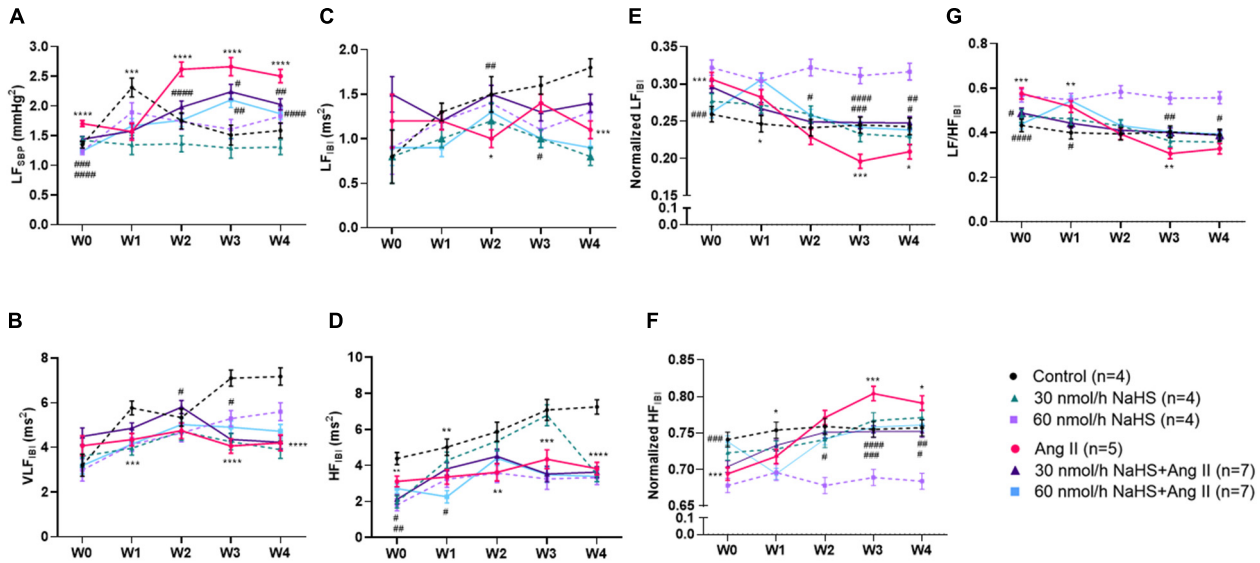

FIGURE 2 | Chronic intracerebroventricular infusion of NaHS attenuates angiotensin (Ang) II–induced autonomic imbalance in Sprague–Dawley rats. Spectral analysis of blood pressure waveform signal was used to derive **(A)** low frequency (LF) of systolic blood pressure (SBP), **(B)** very low frequency (VLF) ratio of inter-beat interval (IBI), **(C)** low frequency (LF) ratio of IBI, **(D)** high frequency (LF) ratio of IBI, **(E)** normalized LF ratio of IBI, **(F)** normalized HF ratio of IBI, and **(G)** LF/HF ratio of IBI. Data were analyzed by Kruskal–Wallis *H* test followed by Tukey's multiple comparisons test and presented as mean ± SEM. $^{****}p < 0.0001$, $^{***}p < 0.001$, $^{**}p < 0.01$, $^{*}p < 0.05$ control vs. Ang II. $^{\#\#\#\#}p < 0.0001$, $^{\#\#\#}p < 0.001$, $^{\#\#}p < 0.01$, $^{\#}p < 0.05$ Ang II vs. NaHS/Ang II-treated rats.

Effect of Angiotensin II HTN and Central Administration of NaHS on Circulating H_2S Levels

Considering the increase in the sulfate-reducing *Desulfovibrionales* in the Ang II group (**Figure 4E**) and a significant decrease in Shannon (alpha) cecal bacterial diversity in the 60 nmol/h NaHS/Ang II group (**Figure 4A**), we measured circulating H_2S levels in all rats at endpoint (W4) using methylene blue method (Shen et al., 2011; Donertas Ayaz and Zubcevic, 2020). We observed no difference in circulating H_2S levels in any of the treatment groups (**Figure 5**). These data suggest that rodent HTN induced by systemic Ang II infusion (200 ng/kg/min) may be independent of any changes in circulating H_2S. In addition, ICV infusion of NaHS can reduce Ang II-dependent increase in sulfate-reducing cecal *Desulfovibrionales* with no effect on circulating H_2S.

DISCUSSION

Our data reveal the following findings: (1) Central administration of NaHS, an H_2S donor, attenuated Ang II-induced increase in BP in a dose-dependent manner. This may be in part due to improvement in the autonomic regulation of BP, largely reflecting in effects on the sympathetic vasomotor drive derived from spectral analysis of SBP waveform signal. (2) Central administration of NaHS alleviated Ang II-dependent increase in the Iba1$^+$ cells in the PVN. These data provide further support for a role of central H_2S in regulation of cardiovascular function (Ufnal et al., 2008; Sikora et al., 2014; Duan et al., 2015; Yu et al., 2015; Liang et al., 2017). (3) Ang II infusion increased the abundance of select gut bacteria, which was prevented by ICV co-administration of NaHS. As we observed no change in circulating H_2S in any of the treatment groups, this suggests that the anti-hypertensive effects of H_2S are primarily mediated via the CNS in the current study.

Both the gut bacteria and their host reportedly produce H_2S (Kimura, 2014; Donertas Ayaz and Zubcevic, 2020) and gut-derived H_2S may contribute to the regulation of BP (Tomasova et al., 2016; Huc et al., 2018). In line with the latter, we have recently shown a positive correlation between the gut bacterial and circulating H_2S levels in the spontaneously hypertensive rat (Donertas Ayaz and Zubcevic, 2020). Indeed, host microbiota may play an important role in controlling H_2S bioavailability and metabolism (Shen et al., 2013) and gut dysbiosis can have an effect on the plasma H_2S (Weber et al., 2016). As reduced systemic H_2S levels are reported in rodent and human HTN (Chen et al., 2007; Xiao et al., 2018; Donertas Ayaz and Zubcevic, 2020), we also investigated circulating H_2S levels in Ang II-induced rodent HTN. We show no association between Ang II rodent HTN and plasma H_2S in the current experimental paradigm. Interestingly, we did observe an increased abundance of sulfate-reducing *Desulfovibrio* in rats with Ang II HTN. It has previously been shown that increased H_2S production in the gut can lead to localized gastrointestinal inflammation (Singh and Lin, 2015), and Ang II is also implicated in inflammation (Benigni et al., 2010; Santisteban et al., 2015; Zubcevic et al., 2017; Satou et al., 2018). Although we did not measure fecal H_2S, unchanged circulating H_2S in Ang II-infused rats suggests that the H_2S effects observed

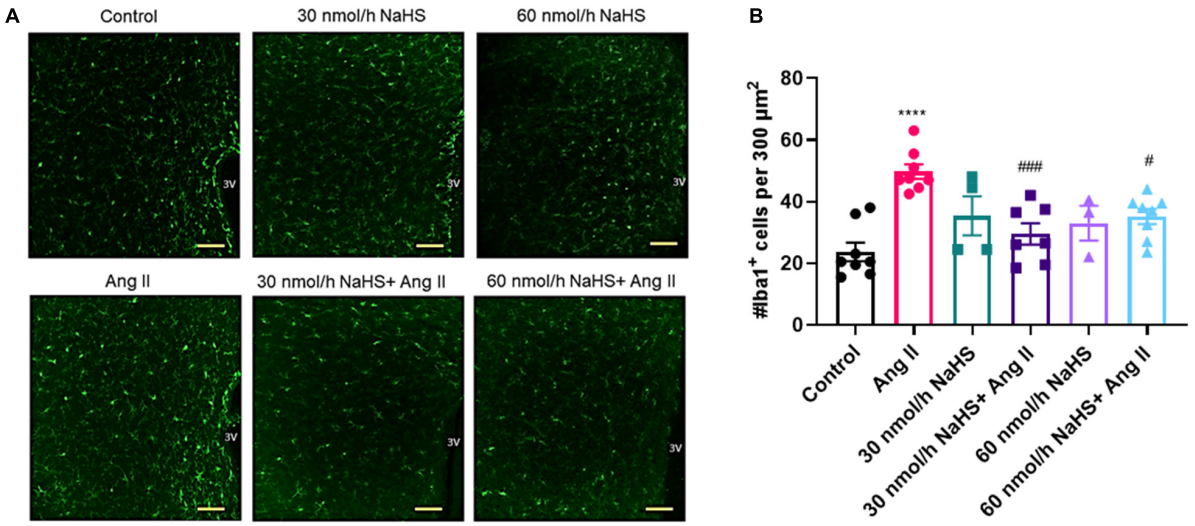

FIGURE 3 | Chronic intracerebroventricular infusion of NaHS reduces angiotensin (Ang) II–induced elevation in ionized calcium binding adaptor molecule 1–positive (Iba1$^+$) cells in the paraventricular nucleus (PVN) of Sprague–Dawley rats. **(A)** Representative images of Iba1$^+$ cells in the PVN in control, Ang II-treated, and NaHS/Ang II-treated rats (magnification: ×20, scale bar = 100 µm, –0.72 mm to –1.92 mm from Bregma, Paxinos and Watson Rat Brain Atlas). **(B)** Quantification of Iba1$^+$ cells per 300 µm^2 in the PVN of control (n = 5), Ang II (n = 4), 30 nmol/h NaHS (n = 3), 60 nmol/h NaHS (n = 2), 30 nmol/h NaHS/Ang II (n = 3), and 60 nmol/h NaHS/Ang II (n = 4). $^{****}p < 0.0001$, Ang II vs. control. $^{###}p < 0.001$, $^{\#}p < 0.05$ Ang II vs. NaHS/Ang II-treated rats. Data are presented as the mean ± SEM, one-way ANOVA, Dunn's multiple comparisons test.

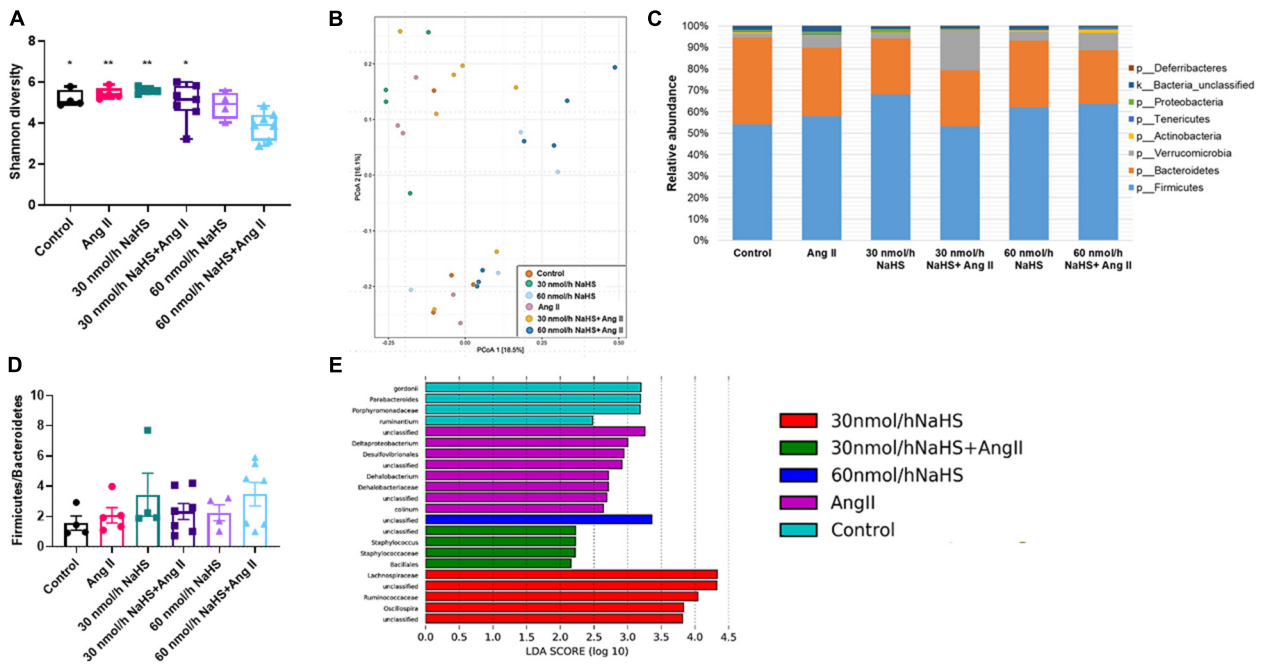

FIGURE 4 | Alterations in cecal microbial composition of Sprague–Dawley rats with angiotensin (Ang) II hypertension and after intracerebroventricular NaHS administration. **(A)** Gut bacterial alpha diversity (Shannon index). Data were analyzed by one-way ANOVA, Tukey's multiple comparisons test, and presented as minimum to maximum with a median. $^{*}p < 0.05$, $^{**}p < 0.01$ vs. 60 nmol/h NaHS/Ang II. **(B)** Gut bacterial beta diversity (principal coordinate analysis, PCoA) determined by permutational analysis of variance (adonis R function or PERMANOVA). Operational taxonomical unit (OTU) abundance is summarized into Bray–Curtis dissimilarities and performed a PCoA ordination. **(C)** Mean relative abundance of gut bacterial phyla identified in cecal samples in each experimental group. **(D)** Ratio of *Firmicutes* to *Bacteroidetes*. Data were analyzed by one-way ANOVA followed by Kruskal–Wallis test and presented as mean ± SEM. **(E)** Linear discriminant analysis effect size (LEfSe) analysis showing enriched taxa in each group. Control (n = 4), Ang II (n = 5), NaHS (n = 4), and NaHS/Ang II-treated rats (n = 7).

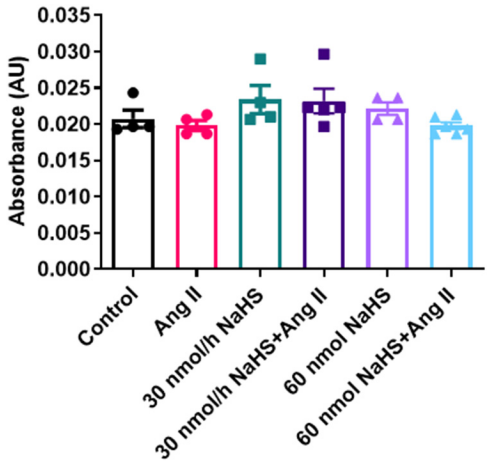

FIGURE 5 | Hydrogen sulfide levels in plasma of Sprague–Dawley rats with angiotensin (Ang) II hypertension and after intracerebroventricular NaHS administration as measured by methylene blue method. Data were analyzed by one-way ANOVA followed by Kruskal–Wallis test and presented as mean ± SEM. AU: arbitrary unit. Control (n = 4), Ang II (n = 5), NaHS (n = 4), and NaHS/Ang II-treated rats (n = 7).

in the current study were not mediated via systemic H_2S. From this, the anti-hypertensive effects of ICV infusion of NaHS appear to be primarily mediated via the CNS, as increasing the availability of central H_2S modified cardiovascular responses without affecting the systemic H_2S levels. It is noteworthy that the current study used methylene blue method for detection of H_2S in plasma (Zhuo et al., 2009; Donertas Ayaz and Zubcevic, 2020). Future studies should employ analytical techniques such as gas/ion chromatography, HPLC, and polarographic electrodes among others to increase sensitivity of H_2S detection in gut and plasma (Kolluru et al., 2013).

Ang II in the CNS modulates neurohumoral pathways involved in autonomic control of BP. Ang II receptor activation within the PVN is a major contributor to chronic sympatho-excitation, while Ang II in the nucleus of the solitary tract reduces the parasympathetic control of the heart (Paton and Raizada, 2010). Thus, one goal of the current study was to evaluate the effects of chronic, concomitant ICV administration of NaHS on autonomic effects exerted by Ang II. Our findings show that Ang II infusion increased LF_{SBP}, a marker of sympathetic vasomotor modulation (deBoer et al., 1987; Madwed et al., 1989), which is consistent with reports in other rodent models of HTN (Waki et al., 2006; Zubcevic et al., 2014, 2017; Chaar et al., 2016). Importantly, we show that ICV NaHS co-infusion attenuated the Ang II effects on LF_{SBP}. We used established stereotaxic coordinates for ICV infusion (Li et al., 2006; Jun et al., 2012; Buttler et al., 2017). However, we acknowledge that ICV administration may deliver NaHS to ventricular brain structures other than PVN (Hashimoto et al., 2005; Buttler et al., 2017). Thus, it is possible that effects of NaHS may be exerted via action on several brain nuclei in the current study. We also investigated the effects of our treatments on VLF, LF, and HF of IBI as indices of autonomic modulation of HR. The VLF_{IBI} variable is reportedly related to changes in the renin–angiotensin system and thermoregulation (Taylor et al., 1998; Pumprla et al., 2002) as well as the parasympathetic modulation (Taylor et al., 1998). The HF_{IBI} is considered an index of cardiac vagal efferent modulation, while LF_{IBI} reportedly contains both vagal and cardiac sympathetic components (Shaffer and Ginsberg, 2017). Thus, any changes in these variables are likely to be reflected in modified autonomic input to the heart and potentially changes in BP. However, while the effects of Ang II on these variables are significant, the effect of ICV NaHS treatment on Ang II-induced changes on VLF and LF of IBI is only partial and sporadic, with no significant effect on HF of IBI. Moreover, the effects of NaHS infusion alone on both VLF and LF of IBI appear to be significant at select time points and doses of NaHS, suggesting NaHS alone may have neuromodulatory effects in control conditions. This may potentially be due to effects of H_2S on astrocytes (Nagai et al., 2004; Lu et al., 2008) and/or neurons (Han et al., 2005; Umemura and Kimura, 2007; Garcia-Bereguiain et al., 2008) as changes in calcium currents and effects on GABA and glutamate neurotransmission have previously been observed in astrocytes and neurons, respectively in response to central H_2S. However, we did not investigate these in the current study. Ang II did significantly alter nLF_{IBI} and nHF_{IBI}, which are derived by normalizing the raw values of LF_{IBI} and HF_{IBI}, respectively, to the value of TP_{IBI}, and ICV NaHS co-treatment appeared to have corrected this effect of Ang II on these two variables. Moreover, LF/HF_{IBI}, an index of cardiac autonomic balance, significantly decreased in the Ang II group, and 60 nmol/h ICV NaHS co-treatment partially corrected this decrease. However, interpretation of these changes in IBI variables are challenging due to the reported participation of parasympathetic modulation in both LF and HF components (Billman, 2013). Thus, these results suggest that central H_2S may counteract the effects of Ang II on autonomic function via effects on pre-autonomic neurons that regulate BP.

Interestingly, we observed an increase in the IBI variables including HF_{IBI} over time in the control group (**Table 2**), which aligns with the time-dependent decrease in HR in the same group. We have previously shown that HR can decrease with age in normotensive rodents (Zubcevic et al., 2009). Thus, attenuation of these time-dependent changes in HF_{IBI} and HR in the Ang II group suggests deregulation of cardiac parasympathetic drive after Ang II infusion, as it has previously been reported (Miller and Arnold, 2019; Dorey et al., 2020; Sharma et al., 2021). However, this effect of Ang II on HF_{IBI} was not significantly affected by ICV NaHS co-treatments, suggesting lesser effects of central infusion of NaHS on parasympathetic control of BP in our study. Further studies are needed to fully understand the effects of central NaHS on cardiac autonomic control.

Left ventricular hypertrophy is a secondary manifestation of HTN resulting from adaptation of heart muscle to accommodate the increased cardiac work via the compensatory hypertrophic response (Li et al., 2019a). In line with our BP results, we observed increased LV wall thickness in Ang II-infused group compared with control, which was significantly attenuated by chronic

ICV 60 nmol/h but not the 30 nmol/h NaHS treatment. However, heart weight analysis showed no significant differences between the groups in the current study. Thus, the observed changes in wall thickness may be due to hypertrophy and/or dilation effects. However, we did not perform heart fibrosis and diameter analyses in the current study. Further studies are needed to determine dose-dependent long-term cardiac effects of NaHS in HTN.

Considering the reported anti-inflammatory properties of H_2S, we investigated whether central administration of NaHS can attenuate the previously reported increase in microglial cells in the PVN, a recognized hallmark of rodent HTN (Shi et al., 2010; Shen et al., 2015). Microglial cells in the CNS express Iba1, a microglia/macrophage-specific calcium-binding protein (Sasaki et al., 2001), which is involved in the membrane ruffling processes of macrophages/microglia and confers the motile properties of these cells (Kanazawa et al., 2002). As previously reported, Ang II infusion significantly increased the number of PVN microglial cells (Shi et al., 2010; Santisteban et al., 2015; Sharma et al., 2019). Here, we report that central NaHS treatment reduced $Iba1^+$ cells in the PVN of Ang II-infused rats. Although we did not investigate microglial morphology in the current study, others have previously shown that both NaHS and H_2S can inhibit microglial activation *in vitro* (Hu et al., 2007; Zhang et al., 2014) and *in vivo* (Zhang et al., 2014; Kumar and Sandhir, 2019; Kumar et al., 2020). It is proposed that Ang II can stimulate the production of pro-inflammatory cytokines and reactive oxygen species in both neurons and microglia (Kang et al., 2009; Shi et al., 2010; Jun et al., 2012; Qi et al., 2013; Shen et al., 2015). This may affect neuronal activity and contribute to the increase in the sympathetic outflow and BP in rodent HTN (Kang et al., 2009; Shi et al., 2010; Jun et al., 2012; Qi et al., 2013; Shen et al., 2015). Liang et al. (2017) have previously shown that chronic PVN infusion of a separate H_2S donor, GYY4137, decreased BP and plasma noradrenaline levels in rodent salt HTN while simultaneously reducing reactive oxygen species and IL-1β in the PVN. However, H_2S may also have direct neuronal effects (Szabo, 2021), warranting further investigation of H_2S in regulation of activity of pre-sympathetic neurons (Guo et al., 2011; Centurion et al., 2016; Dominguez-Rodriguez et al., 2017).

An increase in the F/B ratio, a marker of generalized gut dysbiosis, has been reported in several rodent models of HTN (Yang et al., 2015; Durgan et al., 2016; Marques et al., 2017; Chen et al., 2019; Hsu et al., 2020; Robles-Vera et al., 2020) and humans with HTN (Yang et al., 2015; Silveira-Nunes et al., 2020). However, others have reported no change in the F/B ratio in select animal models of HTN (Mell et al., 2015; Galla et al., 2018; Cheema and Pluznick, 2019). In line with the latter, we did not observe a significant change in the F/B ratios in the current study. However, Ang II did produce a significant shift in the abundance of specific bacteria including but not limited to *Desulfovibrio*, *Deltaproteobacterium*, and *Dehalobacterium*. The genus *Desulfovibrio* in the *Deltaproteobacteria* class is one of the most abundant sulfate-reducing bacteria (SRB) in the human colon (Dordevic et al., 2021). Higher abundance of genus *Desulfovibrio* observed in the Ang II group was in agreement with the previous reports of other hypertensive rodent models and human patients (Adnan et al., 2017; Li et al., 2017; Dan et al., 2019; Thomaz et al., 2021). *Desulfovibrio* abundance is also positively correlated with Ang II levels in rats with high-carbohydrate, high-fat diet–induced HTN (Thomaz et al., 2021). These and our findings further support the possible involvement of SRB in HTN. H_2S produced by gut bacteria is an important regulator of gut health, and high concentrations of H_2S are involved in gut inflammation (Dordevic et al., 2021). Thus, reducing gut *Desulfovibrio*, as we have shown in the current study, may be beneficial in regulation of BP. Thus, while CNS H_2S may be beneficial, higher abundance of SRB may be associated with HTN. However, a cause–effect relationship between SRB and HTN is not clear. On one hand, studies suggest H_2S involvement in gut inflammation (Dordevic et al., 2021), and on the other, H_2S may be protective of the mucosal integrity in the gut (Wallace et al., 2018). Further studies employing genomic sequencing of SRB and investigation of fecal and host H_2S levels in rodents and humans with HTN are needed to clarify this matter.

To the best of our knowledge, no study to date has reported an association between *Dehalobacterium* and HTN, but a positive correlation between the abundance of *Dehalobacterium* and obesity and higher body mass index, which are also associated with HTN (Jones et al., 1994; Wilson et al., 2002; Zhang et al., 2019), has been previously reported (Fu et al., 2015; Thomaz et al., 2021). Here, we observe that central administration of NaHS normalized the levels of *Desulfovibrio*, *Deltaproteobacteria*, and *Dehalobacterium* in Ang II-infused rats. These bacterial shifts may be independent of systemic Ang II effects, as systemic Ang II levels remain constant in all experimental groups. We further observed a decrease in *Parabacteroides* and *Porphyromonadaceae* in the Ang II group, but as these also remained less abundant in all other treatment groups, they may not be associated with regulation of BP. Further studies are needed to elucidate the precise mechanisms of host–microbiota interactions and how they may be involved in hypertensive rodent phenotype and generation of H_2S.

Gender-associated differences in BP have been observed in animals and in humans (Reckelhoff, 2001; Lim et al., 2002; Mishra et al., 2016). Thus, one limitation of the current study is the exclusion of female rats, as the potential of sex differences in the responses to NaHS and Ang II may be important. In addition, sex-dependent gut bacterial differences have been reported (Jasarevic et al., 2016; Beale et al., 2019). Future experiments should investigate potential sex-dependent responses to H_2S and NaHS treatment in relation to regulation of BP and HTN.

In conclusion, our present data show that central administration of an H_2S donor, NaHS, attenuates BP increase and improves autonomic function in Ang II HTN independently of circulating H_2S, while also decreasing SRB in the gut despite continuous systemic Ang II infusion. Moreover, centrally administered NaHS attenuated the Ang II-induced increase in microglial cells in the PVN. Thus, H_2S is a potential therapeutic target for neurogenic HTN and the underlying mechanisms of central H_2S effects in HTN warrant future investigation.

DATA AVAILABILITY STATEMENT

The original contributions presented in the study are included in the article/**Supplementary Material**, further inquiries can be directed to the corresponding author/s.

ETHICS STATEMENT

The animal study was reviewed and approved by University of Florida Institutional Animal Care and Use Committee.

AUTHOR CONTRIBUTIONS

BDA designed the study, carried out the research, analyzed and interpreted the results, and wrote the manuscript. ACO contributed to the analysis and interpretation of data and drafting of the manuscript. WLM, TR, AMA, and RKS contributed to data acquisition. BS participated in the design of the study and edited the manuscript. JZ contributed to the design of the study, access to research components, interpretation of the results, and drafting and editing of the manuscript. All authors read and approved the final manuscript version.

FUNDING

The study was supported by the TUBITAK 2214-A award to BDA, AWD07186 award to ACO, and R21AT010192 to JZ.

ACKNOWLEDGMENTS

The authors wish to thank Jessica M. Jiron and Marianthi M. Karas for their technical support and assistance, and Muzaffer Bilgin for assistance in statistical analysis.

SUPPLEMENTARY MATERIAL

The Supplementary Material for this article can be found online at: https://doi.org/10.6084/m9.figshare.16435356.v1

Supplementary Material | Bacterial sequencing ICV NaHS Ang II hypertension.

REFERENCES

Abe, K., and Kimura, H. (1996). The possible role of hydrogen sulfide as an endogenous neuromodulator. *J. Neurosci.* 16, 1066–1071. doi: 10.1523/jneurosci.16-03-01066.1996

Adnan, S., Nelson, J. W., Ajami, N. J., Venna, V. R., Petrosino, J. F., Bryan, R. M. Jr., et al. (2017). Alterations in the gut microbiota can elicit hypertension in rats. *Physiol. Genomics* 49, 96–104. doi: 10.1152/physiolgenomics.00081.2016

Aslami, H., Pulskens, W. P., Kuipers, M. T., Bos, A. P., van Kuilenburg, A. B., Wanders, R. J., et al. (2013). Hydrogen sulfide donor NaHS reduces organ injury in a rat model of pneumococcal pneumosepsis, associated with improved bio-energetic status. *PLoS One* 8:e63497. doi: 10.1371/journal.pone.0063497

Badoer, E. (2001). Hypothalamic paraventricular nucleus and cardiovascular regulation. *Clin. Exp. Pharmacol. Physiol.* 28, 95–99. doi: 10.1046/j.1440-1681.2001.03413.x

Beale, A. L., Kaye, D. M., and Marques, F. Z. (2019). The role of the gut microbiome in sex differences in arterial pressure. *Biol. Sex Differ.* 10:22.

Benigni, A., Cassis, P., and Remuzzi, G. (2010). Angiotensin II revisited: new roles in inflammation, immunology and aging. *EMBO Mol. Med.* 2, 247–257. doi: 10.1002/emmm.201000080

Billman, G. E. (2013). The LF/HF ratio does not accurately measure cardiac sympatho-vagal balance. *Front. Physiol.* 4:26. doi: 10.3389/fphys.2013.00026

Buttler, L., Jordao, M. T., Fragas, M. G., Ruggeri, A., Ceroni, A., and Michelini, L. C. (2017). Maintenance of Blood-Brain Barrier Integrity in Hypertension: a Novel Benefit of Exercise Training for Autonomic Control. *Front. Physiol.* 8:1048. doi: 10.3389/fphys.2017.01048

Centurion, D., De la Cruz, S. H., Gutierrez-Lara, E. J., Beltran-Ornelas, J. H., and Sanchez-Lopez, A. (2016). Pharmacological evidence that NaHS inhibits the vasopressor responses induced by stimulation of the preganglionic sympathetic outflow in pithed rats. *Eur. J. Pharmacol.* 770, 40–45. doi: 10.1016/j.ejphar.2015.11.057

Chaar, L. J., Coelho, A., Silva, N. M., Festuccia, W. L., and Antunes, V. R. (2016). High-fat diet-induced hypertension and autonomic imbalance are associated with an upregulation of CART in the dorsomedial hypothalamus of mice. *Physiol. Rep.* 4:e12811. doi: 10.14814/phy2.12811

Che, X., Fang, Y., Si, X., Wang, J., Hu, X., Reis, C., et al. (2018). The Role of Gaseous Molecules in Traumatic Brain Injury: an Updated Review. *Front. Neurosci.* 12:392. doi: 10.3389/fnins.2018.00392

Cheema, M. U., and Pluznick, J. L. (2019). Gut Microbiota Plays a Central Role to Modulate the Plasma and Fecal Metabolomes in Response to Angiotensin II. *Hypertension* 74, 184–193. doi: 10.1161/hypertensionaha.119.13155

Chen, H. E., Lin, Y. J., Lin, I. C., Yu, H. R., Sheen, J. M., Tsai, C. C., et al. (2019). Resveratrol prevents combined prenatal N(G)-nitro-L-arginine-methyl ester (L-NAME) treatment plus postnatal high-fat diet induced programmed hypertension in adult rat offspring: interplay between nutrient-sensing signals, oxidative stress and gut microbiota. *J. Nutr. Biochem.* 70, 28–37. doi: 10.1016/j.jnutbio.2019.04.002

Chen, L., Ingrid, S., Ding, Y. G., Liu, Y., Qi, J. G., Tang, C. S., et al. (2007). Imbalance of endogenous homocysteine and hydrogen sulfide metabolic pathway in essential hypertensive children. *Chin. Med. J.* 120, 389–393. doi: 10.1097/00029330-200703010-00008

Coote, J. H. (2005). A role for the paraventricular nucleus of the hypothalamus in the autonomic control of heart and kidney. *Exp. Physiol.* 90, 169–173. doi: 10.1113/expphysiol.2004.029041

Dan, X., Mushi, Z., Baili, W., Han, L., Enqi, W., Huanhu, Z., et al. (2019). Differential Analysis of Hypertension-Associated Intestinal Microbiota. *Int. J. Med. Sci.* 16, 872–881. doi: 10.7150/ijms.29322

deBoer, R. W., Karemaker, J. M., and Strackee, J. (1987). Hemodynamic fluctuations and baroreflex sensitivity in humans: a beat-to-beat model. *Am. J. Physiol.* 253, H680–H689.

d'Emmanuele di Villa Bianca, R., Mitidieri, E., Donnarumma, E., Tramontano, T., et al. (2015). Hydrogen sulfide is involved in dexamethasone-induced hypertension in rat. *Nitric Oxide* 46, 80–86. doi: 10.1016/j.niox.2014.11.013

Dominguez-Rodriguez, M., Drobny, H., Boehm, S., and Salzer, I. (2017). Electrophysiological Investigation of the Subcellular Fine Tuning of Sympathetic Neurons by Hydrogen Sulfide. *Front. Pharmacol.* 8:522. doi: 10.3389/fphar.2017.00522

Donertas Ayaz, B., and Zubcevic, J. (2020). Gut microbiota and neuroinflammation in pathogenesis of hypertension: a potential role for hydrogen sulfide. *Pharmacol. Res.* 153:104677. doi: 10.1016/j.phrs.2020.104677

Dordevic, D., Jancikova, S., Vitezova, M., and Kushkevych, I. (2021). Hydrogen sulfide toxicity in the gut environment: meta-analysis of sulfate-reducing and lactic acid bacteria in inflammatory processes. *J. Adv. Res.* 27, 55–69. doi: 10.1016/j.jare.2020.03.003

Dorey, T. W., Moghtadaei, M., and Rose, R. A. (2020). Altered heart rate variability in angiotensin II-mediated hypertension is associated with impaired autonomic nervous system signaling and intrinsic sinoatrial node dysfunction. *Heart Rhythm* 17, 1360–1370. doi: 10.1016/j.hrthm.2020.03.014

Duan, X. C., Liu, S. Y., Guo, R., Xiao, L., Xue, H. M., Guo, Q., et al. (2015). Cystathionine-beta-Synthase Gene Transfer Into Rostral Ventrolateral Medulla Exacerbates Hypertension via Nitric Oxide in Spontaneously Hypertensive Rats. *Am. J. Hypertens* 28, 1106–1113. doi: 10.1093/ajh/hpu299

Durgan, D. J., Ganesh, B. P., Cope, J. L., Ajami, N. J., Phillips, S. C., Petrosino, J. F., et al. (2016). Role of the Gut Microbiome in Obstructive Sleep Apnea-Induced Hypertension. *Hypertension* 67, 469–474. doi: 10.1161/hypertensionaha.115.06672

Fu, J., Bonder, M. J., Cenit, M. C., Tigchelaar, E. F., Maatman, A., Dekens, J. A., et al. (2015). The Gut Microbiome Contributes to a Substantial Proportion of the Variation in Blood Lipids. *Circ. Res.* 117, 817–824. doi: 10.1161/circresaha.115.306807

Galla, S., Chakraborty, S., Cheng, X., Yeo, J., Mell, B., Zhang, H., et al. (2018). Disparate effects of antibiotics on hypertension. *Physiol. Genomics* 50, 837–845. doi: 10.1152/physiolgenomics.00073.2018

Garcia-Bereguiain, M. A., Samhan-Arias, A. K., Martin-Romero, F. J., and Gutierrez-Merino, C. (2008). Hydrogen sulfide raises cytosolic calcium in neurons through activation of L-type Ca2+ channels. *Antioxid. Redox Signal.* 10, 31–42. doi: 10.1089/ars.2007.1656

Geloso, M. C., and D'Ambrosi, N. (2021). Microglial Pruning: relevance for Synaptic Dysfunction in Multiple Sclerosis and Related Experimental Models. *Cells* 10:686. doi: 10.3390/cells10030686

Guo, Q., Jin, S., Wang, X. L., Wang, R., Xiao, L., He, R. R., et al. (2011). Hydrogen sulfide in the rostral ventrolateral medulla inhibits sympathetic vasomotor tone through ATP-sensitive K+ channels. *J. Pharmacol. Exp. Ther.* 338, 458–465. doi: 10.1124/jpet.111.180711

Han, Y., Qin, J., Chang, X., Yang, Z., Bu, D., and Du, J. (2005). Modulating effect of hydrogen sulfide on gamma-aminobutyric acid B receptor in recurrent febrile seizures in rats. *Neurosci. Res.* 53, 216–219. doi: 10.1016/j.neures.2005.07.002

Hashimoto, H., Hyodo, S., Kawasaki, M., Mera, T., Chen, L., Soya, A., et al. (2005). Centrally administered adrenomedullin 2 activates hypothalamic oxytocin-secreting neurons, causing elevated plasma oxytocin level in rats. *Am. J. Physiol. Endocrinol. Metab.* 289, E753–E761.

Hsu, C. N., Hou, C. Y., Chang-Chien, G. P., Lin, S., Yang, H. W., and Tain, Y. L. (2020). Perinatal Resveratrol Therapy Prevents Hypertension Programmed by Maternal Chronic Kidney Disease in Adult Male Offspring: implications of the Gut Microbiome and Their Metabolites. *Biomedicines* 8:567. doi: 10.3390/biomedicines8120567

Hu, L. F., Wong, P. T., Moore, P. K., and Bian, J. S. (2007). Hydrogen sulfide attenuates lipopolysaccharide-induced inflammation by inhibition of p38 mitogen-activated protein kinase in microglia. *J. Neurochem.* 100, 1121–1128. doi: 10.1111/j.1471-4159.2006.04283.x

Huang, P., Chen, S., Wang, Y., Liu, J., Yao, Q., Huang, Y., et al. (2015). Down-regulated CBS/H2S pathway is involved in high-salt-induced hypertension in Dahl rats. *Nitric Oxide* 46, 192–203. doi: 10.1016/j.niox.2015.01.004

Huc, T., Jurkowska, H., Wrobel, M., Jaworska, K., Onyszkiewicz, M., and Ufnal, M. (2018). Colonic hydrogen sulfide produces portal hypertension and systemic hypotension in rats. *Exp. Biol. Med.* 243, 96–106. doi: 10.1177/1535370217741869

Huetteman, D. A., and Bogie, H. (2009). Direct blood pressure monitoring in laboratory rodents via implantable radio telemetry. *Methods Mol. Biol.* 573, 57–73. doi: 10.1007/978-1-60761-247-6_4

Jasarevic, E., Morrison, K. E., and Bale, T. L. (2016). Sex differences in the gut microbiome-brain axis across the lifespan. *Philos. Trans. R. Soc. Lond. B Biol. Sci.* 371:20150122. doi: 10.1098/rstb.2015.0122

Jones, D. W., Kim, J. S., Andrew, M. E., Kim, S. J., and Hong, Y. P. (1994). Body mass index and blood pressure in Korean men and women: the Korean National Blood Pressure Survey. *J. Hypertens* 12, 1433–1437. doi: 10.1097/00004872-199412000-00018

Jun, J. Y., Zubcevic, J., Qi, Y., Afzal, A., Carvajal, J. M., Thinschmidt, J. S., et al. (2012). Brain-mediated dysregulation of the bone marrow activity in angiotensin II-induced hypertension. *Hypertension* 60, 1316–1323. doi: 10.1161/hypertensionaha.112.199547

Jurga, A. M., Paleczna, M., and Kuter, K. Z. (2020). Overview of General and Discriminating Markers of Differential Microglia Phenotypes. *Front. Cell Neurosci.* 14:198. doi: 10.3389/fncel.2020.00198

Kanazawa, H., Ohsawa, K., Sasaki, Y., Kohsaka, S., and Imai, Y. (2002). Macrophage/microglia-specific protein Iba1 enhances membrane ruffling and Rac activation via phospholipase C-gamma -dependent pathway. *J. Biol. Chem.* 277, 20026–20032. doi: 10.1074/jbc.m109218200

Kang, Y. M., Ma, Y., Zheng, J. P., Elks, C., Sriramula, S., Yang, Z. M., et al. (2009). Brain nuclear factor-kappa B activation contributes to neurohumoral excitation in angiotensin II-induced hypertension. *Cardiovasc. Res.* 82, 503–512. doi: 10.1093/cvr/cvp073

Kimura, H. (2014). Production and physiological effects of hydrogen sulfide. *Antioxid. Redox Signal.* 20, 783–793. doi: 10.1089/ars.2013.5309

Kolluru, G. K., Shen, X., Bir, S. C., and Kevil, C. G. (2013). Hydrogen sulfide chemical biology: pathophysiological roles and detection. *Nitric Oxide* 35, 5–20. doi: 10.1016/j.niox.2013.07.002

Kozich, J. J., Westcott, S. L., Baxter, N. T., Highlander, S. K., and Schloss, P. D. (2013). Development of a dual-index sequencing strategy and curation pipeline for analyzing amplicon sequence data on the MiSeq Illumina sequencing platform. *Appl. Environ. Microbiol.* 79, 5112–5120. doi: 10.1128/aem.01043-13

Kumar, M., Arora, P., and Sandhir, R. (2020). Hydrogen Sulfide Reverses LPS-Induced Behavioral Deficits by Suppressing Microglial Activation and Promoting M2 Polarization. *J. Neuroimmune Pharmacol.* 16, 483–499. doi: 10.1007/s11481-020-09920-z

Kumar, M., and Sandhir, R. (2019). Hydrogen sulfide suppresses homocysteine-induced glial activation and inflammatory response. *Nitric Oxide* 90, 15–28. doi: 10.1016/j.niox.2019.05.008

Lee, M., McGeer, E., Kodela, R., Kashfi, K., and McGeer, P. L. (2013). NOSH-aspirin (NBS-1120), a novel nitric oxide and hydrogen sulfide releasing hybrid, attenuates neuroinflammation induced by microglial and astrocytic activation: a new candidate for treatment of neurodegenerative disorders. *Glia* 61, 1724–1734. doi: 10.1002/glia.22553

Lee, M., McGeer, E. G., and McGeer, P. L. (2016). Sodium thiosulfate attenuates glial-mediated neuroinflammation in degenerative neurological diseases. *J. Neuroinflammation* 13:32.

Li, H., Gao, Y., Freire, C. D., Raizada, M. K., Toney, G. M., and Sumners, C. (2006). Macrophage migration inhibitory factor in the PVN attenuates the central pressor and dipsogenic actions of angiotensin II. *FASEB J.* 20, 1748–1750. doi: 10.1096/fj.06-5836fje

Li, J., Kemp, B. A., Howell, N. L., Massey, J., Minczuk, K., Huang, Q., et al. (2019a). Metabolic Changes in Spontaneously Hypertensive Rat Hearts Precede Cardiac Dysfunction and Left Ventricular Hypertrophy. *J. Am. Heart Assoc.* 8:e010926.

Li, J., Teng, X., Jin, S., Dong, J., Guo, Q., Tian, D., et al. (2019b). Hydrogen sulfide improves endothelial dysfunction by inhibiting the vicious cycle of NLRP3 inflammasome and oxidative stress in spontaneously hypertensive rats. *J. Hypertens* 37, 1633–1643. doi: 10.1097/hjh.0000000000002101

Li, J., Zhao, F., Wang, Y., Chen, J., Tao, J., Tian, G., et al. (2017). Gut microbiota dysbiosis contributes to the development of hypertension. *Microbiome* 5:14.

Li, T., Zhao, B., Wang, C., Wang, H., Liu, Z., Li, W., et al. (2008). Regulatory effects of hydrogen sulfide on IL-6, IL-8 and IL-10 levels in the plasma and pulmonary tissue of rats with acute lung injury. *Exp. Biol. Med. (Maywood)* 233, 1081–1087. doi: 10.3181/0712-rm-354

Liang, Y. F., Zhang, D. D., Yu, X. J., Gao, H. L., Liu, K. L., Qi, J., et al. (2017). Hydrogen sulfide in paraventricular nucleus attenuates blood pressure by regulating oxidative stress and inflammatory cytokines in high salt-induced hypertension. *Toxicol. Lett.* 270, 62–71. doi: 10.1016/j.toxlet.2017.02.004

Lim, Y. K., Retnam, L., Bhagavath, B., Sethi, S. K., Bin Ali, A., and Lim, S. K. (2002). Gonadal effects on plasma ACE activity in mice. *Atherosclerosis* 160, 311–316. doi: 10.1016/s0021-9150(01)00576-7

Lu, M., Hu, L. F., Hu, G., and Bian, J. S. (2008). Hydrogen sulfide protects astrocytes against H(2)O(2)-induced neural injury via enhancing glutamate uptake. *Free Radic. Biol. Med.* 45, 1705–1713. doi: 10.1016/j.freeradbiomed.2008.09.014

Madwed, J. B., Albrecht, P., Mark, R. G., and Cohen, R. J. (1989). Low-frequency oscillations in arterial pressure and heart rate: a simple computer model. *Am. J. Physiol.* 256, H1573–H1579.

Mancia, G., and Grassi, G. (2014). The autonomic nervous system and hypertension. *Circ. Res.* 114, 1804–1814.

Marques, F. Z., Nelson, E., Chu, P. Y., Horlock, D., Fiedler, A., Ziemann, M., et al. (2017). High-Fiber Diet and Acetate Supplementation Change the Gut Microbiota and Prevent the Development of Hypertension and Heart Failure in

Hypertensive Mice. *Circulation* 135, 964–977. doi: 10.1161/circulationaha.116.024545

Mell, B., Jala, V. R., Mathew, A. V., Byun, J., Waghulde, H., Zhang, Y., et al. (2015). Evidence for a link between gut microbiota and hypertension in the Dahl rat. *Physiol. Genomics* 47, 187–197. doi: 10.1152/physiolgenomics.00136.2014

Miller, A. J., and Arnold, A. C. (2019). The renin-angiotensin system in cardiovascular autonomic control: recent developments and clinical implications. *Clin. Auton Res.* 29, 231–243. doi: 10.1007/s10286-018-0572-5

Mishra, J. S., Hankins, G. D., and Kumar, S. (2016). Testosterone downregulates angiotensin II type-2 receptor via androgen receptor-mediated ERK1/2 MAP kinase pathway in rat aorta. *J Renin Angiotensin Aldosterone Syst.* 17:1470320316674875.

Montano, N., Ruscone, T. G., Porta, A., Lombardi, F., Pagani, M., and Malliani, A. (1994). Power spectrum analysis of heart rate variability to assess the changes in sympathovagal balance during graded orthostatic tilt. *Circulation* 90, 1826–1831. doi: 10.1161/01.cir.90.4.1826

Nagai, Y., Tsugane, M., Oka, J., and Kimura, H. (2004). Hydrogen sulfide induces calcium waves in astrocytes. *FASEB J.* 18, 557–559. doi: 10.1096/fj.03-1052fje

Ni, X., Zhang, L., Peng, M., Shen, T. W., Yu, X. S., Shan, L. Y., et al. (2018). Hydrogen Sulfide Attenuates Hypertensive Inflammation via Regulating Connexin Expression in Spontaneously Hypertensive Rats. *Med. Sci. Monit.* 24, 1205–1218. doi: 10.12659/msm.908761

Ohsawa, K., Imai, Y., Sasaki, Y., and Kohsaka, S. (2004). Microglia/macrophage-specific protein Iba1 binds to fimbrin and enhances its actin-bundling activity. *J. Neurochem.* 88, 844–856. doi: 10.1046/j.1471-4159.2003.02213.x

Oliveira, A. C., Sharma, R. K., Aquino, V., Lobaton, G., Bryant, A. J., Harrison, J. K., et al. (2018). Involvement of Microglial Cells in Hypoxia-induced Pulmonary Hypertension. *Am. J. Respir. Cell Mol. Biol.* 59, 271–273. doi: 10.1165/rcmb.2018-0042le

Pagani, M., Lombardi, F., Guzzetti, S., Rimoldi, O., Furlan, R., Pizzinelli, P., et al. (1986). Power spectral analysis of heart rate and arterial pressure variabilities as a marker of sympatho-vagal interaction in man and conscious dog. *Circ. Res.* 59, 178–193. doi: 10.1161/01.res.59.2.178

Paolicelli, R. C., and Ferretti, M. T. (2017). Function and Dysfunction of Microglia during Brain Development: consequences for Synapses and Neural Circuits. *Front. Synaptic Neurosci.* 9:9. doi: 10.3389/fnsyn.2017.00009

Paton, J. F., and Raizada, M. K. (2010). Neurogenic hypertension. *Exp. Physiol.* 95, 569–571. doi: 10.1113/expphysiol.2009.047282

Pumprla, J., Howorka, K., Groves, D., Chester, M., and Nolan, J. (2002). Functional assessment of heart rate variability: physiological basis and practical applications. *Int. J. Cardiol.* 84, 1–14. doi: 10.1016/s0167-5273(02)00057-8

Qi, J., Zhang, D. M., Suo, Y. P., Song, X. A., Yu, X. J., Elks, C., et al. (2013). Renin-angiotensin system modulates neurotransmitters in the paraventricular nucleus and contributes to angiotensin II-induced hypertensive response. *Cardiovasc. Toxicol.* 13, 48–54. doi: 10.1007/s12012-012-9184-9

Reckelhoff, J. F. (2001). Gender differences in the regulation of blood pressure. *Hypertension* 37, 1199–1208. doi: 10.1161/01.hyp.37.5.1199

Robles-Vera, I., Toral, M., de la Visitacion, N., Sanchez, M., Gomez-Guzman, M., Romero, M., et al. (2020). Probiotics Prevent Dysbiosis and the Rise in Blood Pressure in Genetic Hypertension: role of Short-Chain Fatty Acids. *Mol. Nutr. Food Res.* 64:e1900616.

Sakai, J. (2020). Core Concept: how synaptic pruning shapes neural wiring during development and, possibly, in disease. *Proc. Natl. Acad. Sci. U. S. A.* 117, 16096–16099. doi: 10.1073/pnas.2010281117

Santisteban, M. M., Ahmari, N., Carvajal, J. M., Zingler, M. B., Qi, Y., Kim, S., et al. (2015). Involvement of bone marrow cells and neuroinflammation in hypertension. *Circ. Res.* 117, 178–191. doi: 10.1161/circresaha.117.305853

Sasaki, Y., Ohsawa, K., Kanazawa, H., Kohsaka, S., and Imai, Y. (2001). Iba1 is an actin-cross-linking protein in macrophages/microglia. *Biochem. Biophys. Res. Commun.* 286, 292–297. doi: 10.1006/bbrc.2001.5388

Satou, R., Penrose, H., and Navar, L. G. (2018). Inflammation as a Regulator of the Renin-Angiotensin System and Blood Pressure. *Curr. Hypertens Rep.* 20:100.

Schloss, P. D., Westcott, S. L., Ryabin, T., Hall, J. R., Hartmann, M., Hollister, E. B., et al. (2009). Introducing mothur: open-source, platform-independent, community-supported software for describing and comparing microbial communities. *Appl. Environ. Microbiol.* 75, 7537–7541. doi: 10.1128/aem.01541-09

Shaffer, F., and Ginsberg, J. P. (2017). An Overview of Heart Rate Variability Metrics and Norms. *Front. Public Health* 5:258. doi: 10.3389/fpubh.2017.00258

Sharma, N. M., Haibara, A. S., Katsurada, K., Nandi, S. S., Liu, X., Zheng, H., et al. (2021). Central Ang II (Angiotensin II)-Mediated Sympathoexcitation: role for HIF-1alpha (Hypoxia-Inducible Factor-1alpha) Facilitated Glutamatergic Tone in the Paraventricular Nucleus of the Hypothalamus. *Hypertension* 77, 147–157. doi: 10.1161/hypertensionaha.120.16002

Sharma, R. K., Oliveira, A. C., Kim, S., Rigatto, K., Zubcevic, J., Rathinasabapathy, A., et al. (2018). Involvement of Neuroinflammation in the Pathogenesis of Monocrotaline-Induced Pulmonary Hypertension. *Hypertension* 71, 1156–1163. doi: 10.1161/hypertensionaha.118.10934

Sharma, R. K., Yang, T., Oliveira, A. C., Lobaton, G. O., Aquino, V., Kim, S., et al. (2019). Microglial Cells Impact Gut Microbiota and Gut Pathology in Angiotensin II-Induced Hypertension. *Circ. Res.* 124, 727–736. doi: 10.1161/circresaha.118.313882

Shen, X., Carlstrom, M., Borniquel, S., Jadert, C., Kevil, C. G., and Lundberg, J. O. (2013). Microbial regulation of host hydrogen sulfide bioavailability and metabolism. *Free Radic. Biol. Med.* 60, 195–200. doi: 10.1016/j.freeradbiomed.2013.02.024

Shen, X., Pattillo, C. B., Pardue, S., Bir, S. C., Wang, R., and Kevil, C. G. (2011). Measurement of plasma hydrogen sulfide in vivo and in vitro. *Free Radic. Biol. Med.* 50, 1021–1031. doi: 10.1016/j.freeradbiomed.2011.01.025

Shen, X. Z., Li, Y., Li, L., Shah, K. H., Bernstein, K. E., Lyden, P., et al. (2015). Microglia participate in neurogenic regulation of hypertension. *Hypertension* 66, 309–316. doi: 10.1161/hypertensionaha.115.05333

Shi, P., Diez-Freire, C., Jun, J. Y., Qi, Y., Katovich, M. J., Li, Q., et al. (2010). Brain microglial cytokines in neurogenic hypertension. *Hypertension* 56, 297–303. doi: 10.1161/hypertensionaha.110.150409

Sidhapuriwala, J. N., Ng, S. W., and Bhatia, M. (2009). Effects of hydrogen sulfide on inflammation in caerulein-induced acute pancreatitis. *J. Inflamm.* 6:35. doi: 10.1186/1476-9255-6-35

Sikora, M., Drapala, A., and Ufnal, M. (2014). Exogenous hydrogen sulfide causes different hemodynamic effects in normotensive and hypertensive rats via neurogenic mechanisms. *Pharmacol. Rep.* 66, 751–758. doi: 10.1016/j.pharep.2014.04.004

Silveira-Nunes, G., Durso, D. F. Jr., de Oliveira, L. R. A., Cunha, E. H. M., Maioli, T. U., Vieira, A. T., et al. (2020). Hypertension Is Associated With Intestinal Microbiota Dysbiosis and Inflammation in a Brazilian Population. *Front. Pharmacol.* 11:258. doi: 10.3389/fphar.2020.00258

Singh, S. B., and Lin, H. C. (2015). Hydrogen Sulfide in Physiology and Diseases of the Digestive Tract. *Microorganisms* 3, 866–889. doi: 10.3390/microorganisms3040866

Streeter, E., Al-Magableh, M., Hart, J. L., and Badoer, E. (2011). Hydrogen Sulfide in the RVLM and PVN has No Effect on Cardiovascular Regulation. *Front. Physiol.* 2:55. doi: 10.3389/fphys.2011.00055

Szabo, C. (2021). Hydrogen Sulfide, an Emerging Regulator of Acid-Sensing Ion Channels. *Function* 2:zqab014.

Tayler, H. M., Palmer, J. C., Thomas, T. L., Kehoe, P. G., Paton, J. F., and Love, S. (2018). Cerebral Abeta40 and systemic hypertension. *J. Cereb. Blood Flow Metab.* 38, 1993–2005.

Taylor, J. A., Carr, D. L., Myers, C. W., and Eckberg, D. L. (1998). Mechanisms underlying very-low-frequency RR-interval oscillations in humans. *Circulation* 98, 547–555. doi: 10.1161/01.cir.98.6.547

Thomaz, F. S., Altemani, F., Panchal, S. K., Worrall, S., and Dekker Nitert, M. (2021). The influence of wasabi on the gut microbiota of high-carbohydrate, high-fat diet-induced hypertensive Wistar rats. *J. Hum. Hypertens* 35, 170–180. doi: 10.1038/s41371-020-0359-8

Tomasova, L., Dobrowolski, L., Jurkowska, H., Wrobel, M., Huc, T., Ondrias, K., et al. (2016). Intracolonic hydrogen sulfide lowers blood pressure in rats. *Nitric Oxide* 60, 50–58. doi: 10.1016/j.niox.2016.09.007

Tsioufis, C., Kordalis, A., Flessas, D., Anastasopoulos, I., Tsiachris, D., Papademetriou, V., et al. (2011). Pathophysiology of resistant hypertension: the role of sympathetic nervous system. *Int. J. Hypertens* 2011:642416.

Ufnal, M., Sikora, M., and Dudek, M. (2008). Exogenous hydrogen sulfide produces hemodynamic effects by triggering central neuroregulatory mechanisms. *Acta Neurobiol. Exp.* 68, 382–388.

Umemura, K., and Kimura, H. (2007). Hydrogen sulfide enhances reducing activity in neurons: neurotrophic role of H2S in the brain? *Antioxid. Redox Signal.* 9, 2035–2041. doi: 10.1089/ars.2007.1802

Waki, H., Katahira, K., Polson, J. W., Kasparov, S., Murphy, D., and Paton, J. F. (2006). Automation of analysis of cardiovascular autonomic function from chronic measurements of arterial pressure in conscious rats. *Exp. Physiol.* 91, 201–213. doi: 10.1113/expphysiol.2005.031716

Wallace, J. L., Motta, J. P., and Buret, A. G. (2018). Hydrogen sulfide: an agent of stability at the microbiome-mucosa interface. *Am. J. Physiol. Gastrointest. Liver Physiol.* 314, G143–G149.

Weber, G. J., Pushpakumar, S., Tyagi, S. C., and Sen, U. (2016). Homocysteine and hydrogen sulfide in epigenetic, metabolic and microbiota related renovascular hypertension. *Pharmacol. Res.* 113, 300–312. doi: 10.1016/j.phrs.2016.09.002

Willis, A. D. (2019). Rarefaction, Alpha Diversity, and Statistics. *Front. Microbiol.* 10:2407. doi: 10.3389/fmicb.2019.02407

Wilson, P. W., D'Agostino, R. B., Sullivan, L., Parise, H., and Kannel, W. B. (2002). Overweight and obesity as determinants of cardiovascular risk: the Framingham experience. *Arch. Intern. Med.* 162, 1867–1872.

Xiao, L., Dong, J. H., Teng, X., Jin, S., Xue, H. M., Liu, S. Y., et al. (2018). Hydrogen sulfide improves endothelial dysfunction in hypertension by activating peroxisome proliferator-activated receptor delta/endothelial nitric oxide synthase signaling. *J. Hypertens* 36, 651–665. doi: 10.1097/hjh.0000000000001605

Xuan, A., Long, D., Li, J., Ji, W., Zhang, M., Hong, L., et al. (2012). Hydrogen sulfide attenuates spatial memory impairment and hippocampal neuroinflammation in beta-amyloid rat model of Alzheimer's disease. *J. Neuroinflammation* 9:202.

Xue, H., Zhou, S., Xiao, L., Guo, Q., Liu, S., and Wu, Y. (2015). Hydrogen sulfide improves the endothelial dysfunction in renovascular hypertensive rats. *Physiol. Res.* 64, 663–672. doi: 10.33549/physiolres.932848

Yan, H., Du, J., and Tang, C. (2004). The possible role of hydrogen sulfide on the pathogenesis of spontaneous hypertension in rats. *Biochem. Biophys. Res. Commun.* 313, 22–27. doi: 10.1016/j.bbrc.2003.11.081

Yan, Q., Gu, Y., Li, X., Yang, W., Jia, L., Chen, C., et al. (2017). Alterations of the Gut Microbiome in Hypertension. *Front. Cell Infect. Microbiol.* 7:381. doi: 10.3389/fcimb.2017.00381

Yang, G., Wu, L., Jiang, B., Yang, W., Qi, J., Cao, K., et al. (2008). H2S as a physiologic vasorelaxant: hypertension in mice with deletion of cystathionine gamma-lyase. *Science* 322, 587–590. doi: 10.1126/science.1162667

Yang, T., Santisteban, M. M., Rodriguez, V., Li, E., Ahmari, N., Carvajal, J. M., et al. (2015). Gut dysbiosis is linked to hypertension. *Hypertension* 65, 1331–1340.

Yu, H., Xu, H., Liu, X., Zhang, N., He, A., Yu, J., et al. (2015). Superoxide Mediates Depressive Effects Induced by Hydrogen Sulfide in Rostral Ventrolateral Medulla of Spontaneously Hypertensive Rats. *Oxid. Med. Cell Longev.* 2015:927686.

Zhang, Q., Yuan, L., Liu, D., Wang, J., Wang, S., Zhang, Q., et al. (2014). Hydrogen sulfide attenuates hypoxia-induced neurotoxicity through inhibiting microglial activation. *Pharmacol. Res.* 84, 32–44. doi: 10.1016/j.phrs.2014.04.009

Zhang, X., and Bian, J. S. (2014). Hydrogen sulfide: a neuromodulator and neuroprotectant in the central nervous system. *ACS Chem. Neurosci.* 5, 876–883. doi: 10.1021/cn500185g

Zhang, Y., Hou, L. S., Tang, W. W., Xu, F., Xu, R. H., Liu, X., et al. (2019). High prevalence of obesity-related hypertension among adults aged 40 to 79 years in Southwest China. *Sci. Rep.* 9:15838.

Zhong, G., Chen, F., Cheng, Y., Tang, C., and Du, J. (2003). The role of hydrogen sulfide generation in the pathogenesis of hypertension in rats induced by inhibition of nitric oxide synthase. *J. Hypertens* 21, 1879–1885. doi: 10.1097/00004872-200310000-00015

Zhu, M. L., Zhao, F. R., Zhu, T. T., Wang, Q. Q., Wu, Z. Q., Song, P., et al. (2021). The antihypertension effect of hydrogen sulfide (H2S) is induced by activating VEGFR2 signaling pathway. *Life Sci.* 267:118831. doi: 10.1016/j.lfs.2020.118831

Zhuo, Y., Chen, P. F., Zhang, A. Z., Zhong, H., Chen, C. Q., and Zhu, Y. Z. (2009). Cardioprotective effect of hydrogen sulfide in ischemic reperfusion experimental rats and its influence on expression of survivin gene. *Biol. Pharm. Bull.* 32, 1406–1410. doi: 10.1248/bpb.32.1406

Zubcevic, J., Jun, J. Y., Kim, S., Perez, P. D., Afzal, A., Shan, Z., et al. (2014). Altered inflammatory response is associated with an impaired autonomic input to the bone marrow in the spontaneously hypertensive rat. *Hypertension* 63, 542–550. doi: 10.1161/hypertensionaha.113.02722

Zubcevic, J., Santisteban, M. M., Perez, P. D., Arocha, R., Hiller, H., Malphurs, W. L., et al. (2017). A Single Angiotensin II Hypertensive Stimulus Is Associated with Prolonged Neuronal and Immune System Activation in Wistar-Kyoto Rats. *Front. Physiol.* 8:592. doi: 10.3389/fphys.2017.00592

Zubcevic, J., Waki, H., Diez-Freire, C., Gampel, A., Raizada, M. K., and Paton, J. F. (2009). Chronic blockade of phosphatidylinositol 3-kinase in the nucleus tractus solitarii is prohypertensive in the spontaneously hypertensive rat. *Hypertension* 53, 97–103. doi: 10.1161/hypertensionaha.108.122341

Conflict of Interest: The authors declare that the research was conducted in the absence of any commercial or financial relationships that could be construed as a potential conflict of interest.

Publisher's Note: All claims expressed in this article are solely those of the authors and do not necessarily represent those of their affiliated organizations, or those of the publisher, the editors and the reviewers. Any product that may be evaluated in this article, or claim that may be made by its manufacturer, is not guaranteed or endorsed by the publisher.

frontiers in Physiology

REVIEW
published: 16 September 2021
doi: 10.3389/fphys.2021.665298

Asymmetry and Heterogeneity: Part and Parcel in Cardiac Autonomic Innervation and Function

*Tjitske E. Zandstra[1], Robbert G. E. Notenboom[2], Jeroen Wink[3], Philippine Kiès[1], Hubert W. Vliegen[1], Anastasia D. Egorova[1], Martin J. Schalij[1], Marco C. De Ruiter[2] and Monique R. M. Jongbloed[1,2]**

[1] Department of Cardiology, Leiden University Medical Center, Leiden, Netherlands, [2] Department of Anatomy and Embryology, Leiden University Medical Center, Leiden, Netherlands, [3] Department of Anesthesiology, Leiden University Medical Center, Leiden, Netherlands

OPEN ACCESS

Edited by:
Lilei Yu,
Wuhan University, China

Reviewed by:
Eberhard Weihe,
University of Marburg, Germany
Richard Sutton,
Imperial College London,
United Kingdom

***Correspondence:**
Monique R. M. Jongbloed
m.r.m.jongbloed@lumc.nl

Specialty section:
This article was submitted to Autonomic Neuroscience, a section of the journal Frontiers in Physiology

Received: 07 February 2021
Accepted: 26 August 2021
Published: 16 September 2021

Citation:
Zandstra TE, Notenboom RGE, Wink J, Kiès P, Vliegen HW, Egorova AD, Schalij MJ, De Ruiter MC and Jongbloed MRM (2021) Asymmetry and Heterogeneity: Part and Parcel in Cardiac Autonomic Innervation and Function. Front. Physiol. 12:665298. doi: 10.3389/fphys.2021.665298

The cardiac autonomic nervous system (cANS) regulates cardiac adaptation to different demands. The heart is an asymmetrical organ, and in the selection of adequate treatment of cardiac diseases it may be relevant to take into account that the cANS also has sidedness as well as regional differences in anatomical, functional, and molecular characteristics. The left and right ventricles respond differently to adrenergic stimulation. Isoforms of nitric oxide synthase, which plays an important role in parasympathetic function, are also distributed asymmetrically across the heart. Treatment of cardiac disease heavily relies on affecting left-sided heart targets which are thought to apply to the right ventricle as well. Functional studies of the right ventricle have often been neglected. In addition, many principles have only been investigated in animals and not in humans. Anatomical and functional heterogeneity of the cANS in human tissue or subjects is highly valuable for understanding left- and right-sided cardiac pathology and for identifying novel treatment targets and modalities. Within this perspective, we aim to provide an overview and synthesis of anatomical and functional heterogeneity of the cANS in tissue or subjects, focusing on the human heart.

Keywords: autonomic nervous system, sympathetic cardiac nerves, vagal cardiac branches, vagus nerve, cardiac autonomic function, regional differences, anatomical sidedness, asymmetry

INTRODUCTION

The cardiac autonomic nervous system (cANS) adapts the responses of the heart to external demands. It consists of a sympathetic part, which adapts cardiac function to physical activity and stress, and a parasympathetic part, which adapts it to a resting and restorative state. Under physiological conditions these systems are balanced and cardiac responses will be fine-tuned to differentiating demands. Under pathophysiological conditions, dysregulation of the cANS can occur as a result of for example cardiac damage and/or failure, and consequently the balance between the sympathetic and parasympathetic

activity is lost. Usually, this is caused by an increased activity of the sympathetic part of the cANS and/or diminished activity of the parasympathetic part and is associated with an adverse prognosis.

Knowledge about the cANS is necessary for understanding cardiac disease and for the identification of treatment targets (Vegh et al., 2016). Much knowledge is derived from studies in patients with left-sided pathology, such as myocardial infarction or left ventricular failure (Cao et al., 2000; Fallavollita et al., 2014; Fukuda et al., 2015; Matsuo et al., 2016; Franciosi et al., 2017). The same principles are considered to apply to the right ventricle (RV). However, the RV is developmentally, morphologically, and functionally different from the left ventricle (LV). Traditional heart failure medication used in patients with left ventricular failure, relying heavily on influencing the cANS, may not have the same effect on patients with congenital heart disease and right ventricular failure, even though the hemodynamic problem is similar (Hechter et al., 2001; Lester et al., 2001; Robinson et al., 2002; Dore et al., 2005; Josephson et al., 2006; Doughan et al., 2007; Giardini et al., 2007; Therrien et al., 2008; Bouallal et al., 2010; Tutarel et al., 2012; Dos et al., 2013; van der Bom et al., 2013; Palma and Benarroch, 2014; Tobler et al., 2017). Likewise, other cardiac diseases show a relation to cardiac sidedness and region and are heavily influenced by autonomic innervation, such as cardiac arrhythmias originating from the region of the pulmonary veins, ligament of Marshall and the RV outflow tract (Wickramasinghe and Patel, 2013).

Although several reports describe the human heart and cANS, a detailed overview focusing specifically on anatomical sidedness and regional differences in cardiac autonomic innervation as related to function, is currently lacking. The selection of adequate treatment, the identification of future treatment targets, the planning of cardiothoracic surgery and catheter ablation procedures for arrhythmias, as well as the use of thoracic epidural anesthesia might be optimized by taking the sidedness and regional differences of the cANS into consideration.

The aim of the current paper is to review the anatomy and physiology of the human cANS with special emphasizes on asymmetry and regional differences in peripheral cardiac autonomic regulation. For a comprehensive overview of central regulation of cardiac autonomic function, we refer to previous excellent work (Anderson et al., 2000; Kirby, 2007; Kawashima, 2011; Hasan, 2013; Palma and Benarroch, 2014; Jamali et al., 2016; Coote and Spyer, 2018). Data from animal studies are cited when human data are unavailable or when data from animal studies offer additional insight. Relevant questions for future research are formulated.

SYMPATHETIC GANGLIA AND NERVES: ANATOMICAL EVIDENCE OF ORIGINS, VARIATIONS AND ASYMMETRY (FIGURE 1A)

Preganglionic cardiac sympathetic fibers originate from neurons located in the intermediolateral cell columns of the upper thoracic spinal cord (usually T1-T4 or T5) and exit the spinal cord through the ventral (anterior) roots of spinal nerves (**Figure 1A**). Subsequently, they synapse on postganglionic sympathetic neurons in the paravertebral ganglia of the sympathetic trunk. The sympathetic trunk is a bilateral structure situated left and right paravertebrally, extending from the cervical to the coccygeal level. The following ganglia of the sympathetic trunk may provide postganglionic fibers to the heart: the left and right superior cervical, middle cervical and vertebral ganglia, the left and right cervicothoracic ganglion (also called stellate ganglion, composed of the inferior cervical ganglion and the first thoracic ganglion), and the upper thoracic ganglia on both sides. However, there still is debate about the upper and lower limits from which postganglionic fibers to the heart originate, and significant interindividual variations exist (Bonica, 1968; Janes et al., 1986; Kawashima, 2011) (reviewed in Wink et al., 2020). Postganglionic sympathetic fibers travel as cardiac nerves from these ganglia toward the cardiac plexus. Defined by the paravertebral ganglion they originate from, these nerves are named as follows (**Figure 1A**): the superior cervical cardiac nerve (originating from the superior cervical ganglion or sympathetic trunk between the superior cervical and middle cervical ganglia), the middle cervical cardiac nerve (originating from the middle cervical ganglion or the vertebral ganglion, or from the sympathetic trunk between the middle cervical and the inferior cervical or cervicothoracic/stellate ganglia, including the ansa subclavia), the inferior cervical cardiac nerve (originating from the inferior cervical ganglion or the cervicothoracic/stellate ganglion), or thoracic cardiac nerves (originating from the thoracic ganglia or the thoracic sympathetic trunk below the inferior cervical or cervicothoracic/stellate ganglion) (Kawashima, 2005; Federative International Programme for Anatomical Terminology, 2019)

Variations and asymmetry in stellate ganglion morphology and cardiac sympathetic nerve origin have been described. In an American human cadaver study, it was observed that the right stellate ganglion was often longer than the left (Kwon et al., 2018). However, in a cohort from Switzerland, the left stellate ganglion was longer (Marcer et al., 2012) and in a Chinese cohort, no differences in length were found between the left and right stellate ganglion (Yin et al., 2015). A study of Pather in humans in South Africa, also reported no significant difference in the length and width of the right and left sides of the adult cardiothoracic ganglia (Pather et al., 2006). In these studies, differing occurrence and asymmetry of the left and right stellate ganglion as well as the other thoracic sympathetic ganglia is consistently described.

A middle cardiac cervical nerve originating from the ansa subclavia (nerve connection between the middle and inferior cervical ganglia) was observed twice as often on the left compared to the right (Kawashima, 2005). Furthermore, asymmetry in the origin and courses of the left and right thoracic cardiac nerves originating from the lower thoracic ganglia (fourth or fifth) was observed (Fukuyama, 1982; Kawashima, 2005). The left lower thoracic cardiac nerves follow a simple course along the aortic arch and thoracic aorta, comparable with most other cardiac nerves, which generally run along the great

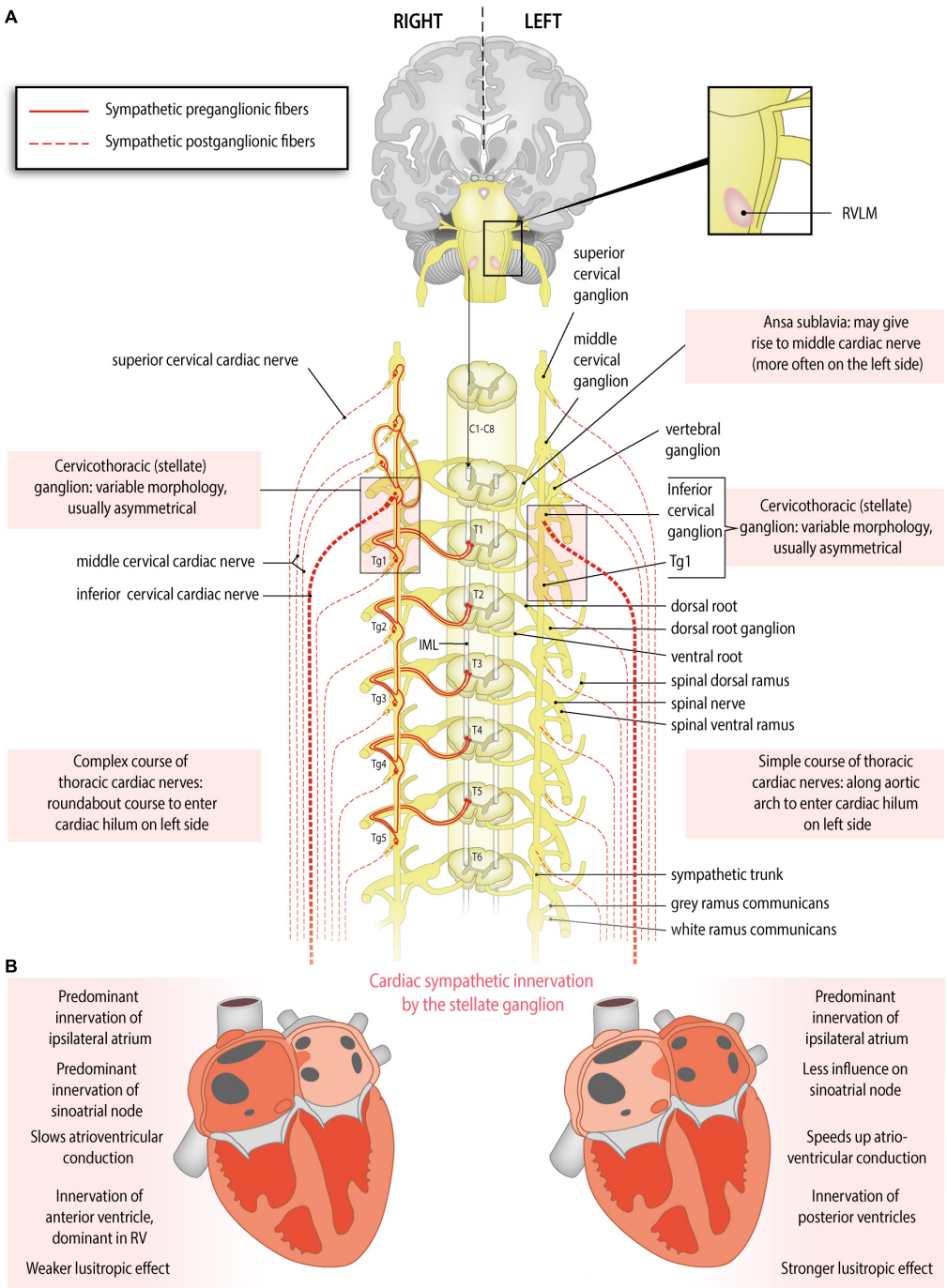

FIGURE 1 | Anatomy of the sympathetic cardiac autonomic nervous system: asymmetry and regional differences. **(A)** Sympathetic cardiac autonomic nervous system. Preganglionic cardiac sympathetic axons (red, solid lines) arise from neurons of the intermediolateral (IML) cell columns in the upper four or five thoracic segments of the spinal cord. These neurons receive excitatory input from the rostral ventrolateral medulla (RVLM). The preganglionic fibers leave the spinal cord through ventral (anterior) roots, enter the ventral (anterior) rami of spinal nerves and pass to the sympathetic chain through white rami communicantes to synapse in the upper thoracic ganglia (Tg) or cervical ganglia; postganglionic fibers (red, dotted lines) from these ganglia form the sympathetic cardiac nerves. At the heart parasympathetic and sympathetic nerves converge to form the cardiac plexus from which atrial and ventricular autonomic innervation is arranged. Sided and regional differences in anatomy are indicated in the boxes. **(B)** Functional anatomy of cardiac sympathetic innervation by the right and left stellate ganglia. Sided and regional differences in function are indicated in the boxes. The right stellate ganglion greatly increases heart rate, slows the atrioventricular conduction, influences the right atrium more strongly than the left, shortens the QT interval, contributes to some extent to myocardial relaxation, and is the predominant source of sympathetic innervation in the right ventricle and the anterior part of both ventricles. The left stellate ganglion increases heart rate to some extent, speeds up the atrioventricular conduction, influences the left atrium more strongly than the right, lengthens the QT interval, contributes greatly to myocardial relaxation, and is the predominant source of sympathetic innervation of the posterior part of the ventricles.

arteries. In contrast, the right lower thoracic cardiac nerves may descend obliquely along the intercostal vessels, turn and ascend along the thoracic aorta, to finally reach the heart through the right venous part of the cardiac hilum or by connecting to the cardiac plexus. This complex, 'roundabout' course may be related to remodeling/regression of the right aortic arch during embryonic development, whereas the left sided arch persists (Gittenberger-de Groot et al., 2006; Kawashima, 2011).

CARDIAC AREAS OF SYMPATHETIC INNERVATION BY THE LEFT AND RIGHT STELLATE GANGLION: FUNCTIONAL EVIDENCE (FIGURE 1B AND TABLE 1)

The stellate ganglia play important and differing roles in cardiac autonomic function and have been studied extensively. The right stellate ganglion is primarily responsible for increasing the heart rate and slowing atrioventricular conduction, whereas the left stellate ganglion has little effect on heart rate and increases atrioventricular conduction (**Figure 1B**). This was concluded from functional studies in humans. A right stellate ganglion block leads to a marked decrease in heart rate, whereas left stellate ganglion block leads to a more discrete decrease in heart rate (Rogers et al., 1978; Yokota et al., 2013). Furthermore, it was demonstrated that right stellate ganglion block leads to faster atrioventricular conduction and left stellate ganglion block leads to slower atrioventricular conduction (Cinca et al., 1985). Interestingly, a dog study suggested that the left stellate ganglion dominates over the right in terms of ventricular refractoriness: left stellate ganglion block led to a net increase in refractoriness, suggesting a decreased sensitivity to ventricular arrhythmias. However, while right stellate ganglion block produced a similar effect in absence of a functional left stellate ganglion, right stellate ganglion block led to a net decrease in refractoriness in the presence of a functional left stellate ganglion. This suggests an overshoot in compensatory sympathetic activity from the left stellate ganglion (Schwartz et al., 1977). Similarly, in humans, left stellate ganglion block shortens the corrected QT interval, whereas right stellate ganglion block lengthens it, suggesting a potential factor in arrhythmogenesis (Egawa et al., 2001). In line with this, left stellate ganglion block is increasingly used to treat ventricular arrhythmias (Meng et al., 2017). Other studies elaborate further on this topic (Lane and Schwartz, 1987; Schwartz et al., 1992; Zhou et al., 2008).

A block of either stellate ganglion in humans, led to prolonged atrial refractory time and a reduction in inducibility of atrial fibrillation. Each stellate ganglion may predominantly innervate the ipsilateral atrium, which, in turn, relays signals to the contralateral atrium (Leftheriotis et al., 2016).

The right stellate ganglion and left stellate ganglion influence both ventricles but unevenly. These regional differences were firstly demonstrated in dogs: the right stellate ganglion primarily influenced the anterior part of the LV and RV, whereas the left stellate ganglion primarily influenced the posterior LV and RV (Yanowitz et al., 1966). Similar to human studies, in this study QT-prolongation was observed after ablation of the right stellate ganglion and after stimulation of the left stellate ganglion (Yanowitz et al., 1966). A similar pattern was found in pigs: stimulation of the right stellate ganglion led to increased echocardiographic radial and circumferential strain in the anterior regions, whereas stimulation of the left stellate ganglion led to increased strain in the inferior/posterior regions (Zhou et al., 2013). This pattern was confirmed by measuring activation-recovery intervals in another pig study (Vaseghi et al., 2013). Additionally, a study by Schlack and Thamer (1996) in dogs demonstrated an improved lusitropic (myocardial relaxation) effect by left stellate ganglion stimulation compared with an impaired relaxation upon right stellate ganglion stimulation. These authors also demonstrated a higher global contractility increase with left stellate ganglion stimulation compared with right stellate ganglion stimulation. In the RV, innervation of the right stellate ganglion may predominate: in a study in dogs, right stellate ganglion stimulation shortened the refractory period more strongly in the RV than in the LV. Left stellate ganglion stimulation shortened the refractory period of the LV and the RV equally (Garcia-Calvo et al., 1992). Whether the same patterns in the ventricles are present in humans, and whether the distribution of innervation is influenced by the dominance of the coronary system, is unknown. It is considered that these differences in effects from the left and right stellate ganglia may play a role in arrhythmias, especially when their activity is unbalanced (Lane and Schwartz, 1987).

TABLE 1 | Summary of functional characteristics of the right and left sided ganglion stellatum.[a]

Right stellate ganglion	Left stellate ganglion
Predominant innervation ipsilateral atrium ++	Predominant innervation ipsilateral atrium ++
Innervation contralateral atrium +	Innervation contralateral atrium +
Predominant innervation of anterior part both ventricles (dogs)	Predominant innervation of posterior part both ventricles (dogs)
Echocardiographic radial and circumferential strain in the anterior regions of the LV ↑ (pigs)	Echocardiographic radial and circumferential strain in the inferior/posterior regions of the LV ↑ (pigs)
Predominant innervation of RV (dogs)	
Myocardial relaxation (lusitropy) + (dogs)	Myocardial relaxation (lusitropy) ++ (dogs)
Myocardial contractility +	Myocardial contractility ++
Cardiac conduction system	
Heart rate ↑↑	Heart rate ↑/=
AV conduction ↓	AV conduction ↑
QT interval ↓	QT interval ↑
Right stellate ganglion block	**Left stellate ganglion block**
Heart rate ↓↓	Heart rate ↓
AV conduction ↑	AV conduction ↓
QTc interval ↑	QTc interval ↓
Atrial refractory time ↑	Atrial refractory time ↑
AF inducibility ↓	AF inducibility ↓

[a]*Data derived from human studies, unless otherwise indicated-for references see text.*

PARASYMPATHETIC INNERVATION: ANATOMICAL EVIDENCE OF ORIGINS AND CONTRIBUTIONS FROM LEFT AND RIGHT VAGAL CARDIAC BRANCHES (FIGURE 2A)

Preganglionic cardiac parasympathetic fibers originate from neurons located in the nucleus ambiguus and the dorsal motor nucleus of the vagus nerve and reach the heart through cardiac branches of this nerve (Standring and Gray, 2016). The vagus nerves (tenth cranial nerve) originate bilaterally from the medulla oblongata and give rise to a recurrent laryngeal nerve that differs in origin (branching site) and course on the two sides. Parasympathetic cardiac branches from these nerves are defined according to their origin as follows (**Figure 2A**): the superior cervical cardiac branch originates from the vagus nerve proximal to the branching site of the recurrent laryngeal nerve. A branch originating from any part of the recurrent laryngeal nerve is called an inferior cervical cardiac branch, and the cardiac branch originating from the vagus nerve distal to the branching site of the recurrent laryngeal nerve is called a thoracic cardiac branch (Kawashima, 2005; Federative International Programme for Anatomical Terminology, 2019). While all cardiac branches are consistently seen on the right side, on the left side, the thoracic cardiac branch was absent in 45% of cases (Kawashima, 2005). In contrast to the preganglionic cardiac sympathetic fibers, which synapse on postganglionic neurons within ganglia of the sympathetic trunk (i.e., remote from the heart), preganglionic cardiac parasympathetic fibers synapse on postganglionic neurons within ganglionated plexuses embedded in the epicardial fat pads and the heart wall. To our knowledge, no further information is available about variations and asymmetry in the parasympathetic cardiac branches.

CARDIAC AREAS OF PARASYMPATHETIC INNERVATION BY THE LEFT AND RIGHT VAGUS NERVE: FUNCTIONAL EVIDENCE (FIGURE 2B AND TABLE 2)

The human sinoatrial node and atria are most likely predominantly influenced by the right vagus nerve, the atrioventricular node is predominantly influenced by the left vagus nerve, and the ventricles are influenced at least by the left vagus nerve but likely by both vagus nerves (Banzett et al., 1999; Lewis et al., 2001; Muppidi et al., 2011; **Figure 2B**). Although human studies are scarce, animal studies are in accordance with this: in the isolated rabbit heart, stimulation of the right vagus nerve had a stronger effect on heart rate, whereas the left vagus nerve had a stronger effect on atrioventricular conduction (Ng et al., 2001). This group also used the same model to explore this in the context of so-called accentuated antagonism (generally, vagal stimulation has a stronger effect when a background level of sympathetic activity is present). During sympathetic stimulation, right and left vagal nerve stimulation may reduce the heart rate differently: there was a trend toward a stronger effect of the right vagus nerve, although this result was not statistically significant (Brack et al., 2004). Animal research also reveals possible regional differences: in pigs, left or right vagus nerve stimulation had a stronger effect on the endocardium than on the epicardium and also on the apex compared to the base. This study also demonstrates that in pigs at least the LV is influenced by both vagus nerves (Yamakawa et al., 2014).

TABLE 2 | Summary of functional characteristics of the right and left sided vagus nerves.[a]

Right vagus nerve	Left vagus nerve
Innervation atria ++?	Innervation atria +?
Sino-atrial node	AV node
Both ventricles	Both ventricles
Influence on endocardium > influence epicardium (pig)	Influence on endocardium > influence epicardium (pig)
Influence on apex > influence on base (pig)	Influence on apex > influence on base (pig)
Cardiac conduction system	
Heart rate ↓↓ (rabbit)	Heart rate ↓
AV conduction ↓	AV conduction ↓↓

[a]*Data derived from human studies, unless otherwise indicated-for references see text.*

CARDIAC AFFERENT NERVE FIBERS: ASYMMETRY AND REGIONAL DIFFERENCES, ANATOMICAL AND FUNCTIONAL ASPECTS

Although visceral afferent fibers, in a strict sense, are not part of the autonomic nervous system (Armour, 1999), given their clinical relevance, regional and asymmetrical features of the afferent (sensory) part of the cardiac nervous system are also considered here. Cardiac afferent nerve fibers are an integral part of the regulatory pathways the cANS is involved in, and transfer sensory signals from the heart to the central nervous system, where they may activate efferent neurons through feedback loops. They convey cardiac nociceptive and reflexive information (Armour, 1999; Kirby, 2007). Like cardiac efferent (autonomic) nerves, these afferents demonstrate regional differences and asymmetry. Studies conducted in humans are rare and most knowledge regarding the organization and function of the cardiac afferent system is derived and extrapolated from animal studies.

The neurites (dendrites) of cardiac afferent neurons are located in the myocardium and their cell bodies lie in the dorsal root ganglia of spinal nerves or the inferior ganglion of the vagus nerve (nodose ganglion) (Anderson et al., 2000; Kirby, 2007; Palma and Benarroch, 2014).

Cardiac spinal or "sympathetic" afferents [named as such because their fibers accompany sympathetic efferent (autonomic) fibers retrogradely in splanchnic nerves] convey mainly nociceptive sensory information from the heart via the

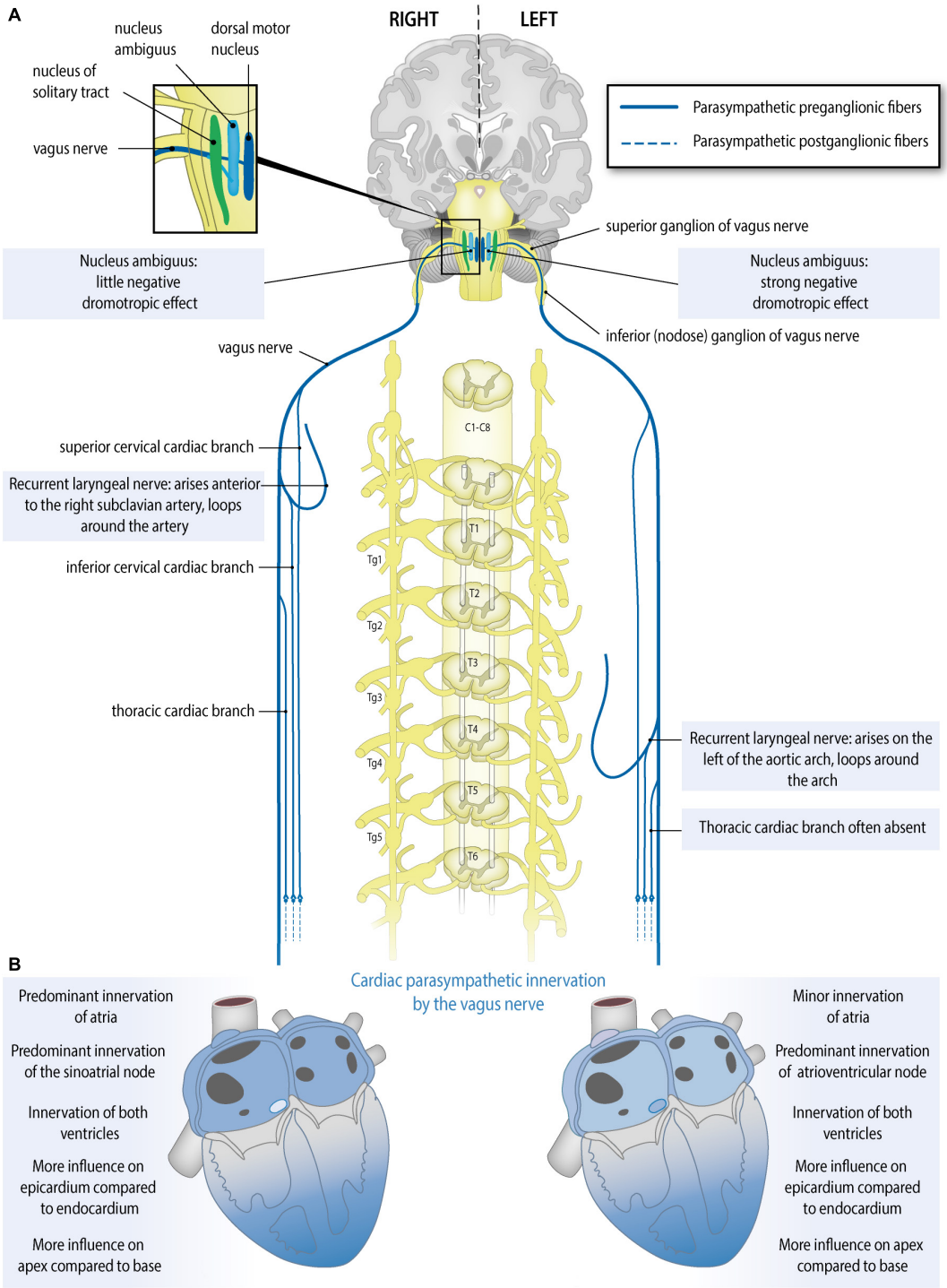

FIGURE 2 | Anatomy of the parasympathetic cardiac autonomic nervous system: asymmetry and regional differences. **(A)** Parasympathetic cardiac autonomic nervous system. Preganglionic cardiac parasympathetic axons (blue, solid lines) arise from neurons in either the nucleus ambiguus or dorsal vagal nucleus; they run in cardiac branches of the vagus nerve to synapse in cardiac plexuses and ganglia from where postganglionic fibers (blue, dotted lines) innervate the sinoatrial node (SAN), atrioventricular node (AVN), coronary arteries, and ventricular myocytes. Sided and regional differences in anatomy are indicated in the boxes. **(B)** Functional anatomy of the right and left vagal nerves. Sided and regional differences in function are indicated in the boxes. The right vagus nerve greatly slows heart rate, may influence the atria more than the left vagus nerve, slows atrioventricular conduction to some extent, influences the epicardium more strongly than the endocardium and influences the apex more strongly than the base. The left vagus nerve slows heart rate to some extent, may influence the atria less than the right vagus nerve, greatly slows atrioventricular conduction, influences the epicardium more strongly than the endocardium and influences the apex more strongly than the base.

splanchnic nerves, sympathetic trunk, spinal nerve and dorsal root (dorsal root ganglia) to the posterior horn of the spinal grey matter, where they synapse on second-order neurons of lamina I. The nociceptive information is further conveyed via ascending pain pathways to the thalamus and other brain regions involved in cardiac pain perception (Palma and Benarroch, 2014). When spinal cardiac afferents are involved in feedback loops via local interneurons projecting to the intermediolateral cell columns of the spinal cord, they can influence sympathetic efferent (motor) activity directly (Armour, 1999; Anderson et al., 2000; Kirby, 2007; Palma and Benarroch, 2014).

Some sympathetic afferents (mainly C-fibers, which are unmyelinated and are slow-conducting) produce substance P as their neurotransmitter. Substance P mediates nociception and also has efferent effects. Nerves containing substance P in the human heart are especially found around coronary arteries and other small blood vessels, and inside intrinsic cardiac ganglia (Weihe et al., 1981; Rechardt et al., 1986; Laine et al., 2000; Hoover et al., 2009). Substance P may be upregulated under pathological conditions. In conditions of ischemia-reperfusion, substance P can have a beneficial effect through increasing coronary blood flow (which was demonstrated in dogs). Conversely, in non-ischemic conditions such as myocarditis and volume overload, substance P may contribute to inflammation, apoptosis, and long-term reduction of LV-function (as was shown in various rodent models) (Dehlin and Levick, 2014).

Cardiac vagal afferents, of which unmyelinated, slow-conducting C-fibers constitute an important part, as was shown in studies in amongst others dogs and rats (Ditting et al., 2005) run centrally in the vagus nerves and convey mainly reflexive (mechano- and chemosensory) information from the heart via the nodose ganglion to the (caudal part of the) solitary nucleus (nucleus tractus solitarii) (**Figure 2A**). They can activate feedback loops through the thalamus and the parabrachial nucleus, and nucleus ambiguus, which lead to increased parasympathetic or decreased sympathetic outflow to the heart (Armour, 1999; Kirby, 2007; Palma and Benarroch, 2014). Of interest, cardiac afferent fibers have also been described to interact directly with postganglionic sympathetic neurons in the stellate ganglia and with parasympathetic postganglionic neurons or interneurons in the intrinsic cardiac ganglia, forming part of intrathoracic feedback loops, bypassing the central nervous system (Crick et al., 2000; Kirby, 2007).

The distribution of cardiac afferent nerve fibers in human can differ per cardiac region. The often observed bradycardia specifically accompanying inferoposterior myocardial infarctions may be a consequence of activation of vagal afferents on the inferior wall of the LV which trigger parasympathetic reflexes (Perez-Gomez et al., 1979; Flapan et al., 1993). The same pattern was observed in an experimental study in dogs (Thames et al., 1978). Interestingly, patients with an anterior myocardial infarction also had worse baroreflex sensitivity and heart rate variability at follow-up compared with patients with inferior/posterior infarctions, which may also be due to this distribution, although it must be noted that the left ventricular ejection fraction was also lower in the anterior infarction group (La Rovere et al., 1998).

Distribution of vagal afferents in the heart was studied in guinea pigs by retrograde labeling of the nodose ganglia. Most vagal afferents were concentrated in the posterior atrial wall (mostly on the ipsilateral atrium of the labeled nodose ganglion), the pulmonary arterial wall, and around the coronary arteries (Quigg et al., 1988). From a physiological study in cats, it was concluded that cardiac afferents (vagal or spinal not specified) were located throughout the heart wall. In the ventricles, they were present mostly in the endocardium. In the atria, they were present equally endo- and epicardially (Malliani et al., 1973).

In conclusion, the anatomy and physiology of cardiac afferents are still largely to be elucidated, especially in humans.

ASYMMETRY OF THE CARDIAC PLEXUS AND CORONARY CARDIAC NERVES: ANATOMICAL EVIDENCE (FIGURE 3)

Human left and right sympathetic and parasympathetic cardiopulmonary nerves connect in the mediastinum, where they form the cardiac plexus. A distinction is made between the superficial (ventral) cardiac plexus, located in between the pulmonary trunk and aortic arch, and the deep (dorsal) cardiac plexus, located between the aorta and trachea (De Gama et al., 2012; **Figure 3**). The superficial and deep cardiac plexuses are not as discrete and confined as for example the cervical and thoracic paravertebral ganglia, but rather describe the locations of interconnecting nerve networks where the number of nerve fibers gradually increases and nerve fibers tend to be more mixed (including sympathetic, parasympathetic and visceral afferent fibers). Plexus formation tends to start higher on the right side (level of the brachiocephalic trunk) than on the left side (level of the aortic arch) (Kawashima, 2011; **Figure 3**; **Table 3**). Possibly, this can be attributed to regional differences during embryonic development, as the initially symmetrical pharyngeal arch arterial system, giving rise to part of the putative arterial vasculature, will show a left-sided dominance, with disappearance of the right sixth pharyngeal arch artery and disappearance/remodeling of the right aortic arch artery. The right fourth pharyngeal arch artery will form the proximal part of the right subclavian artery, below which the right laryngeal recurrent nerve will eventually course (Gittenberger-de Groot et al., 2006).

Among many smaller nerves, three large mixed nerves arise from these plexuses that will innervate the atria and ventricles: from the deep/dorsal cardiac plexus, the left coronary cardiac nerve (which runs along the left anterior descending coronary artery) and the left lateral cardiac nerve (which runs along the circumflex coronary artery) arise. From the ventral plexus, the right coronary cardiac nerve (which runs along the right coronary artery) arises (Janes et al., 1986). Additional cardiopulmonary nerves connect to these (coronary) cardiac nerves distal from the plexuses. Surprisingly, the left coronary cardiac nerve is composed mainly of contributions of right-sided cardiac nerves, largely originating from the right stellate ganglion, which pass through the deep (dorsal) cardiac plexus. The right coronary cardiac nerve is composed mainly of contributions of left-sided cardiac nerves, largely originating from the left stellate ganglion,

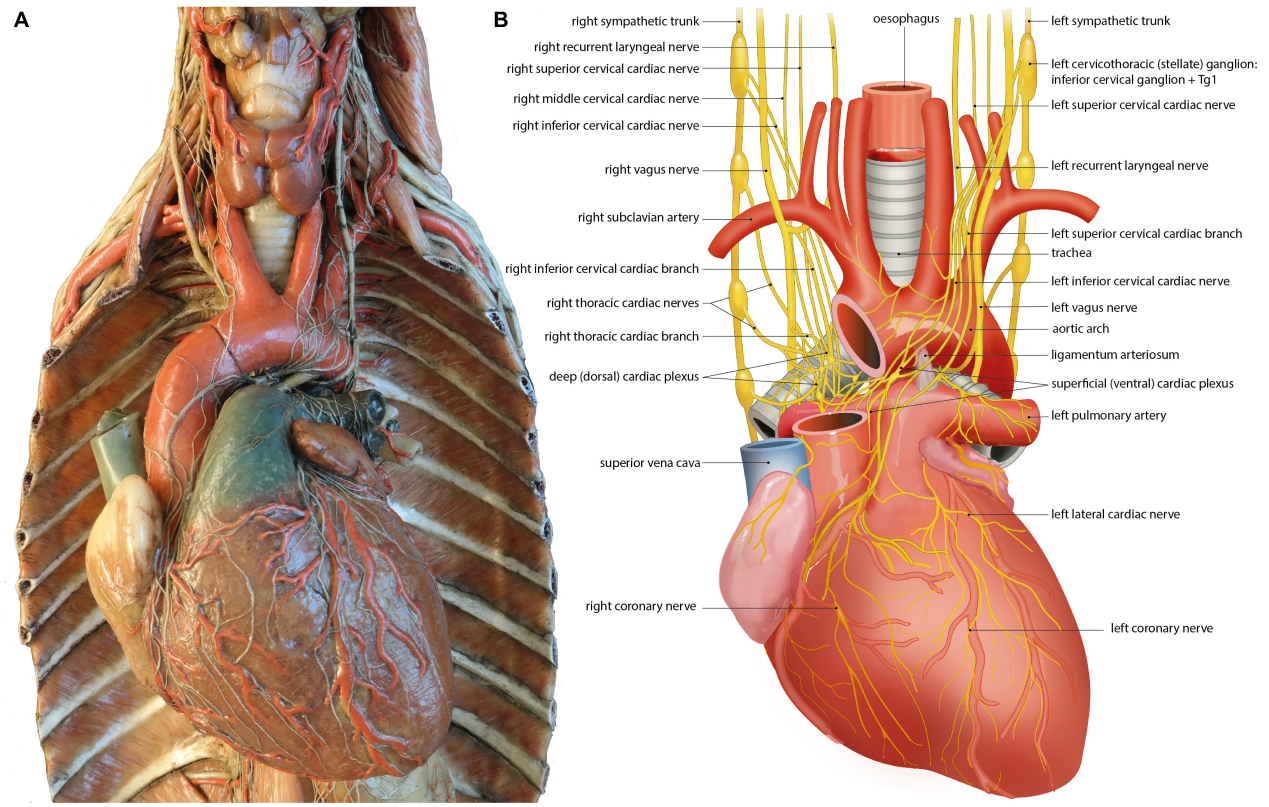

FIGURE 3 | The left and right cardiac nerves and superficial and deep cardiac plexus. **(A)** Wax mold (Museo delle Cere Anatomiche "Luigi Cattaneo", Bologna, Italy) demonstrating sympathetic and parasympathetic (vagal) cardiac nerves and superficial and deep cardiac plexus. Photomicrograph courtesy of Dr. E.A.J.F. Lakke. With permission of the Museo delle Cere Anatomiche "Luigi Cattaneo", University Museum System, Alma Mater Studiorum – University of Bologna, Italy. **(B)** Annotated drawing, details depiction of cardiac nerves and plexus depicted in the left panel. At the heart sympathetic and parasympathetic nerves converge to form the superficial and deep cardiac plexus from which atrial and ventricular autonomic innervation is arranged. For further explanation see text.

which pass through the superficial (ventral) cardiac plexus (Janes et al., 1986; **Table 3**).

INTRINSIC CARDIAC GANGLIA: ANATOMICAL EVIDENCE OF REGIONAL ORGANIZATION AND GRADIENT IN (PARA)SYMPATHETIC DOMINANCE (FIGURE 4)

Apart from nerves that conduct signals from the central nervous system to the human heart (i.e., extrinsic cardiac nerves), an intrinsic cardiac nervous system is also present. A network of over 800 ganglia can be found on the posterior surfaces of the atria, around the base of the aorta and pulmonary artery, dorsal and ventral to the pulmonary veins, and on the ventricular myocardium near the coronary arteries (Singh et al., 1996; Armour et al., 1997; Pauza et al., 2000; Wake and Brack, 2016). These ganglia are usually embedded in epicardial adipose tissue and are more or less organized into seven regions, called ganglionated (sub)plexuses: the right dorsal atrial plexus, the ventral right atrial plexus, the left dorsal plexus, the ventral left atrial plexus, the middle dorsal plexus, the right coronary plexus, and the left coronary plexus (Pauza et al., 2000; Wake and Brack, 2016). Nerve fibers in these plexuses are sympathetic, parasympathetic, or mixed. The dorsal and ventral right atrial ganglionated subplexuses (supplying also the sinoatrial node) are predominantly parasympathetic. The left and right coronary epicardiac subplexuses (supplying mostly the ventricles) are predominantly sympathetic (Petraitiene et al., 2014; **Table 3**). There is a predominance of parasympathetic neurons in plexuses on the atria and sympathetic neurons in plexuses on the ventricles (Wake and Brack, 2016). A considerable part of the intrinsic cardiac ganglion cells show co-expression of sympathetic and parasympathetic markers, as was shown in rhesus monkeys as well as humans (Weihe et al., 2005). This network has a function in passing down vagal impulses further and also in integrating sympathetic, parasympathetic, and sensory information in complex cardiac responses (Armour et al., 1997; Hasan, 2013; Wake and Brack, 2016).

Interestingly, in the experimental treatment of refractory vagally mediated reflex syncope, ablation of both left- and right atrial sites of parasympathetic innervation has shown promising results. Even though an anatomical substrate for these conditions may be difficult to locate, it appears that damaging

TABLE 3 | Summary of asymmetrical and regional features of the extrinsic cardiac plexus, coronary cardiac nerves, and intrinsic cardiac plexus (all human studies).

- Right-sided extrinsic cardiac plexus formation located more superiorly (level of brachiocephalic trunk) than left-sided extrinsic cardiac plexus (level of aortic arch) {Kawashima, 2011 #222}
- Right coronary cardiac nerve: composed largely from contributions of left stellate ganglion {Janes et al., 1986, #35}
- Left coronary cardiac nerve: composed largely from contributions of right stellate ganglion {Janes et al., 1986, #35}
- Dorsal and ventral right atrial intrinsic cardiac plexuses: mainly parasympathetic {Petraitiene et al., 2014 #410}
- Left and right coronary epicardiac plexuses: mainly sympathetic {Petraitiene et al., 2014, #410}
- Predominance of parasympathetic neurons in plexuses on the atria {Wake and Brack, 2016, #167}
- Predominance of sympathetic neurons in plexuses on the ventricles {Wake and Brack, 2016, #167}

parasympathetic control of the heart on either side may prevent recurring episodes (Pachón et al., 2005; Sun et al., 2016).

ANATOMICAL EVIDENCE OF REGIONAL DIFFERENCES IN CARDIAC INNERVATION DENSITY: SYMPATHETIC AND PARASYMPATHETIC

Generally, in humans, innervation density is higher in the atria than in the ventricles, and a gradient in innervation density (higher to lower) is present from the ventricular base to the apex (Kawano et al., 2003). In the atria, most nerve endings are parasympathetic, and in the ventricles, most nerve endings are sympathetic (Kawano et al., 2003). The right atrium (RA) has a higher density of sympathetic innervation than the left atrium (LA) (Kawano et al., 2003). The RA and RV have a higher density of parasympathetic innervation than the LA and LV (Kawano et al., 2003; **Figure 4**).

Specifically in the human conduction system, there is an innervation gradient ranging from the most dense innervation in the sinoatrial node to less innervation in the atrioventricular node, penetrating bundles, and bundle branches (Crick et al., 1994; Chow et al., 2001). As a whole, the conduction system is more densely innervated than the atrial and ventricular myocardium (Crick et al., 1994; Chow et al., 2001). The normal adult conduction system is innervated by both sympathetic and parasympathetic nerve branches (Crick et al., 1994; Chow et al., 2001). The sinoatrial node and atrioventricular node predominantly show parasympathetic innervation, whereas the penetrating bundle and the bundle branches predominantly show sympathetic innervation (Crick et al., 1994; Chow et al., 2001; **Figures 4A,B**).

Interestingly, the innervation of the human conduction system changes considerably with age. In infants, more sympathetic nerves are present in all regions of the conduction system compared to parasympathetic nerves. During childhood and adulthood, the number of parasympathetic nerves increases to the extent that the levels of sympathetic and parasympathetic nerves are equalized. In the elderly, there is a decline in both types of nerves (Chow et al., 2001). These data implicate that the autonomic innervation of the human cardiac conduction system changes with age.

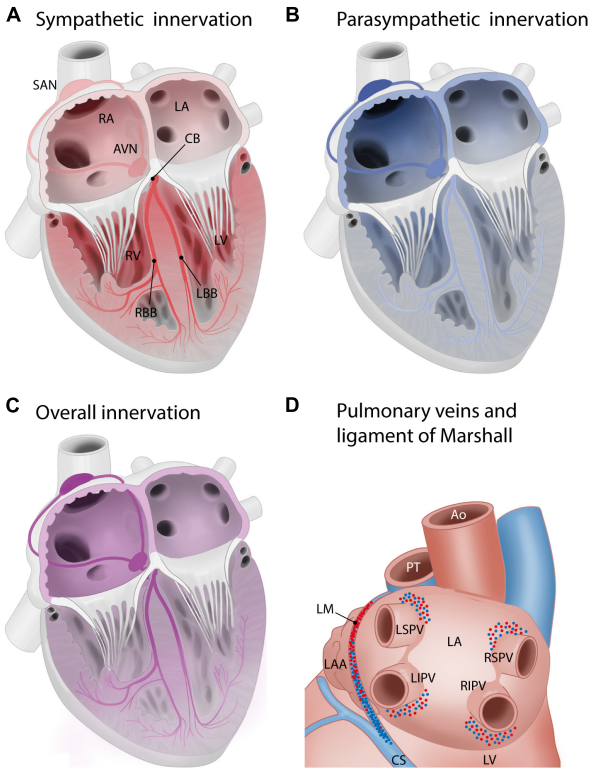

FIGURE 4 | Innervation of the cardiac muscle, including the cardiac conduction system. Red: sympathetic innervation, blue: parasympathetic innervation. **(A,B)** Schematic overview of sympathetic **(A)** and parasympathetic **(B)** innervation of the cardiac compartments and cardiac conduction system. Innervation gradient ranging from the most to least dense innervation: sinoatrial node > atrioventricular node > penetrating bundles > bundle branches. The conduction system is more densely innervated than surrounding myocardium. Sinoatrial node and atrioventricular node: predominantly parasympathetic innervation, penetrating bundle and the bundle branches: predominantly sympathetic (Crick et al., 1994; Chow et al., 2001). **(C)** Global innervation densities in cardiac areas. Innervation density in the atria > innervation density in the ventricles. Gradient in innervation density (higher to lower) from base to the apex. Atria: most nerve endings parasympathetic. Ventricles: most nerve endings sympathetic. Sympathetic innervation density right atrium > left atrium. Right atrium and right ventricle: higher density of parasympathetic innervation than left atrium and left ventricle (Kawano et al., 2003). **(D)** Innervation of the pulmonary veins and ligament of Marshall, posterior view of the left atrium. Sympathetic and parasympathetic innervation density: highest above superior pulmonary veins and below inferior pulmonary veins (Tan et al., 2006). The ligament of Marshall is densely sympathetically and parasympathetically innervated (Han et al., 2010; Rodríguez-Mañero et al., 2016). From superior to inferior, it shifts from predominantly sympathetic to predominantly parasympathetic. AVN, atrioventricular node; AVB, atrioventricular/His bundle; CB, common bundle; LA, left atrium; LBB, left bundle branch; LIPV, left inferior pulmonary vein; LSPV, left superior pulmonary vein; LV, left ventricle; SAN, sinoatrial node; RA, right atrium; RBB, right bundle branch; RIPV, right inferior pulmonary vein; RSPV, right superior pulmonary vein; RV, right ventricle.

In the adult human LA, the area around the pulmonary veins is densely innervated (**Figure 4D**): many ganglionated plexuses with both sympathetic and parasympathetic fibers are found in this area. The right pulmonary veins are mostly innervated by the dorsal right atrial subplexus and the middle dorsal subplexus, whereas the left superior pulmonary vein is innervated by the left dorsal subplexus and the left inferior pulmonary vein is innervated by the left and middle dorsal subplexus (Vaitkevicius et al., 2008, 2009; Wickramasinghe and Patel, 2013). Sympathetic and parasympathetic innervation density are both especially high in the superior aspects of the superior pulmonary veins and the inferior aspects of the inferior pulmonary veins. Innervation density was also higher epicardially than endocardially (Tan et al., 2006). The pulmonary venous myocardium is infamous for its potential for arrhythmogenesis (Haïssaguerre et al., 1998), and autonomic innervation has been recognized as a potential modulating factor (Chen et al., 2014). Of interest, the potential for arrhythmogenicity appears to differ between different pulmonary veins, with more foci found in the superior pulmonary veins as compared to the inferior veins (Haïssaguerre et al., 1998; Chen et al., 1999). Transient autonomic dysfunction and neural injury has been described after catheter ablation of pulmonary vein for atrial fibrillation (Hsieh et al., 1999; Scherschel et al., 2019). The ligament of Marshall, a remnant of the left vena cava inferior that regresses during embryonic development, is surrounded by a dense network of both sympathetic and parasympathetic fibers. From superior to inferior, in humans, the innervation of the ligament of Marshall shifts from predominantly sympathetic (nerve density) to predominantly parasympathetic (presence of parasympathetic ganglia) (Makino et al., 2006; Han et al., 2010; Rodríguez-Mañero et al., 2016; **Figure 4D**). The ligament of Marshall has nerve connections with the LA which are implicated in the genesis of atrial fibrillation (Han et al., 2010).

Animal studies reveal additional, potentially clinically relevant regional differences: in pigs, the RV was more densely innervated than the LV, whereas the left ventricular endocardium was more densely innervated than the right ventricular endocardium (Ulphani et al., 2010). In the RV outflow tract in dogs, sympathetic axons are found in the subendocardium as well as in the subepicardium, whereas in the remainder of the RV and the LV, sympathetic axons are only found in the subepicardium (Ito and Zipes, 1994), indicating a denser sympathetic innervation of the RV outflow tract as compared to the remainder of the RV. Whether this is also the case in humans is yet to be confirmed.

SIDEDNESS AND REGIONAL DIFFERENCES IN CARDIAC SYMPATHETIC RECEPTORS AND RESPONSES: ANATOMICAL AND FUNCTIONAL EVIDENCE

In preganglionic sympathetic nerve terminals, acetylcholine is the primary neurotransmitter. In postganglionic sympathetic nerve terminals, norepinephrine (NE) is the neurotransmitter primarily involved. Postganglionic sympathetic nerve fibers activate adrenergic receptors (the α1-, β1-, and β2-adrenergic receptors, of which the β-receptors greatly outnumber the α-receptors). β1-receptors, the predominant receptors in the heart, outnumber the β2-receptors in the atria and even more so in the ventricles. As the total β-receptor density is similar in the myocardial walls of all four cardiac chambers (Steinfath et al., 1992; Brodde et al., 2001), differences in the ratio β1 versus β2 receptors may be present between atria and ventricle or within the different cardiac compartments. Generally, stimulation of adrenergic receptors causes positive inotropy and an increase in heart rate. Though mostly present in the vascular wall, there are also α-adrenergic receptor in the ventricular myocardium, accounting for approximately 15% of the cardiac adrenergic receptors. Stimulation of the α1-myocardial receptors results in a weak positive inotropic response (Bristow et al., 1988; **Table 4**).

Linked to differences in recruitability of the systemic and pulmonary vasculature, the LV and the RV show differences in responses to adrenergic stimulation. In athletes, it was shown that during exercise, there is a greater relative increase of wall stress in the RV compared with the LV (La Gerche et al., 2011). In dogs receiving sympathetic stimulation, a stronger increase in systolic pressure was seen in the RV compared with the LV. This is likely mediated by β-receptors, as it was not affected by α-receptor blockade (Abe et al., 1987). A more recent study in dogs showed similar results: a stronger relative increase of contractility was seen in the RV compared with the LV after β-stimulation, which appeared to be related to interventricular differences in phosphodiesterase metabolism underlying the response to β-stimulation (Molina et al., 2014).

Adrenergic stress, for example treatment with inotropes, can cause dynamic RV outflow tract obstruction in humans, even without right ventricular hypertrophy (Denault et al., 2006). A study in pigs shows that the RV outflow tract indeed demonstrates an augmented response to adrenergic stimulation compared to the inflow tract, which was suggested by the authors as a possible mechanism to prevent excessive blood flow to the pulmonary circulation (Heerdt and Pleimann, 1996). This may be related to the additional presence of sympathetic axons in the deep myocardium specifically in the RV outflow tract, as was demonstrated in dogs (Ito and Zipes, 1994).

Furthermore, animal research shows that the RV and the LV may differ in their responses to sympathetic stimulation. *Ex vivo* stimulation of the α1-receptor with phenylephrine in ventricular trabeculae in mice resulted in negative inotropy in the RV and in positive inotropy in the LV (Wang et al., 2006).

Nerve growth factor (NGF), an important factor in nerve (re)growth which likely acts on the p75 neurotrophin receptor and tropomyosin-related receptor A (Li and Li, 2015), was investigated in rats of different ages (Saygili et al., 2012). Across all ages, nerve growth factor expression was higher in the ventricles than in the atria, and higher in the LA than in the RA. In the atria, nerve growth factor expression increased with age. In the ventricles, nerve growth factor expression was highest in neonatal rats. It decreased from neonatal to young age, to increase again at old age. These results may be related with an increase in sympathetic activation with age (Saygili et al., 2012). It is unknown whether these patterns can be extrapolated to humans.

TABLE 4 | Asymmetry and regional differences in the distribution and response of cardiac autonomic receptors and modulating factors.

Autonomic division	Receptor or modulating factor	Cardiac distribution	Asymmetrical/regional features of action
Sympathetic	Adrenergic	β1-receptors > β2-receptors in all chambers (human tissue)	Relative increase in inotropy after β-stimulation RV > LV (dogs)
		β-receptors > α-receptors in all chambers (human tissue)	Adrenergic stress may specifically lead to RVOT obstruction (dogs)
			α1-receptor stimulation: negative inotropy in RV, positive inotropy in LV (mice)
	NGF	NGF concentration ventricles > atria (rats)	
		NGF concentration LA > RA (rats)	
Parasympathetic	Muscarinic	M2-receptor concentration atria > ventricles (human tissue)	
		M2-receptor-specific tracer binding LV > RV > atria (human radioactive tracer imaging)	
	NOS	Expression eNOS left ventricular epicardium > RV > left ventricular endocardium (ferrets)	
		Expression nNOS left ventricular endocardium > left ventricular epicardium and RV (ferrets)	

eNOS, endothelial nitric oxide synthase; LA, left atrium; LV, left ventricle; NGF, nerve growth factor; nNOS, neuronal nitric oxide synthase; NOS, nitric oxide synthase; RA, right atrium; RV, right ventricle.

Regional differences in nerve growth factor expression in the human heart have not yet been investigated.

An important regulator of cardiac beta-adrenoreceptor signaling is the opioid receptor system. Three subtypes of endogenous opioids exist, all three of which have effects on the heart through their specific receptors: the μ opioid receptor, δ opioid receptor, and κ opioid receptor (Barron, 1999). The cardiac opioid system may especially be important as part of a negative feedback loop: conditions such as exercise and hypertension lead to increased cardiac opioid content, which depresses neurotransmitter release at adrenergic and/or vagal nerve terminals. Distribution of these receptors appears to be asymmetrical in rat studies: more δ opiate receptors are present on the right side of the heart compared to the left, and more receptors are furthermore present in the atria compared to the ventricles (Krumins et al., 1985). Activity of endogenous opioids (enkephalins), the ligands for these receptors, was generally higher in the atria than in the ventricles in a study in guinea pigs (Weihe et al., 1985).

The asymmetry and regional differences in the distribution and response of cardiac sympathetic receptors and modulating factors are summarized in **Table 4**.

ASYMMETRY AND REGIONAL DIFFERENCES IN CARDIAC PARASYMPATHETIC RECEPTORS AND RESPONSES: ANATOMICAL EVIDENCE

Acetylcholine is the neurotransmitter employed in pre- and postganglionic parasympathetic nerve terminals. Postganglionic parasympathetic fibers mainly activate the muscarinic (M)2-cholinergic receptor. Stimulation of the M2-cholinergic receptor causes a negative inotropic effect and a decrease in heart rate (Brodde et al., 2001). An *in vitro* study in diseased human hearts showed a higher density of M2-receptors in the atria than in the ventricles (Deighton et al., 1990; **Table 4**). However, a radioactive tracer-imaging study in mainly healthy volunteers shows that the human LV and septum show the highest concentrations of the M2-receptor-specific tracer. Therefore, in physiological conditions the LV and septum may contain most of the physiologically active population of M2-receptors (Syrota et al., 1985; **Table 4**). In humans, the M2-receptor density decreases with age, as was shown by both functional evidence and *in vitro* study of the human RA (Brodde et al., 1998).

Nitric oxide (NO) plays an important role in parasympathetic regulation, as was demonstrated in animal models: under physiological circumstances, NO promotes acetylcholine release and reduces NE release from nerve terminals (Herring and Paterson, 2001; Dedkova Elena et al., 2003). Two different isoforms of nitric oxide synthase are primarily responsible for this: neuronal nitric oxide synthase (nNOS) in parasympathetic nerve terminals, and endothelial nitric oxide synthase (eNOS) in cardiac cells (Balligand et al., 2009).

From a clinical point of view, NO is implicated in vasovagal syncope: in young patients, this condition is mostly due to reduced systemic vascular resistance, which can be corrected by antagonizing NO (Stewart et al., 2017). In older patients, vasovagal syncope is mostly due to reduced cardiac output.

The distribution of NOS isoforms may be asymmetrical: in ferrets, eNOS expression is highest in the apical/midventricular epicardium of the LV, moderately high in the right ventricular free wall, and low in the left ventricular endocardium and the left ventricular side of the septum. In the sinoatrial node and the RA, eNOS is present in the majority of cells. The distribution of nNOS follows a more or less inverted pattern: the expression is high in the left ventricular endocardium and the left ventricular side of the septum, and low in the left ventricular epicardium and the RV (Brahmajothi and Campbell, 1999). The exact functional role

and distribution of NOS isoforms in the human heart remains to be elucidated.

The asymmetry and regional differences in the distribution of cardiac parasympathetic receptors and modulating factors are summarized in **Table 4**.

SUMMARY AND CLINICAL IMPLICATIONS

In the current review, we show that the human peripheral cANS shows considerable asymmetry, interindividual variations, and regional differences in anatomical, functional and molecular characteristics.

The right-sided lower thoracic cardiac nerves follow a complex course to reach the heart which differs greatly from the course of the left-sided lower thoracic cardiac nerves. The presence of the left-sided thoracic cardiac branch is highly variable, the localization of the cardiac plexus is higher on the right side compared to the left, and different parts of the cardiac plexus give rise to nerves innervating different parts of the heart. This is important to consider when planning thoracic surgery to avoid complications regarding autonomic function.

The left and right stellate ganglia and the left and right vagus nerves innervate different areas of the heart or have different effects on the same area. In particular, left stellate ganglion block may be used to treat ventricular arrhythmias. The RV outflow tract, pulmonary veins, and the ligament of Marshall have specific innervation gradients. Distribution of cardiac nerves and ganglia differs between regions, showing a parasympathetic predominance in the atria and a sympathetic predominance in the ventricles. The distribution of spinal and vagal afferent nerve fibers may differ between cardiac regions. The RV, the RV outflow tract, and the LV all respond differently to sympathetic stimulation. These factors heavily influence disease manifestation and efficacy of pharmaceutical treatment, and are therefore important to keep in mind. In addition, the risk of clinical procedures such as catheter ablation or stellate ganglion blockade for arrhythmias, may be reduced and their efficacy may be improved by taking asymmetry and regional differences of the cANS into consideration.

Many studies in this field are animal studies, and the RV is often neglected. Future research in human tissue or human subjects focusing for example on specific innervation of the RV outflow tract, distribution of cardiac afferents, regional differences in nerve growth factor or nitric oxide synthase expression, and differing effects of left- or right sided innervation on both the LV and the RV, would be highly valuable to comprehend the influence of cardiac innervation of disease course and potentially adjust treatments for specific cardiac diseases related to cardiac autonomic (dys)function.

AUTHOR CONTRIBUTIONS

TZ performed literature study, drafted the manuscript, co-designed the figures, and implemented suggestions by the co-authors. RN and MD wrote the parts of the manuscript, revised the manuscript and used literature extensively, co-designed the figures, and critically revised and approved of the final manuscript. JW wrote the parts of the manuscript, revised the manuscript and used literature extensively, and critically revised and approved of the final manuscript. PK, HV, and AE guided the process of drafting the manuscript and critically revised and approved of the final manuscript. MS critically revised and approved of the final manuscript. MJ conceived the concept of the manuscript, wrote parts of the manuscript, guided the literature study and the drafting of the manuscript, designed the figures, revised the manuscript and used literature extensively, and critically revised and approved of the final manuscript. All authors contributed to the article and approved the submitted version.

FUNDING

The Department of Cardiology receives research grants from Biotronik (Berlin, Germany), Boston Scientific (Natick, Massachusetts), and Medtronic (Minneapolis, Minnesota). MJ was supported by a personal research grant from NWO ZonMw (projectnr. 91719346). MD and MJ were supported by a grant of the Dutch Bontius Stichting. MD was supported by the Netherlands Heart Foundation (project number 2019B002 OUTREACH). The funders were not involved in the study design, collection, analysis, interpretation of data, the writing of this article or the decision to submit it for publication.

ACKNOWLEDGMENTS

The authors gratefully thank Ron Slagter for drawing the figures.

REFERENCES

Abe, Y., Saito, D., Tani, H., Nakatsu, T., Kusachi, S., Haraoka, S., et al. (1987). The effect of cardiac sympathetic nerve stimulation on the right ventricle in canine heart. *Jpn. Circ. J.* 51, 535–542. doi: 10.1253/jcj.51.535

Anderson, R., Bandler, R., Bohus, B., Buijs, R., Cechetto, D., Clement, C., et al. (2000). *The Nervous System and The Heart*, ed. G. J. Ter Hors Totowa, NJ: Humana Press.

Armour, J. A. (1999). Myocardial ischaemia and the cardiac nervous system. *Cardiovasc. Res.* 41, 41–54. doi: 10.1016/s0008-6363(98)00252-1

Armour, J. A., Murphy, D. A., Yuan, B. X., Macdonald, S., and Hopkins, D. A. (1997). Gross and microscopic anatomy of the human intrinsic cardiac nervous system. *Anat. Rec.* 247, 289–298. doi: 10.1002/(sici)1097-0185(199702)247:2<289::aid-ar15>3.0.co;2-l

Balligand, J. L., Feron, O., and Dessy, C. (2009). eNOS activation by physical forces: from short-term regulation of contraction to chronic remodeling of cardiovascular tissues. *Physiol. Rev.* 89, 481–534. doi: 10.1152/physrev.00042.2007

Banzett, R. B., Guz, A., Paydarfar, D., Shea, S. A., Schachter, S. C., and Lansing, R. W. (1999). Cardiorespiratory variables and sensation during stimulation of the left vagus in patients with epilepsy. *Epilepsy Res.* 35, 1–11.

Barron, B. A. (1999). Opioid peptides and the heart. *Cardiovasc. Res.* 43, 13–16.

Bonica, J. J. (1968). Autonomic innervation of the viscera in relation to nerve block. *Anesthesiology* 29, 793–813. doi: 10.1097/00000542-196807000-00023

Bouallal, R., Godart, F., Francart, C., Richard, A., Foucher-Hossein, C., and Lions, C. (2010). Interest of beta-blockers in patients with right ventricular systemic dysfunction. *Cardiol. Young* 20, 615–619. doi: 10.1017/s1047951110000764

Brack, K. E., Coote, J. H., and Ng, G. A. (2004). Interaction between direct sympathetic and vagus nerve stimulation on heart rate in the isolated rabbit heart. *Exp. Physiol.* 89, 128–139. doi: 10.1113/expphysiol.2003.002654

Brahmajothi, M. V., and Campbell, D. L. (1999). Heterogeneous basal expression of nitric oxide synthase and superoxide dismutase isoforms in mammalian heart : implications for mechanisms governing indirect and direct nitric oxide-related effects. *Circ. Res.* 85, 575–587. doi: 10.1161/01.res.85.7.575

Bristow, M. R., Minobe, W., Rasmussen, R., Hershberger, R. E., and Hoffman, B. B. (1988). Alpha-1 adrenergic receptors in the nonfailing and failing human heart. *J. Pharmacol. Exp. Ther.* 247, 1039–1045.

Brodde, O. E., Bruck, H., Leineweber, K., and Seyfarth, T. (2001). Presence, distribution and physiological function of adrenergic and muscarinic receptor subtypes in the human heart. *Basic Res. Cardiol.* 96, 528–538. doi: 10.1007/s003950170003

Brodde, O. E., Konschak, U., Becker, K., Rüter, F., Poller, U., Jakubetz, J., et al. (1998). Cardiac muscarinic receptors decrease with age. *In vitro* and *in vivo* studies. *J. Clin. Invest.* 101, 471–478. doi: 10.1172/jci1113

Cao, J. M., Fishbein, M. C., Han, J. B., Lai, W. W., Lai, A. C., Wu, T. J., et al. (2000). Relationship between regional cardiac hyperinnervation and ventricular arrhythmia. *Circulation* 101, 1960–1969. doi: 10.1161/01.cir.101.16.1960

Chen, P.-S., Chen, L. S., Fishbein, M. C., Lin, S.-F., and Nattel, S. (2014). Role of the autonomic nervous System in Atrial Fibrillation: pathophysiology and therapy. *Circ. Res.* 114, 1500–1515. doi: 10.1161/circresaha.114.303772

Chen, S.-A., Hsieh, M.-H., Tai, C.-T., Tsai, C.-F., Prakash, V. S., Yu, W.-C., et al. (1999). Initiation of atrial fibrillation by ectopic beats originating from the pulmonary Veins: electrophysiological characteristics, pharmacological responses, and effects of radiofrequency ablation. *Circulation* 100, 1879–1886. doi: 10.1161/01.cir.100.18.1879

Chow, L. T., Chow, S. S., Anderson, R. H., and Gosling, J. A. (2001). Autonomic innervation of the human cardiac conduction system: changes from infancy to senility–an immunohistochemical and histochemical analysis. *Anat. Rec.* 264, 169–182. doi: 10.1002/ar.1158

Cinca, J., Evangelista, A., Montoyo, J., Barutell, C., Figueras, J., Valle, V., et al. (1985). Electrophysiologic effects of unilateral right and left stellate ganglion block on the human heart. *Am. Heart J.* 109, 46–54. doi: 10.1016/0002-8703(85)90414-4

Coote, J. H., and Spyer, K. M. (2018). Central control of autonomic function. *Brain Neurosci. Adv.* 2:2398212818812012.

Crick, S. J., Sheppard, M. N., and Anderson, R. H. (2000). "Nerve supply of the heart," in *The Nervous System and the Heart*, ed. G. J. Ter Horst (Totowa, NJ: Humana), 3–54.

Crick, S. J., Wharton, J., Sheppard, M. N., Royston, D., Yacoub, M. H., Anderson, R. H., et al. (1994). Innervation of the human cardiac conduction system. A quantitative immunohistochemical and histochemical study. *Circulation* 89, 1697–1708.

De Gama, B. Z., Lazarus, L., Partab, P., and Satyapai, K. S. (2012). The sympathetic and parasympathetic contributions to the cardiac plexus: a fetal study. *Int. J. Morphol.* 30, 1569–1576.

Dedkova Elena, N., Ji, X., Wang Yong, G., Blatter Lothar, A., and Lipsius Stephen, L. (2003). Signaling mechanisms that mediate nitric oxide production induced by acetylcholine exposure and withdrawal in cat atrial myocytes. *Circ. Res.* 93, 1233–1240.

Dehlin, H. M., and Levick, S. P. (2014). Substance P in heart failure: the good and the bad. *Int. J. Cardiol.* 170, 270–277.

Deighton, N. M., Motomura, S., Borquez, D., Zerkowski, H. R., Doetsch, N., and Brodde, O. E. (1990). Muscarinic cholinoceptors in the human heart: demonstration, subclassification, and distribution. *Naunyn Schmiedebergs Arch. Pharmacol.* 341, 14–21.

Denault, A. Y., Chaput, M., Couture, P., Hebert, Y., Haddad, F., and Tardif, J. C. (2006). Dynamic right ventricular outflow tract obstruction in cardiac surgery. *J. Thorac. Cardiovasc. Surg.* 132, 43–49.

Ditting, T., Hilgers, K. F., Scrogin, K. E., Stetter, A., Linz, P., and Veelken, R. (2005). Mechanosensitive cardiac C-fiber response to changes in left ventricular filling, coronary perfusion pressure, hemorrhage, and volume expansion in rats. *Am. J. Physiol. Heart Circ. Physiol.* 288, H541–H552.

Dore, A., Houde, C., Chan, K. L., Ducharme, A., Khairy, P., Juneau, M., et al. (2005). Angiotensin receptor blockade and exercise capacity in adults with systemic right ventricles: a multicenter, randomized, placebo-controlled clinical trial. *Circulation* 112, 2411–2416.

Dos, L., Pujadas, S., Estruch, M., Mas, A., Ferreira-Gonzalez, I., Pijuan, A., et al. (2013). Eplerenone in systemic right ventricle: double blind randomized clinical trial. The evedes study. *Int. J. Cardiol.* 168, 5167–5173.

Doughan, A. R., Mcconnell, M. E., and Book, W. M. (2007). Effect of beta blockers (carvedilol or metoprolol XL) in patients with transposition of great arteries and dysfunction of the systemic right ventricle. *Am. J. Cardiol.* 99, 704–706.

Egawa, H., Okuda, Y., Kitajima, T., and Minami, J. (2001). Assessment of QT interval and QT dispersion following stellate ganglion block using computerized measurements. *Reg. Anesth. Pain Med.* 26, 539–544.

Fallavollita, J. A., Heavey, B. M., Luisi, A. J. Jr., Michalek, S. M., Baldwa, S., Mashtare, T. L. Jr., et al. (2014). Regional myocardial sympathetic denervation predicts the risk of sudden cardiac arrest in ischemic cardiomyopathy. *J. Am. Coll. Cardiol.* 63, 141–149. doi: 10.1016/j.jacc.2013.07.096

Federative International Programme for Anatomical Terminology (2019). *Terminologia Anatomica*. Available online at: https://fipat.library.dal.ca/ (accessed January 9, 2021).

Flapan, A. D., Wright, R. A., Nolan, J., Neilson, J. M., and Ewing, D. J. (1993). Differing patterns of cardiac parasympathetic activity and their evolution in selected patients with a first myocardial infarction. *J. Am. Coll. Cardiol.* 21, 926–931. doi: 10.1016/0735-1097(93)90349-6

Franciosi, S., Perry, F. K., Roston, T. M., Armstrong, K. R., Claydon, V. E., and Sanatani, S. (2017). The role of the autonomic nervous system in arrhythmias and sudden cardiac death. *Auton. Neurosci.* 205, 1–11. doi: 10.1016/j.autneu.2017.03.005

Fukuda, K., Kanazawa, H., Aizawa, Y., Ardell, J. L., and Shivkumar, K. (2015). Cardiac innervation and sudden cardiac death. *Circ. Res.* 116, 2005–2019. doi: 10.1161/CIRCRESAHA.116.304679

Fukuyama, U. (1982). Gross anatomy of the extrinsic cardiac nerve branches of human beings. *Acta Anat. Nippon* 57, 357–380.

Garcia-Calvo, R., Chorro, F. J., Sendra, M., Alberola, A., Sanchis, J., Navarro, J., et al. (1992). The effects of selective stellate ganglion manipulation on ventricular refractoriness and excitability. *Pacing Clin. Electrophysiol.* 15, 1492–1503. doi: 10.1111/j.1540-8159.1992.tb02923.x

Giardini, A., Lovato, L., Donti, A., Formigari, R., Gargiulo, G., Picchio, F. M., et al. (2007). A pilot study on the effects of carvedilol on right ventricular remodelling and exercise tolerance in patients with systemic right ventricle. *Int. J. Cardiol.* 114, 241–246. doi: 10.1016/j.ijcard.2006.01.048

Gittenberger-de Groot, A. C., Azhar, M., and Molin, D. G. M. (2006). Transforming growth factor β–SMAD2 signaling and aortic arch development. *Trends Cardiovasc. Med.* 16, 1–6. doi: 10.1016/j.tcm.2005.09.006

Haïssaguerre, M., Jaïs, P., Shah, D. C., Takahashi, A., Hocini, M., Quiniou, G., et al. (1998). Spontaneous initiation of atrial fibrillation by ectopic beats originating in the pulmonary veins. *N. Engl. J. Med.* 339, 659–666. doi: 10.1056/NEJM199809033391003

Han, S., Joung, B., Scanavacca, M., Sosa, E., Chen, P. S., and Hwang, C. (2010). Electrophysiological characteristics of the Marshall bundle in humans. *Heart Rhythm* 7, 786–793. doi: 10.1016/j.hrthm.2010.02.028

Hasan, W. (2013). Autonomic cardiac innervation: development and adult plasticity. *Organogenesis* 9, 176–193. doi: 10.4161/org.24892

Hechter, S. J., Fredriksen, P. M., Liu, P., Veldtman, G., Merchant, N., Freeman, M., et al. (2001). Angiotensin-converting enzyme inhibitors in adults after the Mustard procedure. *Am J Cardiol* 87, 660–663.a611.

Heerdt, P. M., and Pleimann, B. E. (1996). The dose-dependent effects of halothane on right ventricular contraction pattern and regional inotropy in swine. *Anesth. Analg.* 82, 1152–1158. doi: 10.1213/00000539-199606000-00009

Herring, N., and Paterson, D. (2001). Nitric oxide-cGMP pathway facilitates acetylcholine release and bradycardia during vagal nerve stimulation in the guinea-pig *in vitro*. *J. Physiol.* 535, 507–518. doi: 10.1111/j.1469-7793.2001.00507.x

Hoover, D. B., Isaacs, E. R., Jacques, F., Hoard, J. L., Pagé, P., and Armour, J. A. (2009). Localization of multiple neurotransmitters in surgically derived specimens of human atrial ganglia. *Neuroscience* 164, 1170–1179. doi: 10.1016/j.neuroscience.2009.09.001

Hsieh, M.-H., Chiou, C.-W., Wen, Z.-C., Wu, C.-H., Tai, C.-T., Tsai, C.-F., et al. (1999). Alterations of heart rate variability after radiofrequency catheter ablation of focal atrial fibrillation originating from pulmonary veins. *Circulation* 100, 2237–2243. doi: 10.1161/01.CIR.100.22.2237

Ito, M., and Zipes, D. P. (1994). Efferent sympathetic and vagal innervation of the canine right ventricle. *Circulation* 90, 1459–1468. doi: 10.1161/01.CIR.90.3.1459

Jamali, H. K., Waqar, F., and Gerson, M. C. (2016). Cardiac autonomic innervation. *J. Nucl. Cardiol.* 24, 1558–1570. doi: 10.1007/s12350-016-0725-7

Janes, R. D., Brandys, J. C., Hopkins, D. A., Johnstone, D. E., Murphy, D. A., and Armour, J. A. (1986). Anatomy of human extrinsic cardiac nerves and ganglia. *Am. J. Cardiol.* 57, 299–309. doi: 10.1016/0002-9149(86)90908-2

Josephson, C. B., Howlett, J. G., Jackson, S. D., Finley, J., and Kells, C. M. (2006). A case series of systemic right ventricular dysfunction post atrial switch for simple D-transposition of the great arteries: the impact of beta-blockade. *Can. J. Cardiol.* 22, 769–772. doi: 10.1016/S0828-282X(06)70293-8

Kawano, H., Okada, R., and Yano, K. (2003). Histological study on the distribution of autonomic nerves in the human heart. *Heart Vessels* 18, 32–39.

Kawashima, T. (2005). The autonomic nervous system of the human heart with special reference to its origin, course, and peripheral distribution. *Anat. Embryol.* 209, 425–438. doi: 10.1007/s00429-005-0462-1

Kawashima, T. (2011). Anatomy of the cardiac nervous system with clinical and comparative morphological implications. *Anat. Sci. Int.* 86, 30–49. doi: 10.1007/s12565-010-0096-0

Kirby, M. L. (2007). *Cardiac Development*. Oxford: Oxford University Press.

Krumins, S. A., Faden, A. I., and Feuerstein, G. (1985). Opiate binding in rat hearts: modulation of binding after hemorrhagic shock. *Biochem. Biophys. Res. Commun.* 127, 120–128. doi: 10.1016/S0006-291X(85)80134-0

Kwon, O. J., Pendekanti, S., Fox, J. N., Yanagawa, J., Fishbein, M. C., Shivkumar, K., et al. (2018). Morphological spectra of adult human stellate ganglia: implications for thoracic sympathetic denervation. *Anat. Rec. (Hoboken)* 301, 1244–1250. doi: 10.1002/ar.23797

La Gerche, A., Heidbuchel, H., Burns, A. T., Mooney, D. J., Taylor, A. J., Pfluger, H. B., et al. (2011). Disproportionate exercise load and remodeling of the athlete's right ventricle. *Med. Sci. Sports Exerc.* 43, 974–981.

La Rovere, M. T., Bigger, J. T. Jr., Marcus, F. I., Mortara, A., and Schwartz, P. J. (1998). Baroreflex sensitivity and heart-rate variability in prediction of total cardiac mortality after myocardial infarction. ATRAMI (Autonomic Tone and Reflexes After Myocardial Infarction) Investigators. *Lancet* 351, 478–484.

Laine, P., Naukkarinen, A., Heikkilä, L., Penttilä, A., and Kovanen, P. T. (2000). Adventitial mast cells connect with sensory nerve fibers in atherosclerotic coronary arteries. *Circulation* 101, 1665–1669. doi: 10.1161/01.CIR.101.14.1665

Lane, R. D., and Schwartz, G. E. (1987). Induction of lateralized sympathetic input to the heart by the CNS during emotional arousal: a possible neurophysiologic trigger of sudden cardiac death. *Psychosom. Med.* 49, 274–284. doi: 10.1097/00006842-198705000-00006

Leftheriotis, D., Flevari, P., Kossyvakis, C., Katsaras, D., Batistaki, C., Arvaniti, C., et al. (2016). Acute effects of unilateral temporary stellate ganglion block on human atrial electrophysiological properties and atrial fibrillation inducibility. *Heart Rhythm* 13, 2111–2117. doi: 10.1016/j.hrthm.2016.06.025

Lester, S. J., Mcelhinney, D. B., Viloria, E., Reddy, G. P., Ryan, E., Tworetzky, W., et al. (2001). Effects of losartan in patients with a systemically functioning morphologic right ventricle after atrial repair of transposition of the great arteries. *Am. J. Cardiol.* 88, 1314–1316. doi: 10.1016/S0002-9149(01)02098-7

Lewis, M. E., Al-Khalidi, A. H., Bonser, R. S., Clutton-Brock, T., Morton, D., Paterson, D., et al. (2001). Vagus nerve stimulation decreases left ventricular contractility *in vivo* in the human and pig heart. *J. Physiol.* 534, 547–552. doi: 10.1111/j.1469-7793.2001.00547.x

Li, C. Y., and Li, Y. G. (2015). Cardiac sympathetic nerve sprouting and susceptibility to ventricular arrhythmias after myocardial infarction. *Cardiol. Res. Pract.* 2015:698368. doi: 10.1155/2015/698368

Makino, M., Inoue, S., Matsuyama, T. A., Ogawa, G., Sakai, T., Kobayashi, Y., et al. (2006). Diverse myocardial extension and autonomic innervation on ligament of Marshall in humans. *J. Cardiovasc. Electrophysiol.* 17, 594–599. doi: 10.1111/j.1540-8167.2006.00375.x

Malliani, A., Recordati, G., and Schwartz, P. J. (1973). Nervous activity of afferent cardiac sympathetic fibres with atrial and ventricular endings. *J. Physiol.* 229, 457–469. doi: 10.1113/jphysiol.1973.sp010147

Marcer, N., Bergmann, M., Klie, A., Moor, B., and Djonov, V. (2012). An anatomical investigation of the cervicothoracic ganglion. *Clin. Anat.* 25, 444–451. doi: 10.1002/ca.21266

Matsuo, S., Nakajima, K., and Nakata, T. (2016). Prognostic value of cardiac sympathetic nerve imaging using long-term follow-up data - ischemic vs. non-ischemic heart failure etiology. *Circ. J.* 80, 435–441. doi: 10.1253/circj.CJ-15-0952

Meng, L., Tseng, C. H., Shivkumar, K., and Ajijola, O. (2017). Efficacy of stellate ganglion blockade in managing electrical storm: a systematic review. *JACC Clin. Electrophysiol.* 3, 942–949. doi: 10.1016/j.jacep.2017.06.006

Molina, C. E., Johnson, D. M., Mehel, H., Spatjens, R. L., Mika, D., Algalarrondo, V., et al. (2014). Interventricular differences in beta-adrenergic responses in the canine heart: role of phosphodiesterases. *J. Am. Heart. Assoc.* 3:e000858. doi: 10.1161/JAHA.114.000858

Muppidi, S., Gupta, P. K., and Vernino, S. (2011). Reversible right vagal neuropathy. *Neurology* 77, 1577–1579. doi: 10.1212/WNL.0b013e318233b3a2

Ng, G. A., Brack, K. E., and Coote, J. H. (2001). Effects of direct sympathetic and vagus nerve stimulation on the physiology of the whole heart - a novel model of isolated langendorff perfused rabbit heart with intact dual autonomic innervation. *Exp. Physiol.* 86, 319–329. doi: 10.1113/eph8602146

Pachón, J. C., Pachón, E., Páchon, J. C., Lobo, T., Pachón, M. Z., Vargas, R. N., et al. (2005). "Cardioneuroablation" – new treatment for neurocardiogenic syncope, functional AV block and sinus dysfunction using catheter RF-ablation. *EP Europace* 7, 1–13. doi: 10.1016/j.eupc.2004.10.003

Palma, J. A., and Benarroch, E. E. (2014). Neural control of the heart: recent concepts and clinical correlations. *Neurology* 83, 261–271. doi: 10.1212/WNL.0000000000000605

Pather, N., Partab, P., Singh, B., and Satyapal, K. S. (2006). Cervico-thoracic ganglion: its clinical implications. *Clin. Anat.* 19, 323–326. doi: 10.1002/ca.20214

Pauza, D. H., Skripka, V., Pauziene, N., and Stropus, R. (2000). Morphology, distribution, and variability of the epicardiac neural ganglionated subplexuses in the human heart. *Anat. Rec.* 259, 353–382. doi: 10.1002/1097-0185(20000801)259:4<353::AID-AR10>3.0.CO;2-R

Perez-Gomez, F., Martin De Dios, R., Rey, J., and Garcia Aguado, A. (1979). Prinzmetal's angina:reflex cardiovascular response during episode of pain. *Br. Heart J.* 42, 81–87. doi: 10.1136/hrt.42.1.81

Petraitiene, V., Pauza, D. H., and Benetis, R. (2014). Distribution of adrenergic and cholinergic nerve fibres within intrinsic nerves at the level of the human heart hilum. *Eur. J. Cardiothorac. Surg.* 45, 1097–1105. doi: 10.1093/ejcts/ezt575

Quigg, M., Elfvin, L.-G., and Aldskogius, H. (1988). Distribution of cardiac sympathetic afferent fibers in the guinea pig heart labeled by anterograde transport of wheat germ agglutinin-horseradish peroxidase. *J. Auton. Nerv. Syst.* 25, 107–118. doi: 10.1016/0165-1838(88)90015-X

Rechardt, L., Aalto-Setälä, K., Purjeranta, M., Pelto-Huikko, M., and Kyösola, K. (1986). Peptidergic innervation of human atrial myocardium: an electron microscopical and immunocytochemical study. *J. Auton. Nerv. Syst.* 17, 21–32. doi: 10.1016/0165-1838(86)90041-X

Robinson, B., Heise, C. T., Moore, J. W., Anella, J., Sokoloski, M., and Eshaghpour, E. (2002). Afterload reduction therapy in patients following intraatrial baffle operation for transposition of the great arteries. *Pediatr. Cardiol.* 23, 618–623. doi: 10.1007/s00246-002-0046-2

Rodríguez-Mañero, M., Schurmann, P., and Valderrábano, M. (2016). Ligament and Vein of Marshall. A therapeutic opportunity in atrial fibrillation. *Heart Rhythm* 13, 593–601. doi: 10.1016/j.hrthm.2015.10.018

Rogers, M. C., Battit, G., Mcpeek, B., and Todd, D. (1978). Lateralization of sympathetic control of the human sinus node: ECG changes of stellate ganglion block. *Anesthesiology* 48, 139–141. doi: 10.1097/00000542-197802000-00009

Saygili, E., Kluttig, R., Rana, O. R., Saygili, E., Gemein, C., Zink, M. D., et al. (2012). Age-related regional differences in cardiac nerve growth factor expression. *Age (Dordr)* 34, 659–667. doi: 10.1007/s11357-011-9262-0

Scherschel, K., Hedenus, K., Jungen, C., Lemoine, M. D., Rübsamen, N., Veldkamp, M. W., et al. (2019). Cardiac glial cells release neurotrophic S100B upon catheter-based treatment of atrial fibrillation. *Sci. Transl. Med.* 11:eaav7770. doi: 10.1126/scitranslmed.aav7770

Schlack, W., and Thamer, V. (1996). Unilateral changes of sympathetic tone to the heart impair left ventricular function. *Acta Anaesthesiol. Scand.* 40, 262–271. doi: 10.1111/j.1399-6576.1996.tb04430.x

Schwartz, P. J., Motolese, M., Pollavini, G., Lotto, A., Ruberti, U. G. O., Trazzi, R., et al. (1992). Prevention of sudden cardiac death after a first myocardial infarction by pharmacologic or surgical antiadrenergic interventions. *J. Cardiovasc. Electrophysiol.* 3, 2–16. doi: 10.1111/j.1540-8167.1992.tb01090.x

Schwartz, P. J., Verrier, R. L., and Lown, B. (1977). Effect of stellectomy and vagotomy on ventricular refractoriness in dogs. *Circ. Res.* 40, 536–540.

Singh, S., Johnson, P. I., Lee, R. E., Orfei, E., Lonchyna, V. A., Sullivan, H. J., et al. (1996). Topography of cardiac ganglia in the adult human heart. *J. Thorac. Cardiovasc. Surg.* 112, 943–953. doi: 10.1016/S0022-5223(96)70094-6

Standring, S., and Gray, H. (2016). *Gray's Anatomy : The Anatomical Basis of Clinical Practice*. Edinburgh: Churchill Livingstone.

Steinfath, M., Lavicky, J., Schmitz, W., Scholz, H., Doring, V., and Kalmar, P. (1992). Regional distribution of beta 1- and beta 2-adrenoceptors in the failing and nonfailing human heart. *Eur. J. Clin. Pharmacol.* 42, 607–611.

Stewart, J. M., Sutton, R., Kothari, M. L., Goetz, A. M., Visintainer, P., and Medow, M. S. (2017). Nitric oxide synthase inhibition restores orthostatic tolerance in young vasovagal syncope patients. *Heart* 103, 1711–1718. doi: 10.1136/heartjnl-2017-311161

Sun, W., Zheng, L., Qiao, Y., Shi, R., Hou, B., Wu, L., et al. (2016). Catheter ablation as a treatment for vasovagal syncope: long-term outcome of endocardial autonomic modification of the left atrium. *J. Am. Heart Assoc.* 5:e003471. doi: 10.1161/JAHA.116.003471

Syrota, A., Comar, D., Paillotin, G., Davy, J. M., Aumont, M. C., Stulzaft, O., et al. (1985). Muscarinic cholinergic receptor in the human heart evidenced under physiological conditions by positron emission tomography. *Proc. Natl. Acad. Sci. U.S.A.* 82, 584–588. doi: 10.1073/pnas.82.2.584

Tan, A. Y., Li, H., Wachsmann-Hogiu, S., Chen, L. S., Chen, P. S., and Fishbein, M. C. (2006). Autonomic innervation and segmental muscular disconnections at the human pulmonary vein-atrial junction: implications for catheter ablation of atrial-pulmonary vein junction. *J. Am. Coll. Cardiol.* 48, 132–143. doi: 10.1016/j.jacc.2006.02.054

Thames, M. D., Klopfenstein, H. S., Abboud, F. M., Mark, A. L., and Walker, J. L. (1978). Preferential distribution of inhibitory cardiac receptors with vagal afferents to the inferoposterior wall of the left ventricle activated during coronary occlusion in the dog. *Circ. Res.* 43, 512–519. doi: 10.1161/01.RES.43.4.512

Therrien, J., Provost, Y., Harrison, J., Connelly, M., Kaemmerer, H., and Webb, G. D. (2008). Effect of angiotensin receptor blockade on systemic right ventricular function and size: a small, randomized, placebo-controlled study. *Int. J. Cardiol.* 129, 187–192. doi: 10.1016/j.ijcard.2008.04.056

Tobler, D., Bouchardy, J., Reto, E., Heg, D., Muller, C., Frenk, A., et al. (2017). Effect of phosphodiesterase-5 inhibition with Tadalafil on SystEmic Right VEntricular size and function - A multi-center, double-blind, randomized, placebo-controlled clinical trial - SERVE trial - Rational and design. *Int. J. Cardiol.* 243, 354–359. doi: 10.1016/j.ijcard.2017.05.079

Tutarel, O., Meyer, G. P., Bertram, H., Wessel, A., Schieffer, B., and Westhoff-Bleck, M. (2012). Safety and efficiency of chronic ACE inhibition in symptomatic heart failure patients with a systemic right ventricle. *Int J Cardiol* 154, 14–16. doi: 10.1016/j.ijcard.2010.08.068

Ulphani, J. S., Cain, J. H., Inderyas, F., Gordon, D., Gikas, P. V., Shade, G., et al. (2010). Quantitative analysis of parasympathetic innervation of the porcine heart. *Heart Rhythm* 7, 1113–1119. doi: 10.1016/j.hrthm.2010.03.043

Vaitkevicius, R., Saburkina, I., Rysevaite, K., Vaitkeviciene, I., Pauziene, N., Zaliunas, R., et al. (2009). Nerve supply of the human pulmonary veins: an anatomical study. *Heart Rhythm* 6, 221–228. doi: 10.1016/j.hrthm.2008.10.027

Vaitkevicius, R., Saburkina, I., Zaliunas, R., Pauziene, N., Vaitkeviciene, I., Schauerte, P., et al. (2008). Innervation of pulmonary veins: morphologic pattern and pathways of nerves in the human fetus. *Ann. Anat.* 190, 158–166. doi: 10.1016/j.aanat.2007.09.002

van der Bom, T., Winter, M. M., Bouma, B. J., Groenink, M., Vliegen, H. W., Pieper, P. G., et al. (2013). Effect of valsartan on systemic right ventricular function: a double-blind, randomized, placebo-controlled pilot trial. *Circulation* 127, 322–330. doi: 10.1161/CIRCULATIONAHA.112.135392

Vaseghi, M., Yamakawa, K., Sinha, A., So, E. L., Zhou, W., Ajijola, O. A., et al. (2013). Modulation of regional dispersion of repolarization and T-peak to T-end interval by the right and left stellate ganglia. *Am. J. Physiol. Heart Circ. Physiol.* 305, H1020–H1030. doi: 10.1152/ajpheart.00056.2013

Vegh, A. M. D., Duim, S. N., Smits, A. M., Poelmann, R. E., Ten Harkel, A. D. J., Deruiter, M. C., et al. (2016). Part and parcel of the cardiac autonomic nerve system: unravelling its cellular building blocks during development. *J. Cardiovasc. Dev. Dis.* 3:28. doi: 10.3390/jcdd3030028

Wake, E., and Brack, K. (2016). Characterization of the intrinsic cardiac nervous system. *Auton. Neurosci.* 199, 3–16. doi: 10.1016/j.autneu.2016.08.006

Wang, G. Y., Mccloskey, D. T., Turcato, S., Swigart, P. M., Simpson, P. C., and Baker, A. J. (2006). Contrasting inotropic responses to alpha1-adrenergic receptor stimulation in left versus right ventricular myocardium. *Am. J. Physiol. Heart Circ. Physiol.* 291, H2013–H2017. doi: 10.1152/ajpheart.00167.2006

Weihe, E., Mcknight, A. T., Corbett, A. D., and Kosterlitz, H. W. (1985). Proenkephalin- and prodynorphin- derived opioid peptides in guinea-pig heart. *Neuropeptides* 5, 453–456. doi: 10.1016/0143-4179(85)90052-6

Weihe, E., Reinecke, M., Opherk, D., and Forssmann, W. G. (1981). Peptidergic innervation (substance P) in the human heart. *J. Mol. Cell. Cardiol.* 13, 331–333. doi: 10.1016/0022-2828(81)90321-7

Weihe, E., Schütz, B., Hartschuh, W., Anlauf, M., Schäfer, M. K., and Eiden, L. E. (2005). Coexpression of cholinergic and noradrenergic phenotypes in human and nonhuman autonomic nervous system. *J. Comp. Neurol.* 492, 370–379. doi: 10.1161/CIRCULATIONAHA.113.001596

Wickramasinghe, S. R., and Patel, V. V. (2013). Local innervation and atrial fibrillation. *Circulation* 128, 1566–1575.

Wink, J., Van Delft, R., Notenboom, R. G. E., Wouters, P. F., Deruiter, M. C., Plevier, J. W. M., et al. (2020). Human adult cardiac autonomic innervation: controversies in anatomical knowledge and relevance for cardiac neuromodulation. *Auton. Neurosci.* 227:102674. doi: 10.1016/j.autneu.2020.102674

Yamakawa, K., So, E. L., Rajendran, P. S., Hoang, J. D., Makkar, N., Mahajan, A., et al. (2014). Electrophysiological effects of right and left vagal nerve stimulation on the ventricular myocardium. *Am. J. Physiol. Heart Circ. Physiol.* 307, H722–H731. doi: 10.1152/ajpheart.00279.2014

Yanowitz, F., Preston, J. B., and Abildskov, J. A. (1966). Functional distribution of right and left stellate innervation to the ventricles. Production of neurogenic electrocardiographic changes by unilateral alteration of sympathetic tone. *Circ. Res.* 18, 416–428. doi: 10.1161/01.RES.18.4.416

Yin, Z., Yin, J., Cai, J., Sui, T., and Cao, X. (2015). Neuroanatomy and clinical analysis of the cervical sympathetic trunk and longus colli. *J. Biomed. Res.* 29, 501–507.

Yokota, S., Taneyama, C., and Goto, H. (2013). Different effects of right and left stellate ganglion block on systolic blood pressure and heart rate. *Open J. Anesth.* 3, 143–147. doi: 10.4236/ojanes.2013.33033

Zhou, S., Jung, B. C., Tan, A. Y., Trang, V. Q., Gholmieh, G., Han, S. W., et al. (2008). Spontaneous stellate ganglion nerve activity and ventricular arrhythmia in a canine model of sudden death. *Heart Rhythm* 5, 131–139. doi: 10.1016/j.hrthm.2007.09.007

Zhou, W., Yamakawa, K., Benharash, P., Ajijola, O., Ennis, D., Hadaya, J., et al. (2013). Effect of stellate ganglia stimulation on global and regional left ventricular function as assessed by speckle tracking echocardiography. *Am. J. Physiol. Heart Circ. Physiol.* 304, H840–H847. doi: 10.1152/ajpheart.00695.2012

Conflict of Interest: The authors declare that the research was conducted in the absence of any commercial or financial relationships that could be construed as a potential conflict of interest.

Publisher's Note: All claims expressed in this article are solely those of the authors and do not necessarily represent those of their affiliated organizations, or those of the publisher, the editors and the reviewers. Any product that may be evaluated in this article, or claim that may be made by its manufacturer, is not guaranteed or endorsed by the publisher.

frontiers in Neurology

CASE REPORT
published: 16 September 2021
doi: 10.3389/fneur.2021.696056

Atypical Posterior Reversible Encephalopathy Syndrome in a Postpartum Woman With Moyamoya Disease: A Case Report and Literature Review

*Ning Zou†, Guixiang Guo†, Fangchao Wan and Xin Li**

Department of Neurology, The First People's Hospital of Changde City, Changde, China

Background: Moyamoya disease is a rare cerebrovascular occlusive disease, which is characterized by stenosis and gradual occlusion of the internal carotid arteries, causing the progression of characteristic collateral vessels. To date, most studies investigating moyamoya disease have focused on medical implications, and the potential implications for neurocognitive and/or neuropsychiatric functioning were inconclusive.

Case Presentation: we present a case of a 26-year-old Chinese postpartum woman who presented to the emergency department with a 19-h history of cognitive decline, vomiting, and convulsions. Blood pressure, heart rate, and respiration rate were 200/120 mmHg, 115 beats/minute, and 30 breaths/minute, respectively, on arrival. The Glasgow Coma Scale, modified RANKIN scale (mRS), and National Institute of Health stroke scale (NIHSS) scores were 3, 5, and 18, respectively. Moyamoya disease was diagnosed using cerebral angiography and digital subtraction angiography. The cognitive functions of orientation, use of language, ability to calculate, and memory significantly improved after 11 days of treatment (Glasgow Coma Scale: 15; mRS: 0; NIHSS: 0).

Conclusions: This patient was diagnosed with reversible posterior leukoencephalopathy syndrome related to moyamoya disease. This case highlights that atypical posterior reversible encephalopathy syndrome can occur in patients with moyamoya disease, and should be considered for the differential diagnosis of cerebral infarcts and hemorrhage in a postpartum female.

Keywords: postpartum woman, reversible posterior leukoencephalopathy syndrome, cerebrovascular occlusive disease, neurocognitive, differential diagnosis

OPEN ACCESS

Edited by:
Yan Yao,
State Key Laboratory of Cardiovascular Disease, Fuwai Hospital, Chinese Academy of Medical Sciences, China

Reviewed by:
Alessandra Rufa,
University of Siena, Italy
Qiuji Shao,
Henan Provincial People's Hospital, China

***Correspondence:**
Xin Li
798664056@qq.com

†These authors have contributed equally to this work

Specialty section:
This article was submitted to Autonomic Neuroscience, a section of the journal Frontiers in Neurology

Received: *16 April 2021*
Accepted: *09 August 2021*
Published: *16 September 2021*

Citation:
Zou N, Guo G, Wan F and Li X (2021) Atypical Posterior Reversible Encephalopathy Syndrome in a Postpartum Woman With Moyamoya Disease: A Case Report and Literature Review. Front. Neurol. 12:696056. doi: 10.3389/fneur.2021.696056

INTRODUCTION

Moyamoya disease is characterized by stenosis or occlusion of the terminal portion of the internal carotid arteries and the branches in the circle of Willis. The etiology of moyamoya disease remains unclear; it can be observed idiopathically or secondary to other diseases. The diagnosis of moyamoya disease based on moyamoya vessels occurred bilaterally (1). Moreover, the angiographic image of moyamoya disease resembles a puff of smoke rifting in the air; the word "moyamoya" means "puff of smoke" in Japanese (2). A study reported that the prevalence of moyamoya disease

was the highest in East Asia (0.35–0.94 per 100,000 of Japanese and Koreans), and the peak ages for moyamoya disease incidence were around 5 years-of-age and 40 years-of-age (2). In addition, Guey et al. reported that moyamoya disease is twice as prevalent in females as males (3). Nearly 10% of patients with moyamoya disease present as having a familial occurrence (4). Alterations in cognitive functioning and neurological symptoms are commonly observed in emergency departments (5). While some may have clear etiology, other less common etiologies must be considered. Therefore, additional laboratory testing and neuroimaging should be applied. This report reviews a rare case of a postpartum patient with moyamoya disease, who presented with altered cognitive function and neurological symptoms. This case highlights the importance of the awareness of uncommon presentations in postpartum patients leading to clinical suspicion of moyamoya disease.

CASE REPORT

Written informed consent was obtained from the patient and ethical approval was granted by the Institutional Review Board of the First People's Hospital of Changde City (2017SK51308). A 26-year-old postpartum woman was admitted to the emergency department presenting with a 19-h history of cognitive decline, vomiting, and convulsions. She had no history of smoking, diabetes mellitus, hypertension, use of aspirin, or use of any recreational drugs. Blood pressure, heart rate, and respiration rate were 200/120 mmHg, 115 beats/minute, and 30 breaths/minute, respectively. The pupils were 3 mm with slow response to light stimulus. A flexion posture was observed in the left limb after tingling, while no movement was detected in the right limb. An initial computed tomography scan showed large infarcts and subarachnoid hemorrhage in the left frontal, temporal, occipital, and basal ganglia areas of the brain (**Figure 1**). The Glasgow Coma Scale (6), modified RANKIN scale (mRS) (7), and National Institute of Health stroke scale (NIHSS) (8) scores were 3, 5, and 18, respectively. Laboratory tests revealed total bilirubin, alanine aminotransferase, and platelet count were 66.0 μmol/L, 286 U/L, and 49 × 109/L, respectively. This indicated that hemolysis, elevated liver enzymes, and low platelets syndrome (HELLP) was occurring. The initial axial cerebral magnetic resonance imaging showed an area of vasogenic edema within the cortex, basal ganglia, and the subcortical white matter of the parieto-occipital lobes (**Figure 2**). Cerebral angiography and digital subtraction angiography were performed and moyamoya disease was diagnosed based on results (**Figure 3**). Treatment strategies: included urapidil (150 mg), cefamandole nafate (1 g/8 h), compound mannitol (125 ml/6 to 12 h), glucose and sodium chloride injection (500 ml), potassium chloride injection (15 ml qd), pantoprazole sodium (40 mg qd), Xingnaojing injection (10 ml qd), levamlodipine benzenesulfonate (5 mg qd), valsartan (80 mg qd), and carvedilol (12.5 mg bid). After 11 days, the Glasgow Coma Scale, mRS, and NIHSS scores were 15, 0, and 0, respectively. The patient's cognitive functions of orientation, use of language, ability to calculate, and memory were significantly improved. Moreover, cerebral magnetic resonance images were normal after treatment (**Figure 4**). Hence, the cognitive and neurological symptoms in a patient with moyamoya disease led to the additional diagnoses of posterior reversible encephalopathy syndrome (PRES), and associated puerperal HELLP syndrome and subarachnoid hemorrhage.

DISCUSSION

PRES was first described in 1996 and is characterized by acute neurological symptoms, including headache, seizures, visual disturbances, and other focal neurological deficits (9). The

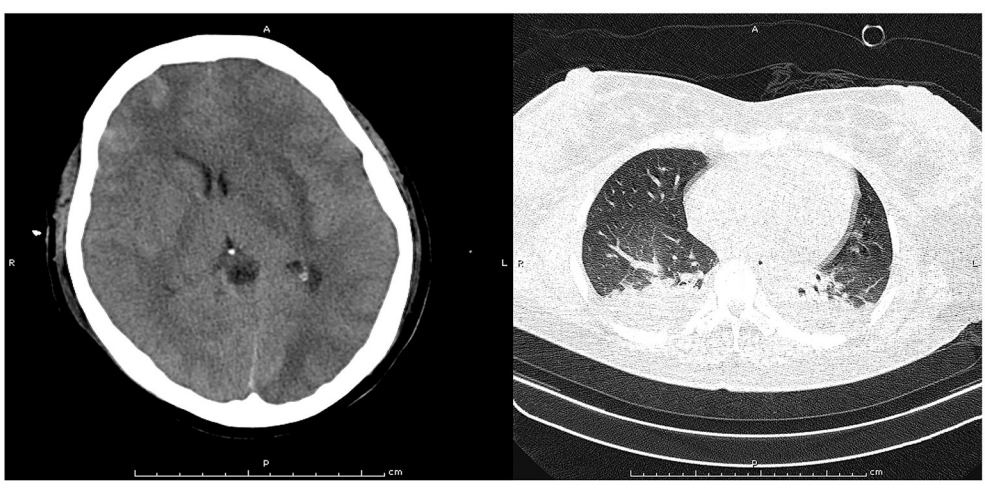

FIGURE 1 | Pre-treatment computed tomography scan at cranial **(A)** and chest **(B)**. The pre-treatment computed tomography scan at cranial indicated obvious cerebral tissue edema, ventricle compression, and subarachnoid hemorrhage. The pre-treatment computed tomography scan at chest found bilateral infection with pleural effusion in lung.

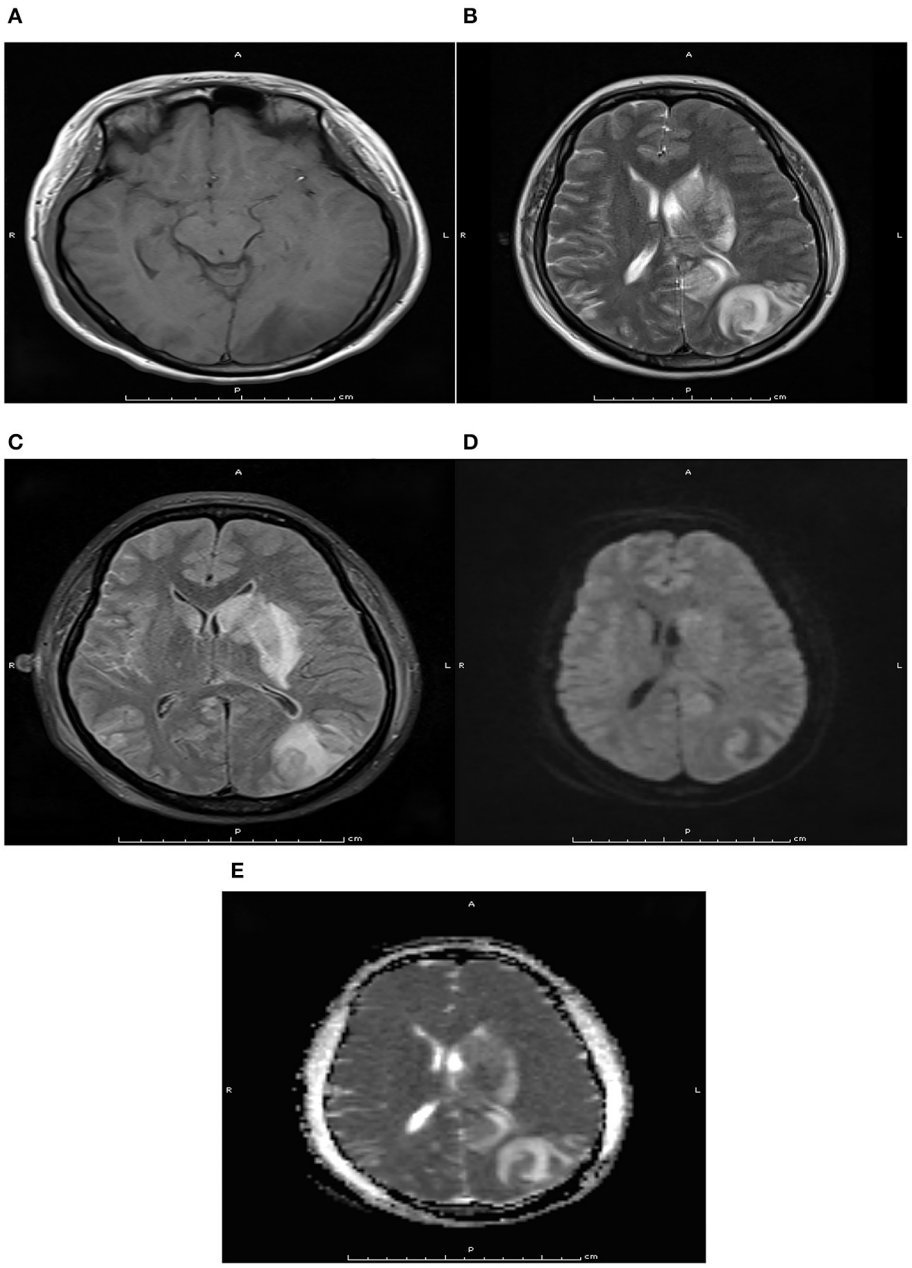

FIGURE 2 | Pre-treatment axial magnetic resonance imaging at T1WI **(A)**, T2WI **(B)**, Flair **(C)**, DWI **(D)**, and ADC **(E)** sequence. Pre-treatment axial magnetic resonance imaging indicated there were long T1 and T2 signals, flair hypersignal, mild limited DWI, and ADC hypersignal in the left occipital lobe and basal ganglia.

severity and acuity of neurological symptoms vary, and PRES generally occurs with rapid onset. PRES has been considered as a dysregulated perfusion disorder, which could cause reversible vasogenic edema. This report presented the case of a postpartum woman with moyamoya disease in which HELLP syndrome and PRES were also observed. Moyamoya is a relatively rare disorder in clinical practice. The diagnosis of moyamoya disease is based on cerebral angiography and digital subtraction angiography. The characteristic angiography results for moyamoya disease was the distal internal carotid arteries and proximal circle of Willis vessels affected by bilateral stenosis, and caused the involvement of prominent collateral vessels. Moreover, the severity of vascular abnormality could staged for predicting further ischemic or hemorrhage risk (10).

In our patient, the potential cause of PRES may have been subarachnoid hemorrhage or eclampsia. The mechanisms for the progression of PRES could be explained by the following: the hyperperfusion and increased cerebral perfusion pressure could cause the breakdown of the blood-brain barrier, which causes the extravasation of plasma and macromolecules into the

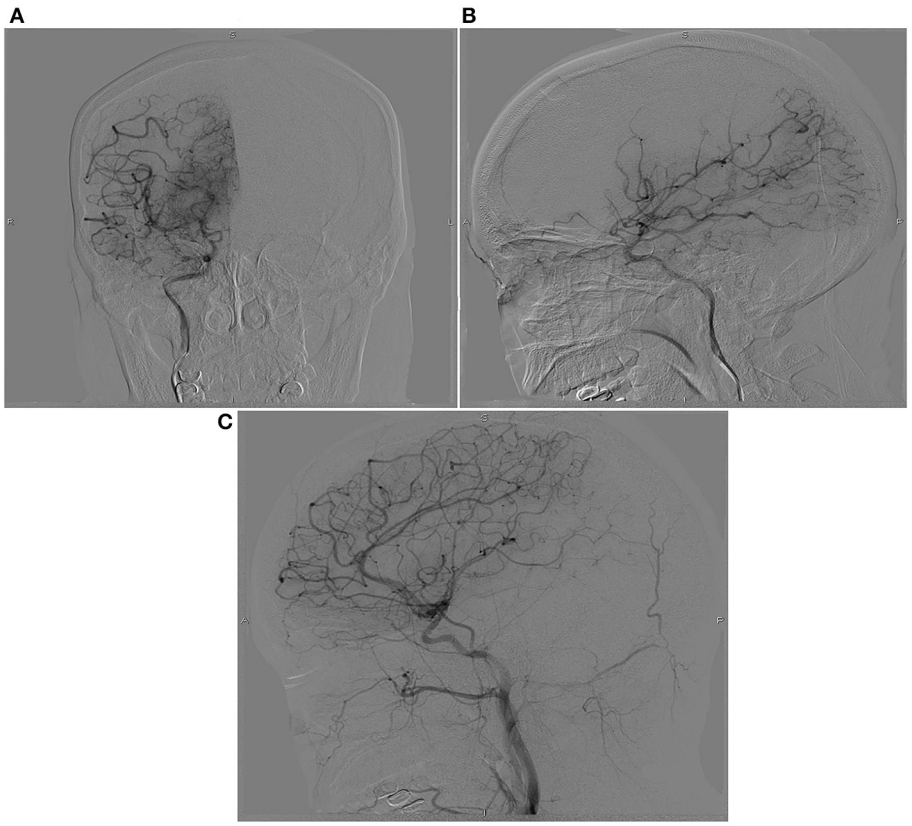

FIGURE 3 | Pre-treatment digital subtraction angiography imaging at anterior **(A)**, posterior **(B)**, and lateral **(C)** projections. Pre-treatment digital subtraction angiography imaging indicated hyperplastic angiography at the end of the internal carotid artery, resembles a puff of smoke rifting in the air.

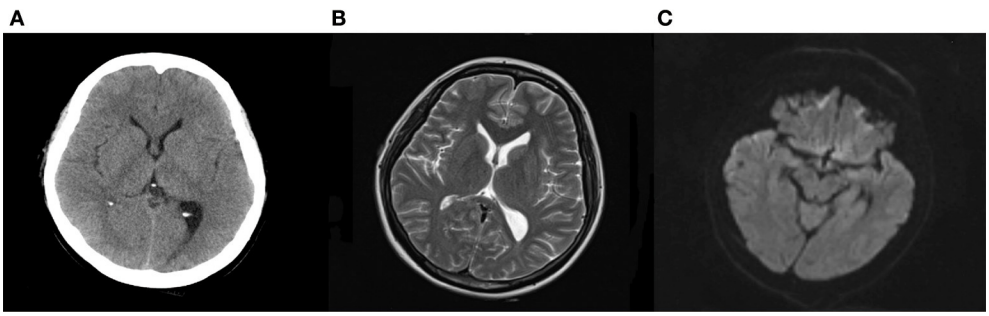

FIGURE 4 | Computed tomography **(A)** and magnetic resonance imaging **(B,C)** after treatments. Computed tomography suggested the edema was disappeared, and the subarachnoid hemorrhage was absorbed after treatments. Magnetic resonance imaging found T2 hypersignal was disappeared, and the DWI signal without hypersignal shadow.

interstitial space through tight junction proteins (11). Moreover, the release of nitric oxide, thromboxane A2, or endothelin-1 from vascular endothelium could mediate cerebral vasospasm and elevate blood pressure, which both play an important role in cerebral autoregulation (12). Furthermore, hypertension is a mutual response to hyperperfusion.

The etiologies of PRES should be mentioned. First, renal injury is an independent risk factor for PRES, and can be explained by the disruption of the renin-angiotensin-aldosterone system (13). Second, individuals infected with COVID-19 could develop cerebrovascular autoregulation disorder, acute renal failure, acute hypertension, hypoxia, inflammation, and endothelial injury; a high prevalence of PRES has been found in COVID-19 infected individuals (14). Third, preeclampsia and eclampsia are significantly associated with PRES. The endothelial dysfunction, elevated blood pressure, thrombocytopenia,

and proteinuria are regarded as important features for the progression of PRES in preeclampsia and eclampsia (15, 16). Fourth, patients with PRES always have autoimmune disorders, including systemic lupus erythematosus, thrombotic thrombocytopenic purpura, Crohn's disease, and scleroderma (17). Finally, the use of immunosuppression and several other medications are significantly associated with increased risk of PRES (18–20).

The clinical presentation of postpartum women with moyamoya disease varies. Maruyama et al. reported a 41-year-old postpartum woman suffering with sudden onset of dysarthria and left extremity weakness 6 days after delivery, and found protein Z deficiency and a hypercoagulation state which are both significantly associated with ischemic stroke in patients with moyamoya disease (21). Kakogawa et al. reported an antepartum intracranial hemorrhage caused by unilateral moyamoya disease (22). Park et al. reported that severely reduced regional cerebrovascular reserve and frequent transient ischemic attacks at antepartum might present as neurologic deterioration during pregnancy, delivery, and puerperium (23). Furthermore, postpartum women with moyamoya disease could experience seizures and subarachnoid hemorrhage (24). These results suggested the most common presenting symptoms for patients with moyamoya disease was ischemic attacks, and hemorrhagic forms were also observed for adults (25). The current report presents a postpartum woman with moyamoya disease, with related HELLP syndrome and PRES. A potential explanation could be that the baseline blood pressure in postpartum women is higher, and this may have contributed to the observed cognitive and neurological symptoms.

CONCLUSIONS

This report presents a rare case of atypical PRES due to moyamoya disease in a patient with HELLP syndrome during the postpartum period. Therefore, moyamoya disease should be regarded as an underlying disease of PRES in postpartum women. However, this study based on single case description, and the association might due to chance. Clinicians should be familiar with the potential complications of moyamoya disease, particularly in pregnant women. The appropriate treatments should be utilized to manage moyamoya disease, and patients need to be closely monitored and referred to appropriate specialists.

DATA AVAILABILITY STATEMENT

The original contributions presented in the study are included in the article/supplementary material, further inquiries can be directed to the corresponding author/s.

ETHICS STATEMENT

The studies involving human participants were reviewed and approved by the Institutional Review Board of the First People's Hospital of Changde City. The patients/participants provided their written informed consent to participate in this study. Written informed consent was obtained from the individual(s) for the publication of any potentially identifiable images or data included in this article.

AUTHOR CONTRIBUTIONS

GG and XL conceived the idea, conceptualized the study, and drafted the manuscript. NZ collected the data. FW analyzed the data. XL reviewed the manuscript. All authors read and approved the final draft.

FUNDING

This work was funded by Hunan Provincial Department of Science and Technology (2017SK51308).

REFERENCES

1. Scott RM, Smith ER. Moyamoya disease and moyamoya syndrome. *N Engl J Med.* (2009) 360:1226–37. doi: 10.1056/NEJMra0804622
2. Kuroda S, Houkin K. Moyamoya disease: current concepts and future perspectives. *Lancet Neurol.* (2008) 7:1056–66. doi: 10.1016/S1474-4422(08)70240-0
3. Guey S, Tournier-Lasserve E, Hervé D, Kossorotoffet M. Moyamoya disease and syndromes: from genetics to clinical management. *Appl Clin Genet.* (2015) 8:49–68. doi: 10.2147/TACG.S42772
4. Bang OY, Fujimura M, Kim SK. The pathophysiology of moyamoya disease: an update. *J Stroke.* (2016) 18:12–20. doi: 10.5853/jos.2015.01760
5. Huff JS, Morris DL, Kothari RU, Gibbs MA; Emergency Medicine Seizure Study Group. Emergency department management of patients with seizures: a multicenter study. *Acad Emerg Med.* (2001) 8:622–8. doi: 10.1111/j.1553-2712.2001.tb00175.x
6. Cook NF. The glasgow coma scale: a european and global perspective on enhancing practice. *Crit Care Nurs Clin North Am.* (2021) 33:89–99. doi: 10.1016/j.cnc.2020.10.005
7. Quinn TJ, Dawson J, Walters MR, Lees KR. Reliability of the modified rankin scale: a systematic review. *Stroke.* (2009) 40:3393–5. doi: 10.1161/STROKEAHA.109.557256
8. Fischer U, Arnold M, Nedeltchev K, Brekenfeld C, Ballinari P, Remonda L, et al. NIHSS score and arteriographic findings in acute ischemic stroke. *Stroke.* (2005) 36:2121–5. doi: 10.1161/01.STR.0000182099.04994.fc
9. Hinchey J, Chaves C, Appignani B, Breen J, Pao L, Wang A, et al. A reversible posterior leukoencephalopathy syndrome. *N Engl J Med.* (1996) 334:494–500. doi: 10.1056/NEJM199602223340803
10. Lee S, Rivkin MJ, Kirton A, deVeber G, Elbers J; International Pediatric Stroke Study. Moyamoya disease in children: results from the international pediatric stroke study. *J Child Neurol.* (2017) 32:924–9. doi: 10.1177/0883073817718730
11. Rabinstein AA, Mandrekar J, Merrell R, Kozak OS, Durosaro O, Fugate JE. Blood pressure fluctuations in posterior reversible encephalopathy syndrome. *J Stroke Cerebrovasc Dis.* (2012) 21:254–8. doi: 10.1016/j.jstrokecerebrovasdis.2011.03.011
12. Creager M, Loscalzo J, Beckman JA. *Vascular Medicine E-book: A Companion to Braunwald's Heart Disease*. Amsterdam: Elsevier Health Sciences (2012).
13. Burrus TM, Mandrekar J, Wijdicks EF, Rabinstein AA. Renal failure and posterior reversible encephalopathy syndrome in patients with thrombotic thrombocytopenic purpura. *Arch Neurol.* (2010) 67:831–4. doi: 10.1001/archneurol.2010.119
14. Parauda SC, Gao V, Gewirtz AN, Parikh NS, Merkler AE, Lantos J, et al. Posterior reversible encephalopathy syndrome in patients with COVID-19. *J Neurol Sci.* (2020) 416:117019. doi: 10.1016/j.jns.2020.117019

15. McDermott M, Miller EC, Rundek T, Hurn PD, Bushnell CD. Preeclampsia: association with posterior reversible encephalopathy syndrome and stroke. *Stroke.* (2018) 49:524–30. doi: 10.1161/STROKEAHA.117.018416
16. Fisher N, Saraf S, Egbert N, Homel P, Stein EG, Minkoff H. Clinical correlates of posterior reversible encephalopathy syndrome in pregnancy. *J Clin Hypertens.* (2016) 18:522–7. doi: 10.1111/jch.12656
17. Fugate JE, Rabinstein AA. Posterior reversible encephalopathy syndrome: clinical and radiological manifestations, pathophysiology, and outstanding questions. *Lancet Neurol.* (2015) 14:914–25. doi: 10.1016/S1474-4422(15)00111-8
18. Largeau B, Le Tilly O, Sautenet B, Salmon Gandonnière C, Barin-Le Guellec C, Ehrmann S. Arginine vasopressin and posterior reversible encephalopathy syndrome pathophysiology: the missing link? *Mol Neurobiol.* (2019) 56:6792–806. doi: 10.1007/s12035-019-1553-y
19. Parikh NS, Schweitzer AD, Young RJ, Giambrone AE, Lyo J, Karimi S, et al. Corticosteroid therapy and severity of vasogenic edema in posterior reversible encephalopathy syndrome. *J Neurol Sci.* (2017) 380:11–5. doi: 10.1016/j.jns.2017.06.044
20. Rosa Júnior M, Borges ÉI, Fonseca APA, Fiorot JL, Balarini L, Valim V. Posterior reversible encephalopathy syndrome during treatment with tocilizumab in juvenile idiopathic arthritis. *Arq Neuropsiquiatr.* (2018) 76:720–1. doi: 10.1590/0004-282x20180093
21. Maruyama K, Akioka N, Kashiwazaki D, Kuwayama N, Kuroda S. Postpartum ischemic stroke in moyamoya disease associated with protein Z deficiency-A case report. *J Stroke Cerebrovasc Dis.* (2016) 25:e158–60. doi: 10.1016/j.jstrokecerebrovasdis.2016.06.036
22. Kakogawa J, Sadatsuki M, Masuya N, Gomibuchi H, Ohno H, Hara T, et al. Antepartum intracranial hemorrhage due to unrecognized unilateral moyamoya disease: a case report. *Arch Gynecol Obstet.* (2011) 283:19–22. doi: 10.1007/s00404-010-1654-3
23. Park W, Ahn JS, Chung J, Chung Y, Lee S, Park JC, et al. Neurologic deterioration in patients with moyamoya disease during pregnancy, delivery, and puerperium. *World Neurosurg.* (2018) 111:e7–17. doi: 10.1016/j.wneu.2017.11.094
24. Varanasi LC, Brown J, Athayde N. Postpartum seizure and subarachnoid haemorrhage secondary to moyamoya disease. *Case Rep Obstet Gynecol.* (2019) 2019:6132835. doi: 10.1155/2019/6132835
25. Gurung S, Gaire S, Bajracharya A, Paudel AK, Budhathoki P. Moyamoya disease in an adult female from Nepal: a case report. *Ann Med Surg.* (2021) 66:102424. doi: 10.1016/j.amsu.2021.102424

Conflict of Interest: The authors declare that the research was conducted in the absence of any commercial or financial relationships that could be construed as a potential conflict of interest.

Publisher's Note: All claims expressed in this article are solely those of the authors and do not necessarily represent those of their affiliated organizations, or those of the publisher, the editors and the reviewers. Any product that may be evaluated in this article, or claim that may be made by its manufacturer, is not guaranteed or endorsed by the publisher.

frontiers in Physiology

ORIGINAL RESEARCH
published: 18 October 2021
doi: 10.3389/fphys.2021.744071

Anti-Heartbeat-Evoked Potentials Performance in Event-Related Potentials-Based Mental Workload Assessment

*Sangin Park[1], Jihyeon Ha[1,2] and Laehyun Kim[1,3]**

[1]Center for Bionics, Korea Institute of Science and Technology, Seoul, South Korea, [2]Department of Biomedical Engineering, Hanyang University, Seoul, South Korea, [3]Department of HY-KIST Bio-Convergence, Hanyang University, Seoul, South Korea

The aim of this study was to determine the effect of heartbeat-evoked potentials (HEPs) on the performance of an event-related potential (ERP)-based classification of mental workload (MWL). We produced low- and high-MWLs using a mental arithmetic task and measured the ERP response of 14 participants. ERP trials were divided into three conditions based on the effect of HEPs on ERPs: ERP_{HEP}, containing the heartbeat in a period of 280–700 ms in ERP epochs after the target; $ERP_{A\text{-}HEP}$, not including the heartbeat within the same period; and ERP_{T}, all trials including $ERP_{A\text{-}HEP}$ and ERP_{HEP}. We then compared MWL classification performance using the amplitude and latency of the P600 ERP among the three conditions. The $ERP_{A\text{-}HEP}$ condition achieved an accuracy of 100% using a radial basis function-support vector machine (with 10-fold cross-validation), showing an increase of 14.3 and 28.6% in accuracy compared to ERP_{T} (85.7%) and ERP_{HEP} (71.4%), respectively. The results suggest that evoked potentials caused by heartbeat overlapped or interfered with the ERPs and weakened the ERP response to stimuli. This study reveals the effect of the evoked potentials induced by heartbeats on the performance of the MWL classification based on ERPs.

Keywords: electroencephalography, heartbeat-evoked potentials, event-related potentials, mental workload, subjective mental effort questionnaire

OPEN ACCESS

Edited by:
Lilei Yu,
Wuhan University, China

Reviewed by:
Austin T. Robinson,
Auburn University, United States
Ian Spence,
The University of Sydney, Australia

***Correspondence:**
Laehyun Kim
laehyunk@kist.re.kr

Specialty section:
This article was submitted to Autonomic Neuroscience, a section of the journal Frontiers in Physiology

Received: *19 July 2021*
Accepted: *27 September 2021*
Published: *18 October 2021*

Citation:
Park S, Ha J and Kim L (2021) Anti-Heartbeat-Evoked Potentials Performance in Event-Related Potentials-Based Mental Workload Assessment. Front. Physiol. 12:744071. doi: 10.3389/fphys.2021.744071

INTRODUCTION

Event-related potentials (ERPs) provide a powerful method for interpreting the relationship between the human mind and the brain. ERPs measure brain responses which are a direct result of a specific input in the form of sensory, cognitive, memory, or motor events (Luck, 2014). Because brain activity in response to a single event or stimulus is not usually visible in electroencephalogram (EEG) signals, the ERP technique is required to measure the response to a stimulus in many trials (Coles and Rugg, 1995; Boudewyn et al., 2018). The brain activity of a single event or stimulus trial would be averaged out, and the relevant or dominant potentials would remain (Coles and Rugg, 1995).

Electroencephalogram signals are often contaminated by various artifacts, such as eyeblinks, ocular movements, and muscular and cardiac activity, which are typically not of interest

(Uriguen and Garcia-Zapirain, 2015). These artifacts can affect EEG signals and interfere with relevant or dominant potentials in ERPs. Thus, many previous studies have sought to remove artifacts, such as muscular activity (Chen et al., 2019; Zou et al., 2020), cardiac activity (Hamaneh et al., 2014; Dai et al., 2019), eyeblinks, and ocular movements (Dimigen, 2020; Egambaram et al., 2020). The effect of noise on ERP analysis has been minimized thanks to the development of methods to remove noise in EEG signals. However, we hypothesized that other factors, such as changes in mental state (i.e., stress, emotion, and cognitive load) and evoked potentials [i.e., heartbeat-evoked potential (HEP)], in addition to noise, could affect the ERP signals, leading to a decrease in performance (Zhang et al., 2020; Zheng et al., 2020). Some previous studies have sought to improve the classification performance by considering the changes in mental state (Ko et al., 2020; Zhang et al., 2020), but no study using HEP has been reported. Evoked potentials are difficult to remove or recover because, unlike noise, they do not cause a change in the dominant pattern of the EEG signal but are instead contained in the EEG signal itself (Schandry and Montoya, 1996; McCraty et al., 2009).

Heartbeat-evoked potentials are characteristic changes in brain waves caused by evoked potentials that can occur due to changes in cardiac activity, such as heart rhythms and heart rate variability (Schandry and Montoya, 1996; McCraty et al., 2009; Park et al., 2015). The vagus nerve transmits cardiac output information *via* the visceral-afferent pathway (medulla, amygdalae, hypothalamic and thalamic nuclei, and nucleus tractus solitarius) from the heart to the brain (Montoya et al., 1993; Janig, 1996; Nieuwenhuys et al., 2007). HEPs reflect a synchronization in the communication between the brain and heart based on efferent and afferent pathways, leading to evoked potentials involving changes in alpha activation in EEG signals (McCraty et al., 2009; Park et al., 2015; Park and Whang, 2018). HEP is divided into two components. The first HEP component (50–250 ms post-R-wave) is defined as the interval required for afferent information from the heart to reach the brain. An increase in afferent processing is indicated by the synchronization of the alpha wave. The second HEP component (250–600 ms post-R-wave) is defined as the time interval needed for blood pressure to reach the brain area from the heart. When the blood pressure wave synchronizes with brain activity, alpha synchronization occurs, which is associated with the higher cognitive centers' processing of the sensory input (Wölk et al., 1989; McCraty et al., 2009; Park et al., 2015).

As previously mentioned, HEP causes evoked potentials in EEG signals due to the synchronization between the brain and heart. HEP is similar to ERP in terms of how it causes evoked potentials in EEG signals based on a trigger point. We believe that HEP can be contained in the ERP when there is little difference in the trigger time between the heartbeat and the event. In ERP analyses, the detection of a significant ERP pattern may be impeded by evoked potentials overlapping a heartbeat. Thus, this study sought to determine the effect of evoked potentials by HEPs on changes in significant patterns in ERP signals during a cognitive task, as well as the ERP-based classification performance of mental workload, by separating ERP trials that are affected by HEP from those that are not.

Abbreviations: HEPs, heartbeat-evoked potentials; ERPs, event-related potentials; MWL, mental workload; ERP_{HEP}, containing the heartbeat in ERP epochs; $ERP_{A\text{-}HEP}$, not containing the heartbeat in ERP epochs; ERP_{T}, $ERP_{A\text{-}HEP}$ and ERP_{HEP} together; RBF-SVM, radial basis function-support vector machine; EEG, electroencephalogram; SMEQ, subjective mental effort questionnaire; CAR, common average referencing; ICA, independent component analysis; F, frontal region; C, central region; P, parietal region; O, occipital region; AUC, area under curve; ROC, receiver operating characteristics; LPPs, late positive potentials; BCI, brain-computer interface; SVEP, steady-state visually evoked potential.

MATERIALS AND METHODS

Participants

Fourteen undergraduate students (seven male and seven female) aged between 22 and 29 years (mean 25.2 ± 3.4) participated in the experiment. Each subject participated voluntarily and was paid 100,000 KRW. All participants were right-handed and had no family or medical history of cardiovascular, autonomic, or central nervous system disorders. All participants were required to abstain from alcohol, cigarettes, and caffeine for 24 h prior to the experiment and to sleep normally. Informed consent was acquired from all participants who were notified of the restrictions and requirements. All experimental protocols were approved by the Sangmyung University Institutional Bioethics Review Board in Seoul, South Korea (BE2019-46).

Experimental Stimuli and Apparatus

ERP Task

A stimulator was designed to measure the ERP response to mental workload based on our previous studies (Mun et al., 2012; Park et al., 2014, 2015, 2019). The stimulator was located on the left and right sides of the screen, and participants were required to focus their attention on the instructed side of the screen according to an arrow (to ignore the left side and attend to the right one, or vice versa). The stimulator consisted of the presentation of 12 alphanumeric characters involving non-targets ("A" to "K") and a target ("5"). The alphanumeric characters were randomly updated at the rate of 6 Hz. One trial consisted of five sequences involving 60 alphanumeric characters lasting 10 s, with an inter-trial interval of 2 s (total 60 s). One block consisted of five trials, and the entire task consisted of 15 blocks. The target was presented with a probability of 5% within each trial, and the interval between targets lasted less than 1 s to avoid overlapping ERPs during analysis, as shown in **Figure 1**.

Mental Workload: Mental Arithmetic Task

The mental arithmetic task was designed to cause mental workload (MWL) based on previous studies (So et al., 2017; Jost et al., 2019) and was divided into two task levels: low- and high-MWL. The low-MWL task consisted of easy questions involving single-digit addition and subtraction (i.e., 3 + 2, 4–1, with numbers ranging from 1 to 9). The high-MWL task consisted of difficult questions involving mixed arithmetic

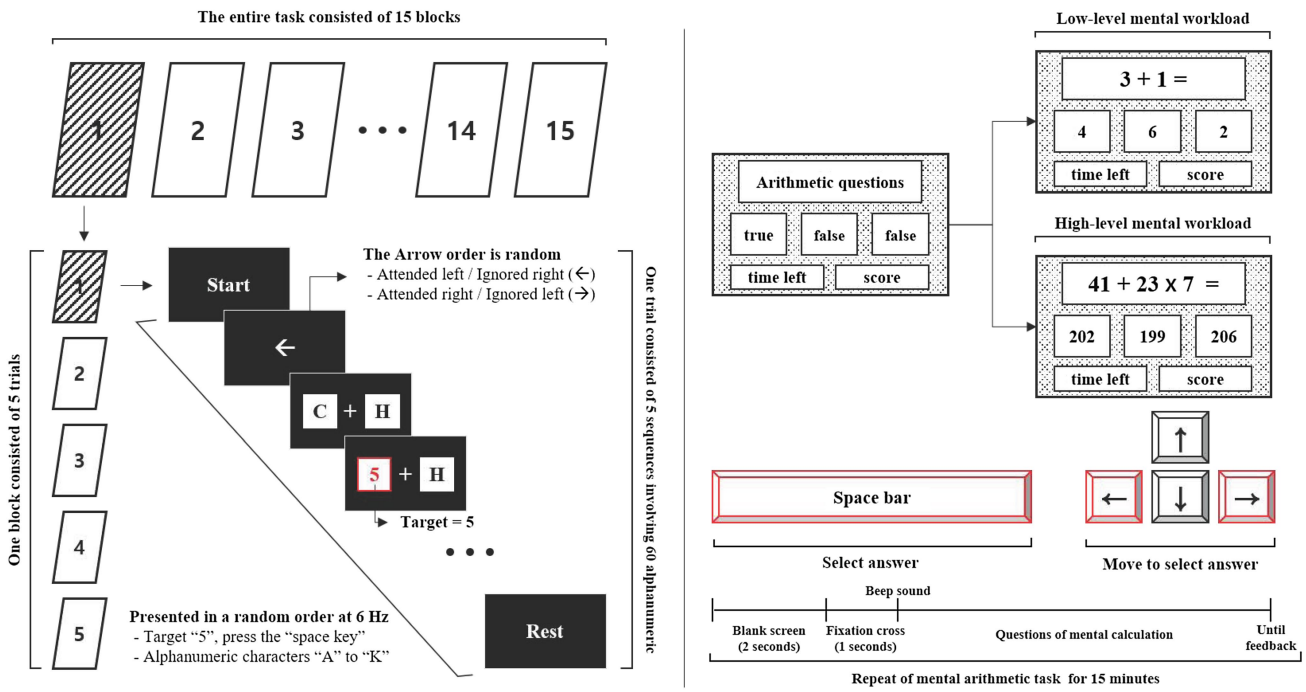

FIGURE 1 | Experimental stimuli to measure ERP responses (left) and cause mental workload (right).

operations (i.e., 36 × 7–24, 43 + 72/9, number range 1–99). The mental arithmetic task questions were randomly presented within a defined range, and included a true answer result and two false confusion results. The two false results were automatically calculated by randomly adding or subtracting a number in the range of 1–5 from the correct answer. Participants were required to select the correct answer using the arrow and spacebar keys of the keyboard, as shown in **Figure 1**. ERP and mental arithmetic tasks were developed using LabVIEW2016 (National Instruments Inc., Austin, TX, United States).

Experimental Procedure

Participants were required to report their MWL state as a subjective rating both before and after the experiment. The subjective mental effort questionnaire (SMEQ) (Sauro and Dumas, 2009), a questionnaire with a 0–150 scale for rating the MWL was used, as shown in **Figure 2**. Participants performed the pre-ERP task for 15 min. Over the course of this session, all participants were required to fixate on a red cross at the center of the screen, 60 cm from the display and press a spacebar key when presented with the target "5." The performance and response times were measured for the target. Following the pre-ERP task, they performed the mental arithmetic task for 15 min. All participants were asked to select the correct answer to the mental arithmetic question, from three options, using the arrow and spacebar keys of the keyboard. For each correct answer, the participant was awarded 10 points, whereas 10 points were deducted for an incorrect answer. In order to increase the subjects' motivation and engagement, those who achieved the top 15% score were paid 150% of the test fee. Participants were divided into low-MWL and high-MWL task groups. On the first day, they performed either the low-MWL or High-MWL task and on the next day, they performed the other MWL task at the same time (e.g., first day low-MWL task and second day high-MWL task; the order randomized across subjects). Participants then performed the post-ERP task, which was the same as the pre-ERP task. The experimental environment and procedure are illustrated in **Figure 3**.

Signal Processing and Data Acquisition

Electroencephalogram signals were recorded at a sampling rate of 2,048 Hz from 64 channels mounted on an EEG electrode cap (Active-two, Biosemi S.V., Amsterdam, Netherlands) based on the international 10–20 montage with separate reference and ground electrodes for each system (common mode sense, CMS and driven right leg, DRL, respectively). Impedance from all electrodes was kept below 5 kΩ (below 10 kΩ for the two eye channels). The measured EEG signals were down-sampled to 512 Hz and re-referenced using a common average referencing (CAR) procedure (Perrin et al., 1989). The CAR was calculated by subtracting the average potential over all the channels from each channel. This re-referencing maintains the activity from local sources while removing the global background activity

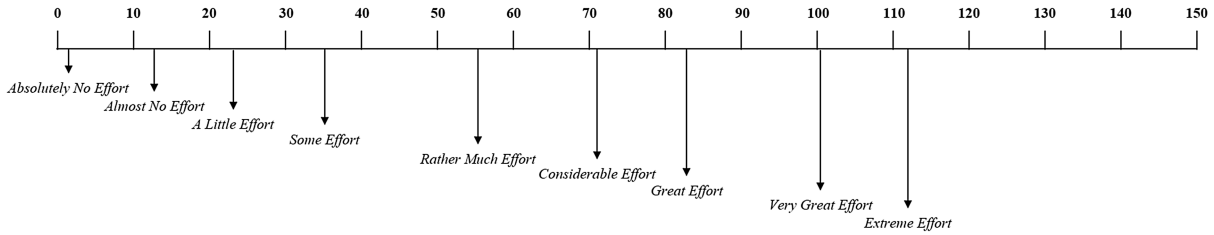

FIGURE 2 | Subjective mental effort questionnaire (SMEQ).

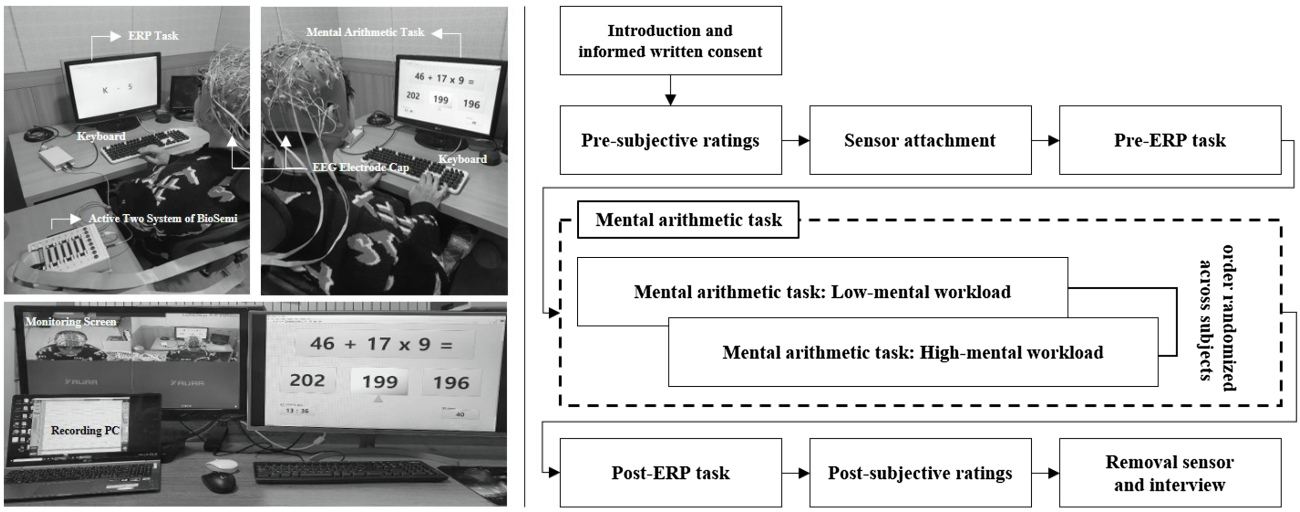

FIGURE 3 | Experimental environment (left) and procedure (right).

(Lew et al., 2012). To avoid contaminating meaningful ERP patterns, we minimized preprocessing by specifying a threshold for each trial. In the trials, where the amplitude exceeded ±100 μV at any electrode, we conducted an independent component analysis to remove oculomotor and muscle artifacts by visual inspection. Additionally, a few trials with anomalous patterns were excluded due to the difficulty of reconstruction (Rampone et al., 2019; Katus et al., 2020; Li et al., 2020).

The ERP analysis procedure was as follows. (1) The EEG signals were divided into epochs of 1,000 ms based on the event (200 ms before target onset to 800 ms after target onset) and averaged. (2) Average ERPs were constructed from trials containing 1,000 ms epochs of raw data, of which the pre-stimulus period (first 200 ms) was used to correct the baseline averaged ERP epochs lasting 800 ms (Mitchell et al., 2016). (3) Next, the P600 latency and amplitude were detected from the averaged ERP epochs. The P600 latency and amplitude were determined from its highest point and mean amplitude, respectively, within a time window between 530 and 750 ms following stimulus presentation (Causse et al., 2016) at the F3, F4, C3, C4, P3, P4, O1, and O2 electrodes (Mun et al., 2014; Park et al., 2015, 2019). Each electrode site corresponds to a brain region identified by a letter: frontal (F), central (C), parietal (P), and occipital (O). These brain areas are associated with the following functions: (1) the frontal area is associated with reasoning, motor skills, higher level cognition, and expressive language; (2) the central area is associated with motor and sensory information; (3) the parietal area is associated with processing of tactile sensations; and (4) the occipital area is associated with interpreting visual stimuli and information (Dimond and Beaumont, 1974). All signal processing and data analyses were performed using EEGlab, a MATLAB toolbox (2020b, Mathworks Inc., Natick, MA, United States).

Participants were required to perform all the 375 trials for the ERP task. In order to assess the effect of the evoked potentials caused by heartbeat (i.e., the alpha activation of HEPs) on the latency and amplitude of the P600 component in ERPs, and the classification performance in distinguishing between low- and high-MWL states, the entire ERP epochs were categorized into two conditions based on the heartbeat within each ERP epoch: including the heartbeat within the ERP epoch (denoted ERP_{HEP}) or not including the heartbeat within the ERP epoch (denoted $ERP_{A\text{-}HEP}$, for anti-HEP). ERP_{HEP} and $ERP_{A\text{-}HEP}$ accounted for 171.79 ± 10.31 and 203.21 ± 10.31 trials, respectively, on average, for each subject. More specifically, ERP_{HEP} was defined as containing the heartbeat during the period from 280 to 700 ms in the ERP epochs after the target was presented. This period was determined by considering the

interval in which the evoked potentials overlapped the heartbeat (50–250 ms after the heartbeat) and events related to P600 (530–750 ms after target). $ERP_{A\text{-}HEP}$ was defined as not including the heartbeat within the same period. Finally, we defined the ERP_T condition as including all the $ERP_{A\text{-}HEP}$ and ERP_{HEP} trials. We divided the $ERP_{A\text{-}HEP}$, ERP_{HEP}, and ERP_T trials from entire ERP epochs, and compared their classification performance in separating low- and high-MWL states and the pattern of latency and amplitude of the P600 component, as shown in **Figure 4**.

Statistical Analysis and Classification

This study followed a within-subject design with respect to low- and high-MWL. A paired *t*-test was used based on the results of the Shapiro–Wilk normality test. Differences between pre- and post-features were calculated to take into account the state before the task. The confidence level in the statistical tests was controlled by the number of individual hypotheses (i.e., $\alpha = 05/n$) based on the Bonferroni correction. Bonferroni correction was performed to assess statistical significance while correcting for multiple comparisons (Dunnett, 1955; Johnson et al., 2019). Thus, the statistically significant levels of performance and ERP measures were set to 0.025 (accuracy and response time, $\alpha = 0.05/2 = 0.025$) and 0.0031 (ERP latency and amplitude at eight electrodes, $\alpha = 0.05/16 = 0.0031$). The effect size based on Hedges' g was calculated to assess not only the statistical significance, but also the practical significance (Hedges and Olkin, 2014). All effect sizes were corrected for small sample sizes according to Hedges' g. We also calculated the expected effect size for the paired t-test (Hedges' g) using G*power software (Faul et al., 2007). The expected effect size in this study was 0.781 (paired *t*-test).

In EEG research, the radial basis function kernel-based support vector machine (RBF-SVM) is considered one of the optimized classifiers (Alomari et al., 2013). We used RBF-SVM to conduct a binary classification for a total of 28 samples × number of features after feature selection and standardization. The optimized kernel scales for each condition were as follows: ERP_T, 117.8; ERP_{HEP}, 2.7; and $ERP_{A\text{-}HEP}$, 21.5. We conducted 10-fold cross-validation and represented the performance of the classification using accuracy, sensitivity, specificity, and area under the curve (AUC) for the receiver operating characteristics curve. Statistical analysis and classification were performed using the Statistics and Machine Learning Toolbox in MATLAB (2020b, Mathworks Inc., Natick, MA, United States).

RESULTS

Subjective Ratings: SMEQ

Figure 5 represents the comparison of the SMEQ scores between low- and high-MWL conditions. In the paired t-test, the SMEQ score of the high-MWL condition was significantly higher than that of the low-MWL condition [$t(13) = -9.238$, Hedges' g = 3.796, 95% CI 2.556–5.036, $p < 0.001$]. The mean (*M*) and standard deviation (*SD*) for each condition were as follows: low-MWL, $M = 13.79$ and $SD = 6.37$; high-MWL, $M = 71.64$ and $SD = 20.59$. Hedges' g satisfied the expected effect size for the paired t-test in this study.

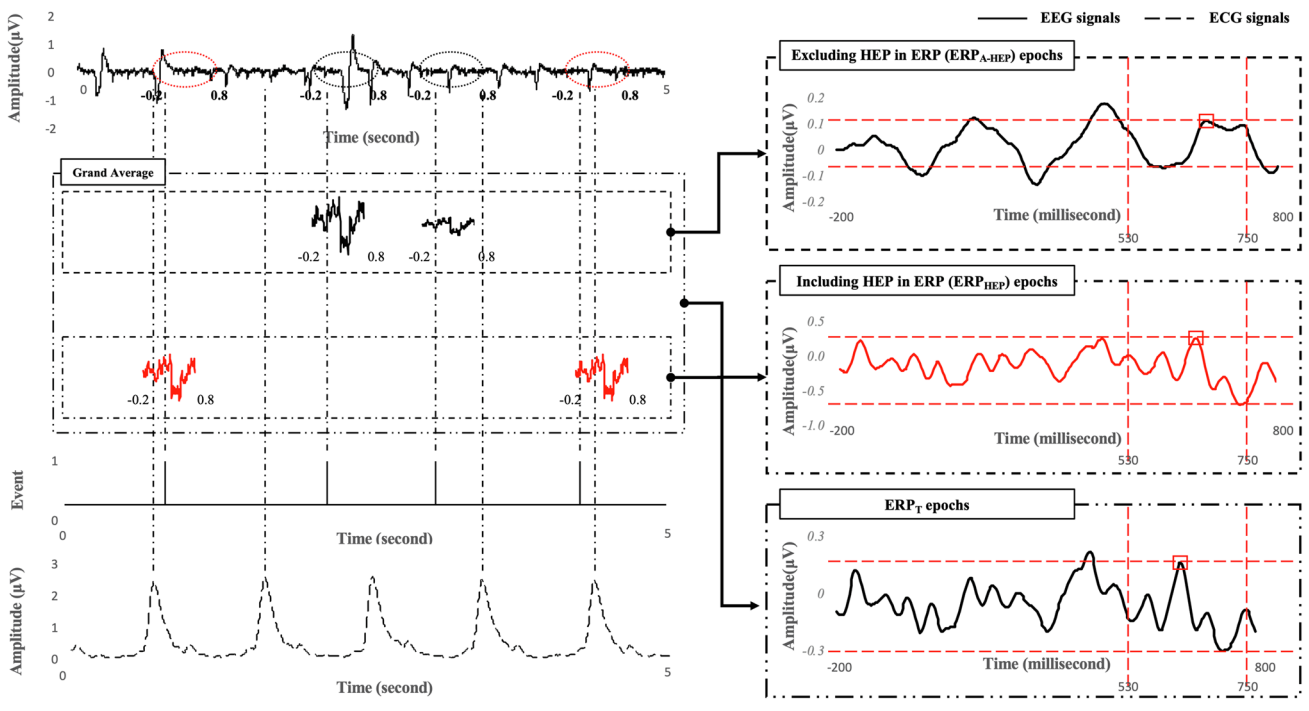

FIGURE 4 | Examples of signal processing compared across $ERP_{A\text{-}HEP}$, ERP_{HEP}, and ERP_T.

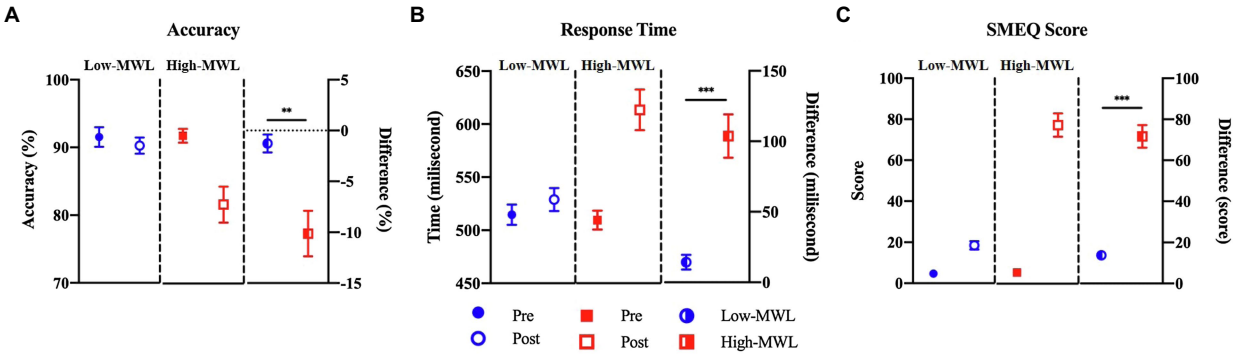

FIGURE 5 | Comparison of accuracy **(A)**, response time **(B)** for target in ERP task, and SMEQ score **(C)** between the low- and high-MWL conditions (paired *t*-test; $^{**}p<0.0031$ and $^{***}p<0.001$).

ERP Task Performance: Accuracy and Response Time

A paired *t*-test of target accuracy in the ERP task showed a significant difference between the low- ($M=-1.27$, $SD=3.29$) and high-MWL ($M=-10.13$, $SD=8.38$) conditions [$t(13)=3.762$, Hedges' g = −1.392, 95% CI −2.217 to −0.566, $p<0.01$]. The response time of the high-MWL ($M=14.30$, $SD=19.54$) condition was significantly delayed compared to the low-MWL ($M=103.67$, $SD=57.76$) condition [$t(13)=-4.643$, Hedges' g = 2.073, 95% CI 1.154 to −2.991, $p<0.001$], as shown in **Figure 5**. Hedges' g for the performance of the ERP task satisfied the expected effect size for the paired t-test in this study.

ERP Waveform: P600 Amplitude and Latency

P600 Amplitude

Figure 6 represents the results of the statistical analysis of the P600 amplitudes, comparing the low- and high-MWL conditions, for the ERP_T, $ERP_{A\text{-}HEP}$, and ERP_{HEP} epochs. In the cases of ERP_T and ERP_{HEP}, no significant differences between low- and high-MWL conditions were found at any electrode site (F3, F4, C3, C4, P3, P4, O1, and O2) after Bonferroni correction ($p>0.0031$). However, in the case of $ERP_{A\text{-}HEP}$, a paired t-test revealed a significant difference between the P600 amplitudes of the low- and high-MWL conditions at F3 [$t(13)=5.505$, Hedges' g = −1.988, 95% CI −2.893 to −1.082, $p<0.001$], F4 [$t(13)=4.787$, Hedges' g = −1.265, 95% CI −2.076 to −0.453, $p<0.001$], P4 [$t(13)=4.383$, Hedges' g = −1.559, 95% CI −2.281 to −0.616, $p<0.001$), and O1 [$t(13)=3.818$, Hedges' g = −1.391, 95% CI −2.217 to −0.566, $p<0.0031$]. No significant differences were found at the other electrode sites (C3, C4, P3, and O2). Detailed results are presented in **Table 1**. Hedges' g for the P600 amplitude satisfied the expected effect size for the paired t-test.

P600 Latency

Figure 7 represents the results of the statistical analysis comparing the P600 latency between the low- and high-MWL conditions for the ERP_T, $ERP_{A\text{-}HEP}$, and ERP_{HEP} epochs. In the case of ERP_T, a paired t-test revealed a significant difference between low- and high-MWL conditions at the O1 site only [$t(13)=-3.935$, Hedges' g = 1.462, 95% CI 0.628 to 2.296, $p<0.0031$], while no significant differences were found at the other electrode sites. In the case of ERP_{HEP}, no significant differences were observed between the P600 latencies of low- and high-MWL conditions at any electrode site after Bonferroni correction ($p>0.0031$). For the $ERP_{A\text{-}HEP}$, P600 latency was significantly prolonged in the high-MWL condition compared with the low-MWL condition at F3 [$t(13)=-4.348$, Hedges' g = 1.823, 95% CI 0.942 to 2.704, $p<0.001$], F4 [$t(13)=-3.833$, Hedges' g = 1.533, 95% CI 0.690 to 2.375, $p<0.001$], P4 [$t(13)=-4.283$, Hedges' g = 1.662, 95% CI 0.803 to 2.521, $p<0.001$], O1 [$t(13)=-5.115$, Hedges' g = 1.714, 95% CI 0.848 to 2.581, $p<0.001$], and O2 [$t(13)=-5.526$, Hedges' g = 1.871, 95% CI 0.983 to 2.760, $p<0.001$] sites. No significant differences were found at the other electrode sites (C3, C4, and P3). Detailed results are presented in **Table 2**. Hedges' g for the P600 latency satisfied the expected effect size for the paired t-test.

To visually confirm the pattern of ERP features between low- and high-MWL, we produced scatterplots with amplitude and latency as the two axes for the ERP_T, ERP_{HEP}, and $ERP_{A\text{-}HEP}$ conditions. As shown in **Figure 8**, only the $ERP_{A\text{-}HEP}$ condition revealed a clear pattern distinguishing the two MWL states. A paired t-test of the heart rate showed no significant difference between the low-MWL (0.81 ± 0.05) and high-MWL (0.79 ± 0.05) conditions [$t(13)=1.479$, $p=0.163$].

Classification and Correlation Results

Classification

We compared the classification performance of ERP_T, ERP_{HEP}, and $ERP_{A\text{-}HEP}$ in distinguishing between low- and high-MWL in order to assess the effect of the HEP on the predictive power of ERPs (10-fold cross-validation). The RBF-SVM was selected as the classification method since it is widely used in EEG-related studies. In the three conditions (ERP_T, ERP_{HEP}, and $ERP_{A\text{-}HEP}$), for all ERP amplitude and latency, the following values of the performance metrics were achieved as: accuracy:

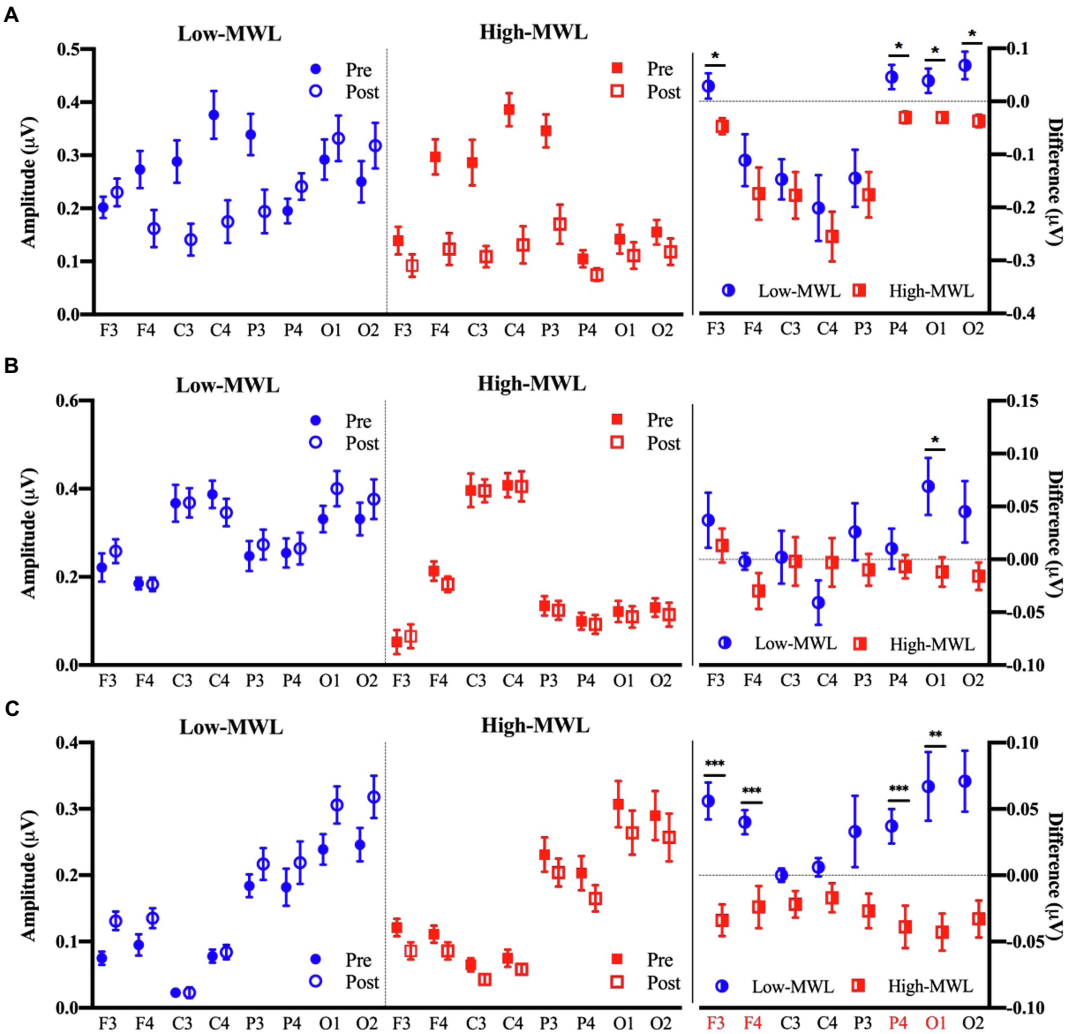

FIGURE 6 | Comparison of the P600 amplitude in ERP between the low- and high-MWL conditions. **(A)** ERP_T condition. **(B)** ERP_{HEP} condition. **(C)** $ERP_{A\text{-}HEP}$ condition (paired *t*-test; $^{*}p<0.05$, $^{**}p<0.0031$, and $^{***}p<0.001$).

85.7,% 71.4, and 100%, respectively; sensitivity, 85.7, 64.3, and 100%; specificity, 85.7, 78.6, and 100%; and AUC: 0.93, 0.76, and 1, as shown in **Table 3** and **Figure 9**.

Correlation

We conducted a correlation analysis among ERP features and SMEQ scores and compared the correlation coefficients for the ERP_T, ERP_{HEP}, and $ERP_{A\text{-}HEP}$ conditions. Specifically, we assessed the partial correlation between post-ERP features and post-SMEQ scores while controlling for two covariates (pre-ERP features and pre-SMEQ scores) to take into account the state before the experiment (Liu, 1988). In the ERP_T, ERP_{HEP}, and $ERP_{A\text{-}HEP}$ conditions, we found significant correlations between SMEQ score and seven, four, and ten ERP features, respectively. The correlation coefficients in the $ERP_{A\text{-}HEP}$ condition (amplitude: 0.410 to 0.885; latency: −0.401 to −0.586) were higher than those of the ERP_T (amplitude: 0.414 to 0.497; latency: −0.432 to −0.483) and ERP_{HEP} (amplitude: 0.440; latency: −0.419 to −0.493) conditions. Detailed correlation results are presented in **Table 4**.

DISCUSSION AND CONCLUSION

This study sought to determine the effect of HEP on the amplitude and latency of the P600 component of ERPs and to compare the classification accuracy for the MWL task among the ERP_T, ERP_{HEP}, and $ERP_{A\text{-}HEP}$ conditions. SMEQ score and MWL performance (accuracy and response time for target) were significantly different between low- and high-MWL tasks. These results confirmed that a difference in the MWL state of participants resulted from low- and high-mental arithmetic tasks. The P600 ERP amplitude and latency were significantly lower and higher, respectively, in the high-MWL than in the low-MWL tasks. This result is consistent with that of previous studies (Baetens et al., 2011; Mun et al., 2012, 2017; Park

TABLE 1 | Comparison by paired *t*-test of the P600 amplitude between low- and high-MWL conditions.

	Site	Condition	N	Mean	SD	t	p	Effect size	
								Hedges' g	95% CI
ERP_T	*F3*	Low-MWL	14	0.03	0.09	2.865	0.0133	−1.046	−1.836 ~ −0.256
		High-MWL	14	−0.05	0.06		(>0.05)		
	P4	Low-MWL	14	0.05	0.09	2.784	0.0155	−1.149	−1.948 ~ −0.349
		High-MWL	14	−0.03	0.04		(>0.05)		
	O1	Low-MWL	14	0.04	0.09	2.556	0.0239	−1.043	−1.833 ~ −0.254
		High-MWL	14	−0.03	0.03		(>0.05)		
	O2	Low-MWL	14	0.07	0.10	3.453	0.0043	−1.444	−2.276 ~ −0.613
		High-MWL	14	−0.04	0.04		(>0.05)		
ERP_{HEP}	*O1*	Low-MWL	14	0.07	0.10	2.658	0.0197	−1.012	−1.799 ~ −0.225
		High-MWL	14	−0.01	0.05		(>0.05)		
$ERP_{A\text{-}HEP}$	*F3*	Low-MWL	14	0.06	0.05	5.505	0.0001	−1.988	−2.893 ~ −1.082
		High-MWL	14	−0.03	0.04		(>0.001)		
	F4	Low-MWL	14	0.04	0.03	4.787	0.0004	−1.265	−2.076 ~ −0.453
		High-MWL	14	−0.02	0.06		(>0.001)		
	P4	Low-MWL	14	0.04	0.05	4.383	0.0007	−1.449	−2.281 ~ −0.616
		High-MWL	14	−0.04	0.06		(>0.001)		
	O1	Low-MWL	14	0.07	0.10	3.818	0.0021	−1.391	−2.217 ~ −0.566
		High-MWL	14	−0.04	0.05		(>0.001)		
	O2	Low-MWL	14	0.07	0.08	3.298	0.0058	−1.499	−2.337 ~ −0.661
		High-MWL	14	−0.03	0.05		(>0.05)		

Results are not shown when the p value is greater than 0.05.

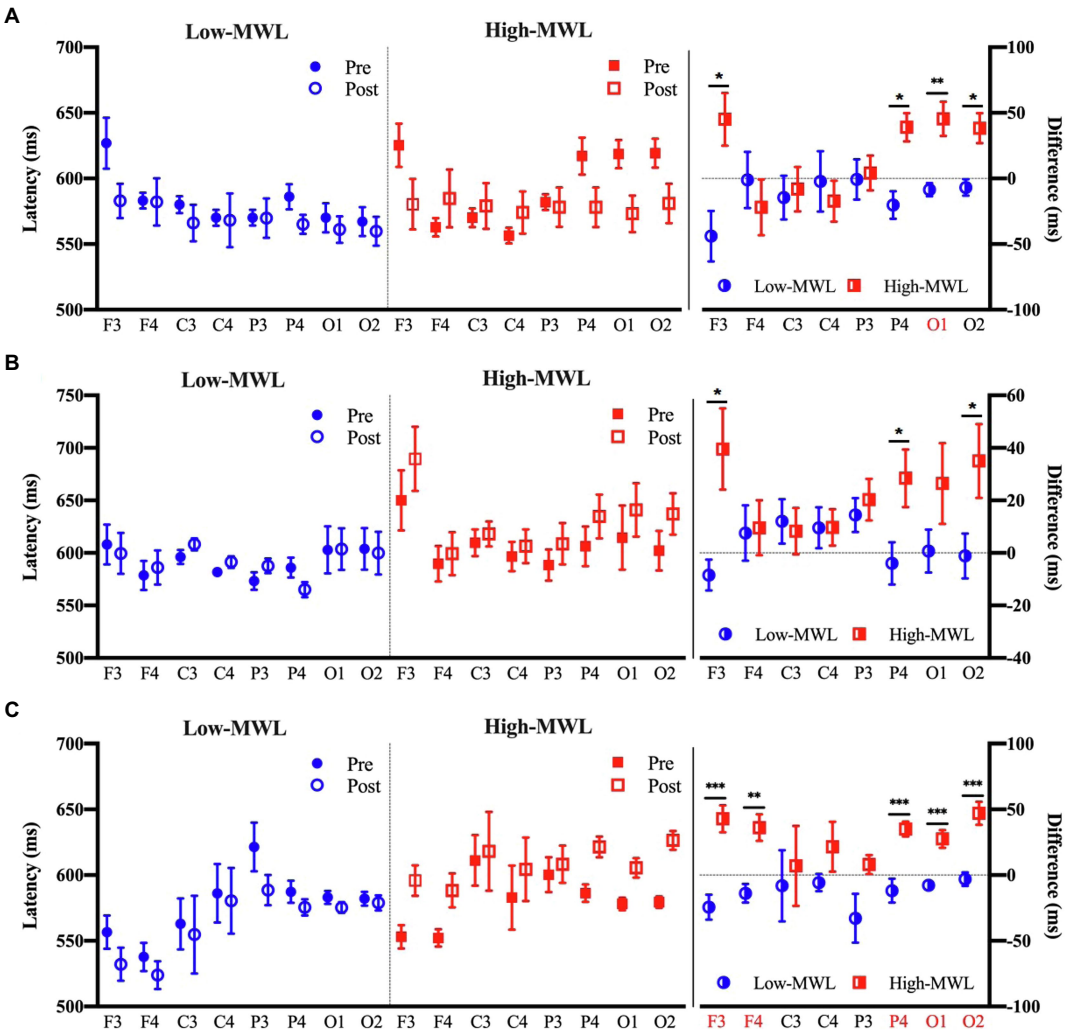

FIGURE 7 | Comparison of the P600 latency in ERP between the low- and high-MWL conditions. **(A)** ERP_T condition. **(B)** ERP_{HEP} condition. **(C)** $ERP_{A\text{-}HEP}$ condition (paired t-test; $^*p < 0.05$, $^{**}p < 0.0031$, and $^{***}p < 0.001$).

et al., 2015, 2019). Late positive potentials (LPPs), such as the P600 and P700 components reflect a high-level MWL required to process difficult tasks (Li et al., 2008; Pastor et al., 2008; Mun et al., 2012, 2014). LPPs are seen as a delayed P300 component and are related to high-level MWL (Friederici et al., 1993; Mun et al., 2012). Reduced LPP amplitudes reflect a decrease in cognitive and neural resources caused by MWL, impairing the attentional allocation mechanisms (Kato et al., 2009; Mun et al., 2012, 2014).

The analysis revealed significant differences in the P600 amplitude and latency among the ERP_T, ERP_{HEP}, and $ERP_{A\text{-}HEP}$ conditions. The number of features (i.e., P600 amplitude and latency in each brain region) with significant differences ($p < 0.0031$) between low- and high-MWL was greater in the $ERP_{A\text{-}HEP}$ (10 significant features) than in the other conditions (ERP_T, one significant feature; ERP_{HEP}, no significant feature). The P600 amplitude and latency in the $ERP_{A\text{-}HEP}$ condition revealed a stronger correlation with SMEQ scores than the other two conditions. These results suggest that the pattern of P600 amplitude and latency in the $ERP_{A\text{-}HEP}$ condition, not affected by the heartbeat, revealed a clearer response to ERP stimuli, without interference from other evoked potentials, compared with other conditions that were affected by the heartbeat.

The vagus nervous system in the heart continuously communicates with the brain *via* efferent and afferent pathways. Neuronal connectivity causes an evoked potential (i.e., alpha rhythms) in brain waves, known as the HEP (Schandry and Montoya, 1996; McCraty et al., 2009; Park et al., 2015). Many previous studies have used the HEP phenomenon in various research fields, such as attention (Petzschner et al., 2019), anxiety (Judah et al., 2018; Pang et al., 2019), mental workload (Park et al., 2015), emotion (Couto et al., 2015), sleep (Lechinger et al., 2015), and medicine (Leopold and Schandry, 2001; Perogamvros et al., 2019; Flasbeck et al., 2020).

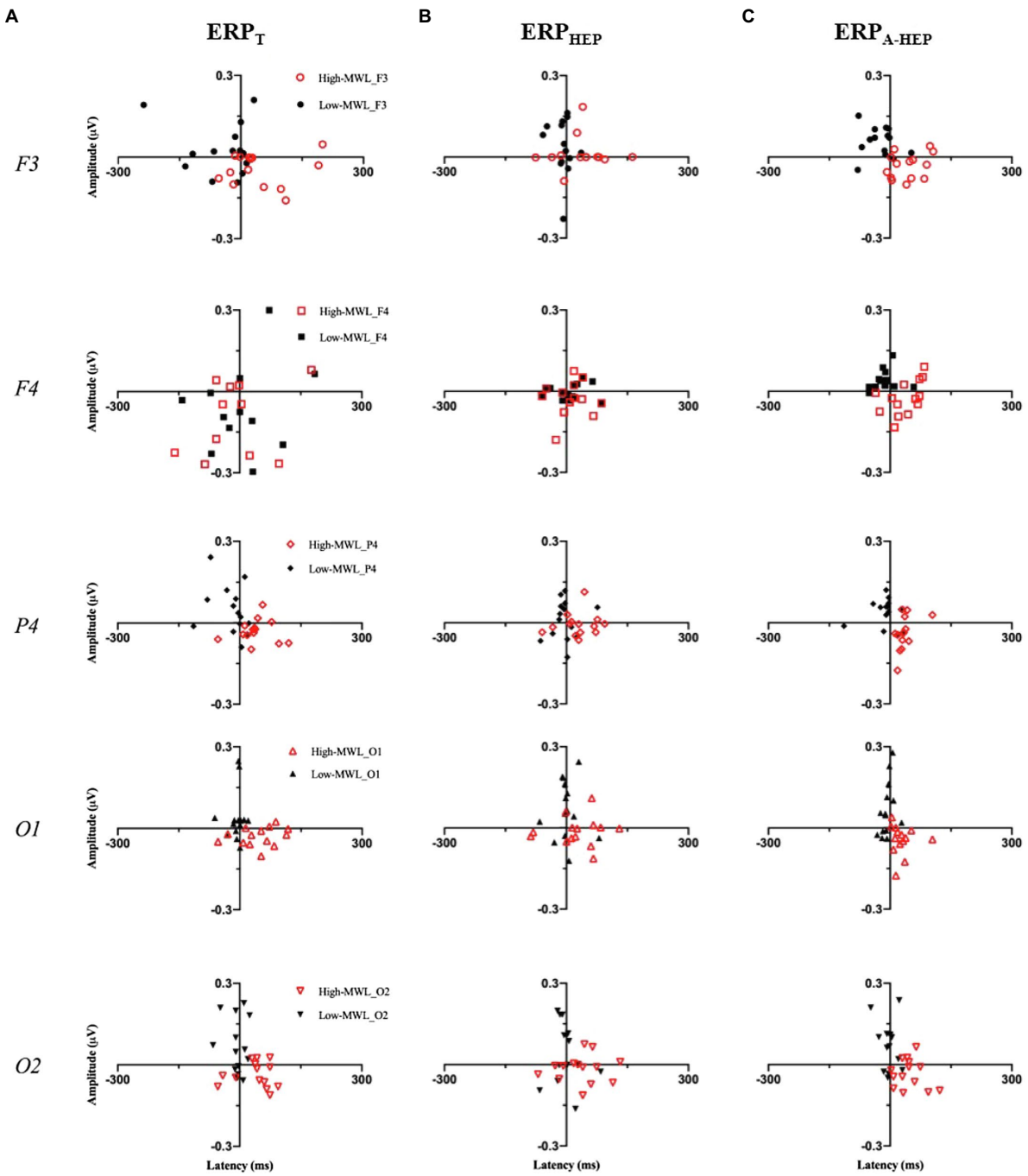

FIGURE 8 | Scatterplots of P600 amplitude (X axis) and latency (Y axis) between low- and high-MWL for the ERP$_T$, ERP$_{HEP}$, and ERP$_{A-HEP}$ conditions.

We divided the ERP trials into three conditions according to whether the heartbeat had an effect on the evoked potential on EEG oscillations. The condition related to the heartbeat (ERP$_{HEP}$) resulted in a change in the P600 amplitude for the target due to the overlap with the evoked potentials induced by the heartbeat, which also led to variations in latency. The phenomenon whereby the evoked potentials caused by the heartbeat affect EEG oscillations has been reported in many previous studies (Wölk et al., 1989; Schandry and Montoya, 1996; McCraty et al., 2009; Park et al., 2015, 2019; Villena-Gonzalez et al., 2017; Perogamvros et al., 2019). Our argument regarding the effect of cardiac activity on the P600 in ERP is supported by the high statistical significance and correlation coefficient we observed in the ERP$_{A-HEP}$ condition compared with the ERP$_{HEP}$ one.

This study also assessed the classification performance using P600 features between low- and high-MWL for the

TABLE 2 | Comparison by paired t-test of the P600 latency the low- and high-MWL conditions.

	Site	Condition	N	Mean	SD	t	p	Effect Size	
								Hedges' g	95% CI
ERP_T	F_3	Low-MWL	14	−44.00	72.29	−3.023	0.0098 (>0.05)	1.208	0.403 ~ 2.014
		High-MWL	14	45.00	75.02				
	P_4	Low-MWL	14	−20.29	39.21	−3.284	0.0059 (>0.05)	1.493	0.655 ~ 2.331
		High-MWL	14	39.00	40.20				
	O_1	Low-MWL	14	−8.57	18.89	−3.935	0.0017 (>0.0031)	1.462	0.628 ~ 2.296
		High-MWL	14	45.43	48.71				
	O_2	Low-MWL	14	−6.86	23.60	−3.067	0.0090 (>0.05)	0.750	−0.016 ~ 1.516
		High-MWL	14	38.29	42.81				
ERP_{HEP}	F_3	Low-MWL	14	−8.43	21.95	−2.425	0.0306 (>0.05)	1.098	0.303 ~ 1.893
		High-MWL	14	39.57	57.79				
	P_4	Low-MWL	14	−4.00	30.09	−3.500	0.0039 (>0.05)	0.903	0.125 ~ 1.680
		High-MWL	14	28.43	40.93				
	O_2	Low-MWL	14	−1.14	31.95	−2.423	0.0308 (>0.05)	0.830	0.058 ~ 1.602
		High-MWL	14	35.00	52.62				
ERP_{A-HEP}	F_3	Low-MWL	14	−24.43	35.54	−4.348	0.0008 (>0.001)	1.823	0.942 ~ 2.704
		High-MWL	14	42.86	38.24				
	F_4	Low-MWL	14	−13.86	26.57	−3.833	0.0021 (>0.001)	1.533	0.690 ~ 2.375
		High-MWL	14	36.14	37.71				
	P_4	Low-MWL	14	−11.86	33.92	−4.283	0.0009 (>0.001)	1.662	0.803 ~ 2.521
		High-MWL	14	35.14	21.18				
	O_1	Low-MWL	14	−7.71	14.42	−5.115	0.0002 (>0.001)	1.714	0.848 ~ 2.581
		High-MWL	14	27.57	25.28				
	O_2	Low-MWL	14	−3.14	19.25	−5.526	0.0001 (>0.001)	1.871	0.983 ~ 2.760
		High-MWL	14	47.00	32.64				

Results are not represented when the value of p is greater than 0.05.

TABLE 3 | Results of the classification by RBF-SVM (10-fold cross-validation) with ERP_T, ERP_{HEP}, and ERP_{A-HEP} epochs ($n = 24$).

	Condition	Accuracy (%)	Sensitivity (%)	Specificity (%)	AUC
RBF-SVM (10-fold cross-validation)	ERP_T	85.7	85.7	85.7	0.93
	ERP_{HEP}	71.4	64.3	78.6	0.76
	ERP_{A-HEP}	100	100	100	1

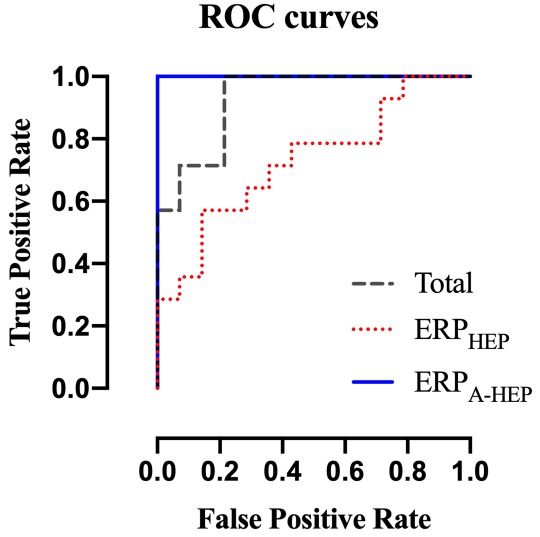

FIGURE 9 | Receiver operating characteristics curves for ERP_T, ERP_{HEP}, and ERP_{A-HEP} according to the RBF-SVM classifier.

three conditions (ERP_T, ERP_{HEP}, and ERP_{A-HEP}), finding that the accuracy in the ERP_{A-HEP} condition increased by 14.3 and 28.6% compared to the ERP_T and ERP_{HEP} conditions, respectively. No previous studies have tried to detect the pure ERP components and improve the MWL classification performance based on ERP while considering the effect of the evoked potentials (i.e., HEP) caused by the cardiac activity (i.e., heartbeat). However, some studies have attempted to improve the accuracy of brain activity classification using approaches similar to that used in our studies. Brain oscillations can be affected by various mental states, such as fatigue, stress, emotion, and mental workload. Changes in mental state can affect EEG oscillations and interfere with the targeting response. This leads to a decrease in classification performance (Lorenz et al., 2014; Myrden and Chau, 2017; Zhang et al., 2020; Zheng et al., 2020). A previous study compared brain-computer interface (BCI) performance under low- and high-stress conditions and reported that the use of steady-state visually evoked

TABLE 4 | Partial correlation analysis between ERP features and SMEQ scores for each condition (ERP_T, ERP_{HEP}, and $ERP_{A\text{-}HEP}$).

		F_3	F_4	C_3	C_4	P_3	P_4	O_1	O_2
P600 Latency in ERP									
SMEQ score	ERP_T	−0.473 ($p > 0.05$)	–	–	–	–	−0.432 ($p > 0.05$)	−0.483 ($p > 0.05$)	−0.440 ($p > 0.05$)
	ERP_{HEP}	−0.440 ($p > 0.05$)	–	–	–	–	−0.493 ($p > 0.05$)	–	−0.419 ($p > 0.05$)
	$ERP_{A\text{-}HEP}$	−0.401 ($p > 0.05$)	–	–	–	–	−0.474 ($p > 0.05$)	−0.496 ($p > 0.05$)	−0.586 ($p > 0.01$)
P600 Amplitude in ERP									
SMEQ score	ERP_T	0.461 ($p > 0.05$)	–	–	–	–	0.414 ($p > 0.05$)	–	0.497 ($p > 0.01$)
	ERP_{HEP}	–	–	–	–	–	0.440 ($p > 0.05$)	–	–
	$ERP_{A\text{-}HEP}$	**0.885 (p > 0.001)**	**0.783 (p > 0.001)**	–	–	0.410 ($p > 0.05$)	**0.612 (p > 0.001)**	0.600 ($p > 0.01$)	**0.632 (p > 0.001)**

Results are not represented when the p value is greater than 0.05 (light gray, $p < 0.05$; dark gray, $p < 0.01$; and bold black, $p < 0.001$).

potential-based BCI under stress leads to a decrease in accuracy and an increase in the required concentration and the resulting fatigue (Zhang et al., 2020). Another study revealed an increase in BCI performance considering the mental focus and lost-in-thought states of participants (Ko et al., 2020). In addition, many studies have sought to improve performance by considering various mental states (Myrden and Chau, 2017; Acı et al., 2019; Zhang et al., 2019; Foong et al., 2020), which is highly relevant to our research approach. Therefore, we believe that the evoked potential caused by the heartbeat must be considered to improve the detection of the evoked potential components in ERPs and that our approach can contribute to the measurement of accurate ERP responses and improve the performance in classifying MWL.

However, this study has several limitations. (1) Only the effects of the HEP on the P600 element of ERP were confirmed, and other components, such as P300, N400, and P200, were not considered. Since our approach selected trials suitable for each ERP element based on the heartbeat, other ERP components may behave similarly to the P600 component, although this needs to be confirmed through further research based on various task environments. (2) Our study sought to confirm a significant difference in MWL classification performance by ERP trials according to whether or not the HEP was affected. In future research, we will conduct a paradigm study that controls the timing of stimuli in ERP tasks based on heartbeats, or a method of training by classifying ERP trials based on whether they are affected by HEP.

In conclusion, this study confirmed that the performance in the classification of MWL states in the $ERP_{A\text{-}HEP}$ condition was significantly superior to that of the ERP_T and the ERP_{HEP} conditions. We interpret these results as showing that the pattern of ERPs in the ERP_T and the ERP_{HEP} conditions, which were affected by the heartbeat, resulted from the overlap of the HEP and the ERPs. On the other hand, the pattern of ERPs in the $ERP_{A\text{-}HEP}$ condition, which was not affected by the heartbeat, showed a clear or pure response to ERP stimuli without the effect of other evoked potentials. Therefore, in ERP studies, the effect of HEPs on ERP patterns (i.e., amplitude and latency in ERP components) needs to be considered in order to obtain a clear and pure ERP response. This study used the P600 component to improve ERP-based MWL classification performance, but the same approach can be used in the application of ERPs to various fields, such as brain-computer interface, emotion recognition, language processing, working memory, and neurotherapy.

DATA AVAILABILITY STATEMENT

The data generated and analyzed in this study are available from the corresponding author upon reasonable request.

ETHICS STATEMENT

All experimental protocols were approved by the Sangmyung University Institutional Bioethics Review Board (SMUIBRB) in Seoul, South Korea (BE2019-46). The patients/participants provided their written informed consent to participate in this study.

AUTHOR CONTRIBUTIONS

SP: conceptualization, methodology, data analysis, experiment, and writing – original draft. JH: investigation, visualization, data analysis, and experiment. LK: conceptualization, writing – review and editing, and supervision. All authors contributed to the article and approved the submitted version.

FUNDING

This work was partly supported by the Institute of Information & Communications Technology Planning & Evaluation (IITP) grant funded by the Korean Government (MSIT) (No. 2017-0-00432), for the development of a non-invasive integrated BCI SW platform to control home appliances and external devices by user's thoughts *via* AR/VR interface.

REFERENCES

Acı, É. İ., Kaya, M., and Mishchenko, Y. (2019). Distinguishing mental attention states of humans via an EEG-based passive BCI using machine learning methods. *Expert Syst. Appl.* 134, 153–166. doi: 10.1016/j.eswa.2019.05.057

Alomari, H. M., Samaha, A., and Alkamha, K. (2013). Automated classification of L/R hand movement EEG signals using advanced feature extraction and machine learning. *Int. J. Adv. Comput. Sci. Appl.* 4. doi: 10.14569/IJACSA.2013.040628

Baetens, K., Der Cruyssen, L. V., Achtziger, A., Vandekerckhove, M., and Van Overwalle, F. (2011). N400 and LPP in spontaneous trait inferences. *Brain Res.* 1418, 83–92. doi: 10.1016/j.brainres.2011.08.067

Boudewyn, M. A., Luck, S. J., Farrens, J. L., and Kappenman, E. S. (2018). How many trials does it take to get a significant ERP effect? It depends. *Psychophysiology* 55:e13049. doi: 10.1111/psyp.13049

Causse, M., Peysakhovich, V., Fabre, E. F. (2016). High working memory load impairs language processing during a simulated piloting task: An ERP and pupillometry study. *Front Hum Neurosci.* 10:240, doi: 10.3389/fnhum.2016.00240

Chen, X., Xu, X. Y., Liu, A. P., Lee, S., Chen, X., Zhang, X., et al. (2019). Removal of muscle artifacts from the EEG: A review and recommendations. *IEEE Sensors J.* 19, 5353–5368. doi: 10.1109/JSEN.2019.2906572

Coles, M.G., and Rugg, M.D. (1995). *Event-Related Brain Potentials: An Introduction*. Oxford: Oxford University Press.

Couto, B., Adolfi, F., Velasquez, M., Mesow, M., Feinstein, J., Canales-Johnson, A., et al. (2015). Heart evoked potential triggers brain responses to natural affective scenes: A preliminary study. *Auton. Neurosci.* 193, 132–137. doi: 10.1016/j.autneu.2015.06.006

Dai, C. X., Wang, J. J., Xie, J. L., Li, W. M., Gong, Y. S., and Li, Y. Q. (2019). Removal of ECG artifacts From EEG using an effective recursive least square notch filter. *IEEE Access* 7, 158872–158880. doi: 10.1109/ACCESS.2019.2949842

Dimigen, O. (2020). Optimizing the ICA-based removal of ocular EEG artifacts from free viewing experiments. *NeuroImage* 207:116117. doi: 10.1016/j.neuroimage.2019.116117

Dimond, S. J., and Beaumont, J. (1974). *Hemisphere Function in the Human Brain*. Hoboken: John Wiley & Sons.

Dunnett, C. W. (1955). A multiple comparison procedure for comparing several treatments with a control. *J. Am. Stat. Assoc.* 50, 1096–1121. doi: 10.1080/01621459.1955.10501294

Egambaram, A., Badruddin, N., Asirvadam, V. S., Begum, T., Fauvet, E., and Stolz, C. (2020). FastEMD-CCA algorithm for unsupervised and fast removal of eyeblink artifacts from electroencephalogram. *Biomed. Signal Process. Control* 57:101692. doi: 10.1016/j.bspc.2019.101692

Faul, F., Erdfelder, E., Lang, A. G., and Buchner, A. (2007). G*power 3: a flexible statistical power analysis program for the social, behavioral, and biomedical sciences. *Behav. Res. Methods* 39, 175–191. doi: 10.3758/BF03193146

Flasbeck, V., Popkirov, S., Ebert, A., and Brune, M. (2020). Altered interoception in patients with borderline personality disorder: a study using heartbeat-evoked potentials. *Borderline Personality Disord. Emotion Dysregulation* 7, 1–13. doi: 10.1186/s40479-020-00139-1

Foong, R., Ang, K. K., Quek, C., Guan, C., Phua, K. S., Kuah, C. W. K., et al. (2020). Assessment of the efficacy of EEG-based MI-BCI With visual feedback and EEG correlates of mental fatigue for upper-limb stroke rehabilitation. *I.E.E.E. Trans. Biomed. Eng.* 67, 786–795. doi: 10.1109/TBME.2019.2921198

Friederici, A. D., Pfeifer, E., and Hahne, A. (1993). Event-related brain potentials during natural speech processing: effects of semantic, morphological and syntactic violations. *Brain Res. Cogn. Brain Res.* 1, 183–192. doi: 10.1016/0926-6410(93)90026-2

Hamaneh, M. B., Chitravas, N., Kaiboriboon, K., Lhatoo, S. D., and Loparo, K. A. (2014). Automated removal of EKG artifact from EEG data using independent component analysis and continuous wavelet transformation. *I.E.E.E. Trans. Biomed. Eng.* 61, 1634–1641. doi: 10.1109/TBME.2013.2295173

Hedges, L. V., and Olkin, I. (2014). *Statistical Methods for Meta-Analysis*. London: Academic Press.

Janig, W. (1996). Neurobiology of visceral afferent neurons: neuroanatomy, functions, organ regulations and sensations. *Biol. Psychol.* 42, 29–51. doi: 10.1016/0301-0511(95)05145-7

Johnson, J. L., Slentz, C. A., Ross, L. M., Huffman, K. M., and Kraus, W. E. (2019). Ten-year legacy effects of three eight-month exercise training programs on Cardiometabolic health parameters. *Front. Physiol.* 10:452. doi: 10.3389/fphys.2019.00452

Jost, P., Cobb, S., and Hämmerle, I. (2019). Reality-based interaction affecting mental workload in virtual reality mental arithmetic training. *Behav. Inform. Technol.* 39, 1062–1078. doi: 10.1080/0144929X.2019.1641228

Judah, M. R., Shurkova, E. Y., Hager, N. M., White, E. J., Taylor, D. L., and Grant, D. M. (2018). The relationship between social anxiety and heartbeat evoked potential amplitude. *Biol. Psychol.* 139, 1–7. doi: 10.1016/j.biopsycho.2018.09.013

Kato, Y., Endo, H., and Kizuka, T. (2009). Mental fatigue and impaired response processes: event-related brain potentials in a Go/NoGo task. *Int. J. Psychophysiol.* 72, 204–211. doi: 10.1016/j.ijpsycho.2008.12.008

Katus, L., Mason, L., Milosavljevic, B., Mccann, S., Rozhko, M., Moore, S. E., et al. (2020). ERP markers are associated with neurodevelopmental outcomes in 1-5 month old infants in rural Africa and the UK. *NeuroImage* 210:116591. doi: 10.1016/j.neuroimage.2020.116591

Ko, L. W., Chikara, R. K., Lee, Y. C., and Lin, W. C. (2020). Exploration of user's mental state changes during performing brain-computer Interface. *Sensors* 20:3169. doi: 10.3390/s20113169

Lechinger, J., Heib, D. P., Gruber, W., Schabus, M., and Klimesch, W. (2015). Heartbeat-related EEG amplitude and phase modulations from wakefulness to deep sleep: interactions with sleep spindles and slow oscillations. *Psychophysiology* 52, 1441–1450. doi: 10.1111/psyp.12508

Leopold, C., and Schandry, R. (2001). The heartbeat-evoked brain potential in patients suffering from diabetic neuropathy and in healthy control persons. *Clin. Neurophysiol.* 112, 674–682. doi: 10.1016/S1388-2457(01)00480-1

Lew, E., Chavarriaga, R., Silvoni, S., and Millan Jdel, R. (2012). Detection of self-paced reaching movement intention from EEG signals. *Front. Neuroeng.* 5:13. doi: 10.3389/fneng.2012.00013

Li, H.-C. O., Seo, J., Kham, K., and Lee, S. (2008). "Measurement of 3D visual fatigue using event-related potential (ERP): 3D oddball paradigm", in *2008 3DTV Conference: The True Vision-Capture, Transmission and Display of 3D Video*: IEEE, Istanbul, Turkey, 213–216.

Li, F. L., Tao, Q., Peng, W. J., Zhang, T., Si, Y. J., Zhang, Y. S., et al. (2020). Inter-subject P300 variability relates to the efficiency of brain networks reconfigured from resting- to task-state: evidence from a simultaneous event-related EEG-fMRI study. *NeuroImage* 205:116285. doi: 10.1016/j.neuroimage.2019.116285

Liu, K. (1988). Measurement error and its impact on partial correlation and multiple linear regression analyses. *Am. J. Epidemiol.* 127, 864–874. doi: 10.1093/oxfordjournals.aje.a114870

Lorenz, R., Pascual, J., Blankertz, B., and Vidaurre, C. (2014). Towards a holistic assessment of the user experience with hybrid BCIs. *J. Neural Eng.* 11:035007. doi: 10.1088/1741-2560/11/3/035007

Luck, S. J. (2014). *An Introduction to the Event-Related Potential Technique* Cambridge: MIT Press.

Mccraty, R., Atkinson, M., Tomasino, D., and Bradley, R. T. (2009). The coherent heart heart-brain interactions, psychophysiological coherence, and the emergence of system-wide order. *Integral Rev.*, 10–115.

Mitchell, M. B., Shirk, S. D., McLaren, D. G., Dodd, J. S., Ezzati, A., Ally, B. A., et al. (2016). Recognition of faces and names: multimodal physiological correlates of memory and executive function. *Brain Imaging Behav.* 10, 408–423. doi: 10.1007/s11682-015-9420-6

Montoya, P., Schandry, R., and Müller, A. (1993). Heartbeat evoked potentials (HEP): topography and influence of cardiac awareness and focus of attention. *Electroencephalography Clin. Neurophysiol./Evoked Potentials Sect.* 88, 163–172. doi: 10.1016/0168-5597(93)90001-6

Mun, S., Kim, E. S., and Park, M. C. (2014). Effect of mental fatigue caused by mobile 3D viewing on selective attention: an ERP study. *Int. J. Psychophysiol.* 94, 373–381. doi: 10.1016/j.ijpsycho.2014.08.1389

Mun, S., Park, M. C., Park, S., and Whang, M. (2012). SSVEP and ERP measurement of cognitive fatigue caused by stereoscopic 3D. *Neurosci. Lett.* 525, 89–94. doi: 10.1016/j.neulet.2012.07.049

Mun, S., Whang, M., Park, S., and Park, M. C. (2017). Effects of mental workload on involuntary attention: A somatosensory ERP study. *Neuropsychologia* 106, 7–20. doi: 10.1016/j.neuropsychologia.2017.08.021

Myrden, A., and Chau, T. (2017). A passive EEG-BCI for single-trial detection of changes in mental state. *IEEE Trans. Neural Syst. Rehabil. Eng.* 25, 345–356. doi: 10.1109/TNSRE.2016.2641956

Nieuwenhuys, R., Voogd, J., and Van Huijzen, C. (2007). *The Human Central Nervous System: A Synopsis and Atlas*. Berlin: Springer Science & Business Media.

Pang, J., Tang, X., Li, H., Hu, Q., Cui, H., Zhang, L., et al. (2019). Altered interoceptive processing in generalized anxiety disorder-A heartbeat-evoked potential research. *Front. Psych.* 10:616. doi: 10.3389/fpsyt.2019.00616

Park, S., Mun, S., Lee, D. W., and Whang, M. (2019). IR-camera-based measurements of 2D/3D cognitive fatigue in 2D/3D display system using task-evoked pupillary response. *Appl. Opt.* 58, 3467–3480. doi: 10.1364/AO.58.003467

Park, S., and Whang, M. (2018). Infrared camera-based non-contact measurement of brain activity From pupillary rhythms. *Front. Physiol.* 9:1400. doi: 10.3389/fphys.2018.01400

Park, S., Won, M. J., Lee, E. C., Mun, S., Park, M. C., and Whang, M. (2015). Evaluation of 3D cognitive fatigue using heart-brain synchronization. *Int. J. Psychophysiol.* 97, 120–130. doi: 10.1016/j.ijpsycho.2015.04.006

Park, S., Won, M. J., Mun, S., Lee, E. C., and Whang, M. (2014). Does visual fatigue from 3D displays affect autonomic regulation and heart rhythm? *Int. J. Psychophysiol.* 92, 42–48. doi: 10.1016/j.ijpsycho.2014.02.003

Pastor, M. C., Bradley, M. M., Low, A., Versace, F., Molto, J., and Lang, P. J. (2008). Affective picture perception: emotion, context, and the late positive potential. *Brain Res.* 1189, 145–151. doi: 10.1016/j.brainres.2007.10.072

Perogamvros, L., Park, H. D., Bayer, L., Perrault, A. A., Blanke, O., and Schwartz, S. (2019). Increased heartbeat-evoked potential during REM sleep in nightmare disorder. *Neuroimage Clin.* 22:101701. doi: 10.1016/j.nicl.2019.101701

Perrin, F., Pernier, J., Bertrand, O., and Echallier, J. F. (1989). Spherical splines for scalp potential and current density mapping. *Electroencephalogr. Clin. Neurophysiol.* 72, 184–187. doi: 10.1016/0013-4694(89)90180-6

Petzschner, F. H., Weber, L. A., Wellstein, K. V., Paolini, G., Do, C. T., and Stephan, K. E. (2019). Focus of attention modulates the heartbeat evoked potential. *NeuroImage* 186, 595–606. doi: 10.1016/j.neuroimage.2018.11.037

Rampone, G., Makin, A. D. J., Tatlidil, S., and Bertamini, M. (2019). Representation of symmetry in the extrastriate visual cortex from temporal integration of parts: An EEG/ERP study. *NeuroImage* 193, 214–230. doi: 10.1016/j.neuroimage.2019.03.007

Sauro, J., and Dumas, J. S. (2009). "Comparison of three one-question, post-task usability questionnaires", in *Proceedings of the SIGCHI Conference on Human Factors in Computing Systems*, Boston, MA, USA, 1599–1608.

Schandry, R., and Montoya, P. (1996). Event-related brain potentials and the processing of cardiac activity. *Biol. Psychol.* 42, 75–85. doi: 10.1016/0301-0511(95)05147-3

So, W. K. Y., Wong, S. W. H., Mak, J. N., and Chan, R. H. M. (2017). An evaluation of mental workload with frontal EEG. *PLoS One* 12:e0174949. doi: 10.1371/journal.pone.0174949

Uriguen, J. A., and Garcia-Zapirain, B. (2015). EEG artifact removal-state-of-the-art and guidelines. *J. Neural Eng.* 12:031001. doi: 10.1088/1741-2560/12/3/031001

Villena-Gonzalez, M., Moenne-Loccoz, C., Lagos, R. A., Alliende, L. M., Billeke, P., Aboitiz, F., et al. (2017). Attending to the heart is associated with posterior alpha band increase and a reduction in sensitivity to concurrent visual stimuli. *Psychophysiology* 54, 1483–1497. doi: 10.1111/psyp.12894

Wölk, C., Velden, M., Zimmermann, U., and Krug, S. (1989). The interrelation between phasic blood pressure and heart rate changes in the context of the "baroreceptor hypothesis". *J. Psychophysiol.* 3, 397–402.

Zhang, H. Y., Stevenson, C. E., Jung, T. P., and Ko, L. W. (2020). Stress-induced effects in resting EEG spectra predict the performance of SSVEP-based BCI. *IEEE Trans. Neural Syst. Rehabil. Eng.* 28, 1771–1780. doi: 10.1109/TNSRE.2020.3005771

Zhang, T., Zhang, X., Zhang, Y., Lu, Z., and Li, H. (2019). "Effects of user fatigue mental state on the facial-expression paradigm of BCI", in *2019 WRC Symposium on Advanced Robotics and Automation* ((WRC SARA): IEEE), Beijing, China, 394–400.

Zheng, X., Xu, G., Zhang, Y., Liang, R., Zhang, K., Du, Y., et al. (2020). Anti-fatigue performance in SSVEP-based visual acuity assessment: A comparison of six stimulus paradigms. *Front. Hum. Neurosci.* 14:301. doi: 10.3389/fnhum.2020.00301

Zou, L., Chen, X., Dang, G., Guo, Y., and Wang, Z. J. (2020). Removing muscle artifacts From EEG data via underdetermined joint blind source separation: A simulation study. *IEEE Trans. Circuits Syst. II Express Briefs* 67, 187–191. doi: 10.1109/TCSII.2019.2903648

Conflict of Interest: The authors declare that the research was conducted in the absence of any commercial or financial relationships that could be construed as a potential conflict of interest.

Publisher's Note: All claims expressed in this article are solely those of the authors and do not necessarily represent those of their affiliated organizations, or those of the publisher, the editors and the reviewers. Any product that may be evaluated in this article, or claim that may be made by its manufacturer, is not guaranteed or endorsed by the publisher.

frontiers in Physiology

BRIEF RESEARCH REPORT
published: 18 November 2021
doi: 10.3389/fphys.2021.689278

Cardiac Stroke Volume Index Is Associated With Early Neurological Improvement in Acute Ischemic Stroke Patients

Joseph Miller[1†], Farhan Chaudhry[2†], Sam Tirgari[1], Sean Calo[3], Ariel P. Walker[2], Richard Thompson[4], Bashar Nahab[5], Christopher Lewandowski[6] and Phillip Levy[2]*

[1] Department of Emergency Medicine and Internal Medicine, Henry Ford Hospital and Wayne State University, Detroit, MI, United States, [2] Department of Emergency Medicine and Integrative Biosciences Center, Wayne State University, Detroit, MI, United States, [3] Central Michigan University College of Medicine, Mount Pleasant, MI, United States, [4] Department of Anesthesiology, University of California, San Francisco, San Francisco, CA, United States, [5] Department of Radiology, Harvard Medical School, Cambridge, MA, United States, [6] Department of Emergency Medicine, Henry Ford Hospital and Wayne State University, Detroit, MI, United States

Early neurological improvement as assessed with the NIH stroke scale (NIHSS) at 24 h has been associated with improved long-term functional outcomes following acute ischemic stroke (AIS). Cardiac dysfunction is often present in AIS, but its association with outcomes is incompletely defined. We performed a pilot study to evaluate the association between non-invasively measured cardiac parameters and 24-h neurological improvement in prospectively enrolled patients with suspected AIS who presented within 12 h of symptom-onset and had an initial systolic blood pressure>140 mm Hg. Patients receiving thrombolytic therapy or mechanical thrombectomy were excluded. Non-invasive pulse contour analysis was used to measure mean arterial blood pressure (MAP), cardiac stroke volume index (cSVI), cardiac output (CO) and cardiac index (CI). Transcranial Doppler recorded mean middle cerebral artery flow velocity (MFV). We defined a decrease of 4 NIHSS points or NIHSS $\leq$ 1 at 24-h as neurological improvement. Of 75 suspected, 38 had confirmed AIS and did not receive reperfusion therapy. Of these, 7/38 (18.4%) had neurological improvement over 24 h. MAP was greater in those without improvement (108, IQR 96–123 mm Hg) vs. those with (89, IQR 73–104 mm Hg). cSVI, CO, and MFV were similar between those without and with improvement: 37.4 (IQR 30.9–47.7) vs. 44.7 (IQR 42.3–55.3) ml/m^2; 5.2 (IQR 4.2–6.6) vs. 5.3 (IQR 4.7–6.7) mL/min; and 39.9 (IQR 32.1–45.7) vs. 34.4 (IQR 27.1–49.2) cm/s, respectively. Multivariate analysis found MAP and cSVI as predictors for improvement (OR 0.93, 95%CI 0.85–0.98 and 1.14, 95%CI 1.03–1.31). In this pilot study, cSVI and MAP were associated with 24-h neurological improvement in AIS.

Keywords: ischemic stroke (IS), cardiac function, heart brain interaction, autonomic dysfunction, stroke outcome and recovery

OPEN ACCESS

Edited by:
Lilei Yu,
Wuhan University, China

Reviewed by:
Emilio Vanoli,
University of Pavia, Italy
Dorota Zyśko,
Wrocław Medical University, Poland

****Correspondence:***
Joseph Miller
Jmiller6@hfhs.org

†These authors share first authorship

Specialty section:
This article was submitted to Autonomic Neuroscience, a section of the journal Frontiers in Physiology

Received: *31 March 2021*
Accepted: *26 October 2021*
Published: *18 November 2021*

Citation:
Miller J, Chaudhry F, Tirgari S, Calo S, Walker AP, Thompson R, Nahab B, Lewandowski C and Levy P (2021) Cardiac Stroke Volume Index Is Associated With Early Neurological Improvement in Acute Ischemic Stroke Patients. Front. Physiol. 12:689278. doi: 10.3389/fphys.2021.689278

Abbreviations: NIHSS,National Institute of Health Stroke Scale; AIS, acute ischemic stroke; ED, emergency department; MAP, mean arterial pressure; CO, cardiac output; CI, cardiac index; cSVI, cardiac stroke volume index; TCD, transcranial Doppler; MCA, middle cerebral artery; MFV, mean flow velocity; IV, intravenous; CAD/PVD, coronary artery or peripheral vascular disease; HRV, heart rate variability; TIA, transient ischemic attack.

INTRODUCTION

Acute ischemic stroke (AIS) is the leading cause of long-term disability and results in worsening functional independence long after initial stroke (Dhamoon et al., 2009; Virani et al., 2020). Twenty-hour neurological improvement, as assessed by the National Institute of Health Stroke Scale (NIHSS), is associated with good long-term functional outcomes following acute stroke (Takagi et al., 2014; Rangaraju et al., 2016; Wouters et al., 2018). Rapid reperfusion strategies have been implemented to rapidly restore blood flow to the penumbra resulting in improved outcomes; however, many patients do not have access to these strategies and/or do not qualify for reperfusion (Bhaskar et al., 2018). Therefore, identification of modifiable factors associated with 24-h neurological improvement in non-reperfused patients could inform their management and prognosis.

AIS diminishes the cerebrovascular autoregulation, thus penumbra blood flow becomes directly dependent on cardiac function (Tranmer et al., 1992). Likewise, AIS can result in sympathetic activation and impaired parasympathetic tone resulting in stroke-induced heart injury, characterized by LV dysfunction (Wrigley et al., 2017; Sposato et al., 2020). Therefore, identifying pertinent aspects of cardiac function associated with 24-h neurological improvement following AIS may have prognostic and acute management implications. Given the acuity associated with AIS management, measurements of cardiac function need to be quick and non-invasive, especially if they are performed on arrival in the emergency department (ED). For this brief research report, we conducted a pilot prospective observational study of AIS patients using a non-invasive monitoring device to test the feasibility of rapidly assessing various cardiac parameters in association with 24-h neurological outcomes.

MATERIALS AND METHODS

Enrollment

We conducted this prospective, observational study of AIS patients at a large, urban, ED, which is part of a comprehensive stroke hospital, Henry Ford Hospital, from July 2014 through September 2016. The study was approved by the hospital's IRB and registered at ClinicalTrials.gov (NCT02056821). We enrolled patients 18–90 years old with suspected AIS presenting within 12-h of symptom onset and with a systolic blood pressure>140 mmHg. AIS was confirmed if symptoms lasted more than 24-h or less than 24 h with ischemic lesion on diffusion-weighted imaging. Exclusion criteria included baseline modified Rankin Scale>3, pregnancy, intracranial hemorrhage on computed tomography, treatment with thrombolytic or mechanical thrombectomy, advanced directive for comfort care/hospice, or requiring endotracheal intubation.

Data Collection

Trained investigators obtained consent and documented baseline demographic and clinical characteristics including age, sex, and past medical history. Localization of stroke was divided into lacunar vs. non-lacunar stroke. Patient treatment with intravenous (IV) fluids and IV antihypertensive were also recorded. NIHSS was documented upon arrival by the stroke neurology team and was then confirmed by an investigator prior to enrollment.

Hemodynamic

Hemodynamic variables were measured with the clinically validated (Nexfin device, Edwards Lifescience, Irvine, CA) (Broch et al., 2012; Martina et al., 2012). This novel non-invasive monitor uses pulse-contour analysis to determine multiple hemodynamic parameters including mean arterial blood pressure (MAP), cardiac stroke volume index (cSVI), cardiac output (CO), and cardiac index (CI). Upon enrollment, a member of the research team placed the device on a non-paretic upper extremity to record beat-to-beat hemodynamic data for 4 h. A trained technician also performed transcranial Doppler imaging (TCD) on all patients looking for middle cerebral artery (MCA) mean flow velocity (MFV) on the affected-side. We averaged all TCD and hemodynamic values over 5-min periods.

Primary Outcome

NIHSS was calculated on arrival and after 24-h. Neurological improvement was defined as a decrease of 4 or more points on the NIHSS or a score equal to or less than one at 24-h (improvement) (National Institute of Neurological Disorders and Stroke rt-Pa Stroke Study Group, 1995).

Statistical Analysis

We reported continuous variables as median with interquartile range (IQR) and binomial variables as counts with percentages (%). Wilcoxon-Mann Whitney test and Fisher's-exact test was performed to compare continuous and categorical variables, respectively, between improvement vs. no improvement. We used a univariate logistic regression model on all identified variables assessing association with 24-h neurologic improvement. We then performed a multivariate logistic regression model to determine which variables were independently associated with 24-h neurologic improvement. Variables were selected using a stepwise logistic regression minimizing the Akaike-information-criterion. We used McFadden pseudo-R^2 to assess the model by quantifying the proportion of the total variability on the outcome from the variables (Louapre et al., 2020). Regression models used 100-iterations maximum to reach convergence. Results were reported as odds ratios (ORs) with 95% confidence intervals (CI). A 2-sided P-value < 0.05 was considered statistically significant. Analysis was completed with R-version 3.6.3.

RESULTS

Patient Enrollment

Seventy five patients met enrollment criteria with suspected AIS, but only 55 were confirmed stroke. We were unable to obtain hemodynamic measurements on 7 patients due to inadequate recording by the device, and 10 patients received thrombolytic

therapy and were also removed, resulting in 38 patients for further analysis.

Baseline Characteristics

7/38 (18.4%) patients showed signs of 24-h neurologic improvement (**Table 1**). There was no significant difference in age, sex, African American race, body mass index (BMI), history of hypertension, coronary artery or peripheral vascular disease (CAD/PVD), diabetes mellitus, transient ischemic attack (TIA)/stroke, anticoagulation use or smoking were noted between those with or without improvement.

Clinical Presentation and Management

Baseline NIHSS was 5 (4–8) and was numerically higher in improved (7[5–11]) vs. unimproved patients (5[4–7]), but this difference was not statistically significant (P = 0.746). Four (57.1%) patients with neurological improvement vs. 12 (38.7%) patients without neurological improvement had lacunar strokes (p = 0.425). The rate of administration of IV-fluids and IV-antihypertensives in the ED were similar between patients that had or did not have neurological improvement.

Hemodynamic Characteristics

MAP was significantly greater in those who did not improve compared to those that did improve. cSVI trended higher in those that improved vs. those that did not. CO, CI, MFV, and HR were similar between the no improvement vs. improvement group. Only cSVI statistically correlated with 24-h NIHSS change from baseline (**Figure 1**) demonstrating that a higher cSVI correlated with a greater reduction in NIHSS from baseline (R = -0.33, P = 0.041).

Logistic Regression Analysis

Only MAP and cSVI were statistically significant predictors for 24-h neurological improvement on univariate analysis (OR 0.944; 95% CI 0.877–0.989, P = 0.0328, and OR 1.1; 95% CI 1.01–1.22, P = 0.0468, **Table 1A** and **Figure 2A**). Step-wise logistic regression retained African American race, MAP and cSVI as variables for multivariate regression. Lower MAP and higher cSVI retained a statistically significant association with 24-h neurological improvement (OR 0.925; 95% CI 0.851–0.981, P = 0.0248 and OR 1.14; 95% CI 1.03–1.31, P = 0.0228). However, African American race did not reach statistical significance (OR

TABLE 1 | Patient demographic, clinical, and hemodynamic data with univariate and multivariate results.

(A) Univariate	All (n = 38)	No Improvement (n = 31)	Improvement (n = 7)	OR	95%CI	P-value
Patient characteristics						
Age in years (IQR)	66.5 (57–73)	67 (58–73.5)	63 (52–70.5)	0.979	0.916–1.05	0.524
Male sex (%)	17/38 (44.7)	14/31 (45.2)	3/7 (42.9)	0.911	0.157–4.81	0.911
African American (%)	28/38 (73.7)	22/31 (71.0)	6/7 (85.7)	0.407	0.0200–2.89	0.435
BMI, kg/m^2 (IQR)	28.1 (23.9–31.0)	28.5 (23.4–33.4)	27.4 (26.6–29.3)	0.976	0.844–1.12	0.735
Past medical history						
Hypertension (%)	32/38 (84.2)	26/31 (83.9)	6/7 (85.7)	1.15	0.146–24.2	0.904
CAD/PVD (%)	7/38 (18.4)	6/31 (19.4)	1/7 (14.3)	0.694	0.0333–5.26	0.756
Diabetes Mellitus (%)	16/38 (42.1)	13/31 (41.9)	3/7 (42.9)	1.04	0.179–5.51	0.964
Previous TIA/Stroke (%)	11/38 (28.9)	10/31 (32.2)	1/7 (14.3)	0.350	0.0170–2.45	0.36
On anticoagulation (%)	16/38 (42.1)	13/31 (41.9)	3/7 (42.9)	1.04	0.179–5.51	0.964
Smoker (%)	14/38 (36.8)	11/31 (35.5)	3/7 (42.9)	1.36	0.233–7.32	0.716
Clinical presentation						
NIHSS (IQR)	5 (4.00–7.75)	5 (4–7)	7 (3.5–11)	1.05	0.846–1.25	0.637
Lacunar localization (%)	16/38 (42.1)	12/31 (38.7)	4/7 (57.1)	2.11	0.399–12.4	0.378
IV-fluids given (%)	24/38 (63.2)	20/31 (64.5)	4/7 (57.1)	0.733	0.137–4.29	0.716
IV-antihypertensives given (%)	6/38 (15.8)	5/31 (16.1)	1/7 (14.2)	0.867	0.0410–6.86	0.904
Hemodynamic characteristics						
Heart rate, BPM (IQR)	77.5 (68–87.25)	78 (69.8–88.5)	62 (46.5–70.8)	0.970	0.918–1.02	0.219
Mean arterial blood pressure, mmHg (IQR)	105 (91.5–122.3)	108 (96.2–123)	89.1 (73.0–104)	0.944	0.887–0.989	0.0328*
Cardiac output, mL/min (IQR)	5.27 (4.29–6.67)	5.24 (4.19–6.62)	5.3 (4.7–6.73)	1.15	0.721–1.83	0.542
Cardiac stroke volume index, mL/m^2 (IQR)	39.6 (31.5–48.4)	37.4 (30.9–47.7)	44.7 (42.3–55.3)	1.10	1.01–1.22	0.0468*
MCA mean flow velocity, cm/s (IQR)	38.4 (30.6–46.7)	39.9 (32.1–45.7)	34.4 (27.1–49.2)	0.983	0.909–1.05	0.617
Cardiac index L/min/m^2 (IQR)	2.83 (2.36–3.26)	2.79 (2.34–3.25)	2.92 (2.88–3.27)	1.85	0.706–5.38	0.211
(B) Multivariate						
African American				0.093	0.002–1.15	0.112
Stroke Volume Index				1.14	1.03–1.31	0.0228*
Mean arterial pressure				0.925	0.851–0.981	0.0248*

*Table shows patient demographic, clinical, and hemodynamic data for each variable. Continuous variables expressed as median (Interquartile range, IQR). Categorical variables expressed as count (percent,%). Table separated by **(A)** univariate and **(B)** multivariate logistic regression results expressed as odds ratio (OR) and 95% CI with P-values. *$P < 0.05$. $^{\&}P < 0.05$ assessed by group comparisons.*

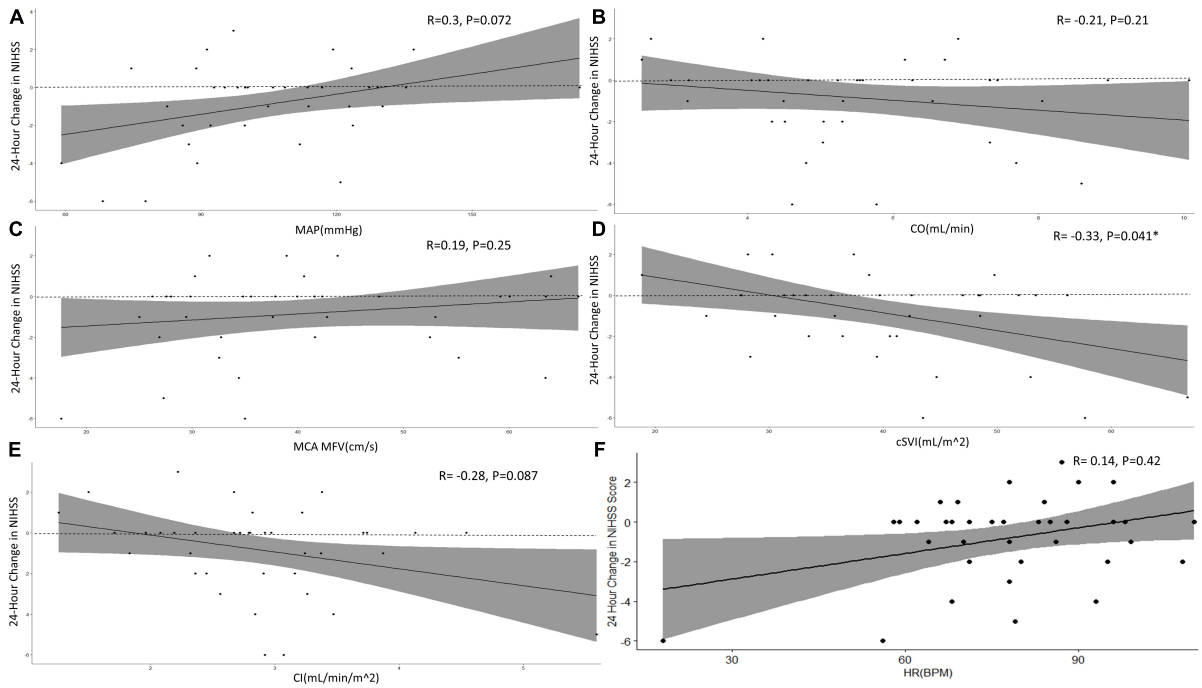

FIGURE 1 | Correlations between hemodynamic measurements with 24-h change in NIHSS score. Figure shows Spearman-Rank correlations between hemodynamic parameters, **(A)** MAP, **(B)** CO, **(C)** MFV, **(D)** cSVI, and **(E)** CI with total 24-h NIHSS score change from baseline (dashed line). Line graphs are shown with error shaded in and respective *R*- and *P*-values. $^*P < 0.05$.

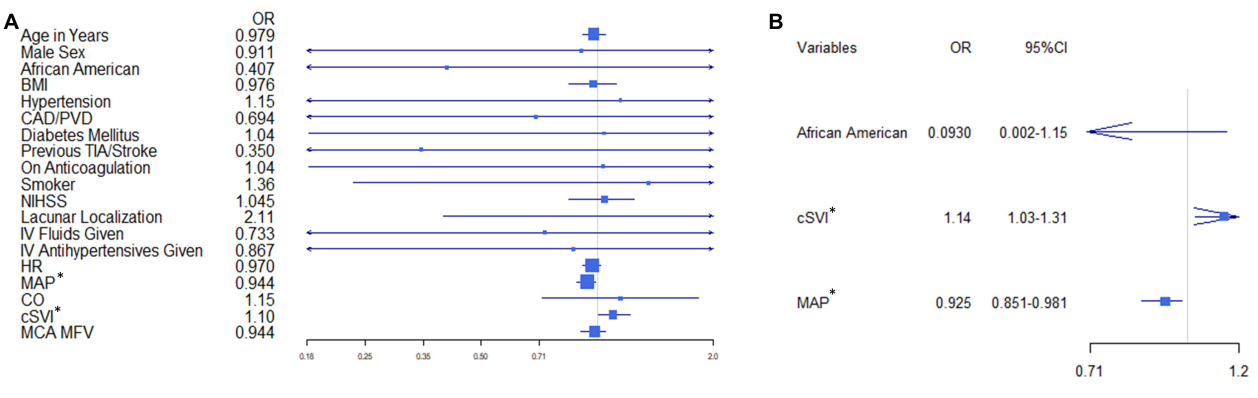

FIGURE 2 | Univariate and multivariate odds ratio (OR) forest plots. Shows the OR forest plot for each variable with confidence intervals for **(A)** univariate and **(B)** multivariate models. $^*P < 0.05$.

0.093; 95% CI 0.002–1.15, $P = 0.112$, **Table 1B** and **Figure 2B**). Pseudo-R^2 for African American race, MAP and cSVI were 0.0195, 0.168, 0.133, while cumulative pseudo-R^2 was 0.396.

DISCUSSION

Independent Predictors Associated With Neurologic Improvement

In this prospective pilot study, we showed preliminary evidence for cSVI as an independent predictor for 24-h neurological improvement following AIS, correlating well with a larger reduction in NIHSS from baseline. Our findings add to the growing evidence associating cardiac function with AIS outcomes (Battaglini et al., 2020). AIS is associated with cerebrovascular autoregulation irregularities leading to significant blood pressure fluctuations, abnormal cerebral perfusion pressures, suboptimal penumbral perfusion and thus poorer neurological recovery (Reinhard et al., 2012). We found that MAP was an independent predictor of worsening 24-h neurological function; however, MAP along with CO and CI did not show a linear correlation with 24-h NIHSS change from baseline. Our findings corroborate with other studies, which have shown a lack of linear correlation between MAP and cerebral perfusion or post-AIS outcomes

(Leonardi-Bee et al., 2002; Fuhrer et al., 2017; Rasmussen et al., 2020). Even though relatively lower BP (140–179 mmHg systolic) is associated with better neurologic outcomes post-stroke, the relationship between BP and has U shaped (Robinson et al., 1997; Leonardi-Bee et al., 2002). Extremely low BP (<120 mmHg systolic) post-stroke is rare, but at these ranges are in fact associated with worse outcomes (Leonardi-Bee et al., 2002). This is most likely caused by the failure of cerebral blood vessels to autoregulate efficiently to radical changes in BP. Cerebral perfusion pressure then becomes heavily dependent on parameters more associated with cardiac function (Tranmer et al., 1992).

Autonomic Instability in Acute Ischemic Stroke and Cardiac Function

Autonomic imbalances, specifically reduced heart rate variability (HRV) and poor baroreceptor sensitivity, result in worse neurological function after AIS (Korpelainen et al., 1996; Robinson et al., 2003; Colivicchi et al., 2004; Xiong et al., 2018). Overall autonomic dysfunction assessed by Ewing battery, independently predicted worse 3-month functional outcomes in AIS patients (OR 3.26; 95% CI 1.14–9.34, $P = 0.027$) (Xiong et al., 2018). AIS, especially of the insular cortex or other cerebral structures that control heart function, results in both systemic and local sympathetic catecholamine release and also inflammation which can cause cardiac injury and dysfunction (Sposato et al., 2020). This in turn could result in worse cerebral perfusion to the penumbra leading to poorer neurological recovery. Therefore, it has been theorized that maintaining adequate cardiac function following AIS could improve neurological function (Fuhrer et al., 2017). Unfortunately, given the multifactorial effects on cardiac function in the setting of AIS, it is unknown as to which cardiac function parameter would be an adequate predictor for neurological recovery following AIS. To further complicate the issue, various hemodynamic variables do not respond to one another as they would under normal physiological conditions (Fuhrer et al., 2016).

Small preliminary studies did show a correlation between CO and cerebral blood flow in cerebral ischemic areas, but its role on neurological improvement has not been studied (Tranmer et al., 1992; Fuhrer et al., 2017). In this pilot study, we failed to find a strong association between CO or CI and neurological function, and there was a minimal difference in CO and CI in AIS patients that improved vs. those that did not improved. It is known that CO variability greatly increases following unopposed sympathetic activity during cholinergic blockade (Toska and Eriksen, 1993). Consequently, utilizing an absolute CO value may not be the most reliable indicator for cardiac function following autonomic dysregulation in AIS, but increased CO variability may indicate autonomic dysregulation and worse neurological prognosis. This coincides with our findings as CO and CI had significantly wide confidence intervals, possibly precluding their significance. CO variability in the setting of AIS warrants further study.

One would expect then that since CO = stroke volume x HR, decreased HRV would be compensated by an increase in stroke volume variability to maintain a consistent CO. Contrarily, though, in the setting of cholinergic blockade, cardiac stroke volume variability remains the same and does not equilibrate to the significant decrease in HRV (Akselrod et al., 1985; Toska and Eriksen, 1993). This most likely explains why CO, and therefore CI, variability increases following cholinergic blockade as all the CO variability will now be derived from the stroke volume variability (Elstad et al., 2011). Stroke volume variability most likely is independent to HRV because cardiac contractility is regulated by a different autonomic neural mechanism (Liu et al., 2004). In cats, it was shown that there are distinct cardiac ganglia found within the fat pad on the surface of the left ventricle (Gatti et al., 1997). This ganglion will selectively mediate any negative inotropic effect from vagal innervation to the left ventricle, independent from vagal stimulation to the sinoatrial node, which controls rate. Furthermore, there are significantly more post-ganglionic sympathetic nerves at the atria than the ventricles implicating less potential sympathetic damage to the ventricles than sinoatrial node following AIS autonomic dysregulation (Balint et al., 2019). Consequently, multiple studies have shown that autonomic changes to HRV did not correspond to changes in cardiac stroke volume variability (Toska and Eriksen, 1993; Akselrod et al., 2000; Liu et al., 2004). Thus, cardiac stroke volume variability is more likely influenced by mechanical factors based on Frank-Sterling's Law, possibly making stroke volume a less variable cardiac parameter in the setting of autonomic dysregulation.

Cardiac Stroke Volume Index Dynamics Following Acute Ischemic Stroke

Our study did show a possible association between cSVI and 24-h neurological function following AIS. Importantly, cSVI was the only parameter which had a linear association with 24-h NIHSS change from baseline. Cardiac stroke volume decreases significantly in patients with autonomic dysregulation and is a strong predictor for MFV in response to blood volume changes (Timmers et al., 2002; Fu et al., 2010; Bronzwaer et al., 2014). Furthermore, related literature shows that reduced left ventricular ejection fraction (LVEF), which is directly proportional to stroke volume, has been associated with worse longer-term functional outcome, though not with short-term outcomes, after adjusting for covariates (Mathias et al., 2013; Milionis et al., 2013; Byun et al., 2014). These findings indicate that inotropic status plays an important role in AIS functional outcomes. Post-AIS CT perfusion studies have shown that patients with reduced LVEF had larger hypoperfusion AIS lesion volumes (Garcia-Esperon et al., 2020). Although the exact pathophysiology behind this is unknown, one strong possibility is that patients with reduced LVEF have less blood flow to collateral circulation resulting in poorer perfusion to the penumbra (Hong et al., 2019; Garcia-Esperon et al., 2020). Since the extent of penumbra perfusion is a powerful predictor of post-AIS clinical outcomes, it is expected then that LVEF/stroke volume status would be a predictor for post-AIS neurological outcomes.

cSVI is equal to stroke volume divided by the body surface area, which allows for a more standardized comparison of stroke

volume between patients regardless of body size. Therefore, cSVI maybe a more consistent and direct method to assess brain perfusion in the presence of autonomic dysregulation. More studies are required to investigate the mechanistic associations between cSVI and AIS.

LIMITATIONS AND CONCLUSION

A significant limitation to our preliminary study was the small sample size, in which the overall range of cardiac hemodynamic parameters and stroke severity was small. The study aimed to enroll patients as early as possible in their stroke care; however, given the challenges of confirming the diagnosis of stroke and requirements for informed consent, the final study cohort was smaller than anticipated and incorporated mild to moderate strokes. Furthermore, we did not assess long-term clinical outcomes, which carry greater weight than 24-h improvement. Nonetheless, 24-h improvement has been shown to strongly predict long term functional outcomes in AIS, thus 24-h improvement still holds significant prognostic importance (Takagi et al., 2014; Rangaraju et al., 2016). Additionally, we did not include patients who were treated with tPA, which is the mainstay treatment for AIS. However, more than 40% of patients present outside the treatment window for tPA and approximately 25% of tPA-eligible patients do not receive tPA due to late presentation or other contraindications. Therefore, there is still a significant clinical need to study AIS patients who do not receive tPA (Messé et al., 2016). Finally, our hemodynamic measurements only utilized non-invasive monitoring, without echocardiographic or invasive confirmation; still, the Nexfin device has shown in previous studies to provide reliable measurements of various hemodynamic parameters and is both quick to use and does not require extensive training before use (Broch et al., 2012; Martina et al., 2012). Given that the assessment and management of AIS must be quick and efficient, measurements of any pertinent clinical values must also be quick and efficient. Therefore, the Nexfin device has the potential to be readily utilized in the rapid assessment of AIS.

In this preliminary study assessing various hemodynamic parameters in AIS patients, we found cSVI and MAP to be associated with 24-h neurological improvement. Of which, cSVI was the only parameter which showed a linear association with NIHSS improvement from baseline. Therefore, cSVI is a unique parameter which warrants further study to determine its prognostic value and possible therapeutic implications.

DATA AVAILABILITY STATEMENT

The raw data supporting the conclusions of this article will be made available by the authors, without undue reservation.

ETHICS STATEMENT

The studies involving human participants were reviewed and approved by the Henry Ford Hospital International Review Board. The patients/participants provided their written informed consent to participate in this study.

AUTHOR CONTRIBUTIONS

All authors affirm that the manuscript complies with author instructions, including author requirements. JM, CL, and PL applied for funding and designed the study. SC, RT, BN, and JM performed to data collection and analysis. JM and FC contributed equally to the creation of this manuscript. All other authors contributed to different aspects of manuscript preparation. This manuscript has not been published elsewhere. IRB approval was obtained for the study.

FUNDING

This study was supported through an institutional physician-scientist grant (A20030, Henry Ford Hospital).

REFERENCES

Akselrod, S., Amitay, Y., Lang, R. M., Mor-Avi, V., and Keselbrener, L. (2000). Spectral analysis of left ventricular area variability as a tool to improve the understanding of cardiac autonomic control. *Physiol. Meas.* 21, 319–331. doi: 10.1088/0967-3334/21/2/311

Akselrod, S., Gordon, D., Madwed, J. B., Snidman, N. C., Shannon, D. C., and Cohen, R. J. (1985). Hemodynamic regulation: investigation by spectral analysis. *Am. J. Physiol.* 249(4 Pt 2), H867–H875.

Balint, B., Jaremek, V., Thorburn, V., Whitehead, S. N., and Sposato, L. A. (2019). Left atrial microvascular endothelial dysfunction, myocardial inflammation and fibrosis after selective insular cortex ischemic stroke. *Int. J. Cardiol.* 292, 148–155. doi: 10.1016/j.ijcard.2019.06.004

Battaglini, D., Robba, C., Lopes da Silva, A., Dos Santos Samary, C., Leme Silva, P., Dal Pizzol, F., et al. (2020). Brain-heart interaction after acute ischemic stroke. *Crit. Care.* 24:163.

Bhaskar, S., Stanwell, P., Cordato, D., Attia, J., and Levi, C. (2018). Reperfusion therapy in acute ischemic stroke: dawn of a new era? *BMC Neurol.* 18:8. doi: 10.1186/s12883-017-1007-y

Broch, O., Renner, J., Gruenewald, M., Meybohm, P., Schöttler, J., Caliebe, A., et al. (2012). A comparison of the Nexfin® and transcardiopulmonary thermodilution to estimate cardiac output during coronary artery surgery. *Anaesthesia* 67, 377–383. doi: 10.1111/j.1365-2044.2011.07018.x

Bronzwaer, A.-S. G. T., Stok, W. J., Westerhof, B. E., and van Lieshout, J. J. (2014). Arterial pressure variations as parameters of brain perfusion in response to central blood volume depletion and repletion. *Front. Physiol.* 5:157. doi: 10.3389/fphys.2014.00157

Byun, J.-I., Jung, K.-H., Kim, Y.-D., Kim, J.-M., and Roh, J.-K. (2014). Cardiac function and outcome in patients with cardio-embolic stroke. *PLoS One* 9:e95277. doi: 10.1371/journal.pone.0095277

Colivicchi, F., Bassi, A., Santini, M., and Caltagirone, C. (2004). Cardiac autonomic derangement and arrhythmias in right-sided stroke with insular involvement. *Stroke* 35, 2094–2098.

Dhamoon, M. S., Moon, Y. P., Paik, M. C., Boden-Albala, B., Rundek, T., Sacco, R. L., et al. (2009). Long-term functional recovery after first ischemic stroke: the Northern manhattan study. *Stroke* 40, 2805–2811.

Elstad, M., Walløe, L., Chon, K. H., and Toska, K. (2011). Low-frequency fluctuations in heart rate, cardiac output and mean arterial pressure in humans:

what are the physiological relationships? *Journal of Hypertens.* 29, 1327–1336. doi: 10.1097/HJH.0b013e328347a17a

Fu, Q., Vangundy, T. B., Galbreath, M. M., Shibata, S., Jain, M., Hastings, J. L., et al. (2010). Cardiac origins of the postural orthostatic tachycardia syndrome. *J. Am. Coll. Cardiol.* 55, 2858–2868.

Fuhrer, H., Reinhard, M., and Niesen, W. D. (2017). Paradigm change? cardiac output better associates with cerebral perfusion than blood pressure in ischemic stroke. *Front. Neurol.* 8:706. doi: 10.3389/fneur.2017.00706

Fuhrer, H., Weiller, C., and Niesen, W.-D. (2016). Is mean arterial pressure the best parameter in ischemic stroke? *Clin. Case Rep.* 4, 236–239.

Garcia-Esperon, C., Spratt, N. J., Gangadharan, S., Miteff, F., Bivard, A., Lillicrap, T., et al. (2020). Computed tomography perfusion identifies patients with stroke with impaired cardiac function. *Stroke* 51, 498–503. doi: 10.1161/strokeaha.119.027255

Gatti, P. J., Johnson, T. A., McKenzie, J., Lauenstein, J.-M., Gray, A., and Massari, V. J. (1997). Vagal control of left ventricular contractility is selectively mediated by a cranioventricular intracardiac ganglion in the cat. *J. Auton. Nerv. Syst.* 66, 138–144.

Hong, L., Cheng, X., Lin, L., Bivard, A., Ling, Y., Butcher, K., et al. (2019). The blood pressure paradox in acute ischemic stroke. *Ann. Neurol.* 85, 331–339.

Korpelainen, J. T., Huikuri, H. V., Sotaniemi, K. A., and Myllylä, V. V. (1996). Abnormal heart rate variability reflecting autonomic dysfunction in brainstem infarction. *Acta Neurol. Scand.* 94, 337–342. doi: 10.1111/j.1600-0404.1996.tb07076.x

Leonardi-Bee, J., Bath, P. M., Phillips, S. J., Sandercock, P. A., and Group, I. S. T. C. (2002). Blood pressure and clinical outcomes in the international stroke trial. *Stroke* 33, 1315–1320.

Liu, H., Yambe, T., Sasada, H., Nanka, S., Tanaka, A., Nagatomi, R., et al. (2004). Comparison of heart rate variability and stroke volume variability. *Auton. Neurosci.* 116, 69–75.

Louapre, C., Collongues, N., Stankoff, B., Giannesini, C., Papeix, C., Bensa, C., et al. (2020). Clinical characteristics and outcomes in patients with coronavirus disease 2019 and multiple sclerosis. *JAMA Neurol.* 77, 1079–1088.

Martina, J. R., Westerhof, B. E., van Goudoever, J., Steffen, C., Wappler, F., and Sakka, S. G. (2012). Noninvasive continuous arterial blood pressure monitoring with Nexfin® . *Anesthesiology* 116, 1092–1103.

Mathias, T. L., Albright, K. C., Boehme, A. K., George, A. J., Monlezun, D., Jones, E., et al. (2013). Cardiac function and short-term outcome in patients with acute ischemic stroke: a cross-sectional study. *J. Cardiovasc. Dis.* 1, 26–29.

Messé, S. R., Khatri, P., Reeves, M. J., Smith, E. E., Saver, J. L., Bhatt, D. L., et al. (2016). Why are acute ischemic stroke patients not receiving IV tPA? Results from a national registry. *Neurology* 87, 1565–1574. doi: 10.1212/wnl.0000000000003198

Milionis, H., Faouzi, M., Cordier, M., D'Ambrogio-Remillard, S., Eskandari, A., and Michel, P. (2013). Characteristics and early and long-term outcome in patients with acute ischemic stroke and low ejection fraction. *Int. J. Cardiol.* 168, 1082–1087. doi: 10.1016/j.ijcard.2012.11.036

National Institute of Neurological Disorders and Stroke rt-Pa Stroke Study Group (1995). Tissue plasminogen activator for acute ischemic stroke. *N Engl. J. Med.* 333, 1581–1588.

Rangaraju, S., Frankel, M., and Jovin, T. G. (2016). Prognostic value of the 24-hour neurological examination in anterior circulation ischemic stroke: a post hoc analysis of two randomized controlled stroke trials. *Interv. Neurol.* 4, 120–129. doi: 10.1159/000443801

Rasmussen, M., Schönenberger, S., Hendèn, P. L., Valentin, J. B., Espelund, U. S., Sørensen, L. H., et al. (2020). Blood pressure thresholds and neurologic outcomes after endovascular therapy for acute ischemic stroke: an analysis of individual patient data from 3 randomized clinical trials. *JAMA Neurol.* 77, 622–631. doi: 10.1001/jamaneurol.2019.4838

Reinhard, M., Rutsch, S., Lambeck, J., Wihler, C., Czosnyka, M., Weiller, C., et al. (2012). Dynamic cerebral autoregulation associates with infarct size and outcome after ischemic stroke. *Acta Neurol. Scand.* 125, 156–162. doi: 10.1111/j.1600-0404.2011.01515.x

Robinson, T., Waddington, A., Ward-Close, S., Taub, N., and Potter, J. (1997). The predictive role of 24-hour compared to casual blood pressure levels on outcome following acute stroke. *Cerebrovasc. Dis.* 7, 264–272. doi: 10.1159/000108206

Robinson, T. G., Dawson, S. L., Eames, P. J., Panerai, R. B., and Potter, J. F. (2003). Cardiac baroreceptor sensitivity predicts long-term outcome after acute ischemic stroke. *Stroke* 34, 705–712. doi: 10.1161/01.STR.0000058493.94875.9F

Sposato, L. A., Hilz, M. J., Aspberg, S., Murthy, S. B., Bahit, M. C., Hsieh, C.-Y., et al. (2020). Post-stroke cardiovascular complications and neurogenic cardiac injury: JACC state-of-the-art review. *J. Am. Coll. Cardiol.* 76, 2768–2785. doi: 10.1016/j.jacc.2020.10.009

Takagi, T., Kato, T., Sakai, H., and Nishimura, Y. (2014). Early neurologic improvement based on the national institutes of health stroke scale score predicts favorable outcome within 30 minutes after undergoing intravenous recombinant tissue plasminogen activator therapy. *J. Stroke Cerebrovasc. Dis.* 23, 69–74. doi: 10.1016/j.jstrokecerebrovasdis.2012.09.013

Timmers, H. J., Wieling, W., Soetekouw, P. M., Bleijenberg, G., Van Der Meer, J. W., and Lenders, J. W. (2002). Hemodynamic and neurohumoral responses to head-up tilt in patients with chronic fatigue syndrome. *Clin. Auton. Res.* 12, 273–280. doi: 10.1007/s10286-002-0014-1

Toska, K., and Eriksen, M. (1993). Respiration-synchronous fluctuations in stroke volume, heart rate and arterial pressure in humans. *J. Physiol.* 472, 501–512. doi: 10.1113/jphysiol.1993.sp019958

Tranmer, B. I., Keller, T. S., Kindt, G. W., and Archer, D. (1992). Loss of cerebral regulation during cardiac output variations in focal cerebral ischemia. *J. Neurosurg.* 77:253. doi: 10.3171/jns.1992.77.2.0253

Virani, S. S., Alonso, A., Benjamin, E. J., Bittencourt, M. S., Callaway, C. W., Carson, A. P., et al. (2020). Heart disease and stroke statistics-2020 update: a report from the american heart association. *Circulation* 141, e139–e596. doi: 10.1161/CIR.0000000000000757

Wouters, A., Nysten, C., Thijs, V., and Lemmens, R. (2018). Prediction of outcome in patients with acute ischemic stroke based on initial severity and improvement in the first 24 h. *Front. Neurol.* 9:308. doi: 10.3389/fneur.2018.00308

Wrigley, P., Khoury, J., Eckerle, B., Alwell, K., Moomaw, C. J., Woo, D., et al. (2017). Prevalence of positive troponin and echocardiogram findings and association with mortality in acute ischemic stroke. *Stroke* 48, 1226–1232.

Xiong, L., Tian, G., Leung, H., Soo, Y. O. Y., Chen, X., Ip, V. H. L., et al. (2018). Autonomic dysfunction predicts clinical outcomes after acute ischemic stroke: a prospective observational study. *Stroke* 49, 215–218. doi: 10.1161/strokeaha.117.019312

Conflict of Interest: JM discloses that Edwards Lifesciences provided the Nexfin device at no cost but provided no other financial support. The Henry Ford Health System funded the study through an investigator initiated grant. PL discloses the receipt of unrelated research funding from Edwards Lifesciences.

The remaining authors declare that the research was conducted in the absence of any commercial or financial relationships that could be construed as a potential conflict of interest.

Publisher's Note: All claims expressed in this article are solely those of the authors and do not necessarily represent those of their affiliated organizations, or those of the publisher, the editors and the reviewers. Any product that may be evaluated in this article, or claim that may be made by its manufacturer, is not guaranteed or endorsed by the publisher.

frontiers in Physiology

ORIGINAL RESEARCH
published: 16 December 2021
doi: 10.3389/fphys.2021.687424

Proteomic Sequencing of Stellate Ganglions in Rabbits With Myocardial Infarction

Lijun Cheng, Xinghua Wang, Hongda Chou, Tong Liu, Huaying Fu and Guangping Li**

Tianjin Key Laboratory of Ionic-Molecular Function of Cardiovascular Disease, Department of Cardiology, Tianjin Institute of Cardiology, The Second Hospital of Tianjin Medical University, Tianjin, China

The stellate ganglion (SG) of the autonomic nervous system plays important role in cardiovascular diseases (CDs). Myocardial infarction (MI) is associated with sustained increasing cardiac sympathetic nerve activity. Expressions and functions of proteins in SG tissue after MI are remaining unclear. This study is to explore the expression characteristics of proteins in SGs associated with MI. Japanese big-ear white rabbits ($n = 22$) were randomly assigned to the control group and MI group. The MI model was established by left anterior descending coronary artery ligation and confirmed by serum myocardial enzymes increasing 2,3,5-triphenyltetrazolium (TTC) staining and echocardiography. The expressions of proteins in rabbit SGs after MI were detected using tandem mass tags (TMT) quantitative proteomic sequencing. There were 3,043 credible proteins were predicted in rabbit SG tissues and 383 differentially expressed proteins (DEPs) including 143 upregulated and 240 downregulated proteins. Gene ontology (GO) and Kyoto Encyclopedia of Genes and Genomes (KEGG) analysis showed that the DEPs involved in adrenergic signaling in cardiomyocytes, positive regulation of ERK1 and ERK2 cascade, and other biological processes. Three kinds of proteins directly correlated to CDs were selected to be validated by the subsequent western blot experiment. This study first identified the characterization of proteins in rabbit SG after MI, which laid a solid foundation for revealing the mechanism of roles of SG on the MI process.

Keywords: stellate ganglion, myocardial infarction, TMT quantitative proteomic sequencing, rabbit, KEGG analysis, GO analysis

OPEN ACCESS

Edited by:
Lilei Yu,
Wuhan University, China

Reviewed by:
Hong Jiang,
Renmin Hospital of Wuhan University, China
Elham Mahmoudi,
Universal Scientific Education and Research Network, Iran

****Correspondence:***
Huaying Fu
fuhuaying@tmu.edu.cn
Guangping Li
tic_tjcardiol@126.com

Specialty section:
This article was submitted to Autonomic Neuroscience, a section of the journal Frontiers in Physiology

Received: *29 March 2021*
Accepted: *17 November 2021*
Published: *16 December 2021*

Citation:
Cheng L, Wang X, Chou H, Liu T, Fu H and Li G (2021) Proteomic Sequencing of Stellate Ganglions in Rabbits With Myocardial Infarction. Front. Physiol. 12:687424. doi: 10.3389/fphys.2021.687424

INTRODUCTION

Myocardial infarction (MI) is a common cardiovascular disease (CD), which seriously endangers the health of middle-aged and elderly people. The stellate ganglion (SG) in the autonomic nervous system provides sympathetic outflow and plays an integrative role in regulating cardiovascular function (Yu et al., 2017a). The SG has been implicated in the pathogenesis of various CDs. Following MI, SG was involved in the process of catecholamine released and promoted cardiac arrhythmogenesis (Richardt et al., 2006; Wu et al., 2012). Also, morphological, neurochemical, and electrophysiological changes in the SG neurons were observed in the areas distant from the infarct zone (Ajijola et al., 2015; Cheng et al., 2016), which may be important factors leading to ventricular arrhythmia after MI. The results of clinical and animal experiments showed that SG blockade can improve and treat CDs (Gu et al., 2012; Meng et al., 2017; Yu et al., 2017b), but it had adverse complications (including Horner's syndrome, hyperhidrosis, and paraesthesia)

(Goel et al., 2019). Many proteins of SG participated in the regulation of cardiac function. The targeted intervention of these proteins can improve cardiac function after myocardial ischemia or infarction. For example, previous studies have shown that the characteristics of ion channels in sympathetic ganglion neurons changed significantly after myocardial ischemia and infarction (Cheng et al., 2016, 2018). Blocking the ion channel of SG neurons can significantly attenuate ischemia-induced ventricular arrhythmia by suppressing the SG activity (Yu et al., 2017a). In addition, the neural chemorepellent Semaphorin 3a overexpression in the SG ameliorated the inducibility of ventricular arrhythmias after MI through attenuation of neural remodeling within the cardiac neuraxis (Yang et al., 2016). P2X7 inhibition can prevent the pathophysiologic processes mediated by P2X7 receptors in the SG after myocardial ischemic injury (Zou et al., 2016). So, it is necessary to find the key proteins in SGs regulating cardiac function, to reduce sympathetic overactivation after MI by target intervention of these proteins safely and effectively. However, analyzing the proteins in ganglia after MI comprehensively and systematically is absent. Discovering differentially expressed proteins (DEPs) in SG after MI is an urgent problem to be solved.

To find DEPs in SGs after MI, in this study, we established the rabbit MI model to reveal the expression characterization of proteins in MI rabbit SG tissues by tandem mass tags (TMT) quantitative proteomic sequencing and screening out the key proteins that are regulating the process of MI in SG tissues, which will provide a reliable experimental basis for finding effective intervention targets in SGs after MI.

MATERIALS AND METHODS

Experimental Animals and Protocol

All animal studies were approved by the Animal Ethical and Welfare Committee of the Chinese Academy Medical Sciences Institute of Radiation Medicine. Japanese big-ear white male rabbits weighing 400–600 g were obtained from Tianjin Yuda Experimental Animal Co. Ltd. (Tianjin, China). They were randomly divided into the control group and MI group (each group $n = 11$). MI injury was induced by ligating the left anterior descending coronary artery (LADCA). First, rabbits were anesthetized using 3% pentobarbital sodium (1 ml/kg) intravenously via the marginal ear vein. A left thoracotomy was performed. Then, the LAD was identified and it was ligated and the thorax was closed. The rabbits in the control group underwent an identical surgical procedure without ligation. Four rabbits died during the experimental process. Randomly selected rabbits were replenished for the experiment, and the number of animals in each group was 11. After 24 h of surgery in two groups, blood samples were obtained. After 7 d of surgery, the animals were sacrificed, hearts and SG tissues were obtained for the following experiments. MI was confirmed using 2,3,5-triphenyltetrazolium chloride (TTC) staining, increasing the levels of the three serum myocardial enzymes, and echocardiography.

Echocardiography

After MI surgery, rabbits in the two groups were anesthetized using 3% pentobarbital sodium to measure transthoracic echocardiography. Echocardiography parameters, including left atrial diameter (LAD), left ventricular end-diastolic dimension (LVDD), left ventricular end-systolic dimension (LVSD), and left ventricular ejection fraction (LVEF), were obtained using a specified small animal ultrasound system (VisualSonics Vevo 2100, USA).

Analyzing Myocardial Enzymes

Blood samples (1-2 ml) were collected from the jugular veins of rabbits in the control and MI groups. Sera were separated using centrifugation and stored in the refrigerator at −20°C. Serum myocardial enzymes including creatine kinase isoenzyme (CK-MB), creatine kinase (CK), and lactate dehydrogenase (LDH) were analyzed following the instructions of the manufacturer (Nanjing Jiancheng Bioengineering Institute, China).

TTC Staining

TTC staining was performed to assess the myocardial infarct size. In brief, the animal was fixed on the table, and the heart was taken out quickly. After washing the residual blood from the heart with the phosphate buffer, the heart was frozen in the refrigerator at −20°C for 30 min. Then the heart was transected into 2–3 mm thick sections. The sections were incubated in 0.5% TTC solution (30 min, 37°C) and fixed with 10% formalin. Normal myocardium was stained in red color, and the infarcted myocardium was stained in white color. Then the stained myocardium was photographed, and the infarct size was calculated.

TMT Quantitative Proteomic Sequencing and Bioinformatics Analysis

In this study, we used the "mix the samples" method to reduce the variation in a single group. In contrast, the SG tissue of a single rabbit is small and cannot meet the weight requirements for sequencing analysis; the SG tissues of two rabbits need to be mixed. Therefore, SGs of two rabbits in the control group were randomly mixed; six rabbits were divided into con1, con2, and con3 ($n = 3$). It was the same as in the MI group; six rabbits were divided into MI1, MI2, and MI3 ($n = 3$). TMT quantitative proteomic sequencing and subsequent bioinformatics analysis were performed using the Shanghai Luming Biological Technology Co. Ltd. (Shanghai, China). Briefly, the process of TMT quantitative proteomic sequencing was as follows: Frozen samples were lysed with 300 μl lysis buffer supplemented with 1 mM PMSF (Amresco, USA). After sonication, the samples were centrifuged to remove insoluble particles and precipitation. Protein concentration was determined using the BCA Protein Assay Kit (ThermoScientific,

Abbreviations: SG, stellate ganglion; MI, myocardial infarction; TMT, tandem mass tags; KEGG, Kyoto Encyclopedia of Genes and Genomes; GO, gene ontology; TTC, 2,3,5-triphenyltetrazolium chloride; LAD, left anterior descending coronary artery; CK, creatine kinase; CK-MB, creatine kinase isoenzyme; LDH, lactate dehydrogenase; PVDF, polyvinylidene fluoride; CALM, calmodulin; TPM1, tropomyosin 1; TPM2, tropomyosin 2; SD, standard deviation; DEPs, differentially expressed proteins; CD, cardiovascular disease.

USA). The amount of protein can be analyzed using the SDS-PAGE electrophoresis method. The 100 μg proteins were hydrolyzed into peptides using 2 μl sequencing-grade trypsin (1 μg/μl). Digested peptides were labeled using a 41 μl TMT reagent (ThermoFisher, USA) and incubated using 8 μl 5% hydroxylamine (Sigma, USA) to terminate the reaction. The High Performance Liquid Chromatography (RPLC) analysis was performed on an 1100 HPLC System (Agilent, USA) using an Agilent Zorbax Extend RP column (5 μm, 150 mm × 2.1 mm). Mass spectrometry analysis was performed using a Q Exactive Mass Spectrometer (Thermo, USA). Samples were loaded and separated using Acclaim RepMap 100 column [100 μm × 2 cm, RP-C18, Acclaim RepMap (Thermo Fisher, USA)] and then separated using Acclaim RepMap RSLC column (15 cm × 75 μm, RP-C18, Thermo Fisher) on an EASY-nLC 1200 system (Thermo, USA).

Western Blot

SG tissues were ground to extract total protein. The total protein concentration was determined using the BCA Protein Assay Kit (Cwbio, China). Equal amounts of proteins were subjected to 10% SDS-PAGE and transferred onto polyvinylidene fluoride (PVDF) membranes (Millipore, Billerica, MA, USA). Membranes were blocked using 5% skimmed milk and subsequently incubated overnight at 4°C with anti-calmodulin (CALM) (Bioss Antibodies, China; 1:1,000), anti-tropomyosin 1 (TPM1) (Boster, China; 1:1,000), anti-tropomyosin 2 (TPM2) (Bioss Antibodies, China; 1:1,000), and anti-β-actin (TransGen Biotech, China; 1:5,000). Then, the membranes were incubated using secondary antibodies, including goat anti-Mouse IgG (H+L) HRP (Promega Corporation, USA; 1:5,000), or goat anti-rabbit IgG (H+L) HRP (Promega Corporation, USA; 1:5,000). Last, protein signals were assessed and analyzed using the ECL western blot detection system (Millipore, Billerica, MA, USA).

Statistical Analysis

Proteome Discoverer (version 2.2) was used to search all of the Q Exactive raw data thoroughly against the sample protein database. The database used was uniprot-proteome_UP000001811-Oryctolagus cuniculus (Rabbit) (Strain Thorbecke inbred) database. The search settings were selected as follows: the sample type was TMT 6 plex (Peptide Labeled), the cysteine alkylation was performed using iodoacetamide, digestion was done using trypsin, and the instrument used was Q Exactive. A global false discovery rate (FDR) was set to 0.01.

According to the search results of the protein database, the original data were obtained. The credible proteins and DEPs were selected, and the subsequent biological information function analysis was carried out based on the DEPs. Several common databases were used for functional annotation analysis of credible proteins. Gene ontology (GO) analysis, Kyoto Encyclopedia of Genes and Genomes (KEGG) analysis, and protein interaction analysis were done in the DEPs. Correlation analysis, expression pattern clustering map, and heat map were performed in the control and MI group proteins.

Data were analyzed using Proteome Discoverer (Thermo Scientific, USA), Origin 6.0 (OriginLab Inc., USA), SPSS 17.0 (SPSS, USA). All data were treated with a normal distribution test and variance homogeneity test. The variables were expressed as mean ± standard deviation (SD) and statistically analyzed using a *t*-test. $P < 0.05$ were considered statistically significant.

RESULTS

Validation of the MI Model

The MI model was confirmed and assessed using TTC staining, higher serum myocardial enzymes, and a decrease in cardiac function. According to the experimental results of TTC staining, there was no MI area in the control group; in contrast, the mean infarct area in the MI group was (42 ± 5.7)% ($n = 6$, $p < 0.05$; **Figure 1A**). The levels of serum myocardial enzymes (CK-MB, CK, and LDH) in the MI group were increased significantly compared with those in the control group ($n = 11$, $p < 0.05$; **Figure 1B**). Compared with the control group, the cardiac chamber dilation and left ventricle function decreased in the MI group, which manifested in the increasing of the inner diameter of the atrium and ventricle and the decreasing of left ventricle ejection fraction ($n = 11$, $p < 0.05$; **Figures 1C,D**).

General Characteristics of Proteins Obtained Using Sequencing

The distribution of peptide numbers corresponding to each qualitative protein in the original off-line data is shown in **Figure 2A**. The protein numbers corresponding to different molecular weights are displayed in **Figure 2B**. In the qualitative process, we compared each peptide segment with that in the background database and obtained the coverage index of the peptide relative to the complete protein sequence using the database search software and made statistics according to the coverage index, as shown in **Figure 2C**.

Differentially Expressed Proteins

After using the database to retrieve the original data, the search results were screened for credible proteins according to the unique peptide ≥1, and the proteins with expression values of more than 50% in the samples were retained. The mean of the samples in one group was filled in the proteins with missing values <50%. Credible proteins were obtained through median normalization and log2 logarithmic conversion. There were 3,043 credible proteins expressed in the SG tissues of rabbits. Based on credible protein, two standards were selected to calculate the difference between samples. Fold change (FC) was used to evaluate the change in the expression level of a protein between samples. The *p*-value was calculated using a *t*-test. The DEPs between the control and MI groups were screened using fold change ≥1.2 and $p < 0.05$. Compared with the control group, there were 383 kinds of DEPs in MI rabbits, which included 143 upregulated and 240 downregulated proteins (shown in **Figure 3A**). By using the Volcano map, we filtered out the DEPs as shown in **Figure 3B**.

Unsupervised hierarchical clustering was based on the R language. The cluster heatmap of the control and MI groups is shown in **Figure 3C**. By using the Pearson algorithm, we analyzed the correlation between the DEPs. The correlation

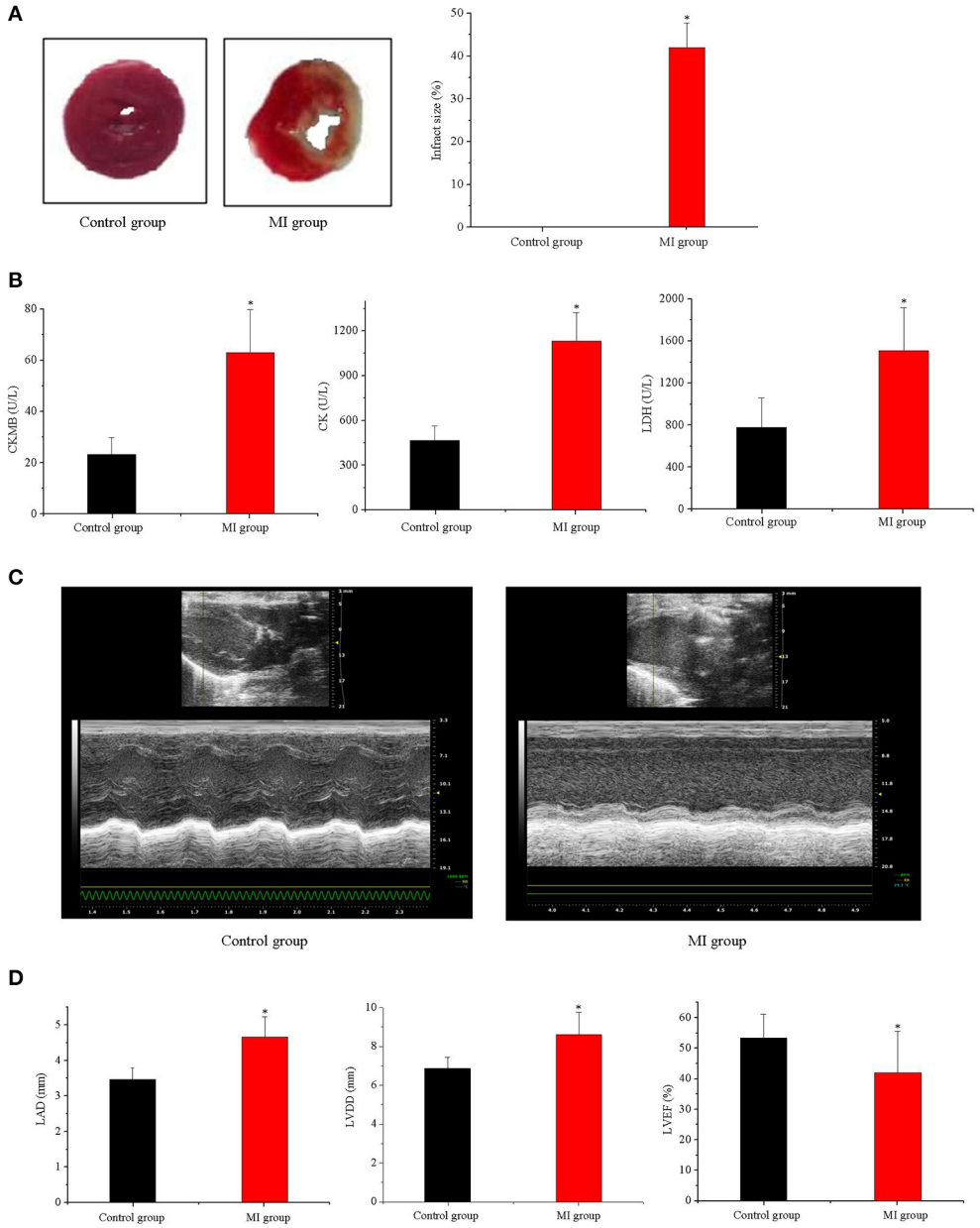

FIGURE 1 | Validation of the MI model. **(A)** TTC staining of MI and the infract size ($n = 6$, $p < 0.05$); **(B)** CK-MB, CK, and LDH in serum in control and MI group ($n = 11$, $p < 0.05$); **(C,D)** the cardiac function in the MI group decreased ($n = 11$, $p < 0.05$). Each point represents mean ± SD, n is the number of animals, $^*p < 0.05$ compared with the control group.

analysis diagram of the top 50 DEPs is shown in **Figure 3D**. The closer the correlation coefficient to 1, the higher the similarity of expression patterns between proteins.

GO and KEGG Analysis of the Differentially Expressed Proteins

After obtaining the DEPs, the DEPs were enriched and analyzed using GO/KEGG to describe their functions. In GO/KEGG functional enrichment analysis method, all credible proteins were considered for the background list and the differential protein list was considered as the candidate list screened from the background list. The hypergeometric distribution test was used to calculate the p-value, and the p-value was corrected using Benjamin-Hochberg multiple tests to obtain FDR.

To gain a deeper understanding of these DEPs after MI, the GO analysis was performed to analyze the function of these DEPs. The proteins were categorized based on the characters of "biological process," "cellular component," and "molecular function." The first 3 categories of the biological process were

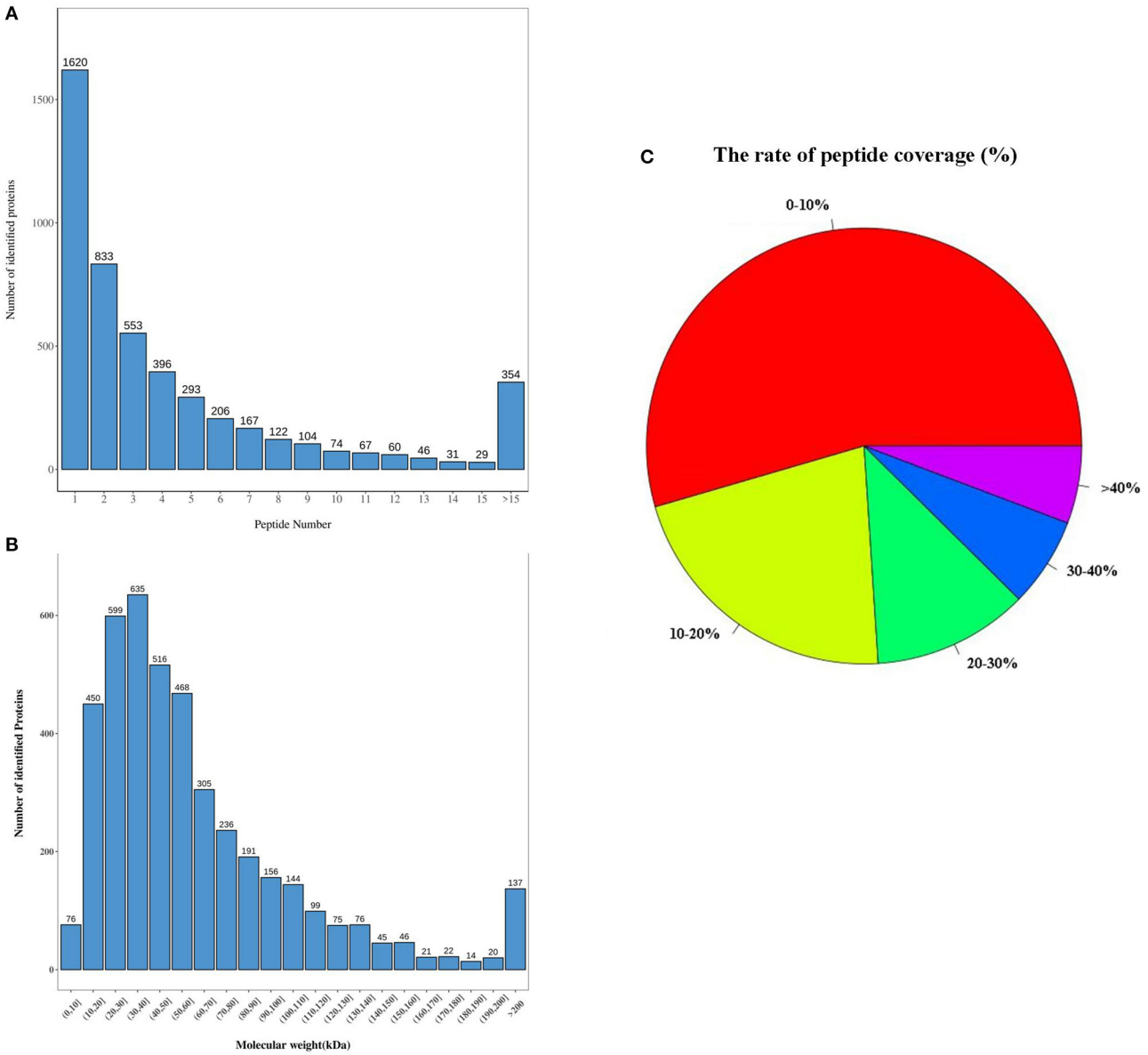

FIGURE 2 | General characteristics of proteins obtained by sequencing. **(A)** The distribution of peptide number corresponding to each qualitative protein; **(B)** the number of proteins corresponding to different molecular weights; **(C)** the rate of peptide coverage (%). Red, the proportion of protein with peptide coverage of 0–10%; yellow, the proportion of protein with peptide coverage of 10–20%; green, the proportion of protein with peptide coverage of 20–30%; blue, the proportion of protein with peptide coverage of 30–40%; purple, the proportion of protein with peptide coverage of >40%. There were three samples in each group of the control and MI groups ($n = 3$).

"positive regulation of ERK1 and ERK2 cascade," "cellular response to interferon-gamma," and "protein polymerization," respectively. The first 3 categories of the cellular component were "cytoplasm," "cytosol," and "endoplasmic reticulum membrane," respectively. The first 3 top categories of molecular function were "calcium ion binding," "identical protein binding," and "structural constituent of the ribosome" (**Figure 4A**). The first 6 items with the number of DEPs excesses than 3 and <50 in each comparison group were selected, which are sorted from large to small according to the $-\log_{10}$ p-value corresponding to each item, and the GO enrichment analysis chord representing the relationship between the selected GO term and the corresponding differential protein list is shown in **Figure 4B**. The KEGG analysis of these DEPs was also carried out to systematically analyze the regulatory role of these proteins. Top 20 KEGG enrichment proteins are shown in **Figure 4C**, and their roles include "adrenergic signaling in cardiomyocytes," "aldosterone synthesis and secretion," "Alzheimer's disease," "aminoacyl-tRNA biosynthesis," and other processes. The distributions of differentially upregulated

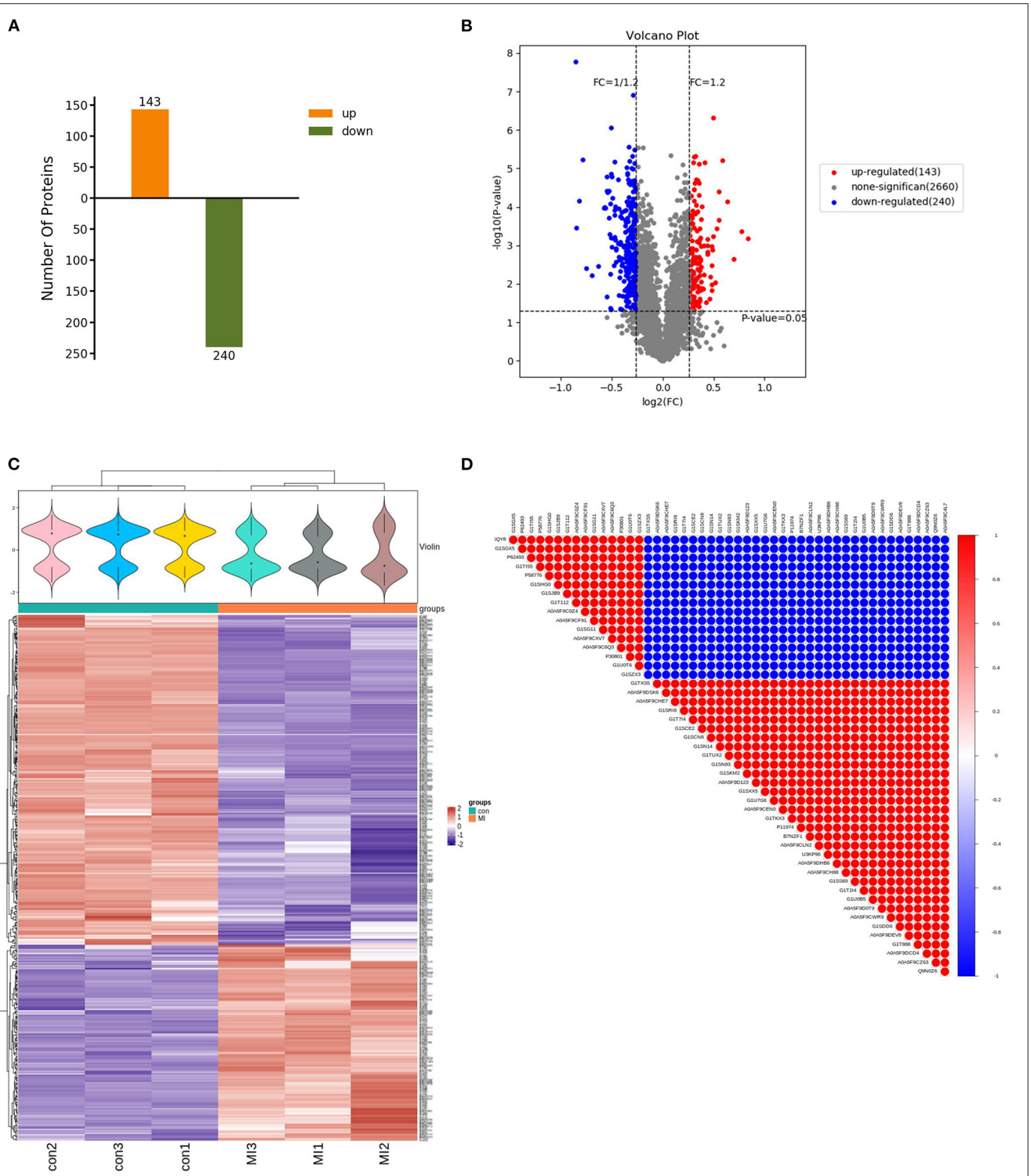

FIGURE 3 | Characteristics of DEPs. **(A)** Totally 383 DEPs in the MI group, including 143 upregulated and 240 downregulated proteins (the abscissa is the comparison group, and the ordinate is the number of differential proteins); **(B)** volcano map filtering out the DEPs [the abscissa of the volcano map is $\log_2$(FC)]. The farther its value is from point 0, the greater the difference is. It is upregulated on the right and downregulated on the left. The ordinate is $-\log_{10}$(*p*-value). The farther the ordinate value from point 0, the greater is the difference. The blue dots indicate downregulated DEPs, red dots indicate upregulated DEPs, and black dots indicate non-significant DEPs; **(C)** cluster heatmap of the 383 differentially expressed proteins (the violin graph in the upper part is a combination of a box plot and density graph). The flatter the violin box, the more concentrated the data. The outline of the box reflected the probability distribution of the expression value. Different color

(Continued)

FIGURE 3 | filled in represents different samples. The "+" in the middle of the violin graph indicates the median of the data; the vertical axis is the protein expression level. Below the violin is the column annotations of the heat map, the samples in the same group correspond to the same color block annotation. The clustering heat map below is clustered according to protein expression level. The red color indicates high expression protein, the blue color indicates low expression protein, and each row indicates the expression level of each protein in each different group, and each column represented the expression of all differential proteins in each group. **(D)** The correlation analysis diagram of the top 50 DEPs (red is a positive correlation, blue is a negative correlation. The darker color means the greater correlation). There were three samples in each group of control and MI group ($n = 3$).

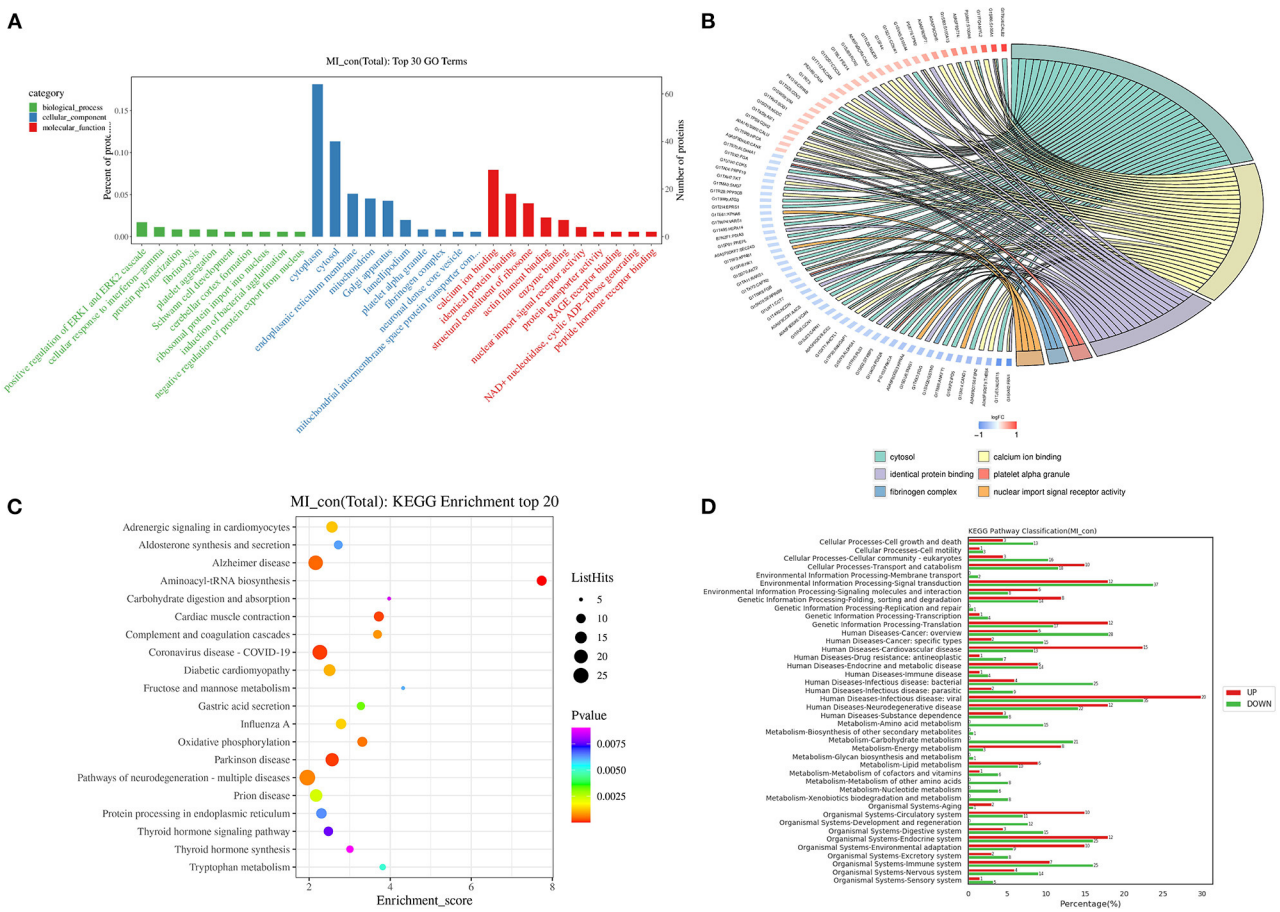

FIGURE 4 | Go and KEGG analysis of the DEPs. **(A)** GO annotation analysis of proteins with top 10 in "biological process," "cellular component," and "molecular function" (the *x*-axis is the name of GO entry, the *y*-axis is the protein quantity and its percentage of the corresponding item); **(B)** go enrichment analysis chord diagram (the protein is on the left: gene name, the red color indicated upregulation, the blue color indicated downregulation. The selected GO term is on the right); **(C)** KEGG enrichment of top 20 (the *x*-axis is the enrichment score, and the *y*-axis is the pathway information of top 20. The larger the bubble means more differential protein numbers. The color of bubbles changed from purple-blue-green to red. The smaller the *p*-value, the greater the significance); **(D)** the distribution of upregulated and downregulated proteins at KEGG level 2 [the *x*-axis is the number and ratio (%) of differentially upregulated and downregulated proteins annotated to each level 2 metabolic pathway. The *y*-axis is the name of the level 2 pathway, and the number on the right side of the column represents the number of DEPs annotated to the level 2 pathway].

and downregulated proteins at KEGG Level 2 are shown in **Figure 4D**.

Verification of the Proteins by Western Blot

Among the DEPs, we focused on the DEPs related to human CDs. We screened 7 items in KEGG results by classification_level1 ("human disease") and classification_level2 ("CDs"). Proteins in these items were involved in the occurrence and development of human CDs. We presented DEPs related to CDs of human diseases. Three of the proteins (meeting the following conditions: at least involved in two items, fold change >1.2 or fold change <0.8, and score sequence HT of protein >50) were selected for verification using Western blot experiment, including tropomyosin 1 (TPM1), tropomyosin 2 (TPM2), and calmodulin (CALM) in **Table 1**. Western blot results showed that three proteins expressions were significantly increased in MI group rabbits, which is consistent with the results of TMT quantitative proteomic sequencing analysis ($n = 5$, $p < 0.05$; **Figure 5**).

TABLE 1 | KEGG analysis related to CD of human diseases.

Id	Classification_level1	Classification_level2	Term	Protein	*p*-value
ocu05415	Human Diseases	CD	Diabetic cardiomyopathy	G1T359: NDUFS1, A0A5F9C1W2: ATP2A2, G1U7G6: G1TVE5: CAMK2D, G1SDD6: AGT, P05772: PRKCB, P10102: PRKCA, G1SD70: AKT2, G1SQA8: ATP5F1B, G1SG11: COX4I1, G1SXI9: O79431: MT-ATP8, G1TMH7: G1TPV7: G1SN66: NDUFB6	0.00106
ocu05418	Human Diseases	CD	Fluid shear stress and atherosclerosis	G1U9R0: G1SXQ0: GSTM3, G1SXP3: G1SD70: AKT2, P62160: CALM	0.51084
ocu05410	Human Diseases	CD	Hypertrophic cardiomyopathy	A0A5F9C1W2: ATP2A2, G1SDD6: AGT, P58776: TPM2, A0A5F9CLU9: TPM1, G1TW48: MYH7, G1TFQ4: MYL2	0.12617
ocu05412	Human Diseases	CD	Arrhythmogenic right ventricular cardiomyopathy	A0A5F9C1W2: ATP2A2, G1TPS9: CDH2	0.80004
ocu05414	Human Diseases	CD	Dilated cardiomyopathy	A0A5F9C1W2: ATP2A2, G1SDD6: AGT, P58776: TPM2, A0A5F9CLU9: TPM1, G1TW48: MYH7, G1TFQ4: MYL2	0.37173
ocu05416	Human Diseases	CD	Viral myocarditis	P41110: EIF4G1, G1TW48: MYH7, G1U0B4: A0A5F9CVI4	0.61311
ocu05417	Human Diseases	CD	Lipid and atherosclerosis	G1TVE5: CAMK2D, P10102: PRKCA, G1TRZ8: PPP3CB, G1SD70: AKT2, P62160: CALM, G1U0B4	0.57190

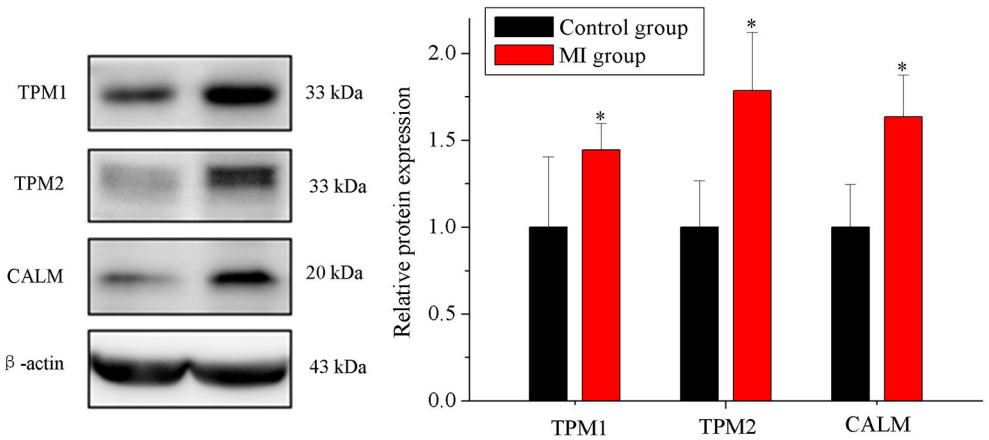

FIGURE 5 | Verification of the proteins using Western blot. Expression of TPM1, TPM2, and CALM in the control and MI groups ($n = 5$, $p < 0.05$). Each point represents mean ± SD; n is the number of animals; *$p < 0.05$ compared with the control group.

Proteins Interaction Network

STRING database is a database for predicting functional correlation between proteins. In the STRING database, we analyzed the interaction relationship of DEPs following MI, visualized the first 25 nodes in terms of node connectivity using the python "networkx" package, and displayed them with protein IDs and gene names (**Figure 6**). Proteins interaction network analysis demonstrated that one protein interacted with another or more other proteins directly or interacted with many proteins indirectly. These results were used to construct a complex and extensive protein regulatory network.

DISCUSSION

We presented the profiled proteins expression in rabbit SG tissues using the TMT quantitative proteomic sequencing in this study first. We identified the DEPs in MI rabbit SG tissues and analyzed the DEPs using GO, KEGG, and proteins interaction analysis. Three of the proteins (meeting the following conditions: at least involved in two items, fold change >1.2 or fold change <0.8, and score sequence HT of protein >50) were selected for verification using Western blot experiment, including TPM1, TPM2, and CALM.

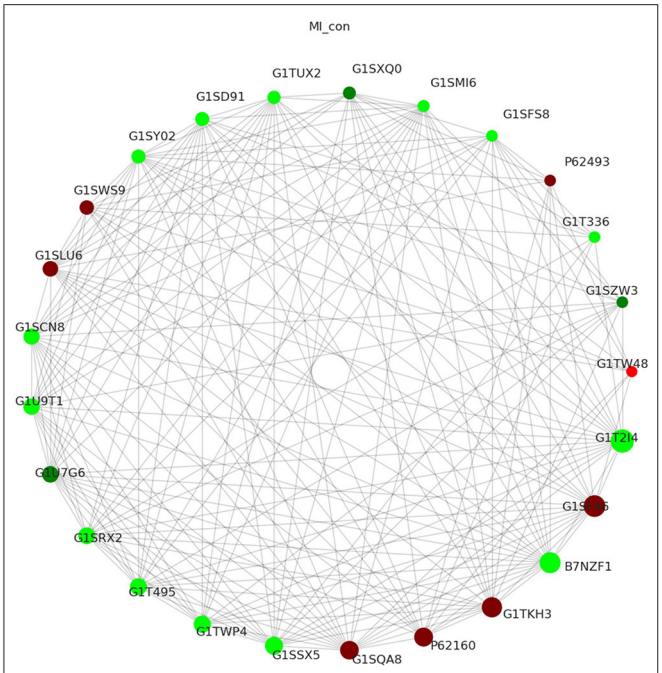

FIGURE 6 | Proteins interaction network shows the interaction between DEPs after MI (the circles in the figure represented differential proteins, the red color represented upregulated protein, and the green color represented downregulated protein. The size of the circle represented the degree of connected correlation, and the larger the circle, the higher the connected correlation).

The MI induced a series of changes including autonomic nervous system remodeling in the heart (Richardson et al., 2015). The SG in the autonomic nervous system played an integrative role in regulating cardiovascular function (Yu et al., 2017b; Boukens et al., 2020). Previous studies have shown that MI can lead to neural remodeling in the SG, including remodeling in the morphology, neurochemistry, electrophysiological remodeling, and sympathetic hyperinnervation (Zhou et al., 2008; Ajijola et al., 2015; Wang et al., 2015; Nakamura et al., 2016), which contributed to MI-induced ventricular arrhythmias (Han et al., 2012; Sheng et al., 2018). Interventions to reduce SG activity can improve cardiac function and reduce ventricular arrhythmogenicity (Gu et al., 2012; Meng et al., 2017; Xiong et al., 2018; Zhou et al., 2019). However, the roles and mechanisms of SG in MI have not been clarified.

Previous clinical and basic studies have shown that SG blockade and denervation can reduce the expression of sympathetic neurohormones and the release of noradrenaline prevent the occurrence of cardiac remodeling, fibrosis, and malignant arrhythmia (Gu et al., 2012; Zhang et al., 2019, 2020). However, the side effects of SG blockade and resection limited its clinical application (Goel et al., 2019). A new method of SG denervation after CDs is promising. A variety of proteins in SG plays regulatory roles in cardiac function. After finding out the intervention of the proteins that played vital roles in SG, we can purposefully change the effect of SG on cardiac remodeling after CDs. Therefore, it is important to clarify the proteins involved in the regulation of SG after MI by sequencing. Studies have shown that cardiac nerve sprouting and sympathetic hyperinnervation were more pronounced at 7 days after MI (Zhou et al., 2004). We identified the DEPs in MI groups. Compared with the control group, there were 383 kinds of DEPs totally in the MI group, including 143 upregulated proteins and 240 downregulated proteins. In a further study, the regulating function of the DEPs on cardiac function after MI will be studied.

The GO and KEGG analysis showed that the DEPs were involved in the process of "adrenergic signaling in cardiomyocytes, positive regulation of ERK1 and ERK2 cascade," and other biological processes. Screening results of the GO and KEGG analysis showed the biological function related to the heart in SGs after MI, including "diabetic cardiomyopathy, fluid shear stress and atherosclerosis, hypertrophic cardiomyopathy, arrhythmogenic right ventricular cardiomyopathy," and so on. Three of the proteins including TPM1, TPM2, and CALM (meeting the conditions: at least involved in two items, fold change >1.2 or fold change <0.8, and score sequence HT of protein >50) were selected for verification using Western blot experiment.

TPM is a thin filament-associated protein and is associated with morphogenesis, cellular migration, and the regulation of actin filaments (Zhang et al., 2018). TPM1 and TPM2 are two gene subtypes of TPM. TPM1 is an essential sarcomeric component that can stabilize the thin filament and facilitate the interaction of actin with myosin (England et al., 2017). TPM1 plays a vital role in cardiogenesis and is closely related to a variety of CDs including inherited cardiomyopathy and dilated cardiomyopathy (Hershberger et al., 2010; Gupte et al., 2015; Deacon et al., 2019). TPM2 is involved in muscle contraction, cell movement, and other biological processes (Xiong et al., 2018). It is also closely related to CDs (Marshall et al., 2012). Studies have shown that TPM2 exhibited potential as a promising diagnostic and therapeutic biomarker for atherosclerosis (Meng et al., 2019). Moreover, TPM protein also played a role in the nervous system (Gray et al., 2017). CALM is a ubiquitous intracellular Ca^{2+} sensing protein that modifies the gating of numerous ion channels (Chazin and Johnson, 2020). It also has notable roles in cell proliferation, cyclic nucleotide metabolism, cellular Ca^{2+} metabolism, gene expression, muscle contraction, and proteolysis (Sharma and Parameswaran, 2018). CALM activity is closely related to MI, arrhythmia, and hyperthyroid CDs (Beghi et al., 2020; Chazin and Johnson, 2020; Hou et al., 2020) and is involved in the occurrence and development of neurological diseases (O'Day, 2020). Both TPM and CALM proteins played important roles in the cardiovascular system and nervous system at the same time. Proteome sequencing also showed that the expression of TPM1, TPM2, and CALM increased in SGs after MI, and the score sequence HT was the highest among the DEPs related to at least two human CDs.

CONCLUSION

We clarified the protein expression in rabbit SG tissue by the TMT quantitative proteomic sequencing and compared the DEPs in the MI group. This study laid a solid foundation for further study on the mechanism of SG in regulating the heart after MI.

LIMITATIONS

This study has some limitations. First, in this study, three proteins related to CDs were selected for validation; however, there may be more important proteins that may play an important role in the development of MI, which should be confirmed in further studies. Second, the SG tissue on the 7th day after MI was used in sequence analysis instead of 1 month after MI when heart remodeling may lead to chronic remodeling of the cardiac nerve sprouting and sympathetic hyperinnervation. Third, the number of samples should be increased in future studies. "Mix the samples" method and the animal-to-animal variation reduced the statistical power of the study.

DATA AVAILABILITY STATEMENT

The datasets presented in this study can be found in online repositories. The names of the repository/repositories and accession number(s) can be found at: ProteomeXchange, accession no: PXD029386.

ETHICS STATEMENT

The animal study was reviewed and approved by Animal Ethical and Welfare Committee of Chinese Academy Medical Sciences Institute of Radiation Medicine.

AUTHOR CONTRIBUTIONS

GL and HF: conception of the work. LC: finishing experiment, analysis data, and drafting of manuscript. HC: submission. XW and TL: data interpretation and critically revised the manuscript. All authors contributed to the article and approved the submitted version.

FUNDING

This work was supported by grants from the National Natural Science Foundation of China (No. 82100342), the Tianjin Natural Science Foundation (Nos. 16JCQNJC12000 and 16JCYBJC25000), the China Postdoctoral Science Foundation (No. 2016M601274), the Key Laboratory of Scientific Research Foundation of the Second Hospital of Tianjin Medical University (Nos. 2017ZDSYS07 and 2019ZDSYS14), and clinical study of Second Hospital of Tianjin Medical University (No. 2019LC03).

ACKNOWLEDGMENTS

The authors thank the Shanghai Luming Biological Technology Co. Ltd. (Shanghai, China) for providing proteomics services and bioinformatics analysis.

REFERENCES

Ajijola, O. A., Yagishita, D., Reddy, N. K., Yamakawa, K., Vaseghi, M., Downs, A. M., et al. (2015). Remodeling of stellate ganglion neurons after spatially targeted myocardial infarction: neuropeptide and morphologic changes. *Heart Rhythm* 12, 1027–1035. doi: 10.1016/j.hrthm.2015.01.045

Beghi, S., Cavaliere, F., and Buschini, A. (2020). Gene polymorphisms in calcium-calmodulin pathway: focus on cardiovascular disease. *Mutat. Res. Rev. Mutat. Res.* 786:108325. doi: 10.1016/j.mrrev.2020.108325

Boukens, B. J., Dacey, M., Meijborg, V. M., Janse, M. J., Hadaya, J., Hanna, P., et al. (2020). Mechanism of ventricular premature beats elicited by left stellate ganglion stimulation during acute ischemia of the anterior left ventricle. *Cardiovasc. Res.* 117, 2083–2091. doi: 10.1093/cvr/cvaa253

Chazin, W. J., and Johnson, C. N. (2020). Calmodulin mutations associated with heart arrhythmia: a status report. *Int. J. Mol. Sci.* 21:1418. doi: 10.3390/ijms21041418

Cheng, L. J., Li, G. P., Li, J., Chen, Y., and Wang, X. H. (2016). Effects of fluvastatin on characteristics of stellate ganglion neurons in a rabbit model of myocardial ischemia. *Chin. Med. J.* 129, 549–556. doi: 10.4103/0366-6999.176991

Cheng, L. J., Wang, X. H., Liu, T., Gary, T., Fu, H. Y., and Li, G. P. (2018). Modulation of ion channels in the superior cervical ganglion neurons by myocardial ischemia and fluvastatin treatment. *Front. Physiol.* 9:1157. doi: 10.3389/fphys.2018.01157

Deacon, D. C., Happe, C. L., Chen, C, Tedeschi, N., Manso, A. M., Li,T., et al. (2019). Combinatorial interactions of genetic variants in human cardiomyopathy. *Nat. Biomed. Eng.* 3, 147–157. doi: 10.1038/s41551-019-0348-9

England, J., Granados-Riveron, J., Polo-Parada, L., Kuriakose, D., Moore, C., Brook, J. D., et al. (2017). Tropomyosin 1: multiple roles in the developing heart and in the formation of congenital heart defects. *J. Mol. Cell. Cardiol.* 106, 1–13. doi: 10.1016/j.yjmcc.2017.03.006

Goel, V., Patwardhan, A. M., Ibrahim, M., Howe, C. L., Schultz, D. M., and Shankar, H. (2019). Complications associated with stellate ganglion nerve block: a systematic review. *Reg. Anesth. Pain Med.* 44, 669–678. doi: 10.1136/rapm-2018-100127

Gray, K. T., Kostyukova, A.S., and Thomas Fath, T. (2017). Actin regulation by tropomodulin and tropomyosin in neuronal morphogenesis and function. *Mol. Cell. Neurosci.* 84:48–57. doi: 10.1016/j.mcn.2017.04.002

Gu, Y., Wang, L., Wang, X., Tang, Y., Cao, F., and Fang, Y. (2012). Assessment of ventricular electrophysiological characteristics at periinfarct zone of postmyocardial infarction in rabbits following stellate ganglion block. *J. Cardiovasc. Electrophysiol.* 1, S29–S35. doi: 10.1111/j.1540-8167.2012.02437.x

Gupte, T. M., Haque, F., Gangadharan, B., Sunitha, M. S., Mukherjee, S., Anandhan, S., et al. (2015). Mechanistic heterogeneity in contractile properties of α-tropomyosin (TPM1) mutants associated with inherited cardiomyopathies. *J. Biol. Chem.* 290, 7003–7015. doi: 10.1074/jbc.M114.596676

Han, S., Kobayashi, K., Joung, B., Piccirillo, G., Maruyama, M., Vinters, H. V., et al. (2012). Electroanatomic remodeling of the left stellate ganglion after myocardial infarction. *J. Am. Coll. Cardiol.* 59, 954–961. doi: 10.1016/j.jacc.2011.11.030

Hershberger, R. E., Norton, N., Morales, A., Li, D. X., Siegfried, J. D., and Gonzalez-Quintana, J. (2010). Coding sequence rare variants identified in MYBPC3, MYH6, TPM1, TNNC1 and TNNI3 from 312 patients with familial or idiopathic dilated cardiomyopathy. *Circ. Cardiovasc. Genet.* 3, 155–161. doi: 10.1161/CIRCGENETICS.109.912345

Hou, R., Jin, X. S., Gao, Y. H., Sun, D. D., Ma, W. P., Sun, P. Y., et al. (2020). Evaluation of the effects of schisandra chinensis on the myocardium of rats with hyperthyroid heart disease by using velocity vector imaging combined with the estimation of p53 expression and calmodulin activity. *Evid. Based Complement. Alternat. Med.* 2020:5263834. doi: 10.1155/2020/5263834

Marshall, P. A., Hernandez, Z., Kaneko, I., Widener, T., Tabacaru, C., Aguayo, I., et al. (2012). Discovery of novel vitamin D receptor interacting proteins that modulate 1,25-dihydroxyvitamin D3 signaling. *J. Steroid Biochem. Mol. Biol.* 132, 147–159. doi: 10.1016/j.jsbmb.2012.05.001

Meng, L., Tseng, C. H., Shivkumar, K., and Ajijola, O. (2017). Efficacy of stellate ganglion blockade in managing electrical storm: a systematic review. *JACC Clin. Electrophysiol.* 3, 942–949. doi: 10.1016/j.jacep.2017.06.006

Meng, L. B., Shan, M. J., Qiu, Y., Qi, R. M., Yu, Z. M., Guo, P., et al. (2019). TPM2 as a potential predictive biomarker for atherosclerosis. *Aging* 11, 6960–6982. doi: 10.18632/aging.102231

Nakamura, K., Ajijola, O. A., Aliotta, E., Armour, J. A., Ardell, J. L., and Shivkumar, K. (2016). Pathological effects of chronic myocardial infarction on peripheral neurons mediating cardiac neurotransmission. *Auton. Neurosci.* 97, 34–40. doi: 10.1016/j.autneu.2016.05.001

O'Day, D. H. (2020). Calmodulin binding proteins and Alzheimer's disease: biomarkers, regulatory enzymes and receptors that are regulated by calmodulin. *Int. J. Mol. Sci.* 21:7344. doi: 10.3390/ijms21197344

Richardson, W. J., Clarke, S. A., Quinn, T. A., and Holmes, J. W. (2015). Physiological implications of myocardial scar structure. *Compr. Physiol.* 5, 1877–1909. doi: 10.1002/cphy.c140067

Richardt, D., Dendorfer, A., Tölg, R., Dominiak, P., and Richardt, G. (2006). Inhibition of nonexocytotic norepinephrine release by desipramine reduces myocardial infarction size. *Can. J. Physiol. Pharmacol.* 84, 1185–1189. doi: 10.1139/y06-066

Sharma, R. K., and Parameswaran, S. (2018). Calmodulin-binding proteins: a journey of 40 years. *Cell Calcium* 75, 89–100. doi: 10.1016/j.ceca.2018.09.002

Sheng, X., Dan, Y., Dai, B., Guo, J., Ji, H., Zhang, X., et al. (2018). Knockdown the P2X3 receptor in the stellate ganglia of rats relieved the diabetic cardiac autonomic neuropathy. *Neurochem. Int.* 120, 206–212. doi: 10.1016/j.neuint.2018.09.002

Wang, S. Y., Zhou, X. Y., Huang, B., Wang, Z., Liao, K., Saren, G., et al. (2015). Spinal cord stimulation protects against ventricular arrhythmias by suppressing left stellate ganglion neural activity in an acute myocardial infarction canine model. *Heart Rhythm* 12, 1628–1635. doi: 10.1016/j.hrthm.2015.03.023

Wu, X. L., Jiang, H., Yu, L. L., Hu, X., and Liu, W. (2012). Desipramine pretreatment improves sympathetic remodeling and ventricular fibrillation threshold after myocardial ischemia. *J. Biomed. Biotechnol.* 2012:732909. doi: 10.1155/2012/732909

Xiong, L., Liu, Y., Zhou, M. M., Wang, G., Quan, D., Shen, C., et al. (2018). Targeted ablation of cardiac sympathetic neurons improves ventricular electrical remodelling in a canine model of chronic myocardial infarction. *Europace* 20, 2036–2044. doi: 10.1093/europace/euy090

Yang, L. C., Zhang, P. P., Chen, X. M., Li, C. Y., Sun, J., Hou, J. W., et al. (2016). Semaphorin 3a transfection into the left stellate ganglion reduces susceptibility to ventricular arrhythmias after myocardial infarction in rats. *Europace* 18, 1886–1896. doi: 10.1093/europace/euv276

Yu, L. L., Wang, M. L., Hu, D., Huang, B., Zhou, L. P., Zhou, X. Y., et al. (2017a). Blocking the Nav1.8 channel in the left stellate ganglion suppresses ventricular arrhythmia induced by acute ischemia in a canine model. *Sci. Rep.* 7:534. doi: 10.1038/s41598-017-00642-6

Yu, L. L., Zhou, L. P., Cao, G., Po, S. S., Huang, B., Zhou, X., et al. (2017b). Optogenetic modulation of cardiac sympathetic nerve activity to prevent ventricular arrhythmias. *J. Am. Coll. Cardiol.* 70, 2778–2790. doi: 10.1016/j.jacc.2017.09.1107

Zhang, J. F., Zhang, J., Xu, S. P., Zhang, X. Y., Wang, P. Y., Wu, H., et al. (2018). Hypoxia-induced TPM2 methylation is associated with chemoresistance and poor prognosis in breast cancer. *Cell. Physiol. Biochem.* 45, 692–705. doi: 10.1159/000487162

Zhang, M. J., Liu, X. G., Wu, J., Yu, Y. J., Wang, Y. T., and Gu, Y. (2020). Impact of bilateral sympathetic stellate ganglionectomy on TGF-β1 signaling pathway in rats with chronic volume overload. *Front. Physiol.* 11:375. doi: 10.3389/fphys.2020.00375

Zhang, M. J., Zhu, P. F., Wang, Y. T., Wu, J., Yu, Y. J., Wu, X. Y., et al. (2019). Bilateral sympathetic stellate ganglionectomy attenuates myocardial remodelling and fibrosis in a rat model of chronic volume overload. *J. Cell. Mol. Med.* 23, 1001–1013. doi: 10.1111/jcmm.14000

Zhou, M. M., Liu, Y., He, Y., Xie, K., Quan, D. J., Tang, Y. H., et al. (2019). Selective chemical ablation of transient receptor potential vanilloid 1 expressing neurons in the left stellate ganglion protects against ischemia-induced ventricular arrhythmias in dogs. *Biomed. Pharmacother.* 120:109500. doi: 10.1016/j.biopha.2019.109500

Zhou, S., Jung, B. C., Tan, A. Y., Trang, V. Q., Gholmieh, G., Han, S. W., et al. (2008). Spontaneous stellate ganglion nerve activity and ventricular arrhythmia in a canine model of sudden death. *Heart Rhythm* 5, 131–139. doi: 10.1016/j.hrthm.2007.09.007

Zhou, S. M., Chen, L. S., Miyauchi, Y., Miyauchi, M., Kar, S., Kangavari, S., et al. (2004). Mechanisms of cardiac nerve sprouting after myocardial infarction in dogs. *Circ. Res.* 95, 76–83. doi: 10.1161/01.RES.0000133678.22968.e3

Zou, L., Tu, G., Xie, W., Wen, S., Xie, Q., Liu, S., et al. (2016). LncRNA NONRATT021972 involved the pathophysiologic processes mediated by P2X7 receptors in stellate ganglia after myocardial ischemic injury. *Purinergic Signal.* 12, 127–137. doi: 10.1007/s11302-015-9486-z

Conflict of Interest: The authors declare that the research was conducted in the absence of any commercial or financial relationships that could be construed as a potential conflict of interest.

Publisher's Note: All claims expressed in this article are solely those of the authors and do not necessarily represent those of their affiliated organizations, or those of the publisher, the editors and the reviewers. Any product that may be evaluated in this article, or claim that may be made by its manufacturer, is not guaranteed or endorsed by the publisher.

Advantages of publishing in Frontiers

OPEN ACCESS
Articles are free to read for greatest visibility and readership

FAST PUBLICATION
Around 90 days from submission to decision

HIGH QUALITY PEER-REVIEW
Rigorous, collaborative, and constructive peer-review

TRANSPARENT PEER-REVIEW
Editors and reviewers acknowledged by name on published articles

Frontiers
Avenue du Tribunal-Fédéral 34
1005 Lausanne | Switzerland

Visit us: www.frontiersin.org
Contact us: frontiersin.org/about/contact

REPRODUCIBILITY OF RESEARCH
Support open data and methods to enhance research reproducibility

DIGITAL PUBLISHING
Articles designed for optimal readership across devices

FOLLOW US
@frontiersin

IMPACT METRICS
Advanced article metrics track visibility across digital media

EXTENSIVE PROMOTION
Marketing and promotion of impactful research

LOOP RESEARCH NETWORK
Our network increases your article's readership